Role of Plectin in Nuclear Mechano-transduction of Keratinocytes

Submitted in partial fulfilment of the requirements of the Degree of Doctor of Philosophy

by

Filipe Veiga de Macedo Almeida

School of Engineering and Material Sciences

Queen Mary, University of London

November 2015

I, Filipe Veiga de Macedo Almeida, confirm that the research included within this thesis is my own work or that where it has been carried out in collaboration with, or supported by others, that this is duly acknowledged below and my contribution indicated. Previously published material is also acknowledged below.

I attest that I have exercised reasonable care to ensure that the work is original, and does not to the best of my knowledge break any UK law, infringe any third party's copyright or other Intellectual Property Right, or contain any confidential material.

I accept that the College has the right to use plagiarism detection software to check the electronic version of the thesis.

I confirm that this thesis has not been previously submitted for the award of a degree by this or any other university.

Signature: (Filipe Almeida)

Date: 27th November of 2015

Details of collaboration and publications

1) Filipe V Almeida[1,6], Gernot Walko[2], James R McMillan[3], John A McGrath[4], Gerhard Wiche[5], Asa H Barber[1], John T Connelly[6]* "The cytolinker plectin regulates nuclear mechanotransduction in keratinocytes". *Journal Cell Science* (In press)

2) Urszula Stachewicz, Tuya Qiao, Simon C. F. Rawlinson, Filipe V Almeida, Wei-Qi Li, Michael Cattell and Asa H. Barber. (2015) 3D imaging of cell interactions with electrospun PLGA nanofiber membranes for bone regeneration. *Acta Biomaterilia* (In press)

3) Costa P, Almeida F V, Connelly JT. (2012) Biophysical signals controlling cell fate decisions: How do stem cells really feel? *Int J Biochem Cell Biol.,* (12) 00314-7

Abstract

Cell shape dictates nuclear morphology via cytoskeleton remodelling, potentially regulating therefore nuclear architecture and gene expression. Utilising micro-patterned substrates to control cell shape, the physical cell-nuclear integration was investigated. Cells were seeded in patterns with variable sizes and shapes, and the nuclear morphology assessed. The nucleus in spread cells was larger when compared with confined cells as measured by its volume. Actin and keratins are the two main determinants of keratinocytes mechanics and their role in defining nuclear morphology is still unclear. Results here showed that the inhibition of filamentous actin, therefore the formation of stress fibres, was not sufficient to disrupt the physical link between cell shape and nuclear morphology in keratinocytes. Plectin deficient keratinocytes were further investigated as they possess abnormal keratin architecture: their more open network of keratin 14 resulted in a larger and more deformable nucleus. These deformations depended on acto-myosin contractility and the formation of cell-cell contacts. When seeded as cell clusters with a confined adhesive area, *Plec* KO were able to compact to a higher extent and when allowed to migrate outside this confined area, the nucleus of *Plec* KO underwent larger and quicker morphological remodelling in comparison to the WT. Changes in nuclear morphology may influence chromatin remodelling. Confined keratinocytes committed to terminal differentiation, had lower levels of transcriptionally active sites (H3K4me3), and re-distributed heterochromatin markers (H3K27me3). In summary, the present thesis demonstrates that cell shape mediates nuclear morphology and chromatin remodelling, and this cell-nucleus coupling is coordinated by the cross-talk between keratins and actin, in which plectin is a key player.

Acknowledgments

I would like to thank, first of all, to Prof. Asa Barber to bring me on board in this PhD, for all the motivating words and support. To my mentor Dr John Connelly, a huge thanks for the active patience, enormous support and trust. A special and warm thanks for all the amazing team of post-docs with whom I learnt a lot: Patricia Costa, Vera Martins, Roanne Jones, Matthew Calley, Viviana Castagna, Krystelle Mafina, Valentina Rapisarda, Supatra Marsh, among others. Also to all my dear PhD colleagues from both SEMS and Blizards who helped in crucial occasions: Georgios Theocharidis, Fiona Kenny, Zoe Drymoussi, Alex Kao, Wenjun, Hao, Feng, Barbara Ricci, Aneta, Francesca, Ana Laly, among others. This intense experience was elevated to a level of enjoyment thanks to you guys, being there every day in good and bad moments made it a quite special journey.

One is made of experiences, not only the recent matter. I owe my fascination towards research to Dr. Ana Queiroz and Prof. Jorge Monteiro, the two figures who introduced me in the world of research and most of all believed in me. For that, I'll be for ever grateful.

I could not let my family and friends out, they are the scaffold of my life - they make every effort worth it. To all the kindness, believe and love that was to me provided, an endless thank you. *Mae, Pai, Mariana, Sergio, Tita, Zeca, Gaucho, Eric, Carolina, Mauri e Luis um grande sorriso, pois por voces eu sou a pessoa mais feliz e completa do Mundo ! Diana Leandro, Carlos Gomes, Joao Rola, Joao Torres, Liliana Reis, Luis Filipe Rodrigues, Victor Sousa, Ben Johnson, voces tambem sao familia, portanto o mesmo de aplica ehehe. Obrigado a todos. Thank you all.*

Table of contents

List of Figure

List of Tables

List of Equations

Abbreviations

ABD – Actin-binding domain

AFM - Atomic force microscopy

AJ – Adherens junctions

Akt – Protein kinase B

ATRP – Atom Transfer Radical Polymerisation

BM – Basement membrane

BPAG – Bullous pemphigoid antigen

CH – Calponin-homology

CP – Contact point

DAPI - 4,6-diamidino-2-phenylindole

DMEM - Dulbecco's modified Eagle media

DMAP – 4(dimethylamina) pyridine

DMPK – Dystrophia Myotonica-Protein Kinase

DMSO - Dimethyl sulfoxide

DN-KSH – Dominant-negative KASH

DSC – N,N' – disuccinimidyl carbonate

EDC – Epithelial differentiation complex

EBS – Epidermolysis bullosa simplex

ECM – Extracellular matrix

EDTA – Ethylenediaminetetraacetic acid

EGF – Epithelial growth factor

EMT – Epithelial-mesenchymal transition

ER – Endoplasmic reticulum

ERK1 – Extracellular signal-regulated kinases 1

ERK2 – Extracellular signal-regulated kinases 2

FA - Focal adhesion

FAK - Focal adhesion kinase

FBS – Fetal bovine serum

FFT – Fast fourier transform

FIB – Focused ion beam

G-actin – Globular actin

GFOGER – glycine-phenulalanine-hydroxyproline-glycine-glutamate-arginine

GFAP – Glial fibrillary acidic protein

GSTF – Gene-specific transcription factor

HB-EGF – Heparin-binding EGF

HD – Hemidesmosomes

HEPES – 2-[4-(2-hydroxyethyl)piperazin-1-yl]ethanesulfonic acid

HP1 – Heterchromatin protein 1

ICC – Immunocytochemistry

IF – Intermediate filaments

IHC – Immunohistochemistry

ILK –Integrin-linked kinase

INM – Inner nuclear membrane

IVL – Involucrin

JNK – c-Jun N-terminal kinases

KASH – Klarsicht, ANC-1, Syne Homology

KDM – Lysine methyltransferase

KMT – Lysine demethyltransferase

LAP – Lamin-assossiated protein

LBR – Lamin B receptor

LED – Light emitter diode

LINC – Linker of Nucleoskeleton and Cytoskeleton

LSCM – Laser scanning confocal microscopy

MAPK – Mitogen-activated phosphatase kinase

MCF7 – Michigan Cancer Foundation-7

MDCK – Madin-Darby canine kidney

MEF – Mouse embryonic fibroblasts

MKL1 – Megakaryoblastic leukemia 1 protein

MP – Mega pixel

MRTF – Myocardin-related transcription factors

MSC – Mesenchymal stem cell

MT – Microtubules

NE – Nuclear envelope

NPC – Nuclear pore complex

OKA – Okadaic acid

ONM – Outer nuclear membrane

PBS – Phosphate buffer saline

PDMS – Polydimethylsiloxane

PFA – Paraformaldehyde

pHK – primary human keratinocytes

PI3K – Phosphatidylinositol-3OH kinase

PIC – Pre-initiation complex

PKC – Protein kinase C

PML – Promyelocytic leukemia

POEGMA – Poly(oligo-ethane glycol)methyl acid

PP1 – Protein phosphatase 1

PP2 – Protein phosphatase 2

PRD – Plakin-repetitive domain

RA – Retinoic acid

RAR – Retinoic acid receptor

RMS – Root mean square

RNAPII – RNA Polymerase II

ROCK – Rho kinase

RT – Room temperature

SEM – Scannning Electron Microscopy / Standard error mean

SF – Shape factor

siRNA – Small-interfering RNA

SRF – Serum response factor

SUN – Sad1p and UNC-84 homology

TJ – Tight junction

UV – Ultraviolet

Chapter 1. Introduction

1.1 Introduction

The way eukaryotic cells sense the surrounding environment and respond accordingly is a fundamental question in current cell biology. The behaviour of tissues and cells in response to mechanical stimuli for long time has been the focus of many studies, yet the mechanistic basis of such events is poorly understood. Currently, it is known that mechanical forces lead to nuclear deformation (Maniotis et al. 1997), and that such forces are translated into genetic information. This adaptive behaviour is thought to depend upon cell shape, which dictates nuclear morphology via cytoskeleton remodelling, and consequently tuning gene expression. Few studies have mechanistically characterised the changes in nuclear morphology in response to cell shape, and none have investigated nuclear mechano-transduction in primary keratinocytes.

The cytoskeleton is composed by three major cytoskeletal protein families: microtubules, actin and intermediate filaments. They define cellular integrity and mechanics. Whether they are exclusively dedicated in transmitting forces to the nucleus and this way regulate its activity is still an open question. Actin, in particular, has been intensively studied for its involvement in cell growth, apoptosis, motility, and differentiation, among others. Also, its role in regulating cell-nucleus shape is reported for several cell types including endothelial, smooth muscle cells and fibroblasts. Nevertheless, intermediate filaments are also likely to be involved in nuclear morphology regulation, as it was shown recently for keratinocytes (Lee et al., 2012). In fact, actin and keratins (largest subset of proteins from intermediate filament family) are central determinants of skin barrier function and overall tissue homeostasis as they intervene in cell-cell

and cell-extracellular matrix contacts. Keratins form a complex and extremely resilient network throughout the cytoplasm of keratinocytes and contribute to cell mechanics. Other than providing physical integrity to the tissue, keratins are also involved in the regulation of proliferation and differentiation of keratinocytes. Mutations in keratins lead to several skin diseases, generally affecting the overall barrier function of the epidermis and mechanical integrity. One of the most common disease families caused by abnormal expression of keratins (e.g. K14 and K5) is epidermolysis bullosa simplex. The severity of these cases depends on the keratin sub-type affected and it may affect other tissues such as muscle and brain. Interestingly, mutations in plectin (plakin family of proteins) lead to similar symptoms. Cellular studies demonstrate that plectin regulates cytoskeleton architecture. Indeed, keratinocytes with mutant plectin display abnormal keratin architecture. The consequences of having an abnormal keratin network in nuclear mechano-transduction are still unknown and therefore addressed here.

The field of mechano-biology emerged from evidence showing that forces do convert into biochemical information. Deformations imposed upon the large and highly organised nucleus could regulate gene expression via a range of mechanisms, including chromatin remodelling. The conformation of chromatin is thought to define the accessibility of DNA to transcription machinery and is regulated epigenetically by covalent modification at histone residues. Throughout the epidermis, the nucleus undergoes several epigenetic changes, including the reduction of transcriptionally active genes and positioning of heterochromatin during terminal differentiation (Gdula et al., 2013). Using micro-patterning technology, we investigate these events in more detail, with particular

focus on how euchromatin and heterochromatin regions correlate with keratinocytes differentiation induced by the loss of substrate adhesions. The role of plectin in the regulation of nuclear mechanics and epigenetic modifications are also investigated.

Aims and objectives

The aim of the present work is to determine the role of the cytoskeleton in nuclear mechano-transduction in primary keratinocytes. The hypothesis underlying this study is that the both actin and keratin networks cooperate via plectin in transmitting forces towards the nucleus and therefore causing its deformation. The repercussions of such deformations were further investigated by the analysis of chromatin remodelling. In order to address this hypothesis, the following aims were investigated:

1. Examination of how cell shape regulates nuclear morphology and whether this is dependent on actomyosin contractility

2. Investigation of how plectin leads to abnormal keratin network and how this affects nuclear mechano-transduction in different environments

3. Analysis of chromatin remodelling in response to cell shape and the influence of plectin in this process

Chapter 2. Literature Review

2.1 The eukaryotic cell

The cell is the basic unit of all living organisms and is composed of several supramolecular structures, the organelles. The cellular membrane, a bilayer of phospholipids, serves as the physical barrier between the cytoplasm and the external environment. Within the cytoplasm, most of organelles are dispersed in a non-random fashion, each responsible for specific function(s). In this section, cellular structural-functional relationships will be explored with special focus on how the organisation and structure of subcellular structures (*i.e.* cytoskeleton and nucleus) regulate mechano-sensation of cells.

2.2 The cytoskeleton

Cells must be capable to re-arrange their internal components as they grow, move, divide and adapt to changing circumstances. These spatial and mechanical functions depend on the cytoskeleton, a system of biopolymers composed by filamentous entities. Generally, the cytoskeleton is responsible for cell motility, transport of nutrients, and the balancing of internal and external forces, (Cooper and Hausman, 2004). Actin filaments (F-actin), microtubules (MTs) and intermediate filaments (IFs) are the three major cytoskeleton proteins whose role in cellular integrity and tissue morphogenesis has been appreciated for decades now (Ingber et al., 1994, Wang and Ingber, 1994). Each filament system is built from a family of subunit proteins with cell-tissue specific expression. F-actin and MTs are well conserved amongst eukaryotic cells, with a homology of 90 and 75%, respectively (Bruce Alberts et al., 2015). Intermediate filaments are by far the most variable of the cytoskeletal proteins with at least 70 different IF proteins subcategorised into six broad subtypes

(Type I to VI) based on tissue-specific expression patterns, sequence similarity and protein structure (Chamcheu et al., 2011). All three cytoskeleton proteins interact with hundreds of accessory proteins that may regulate their dynamics, structure and the interaction with other components in the cell. In addition, cytoskeletal proteins may directly and/or indirectly interact with each other (e.g. F-actin with MTs). Each of the cytoskeleton protein families forms filamentous structures with distinct architecture, function and mechanics. As the aim of the current study is focused on scrutinising the role of cytoskeletal proteins in nuclear mechano-transduction of keratinocytes, only actin and keratins are approached here in detail. Recent studies have identified these structures as their main mechanical determinants (Ramms et al., 2013, Seltmann et al., 2013a) and are therefore postulated to regulate the varying nuclear morphology throughout epidermis (Lee et al., 2012, Gdula et al., 2013).

2.2.1 Actin

Actin is the most abundant intracellular protein in a eukaryotic cell (Lodish H. et al., 2000) and it regulates several cellular processes such as motility and apoptosis. In vertebrates, there are 3 isoforms of actin: α-, β- and γ-actin. α-actin is expressed only in muscle cells, while the other two are widely expressed in non-muscle cells. Globular actin (G-actin) monomers assemble head-to-tail to form an 8nm wide right-handed helix of filamentous actin (F-actin). Filaments are polar and have structurally different ends: the fast-growing end, called the “barbed end”, and the slow-growing end, designated as the “pointed end”. As G-actin is energetically stable, the formation of F-actin requires the assembly of monomeric G-actin into an initial aggregate (the nucleus), which is stabilised by multiple monomer-monomer contacts and can

then elongate rapidly by addition of more monomeric subunits. Several actin-binding proteins mediate the dynamics of actin polymerisation and organisation through spatial and temporal control of monomer availability for filament nucleation, elongation and depolymerisation. The dynamics of actin in different subcellular locations is thought to be dependent on the balance between stabilising and destabilising accessory proteins.

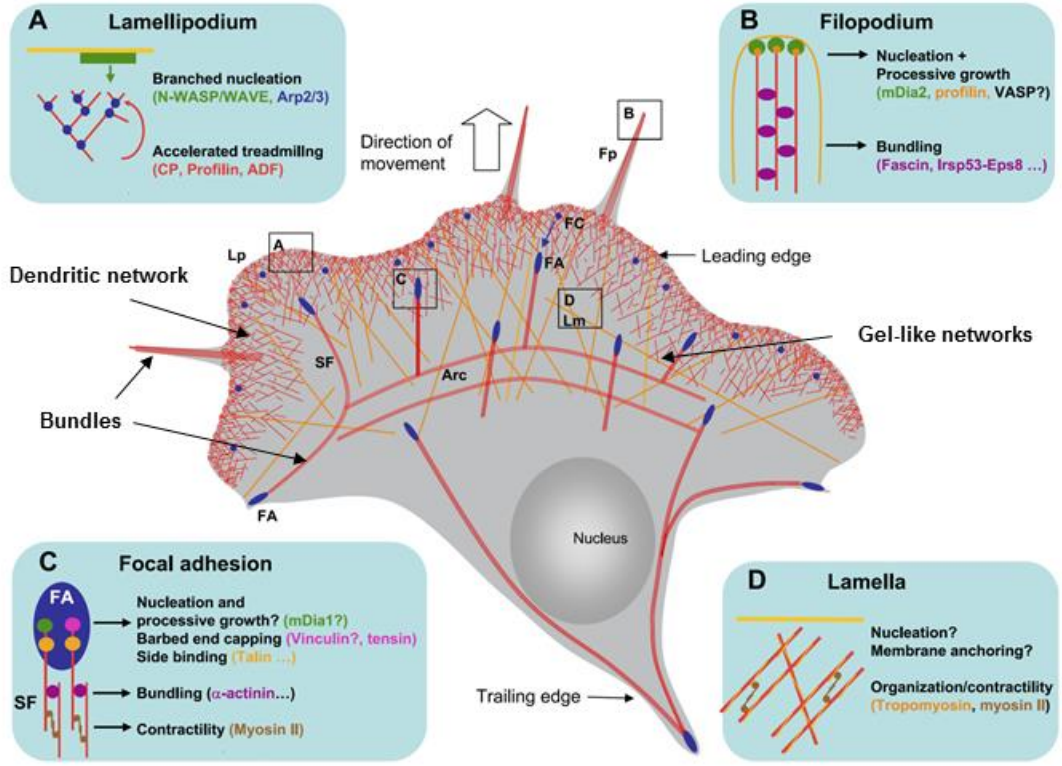

Figure 2.1 - Schematic illustration of the actin cytoskeleton in a migrating cell.

This schematic cell contains the major structures found in migrating cells but does not correspond to a precise cell type. (Addapted from Le Clainche and Carlier, 2008)

Motile cells extend a flat leading edge rich in actin filaments, called the lamella (Ponti et al., 2004). Here, the different architectures into which actin filaments may organise are found: branched, bundles and gel-like (Figure 2.1). At the leading edge, actin forms a dense and heavily cross-linked network, the lamellipodia. At this site, the predominant protein complex Arp2/3 is responsible for nucleation and consequent branching actin filaments. Arp2/3 activity is shown to generate forces and hence facilitating cell crawling (Bernheim-Groswasser et al., 2002, Boukellal et al., 2004, Cameron et al., 1999, Loisel et al., 1999, Noireaux et al., 2000). Branching elongation is limited by capping proteins and thought to be important for force production and therefore motility (Achard et al., 2010, Akin and Mullins, 2008, Dayel et al., 2009, Kawska et al., 2012, Vignjevic et al., 2006, Vignjevic et al., 2003). Other than branched networks, actin filaments are cross-linked together by various other proteins in order to control cell shape and mechanics. The spacing between cross-linked filaments is essential for the architecture of resulting network. Cross-linkers that impose small cross-linking distances pack the filaments into bundles, which may be oriented in a parallel, anti-parallel, or mixed polarity fashion depending on the cross-linker (Lieleg et al., 2009, Skau et al., 2011). In contrast, larger cross-linkers, such as filamin or α-actinin, are present in either bundles or networks depending on their concentration (Courson and Rock, 2010, Kasza et al., 2010, Meyer and Aebi, 1990, Schmoller et al., 2008, Wachsstock et al., 1993, Wachsstock et al., 1994). In addition, the rate of assembly is another important factor for the accessibility of cross-linkers as it was investigated for the case of α-actinin: increased actin polymerisation rate resulted in the formation of bundles and therefore limited motility (Falzone et al., 2012).

The spatial organisation of F-actin is complex and depends on actin-associated proteins. Also at the lamella, actin bundles organise into transverse arcs, ventral stress fibres and dorsal stress fibres (Figure 2.1). Importantly, a thin layer of actin, called the cell cortex or cortical actin, coats the plasma membrane at the back and sides of the cell, vital for cell shape maintenance (Blanchoin et al., 2014). In turn, it is believed that mechanical cues feed-back to control the biochemical activity of actin filaments and actin-binding proteins (Blanchoin et al., 2014).

Motor proteins are specific actin-associated proteins crucial in cell mechanics. Motor proteins, such as non-muscle myosin (myosin II), are associated with cell contractility, which is important for cell shape maintenance and F-actin architecture. Also, myosins regulate signalling pathways by altering the configurations and therefore activity of e.g. enzymes and receptors (Blanchoin et al., 2014, Burnette et al., 2014, Vogel and Sheetz, 2006). ATP-dependent movement of myosin II along anti-parallel F-actin (Sheetz and Spudich, 1983) leads to the generation of tension by sliding two anti-parallel filaments. In crawling cells, myosin II is preferentially enriched in transversal arcs (Figure 2.1), which recently was shown to regulate cell shape (Burnette et al., 2014).

Actin interacts with a plethora of other molecules (Pollard and Cooper, 1986). The direct or indirect binding of F-actin to focal adhesion complexes and intercellular junctions is central in tissue morphogenesis, mechanical integrity and homeostasis. Cells adhere to extracellular components via a cluster of different proteins designated as focal adhesions, which assemble in an actin-dependent in fashion. Here, several intracellular proteins e.g. talin, paxillin and

vinculin bind to a cluster of transmembrane ECM receptors – the integrins. These form heterodimeric structures that interact non-covalently with specific compound(s) of surrounding substratum (Hynes, 2002). As will be covered in more detail further in section 2.3, F-actin binds to FAs via vinculin and Kindlin-1 and potentially to the nucleus via LINC-complex proteins. This integration is thought to have major implications in cell sensing and mechanics. Importantly, increasing evidence suggests that F-actin and other cytoskeletal proteins team up in the regulation of nuclear mechano-transduction (Huber et al., 2015).

Table 2.1. – Acting-binding proteins and their function.

Actin-binding protein	Function
Arp 2/3	Nucleation - Branched actin
Formins	Nucleation - Unbranched actin
Profilin	Elongation enhancer
Thymosin	Elongation blocker
Tropomodulin	Capping (pointed end)
CapZ	Capping (barbed end)
Cofilin	Destabiliser
Tropomyosin	Stabiliser; Promotes contractility
α-actinin	Cross-linker
Fimbrin	Cross-linker

2.2.2 Intermediate Filaments

Intermediate filaments are only present in some metazoans (including vertebrates, nematodes, and mollusks), in particular in cells that are subjected to mechanical stress (Bruce Alberts et al., 2015). Intermediate filaments are encoded in the human genome by 70 different genes in six subfamilies (Table 2.2). This large multigene family is associated with 99 discrete clinical disorders, a number that is growing as the new clinical cases emerge (Szeverenyi et al., 2008). Unlike F-actin and MTs, IF assembly is energetically favourable and quick: the formation of unit-length filament (Figure 2.2) occurs in seconds (Brennich et al., 2011).

In epithelial cells, keratins (or cytokeratins) are the most abundantly expressed IFs (Fuchs, 1995). Twenty-eight type I and 26 type II keratins encode the biggest family of IFs. The 10-nm keratin bundles are heteropolymers, with type I and type II proteins occurring in a 1:1 molar ratio. This requirement explains the coordinated transcription of at least one of each of the two subtypes of keratin genes in epithelial cells (Pan et al., 2013). Each keratin pair is characteristic of a particular epithelial differentiation programme; some epithelial cells express more than one pair. A single epithelial cell may express several types of keratins, which forms a unique copolymerised network.

IFs are dispersed throughout the cytoplasm in a non-random fashion. They interact with major structural determinants in the cell, including F-actin and MTs, membrane adhesion both at cell-cell and cell-ECM contacts (Fuchs and Green, 1980, Jefferson et al., 2004, Svitkina et al., 1996). In contrast with actin, few

Table 2.2 – Intermediate filament families, designation and expression in human cells (Based on Szeverenyi et al., 2008)

Type	Designation	Expressing cell types / Subcellular location
I and II	Keratins	Epithelial cells, tumour cells
III	Desmin	Muscle cells
	Vimentin	Fibroblasts, lymphocytes, endothelial
	Peripherin	peripheral neurons
	Syncoilin	Skeletal muscle cells
	Glial Fibrillary Acidic Protein (GFAP)	Astrocytes and Glial cells
IV	α-internexin	Nerve cells
	NF-H	Nerve cells
	NF-L	Nerve cells
	NF-M	Nerve cells
	Nestin	Nerve cells
	Synemin α	Muscle cells
	Synemin β	Muscle cells
V	Lamin A	Differentiated cells (nucleus)
	Lamin B1	Ubiquitous (nucleus)
	Lamin B2	Ubiquitous (nucleus)
	Lamin C1	Differentiated cells (nucleus)
	Lamin C2	Differentiated cells (nucleus)
VI	Phakinin (CP49 or BFSP2)	Eye lens fibres
	Filensin (CP115 or BFSP1)	Eye lens fibres

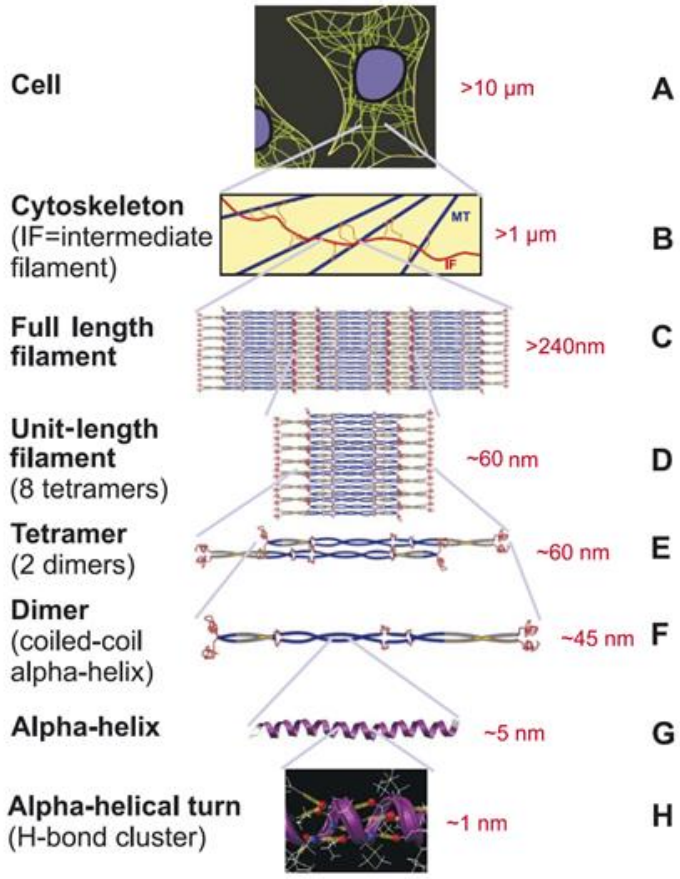

Figure 2.2 – The hierarchical structure of the intermediate filament, from atomic to cellular scale.

A) Schematic representation of IF cytoskeleton within a cell; (B) Schematic representation of IF filament interlaced with MTs; C) Full-length IF filament at molecular level; D) Unit-length filament composed by eight tetramers; E) Tetramer composed by two coiled-coil dimer; F) Representation of coiled-coil dimer formation; G) Molecular structure of α-helix IF monomer; (H) Molecular structure over H-bond cluster within α-helix IF monomer. (Qin et al., 2010)

studies have examined the architecture of IFs within the cell. Both keratins and vimentin form a dense cage around the nucleus, unfolding in cross-linked network of bundles. The network may be presented as an “alveolar-like” web throughout the cytoplasm and apical to the nucleus, ending as a thick wave-like

structure at the periphery of the cell (Figure 2.3). A rectilinear pattern “zip-like” is formed at cell-cell contacts at desmosomes (Portet et al., 1999). How the architecture of IFs contributes for cell mechanics is still unclear. Dedicated

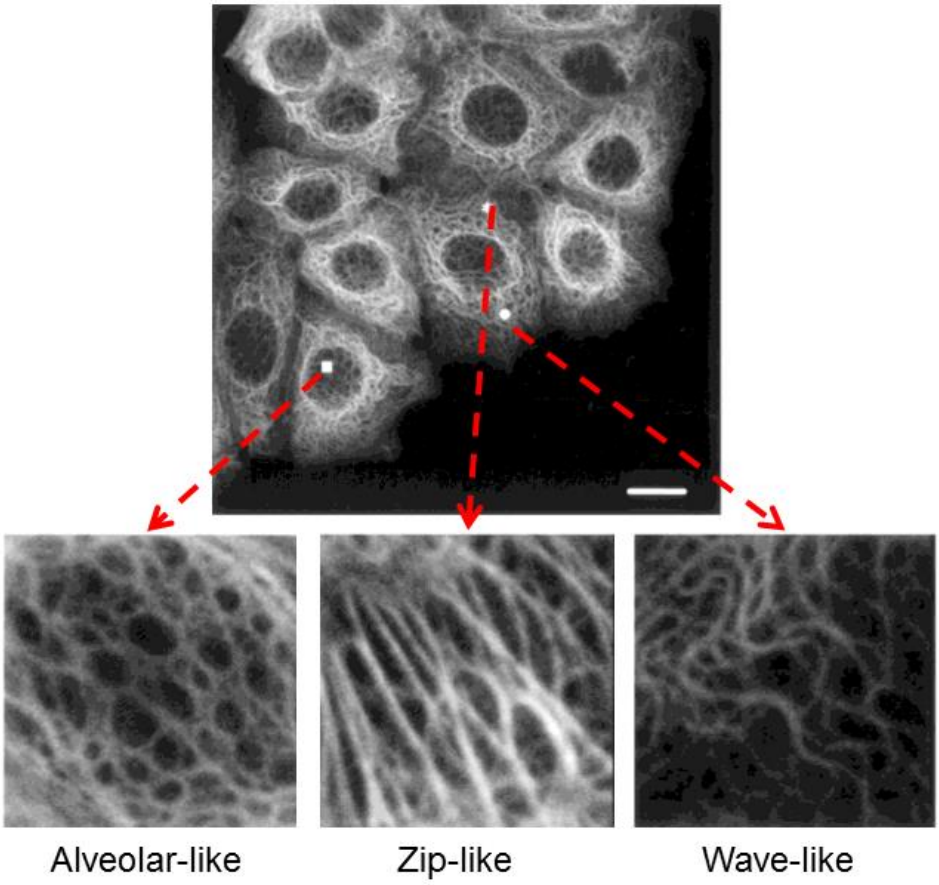

Figure 2.3 – Representative images of keratin network organisation proposed by Portet et al. (1999).

Immuno-fluorescent image of MCF7 cells, labelled against K8. (adapt. from Portet et al. 1999). Three distinct patterns were proposed, exemplified in the lower set of zoomed-in images. According with the Portet and co-workers, alveolar-like pattern is preferentially seen on top of the nucleus; zip-like patern at cell-cell contacts; and wave-like pattern at the periphery of the cell. Scale bar 10µm.

studies addressing the relationship between the structure and function of keratins might bring new insights into the role of these complex networks in living cells. Intermediate filaments have tissue specific functions. In epithelial cells, keratins have two fundamental roles: 1) provide structural and mechanical support and 2) regulate metabolic processes and pathways governing growth, proliferation, migration and apoptosis (Kim and Coulombe, 2007). In addition, keratins play a protective role against toxins of foreign entities and stress: K8 and K18 are instrumental in the ability of liver hepatocytes to cope with a broad variety of metabolic, oxidative and chemical stresses (Ku et al., 2007, Zhou et al., 2005, Toivola et al., 2004). The adaptation to stresses is mediated by glycosylation of K18, which positively regulates the activity of pro- survival Akt and PKC kinases, thereby protecting cells against apoptosis (Ku et al., 2010). Emerging evidence show that keratins are also involved in other cellular processes, for instance in embryonic development and epithelial cell mechano-transduction (Goldman et al., 2012, Pan et al., 2013).

Keratin networks consist of a perpetual cycle of assembly-disassembly as suggested by Leube and co-workers (Windoffer et al., 2011, Leube et al., 2011, Kolsch et al., 2010). Nucleation of keratins takes place at the cell periphery, followed by elongation through the addition of soluble oligomeric units, (Windoffer et al., 2006, Woll et al., 2005, Windoffer et al., 2004). Integration and bundling of keratin filaments follow as they move towards the nucleus, followed by either maturation (formation of stable keratin cage around the nucleus) or its disassembly. In addition, keratins do exist in a soluble oligomeric form throughout the cytoplasm, showing that active transport machinery is not necessary to deliver mobile keratins to cell’s periphery (Kolsch et al., 2010).

Insights into the dynamics and architecture of keratin may be investigated using live fluorescent microscopy (e.g. as published recently in Moch et al., 2013, Portet et al., 2015). Recently, the inward movement of keratin from cell periphery towards the nucleus was characterised, which interestingly was accelerated by EGF levels and decreased when cells establish adhesions (Moch et al., 2013). This shows that cell-ECM contacts do play a central role in dictating keratins dynamic, and further studies applying live-cell imaging technology will help scrutinizing the role of keratins in cell mechanics and behaviour.

2.2.3 Cytoskeleton mechanics

The cytoskeleton is the main structural determinant in animal eukaryotic cells, yet its mechanical properties are still not fully understood, in big part because of its complex architecture and dynamic nature. A plethora of different techniques are available to probe the mechanical properties of the cytoskeleton (Van Vliet et al., 2003), including magnetic tweezers, atomic force microscopy (AFM), substrate strain testing, parallel plate compression, micro-needle, ballistic rheology, among others. These techniques allow the *in situ* testing of different compartments of the cell, each with specific advantages and also limitations. Common to all, the dissociation of the individual contributions of particular cytoskeletal structure is a challenge. Alternatively, *in vitro* experiments analysing the mechanics of purified cytoskeleton proteins in solutions are performed. In polymer physics, repetitive macromolecular structures are distinguished in three differing stiffness regimes: flexible, semi-flexible, and stiff. Stiffness of the chain can be determined by the ratio between the persistent length (l_p) of the filament and the contour length (l_c). At non-zero temperature,

a polymer filament is subjected to thermal fluctuations, and the resistance against these fluctuations are characterised by tangent vectors $\vec{t}$ to each point throughout its contour s ($\langle \vec{\boldsymbol{t}}(\boldsymbol{s}).\vec{\boldsymbol{t}}(\boldsymbol{s'})\rangle = \boldsymbol{e}^{-|s-s'|/l_p}$ Equation 2.1).

$$\langle \vec{\boldsymbol{t}}(\boldsymbol{s}).\vec{\boldsymbol{t}}(\boldsymbol{s'})\rangle = \boldsymbol{e}^{-|s-s'|/l_p} \qquad \textbf{Equation 2.1}$$

The correlation of tangent vectors along the polymer contour decay exponentially with the persistence length l_p (Figure 2.4). The persistence length is then defined as the length along a filament over which its direction (i.e. longitudinal tangent) becomes nearly uncorrelated (Li et al., 2010). This measurable quantity may also be determined as in $\boldsymbol{l_p} = \frac{\boldsymbol{B}}{\boldsymbol{kT}}$ Equation 2.2.

$$\boldsymbol{l_p} = \frac{\boldsymbol{B}}{\boldsymbol{kT}} \qquad \textbf{Equation 2.2}$$

where B defined the bending modulus of the filament and kT the thermal energy (i.e. k is the Boltzmann constant, $1.38 \times 10^{-16}\, erg.K^{-1}$). Therefore, one can simply determine the stiffness of macromolecular chains by examining a biopolymer's bending fluctuations in a microscope (MacKintosh, 2006). When $l_p \gg l_c$, filaments are stiff resembling marginal transverse thermal undulations, although being still able to move in solution as rigid rods driven by thermal energy. In contrast, filaments are considered flexible when $l_c \gg l_p$ – thermal fluctuations lead to large transverse fluctuations. Semi-flexible filaments lie between these two limits, l_p and l_c are of the same order of magnitude. Interestingly, the three types of cytoskeleton filaments fall distinctly into these three stiffness regimes (Figure 2.4).

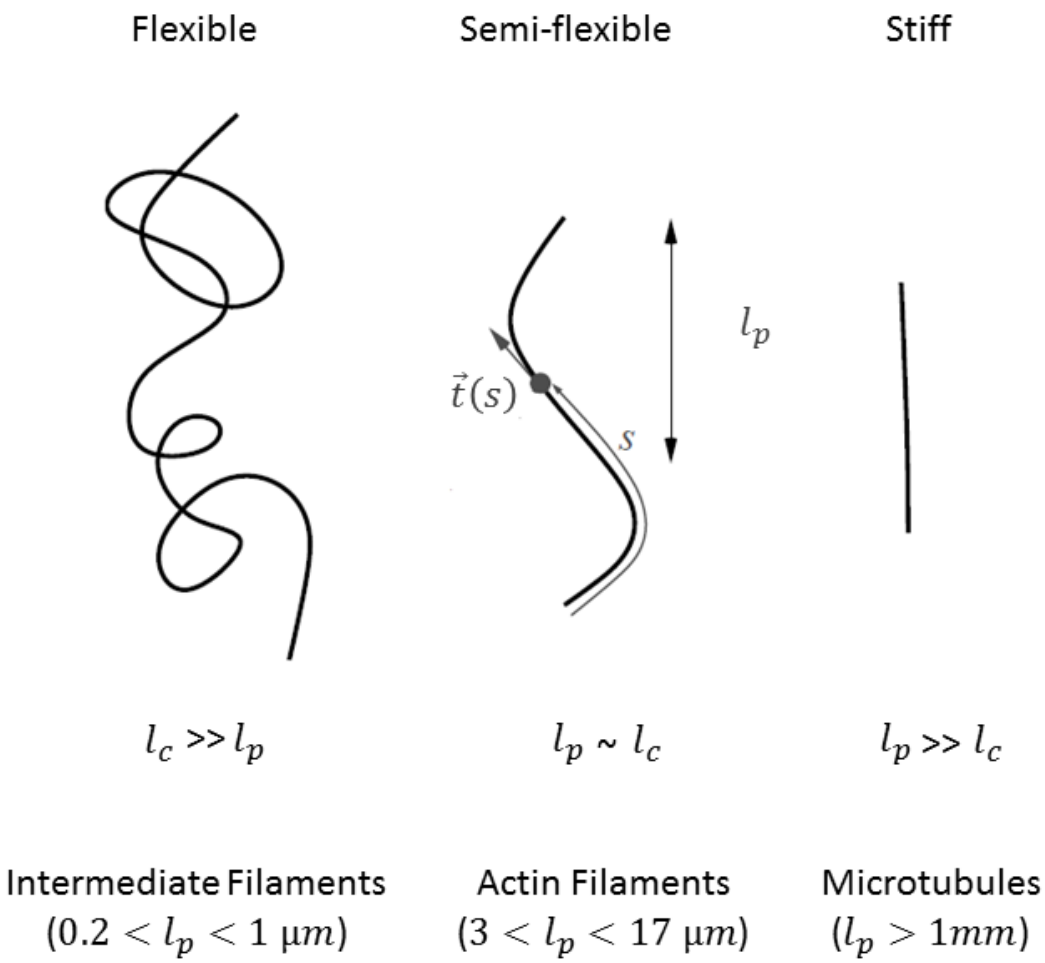

Figure 2.4 – Polymeric network stiffness and how cytoskeleton filaments fall into each category.

Network mechanics is defined by the ratio between l_p and l_c. Tangent vector over filament position s and respective persistent length l_p are represented in semi-flexible illustrative cartoon. Each cytoskeleton protein falls into distinct stiffness ranges: IFs < F-actin < MTs. (Addap. Liverpool, 2006)

IFs are the softest family of cytoskeleton proteins, followed by F-actin and then MTs. Importantly, in comparison with F-actin and MTs, IFs possess superior resiliency, which reflect the total energy absorbed by a material within the elastic regime (Janmey et al., 1998, Janmey et al., 1991). This explains why IFs such as vimentin, keratins and desmin, provide mechanical strength and

resiliency to cells (Wang et al., 1993, Fudge et al., 2008, Mendez et al., 2014, Beriault et al., 2012). Under stretching, keratins do provide resiliency to cells in monolayers, allowing them to stretch more than 100% without compromising cell viability (Fudge et al., 2008). In another study, an exceptional ability of these networks to withstand large tensile deformations was observed: a stretch of 3.6-fold of its original length was recorded for desmin filaments adsorbed in mica surface (Kreplak et al., 2005). For this reason, some authors consider the IF cytoskeleton to function as cellular “security belts” (Qin et al., 2010, Kreplak et al., 2008, Kreplak et al., 2005). Indeed, coarse-grained simulations corroborate the hypothesis that IFs dominate the mechanical response of cells to large mechanical stresses (Bertaud et al., 2010).

The three different cytoskeletal structures comprise an extremely complex network, which cross-interact with each other. The study of these systems independently, although fundamental for basic insights into individual properties and function, may be incomplete. The presence of elastic filamentous background around MT (provided by both F-actin and IF) enhance its resistance to buckling over 100-fold, and actin strain-stiffening is favoured by the presence of MT (Brangwynne et al., 2006, Das et al., 2008, Bai et al., 2011). This shows that the overall mechanical behaviour of the cytoskeleton is not a mere sum of the individual properties of its counterparts. Furthermore, the interpenetration and steric interactions among the three cytoskeletal protein networks, plus cytoskeleton-associating proteins such as motors and cross-linkers are likely to positively influence the overall mechanics of the cell (Wiche et al., 2015, Huber et al., 2015). The analysis of individual cytoskeleton structures in response to mechanical cues is therefore incomplete. As the aim of the present work is to

study in more detail how F-actin and keratin network cooperate for nuclear mechano-transduction, MTs will not be covered in detail.

2.3 Physical linkages: cell-ECM adhesions, cell-cell junctions and the nucleus

The cytoskeleton integrates and regulates several organelles within the cell in a tissue-specific way. The link between cell-ECM adhesions and cell-cell junctions to the nucleus is of particular interest in mechano-transduction and therefore cell's ability to sense the environment (Fletcher and Mullins, 2010).

2.3.1 Cell-ECM adhesions

Adherent cells establish focal contacts with the exterior substratum via ECM receptors: the integrins. These are heterodimeric transmembrane receptors, consisting of an α and a β subunit, which integrate the extracellular matrix with the interior of the cell by interacting with the cytoskeleton (Hynes, 2002). Focal adhesions (FAs) and hemidesmosomes (HDs) are the two main integrin-based types of adhesions found in adherent cells, which connect with the F-actin and intermediate filaments, respectively (Figure 2.5). FAs and HDs appear to have distinct functions: FAs are associated with both mechanical and cell signalling as they are able to trigger several pathways (e.g. MAPK and EGF); whereas HDs are thought to stabilise and strengthen cellular adhesion to the underlying ECM. These pathways are key regulators of cell function and mechano-sensitivity as will be explored in more detail later in section 2.4.3 (page 39).

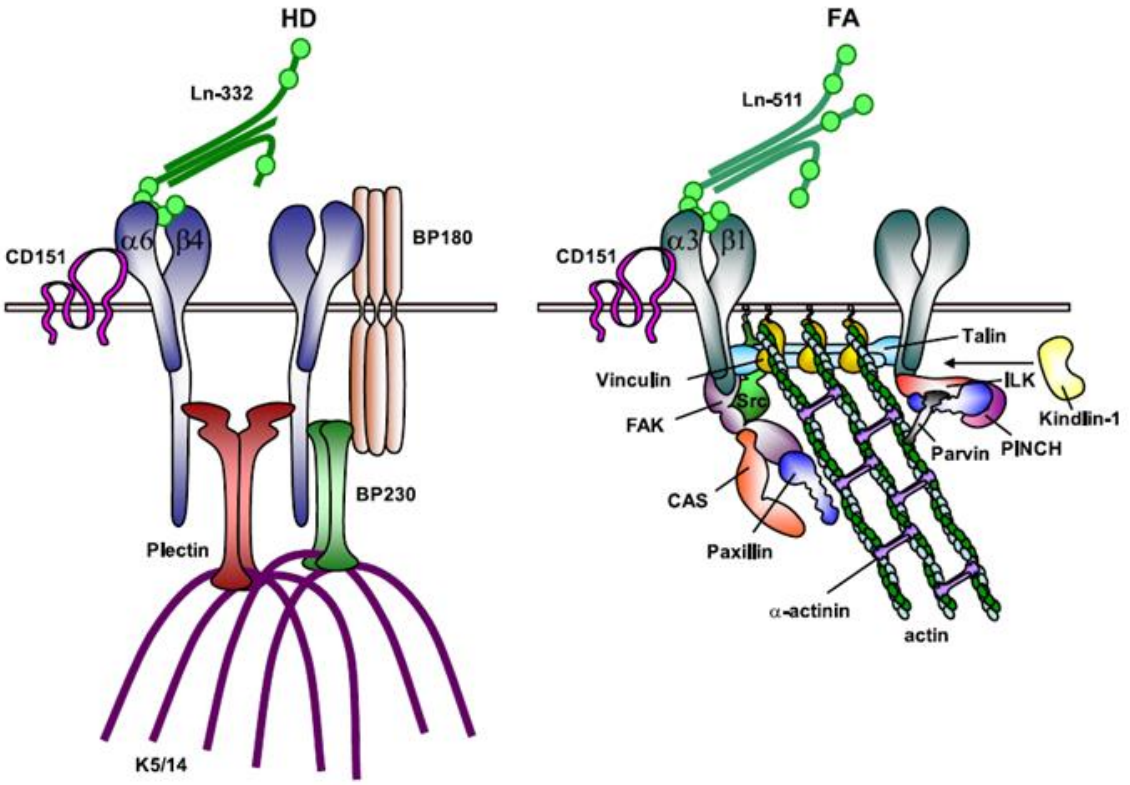

Figure 2.5 – Molecular composition of hemidesmosomes (HDs) and focal adhesions (FAs) (Margadant et al., 2010).

In humans, there are 24 combinations of integrin heterodimers, which define ligand specificity. Integrins are not constitutively active (Hynes, 2002). The ligand-binding activity is determined by their molecular conformation, which is regulated by other molecules such as talin and kindlin (Patil et al., 1999, Shi et al., 2007). Integrins are classically associated with major processes such as cell adhesion and motility, and for that reason implicated in metastatic potential in tumour cells and cancer. They get internalised into endosomal compartments and recycled back to the plasma membrane, hence completing an endo-exocytic cycle (Jones et al., 2006, Rappoport and Simon, 2003). Interestingly, new evidence shows that this endocytosis process is intensified by a shortage

of nutrients, which in turn facilitates cell motility in cancer cells (Rainero et al., 2015). This shows that the metastatic potential of these cells may be enhanced by shortage of nutrients supply.

The signalling properties and functions of integrins are executed by specialised adhesive structures with particular morphology, subcellular localisation, life-time and composition. Nascent focal adhesions are short-lived adhesive structures in membrane protrusions (Choi et al., 2008) that promote the activity of Rho-GTPases such as Rac1. These nascent adhesions may develop into large focal adhesions that initiate multiple signalling pathways, which activate effectors including myosin II. This motor protein exerts contractile forces resulting in adhesion reinforcement and recruitment of more proteins to focal adhesions, which induces a further increase in myosin II activity (Geiger et al., 2009). This feedback signalling to myosin II critically depends on biophysical parameters such as ECM stiffness. In fibroblasts, α5β1 integrins are important in force generation, whereas αv-class integrins mediate the structural adaptations to forces (Schiller et al., 2013). The combination of α_v-class integrin-mediated structure (FA anchoring and stress-fibres formation) with the $\alpha_5\beta_1$-mediated force generation (myosin II – dependent) constitutes a synergistic system, which is important for mechano-sensing (Schiller et al., 2013).

Integrins also provide linkage between the ECM and the keratin cytoskeleton via hemidesmosomes, forming dense adhesive plaques at the basal surface of epithelial cells. These constitute a firm anchorage between the basement membrane and epithelial cells, important for the mechanical integrity of the epithelium. Currently, HDs may be grouped into two distinct types (Walko et al.,

2015): classical type I HDs, constituted integrin α6β4, plectin isoform 1a (P1a), tetraspanin CD151, bullous pemphigoid antigen (BPAG)1 isoform e (BPAG1e, also called BP230) and BPAG2 (also called BP180 or type XVII collagen) (Owaribe et al., 1990); and the type II HDs, formed by integrin α6β4 and plectin and lack the two BP antigens (Fontao et al., 1999, Uematsu et al., 1994). Type I HDs are found in stratified and pseudo-stratified epithelia, for example in the epidermis, whereas type II HDs are found in simple epithelia such as that of the intestine (Walko et al., 2015).

2.3.2 Cell-cell junctions

In mammals, there are four types of cell-cell junctions: adherens junctions (AJ), tight junctions (TJ), desmosomes and gap junctions. Similarly to cell-ECM adhesions, these are other types of transmembrane complexes. AJs and desmosomes connect to the cytoskeleton, F-actin and IFs, respectively (Green et al., 2010). These two subtypes of cell-cell junctions belong to the large cadherin family of calcium-dependent adhesion molecules, which are expressed in a variety of different tissues. The extracellular domains of classical cadherins associate via cis- (between molecules of the same cell) and trans- (between molecules of opposing cells) interactions in the intercellular space, and the cytoplasmic tails bind to the adaptor proteins of the catenin family (e.g. β-catenin, p120-catenin and α-catenin). Members of the catenin family perform various functions, such as stabilisation of cadherins, organisation of the F-actin and are involved in intracellular signalling pathways that control gene transcription (Rudini and Dejana, 2008). Both p120-catenin and β-catenin interact with the cytoplasmic tail of E-cadherin and are thought to stabilise E-cadherin at the plasma membrane (Kourtidis et al., 2013). β-catenin links E-

cadherin to α-catenin, which in turn interacts with F-actin and therefore regulates its architecture (Green et al., 2010, Cucci et al., 2000). The re-arrangement of F-actin is a key step for the subsequent formation of tight junctions and desmosomes. Formation of intermediate filament attachments follows via plaque proteins desmoplakin, which stabilises the desmosomes (Green et al., 2010).

Cell-cell junctions are essential for tissue morphogenesis and homeostasis. In drosophila, epithelial morphogenesis involves the folding and invagination of cell sheets, a process orchestrated by actomyosin contractility and AJs (Blanchard et al., 2009, Martin et al., 2010). Also, forces exerted at tissue level are able to influence cellular processes such as mitosis. Interphase Madin-Darby canine kidney II cell line (MDCK), a model of epithelial cells, did elongate in the direction of the stretch in order to facilitate stress relaxation and restoring cell packing. This is thought to counter balance long-term external forces applied to the tissue, which proves a tissue-level mechanical homeostasis (Wyatt et al., 2015). In skin, these structures are key for the barrier function and wound healing (Green et al., 2010) (section 2.5, page 42). Forces are, therefore, central in maintaining tissue function by regulating cellular processes.

An elegant and novel micro-tensile testing method to probe the mechanics of cellular sheets was recently introduced (Harris et al., 2013, Harris et al., 2014, Moeendarbary et al., 2013, Terry et al., 2012), consisting in a monolayer of cells suspended by two rods, one static and the other one controlled by a manipulator. Using this apparatus, the contribution of subcellular structures to the tissue-level mechanics may be investigated without the introduction of

artefacts arising from ECM or other substrates. In MDCK, F-actin contributes significantly to the elastic modulus of the tissue, whereas intercellular junctions define both tissue's strength (Harris et al., 2012). Contrary to adherens junctions, desmosomes appear to be redundant in the generation of tissue tension at the formation of cell monolayers and therefore tissue's apparent stiffness (Harris et al., 2014). Instead, desmosomes appear to govern the maximal deformation a tissue can withstand before failure.

2.3.3 The nucleus

Focal adhesions generate forces via the cytoskeleton towards the nucleus. Importantly, the cytoskeleton may bind to the nucleus. The nucleus itself is extremely complex in terms of structure, function and its composition. Its core is delimited by a double phospholipid bilayer: the outer nuclear membrane (ONM) and is the inner nuclear membrane (INM). ONM and INM join together at the nuclear pore complexes (NPCs), which are protein-complex gates that allow nuclear-cytoplasm transport of molecules and ions. The ONM is continuous with the endoplasmic reticulum. Across the nuclear membrane, the LINC complex of proteins bridges the cytoskeleton to nuclear lamina. Part of this complex, Nesprins 1 and 2 comprise an actin binding domain, the calponin-homology domain (CH) at the N-terminus, whereas the C-terminal KASH domain that traverses the outer nuclear membrane interacts with the C-termini of SUN proteins in the inter-membrane space (Zhen et al., 2002, Crisp et al., 2006, Sosa et al., 2012). Nesprin-3 binds to IF via plectin, whereas MTs interact with nesprin-4 through kinesin-1-binding protein (Postel et al., 2011, Roux et al., 2009, Wilhelmsen, 2005). SUN proteins and emerin are other members of

LINC-complex, which internally bind to the chromatin and other associated proteins via lamina.

The nuclear lamina forms a meshwork of ~10nm filaments (IF family) which gives the nucleus its shape and stiffness. Nuclear lamina in somatic cells is expressed in four isoforms (lamin A, B1, B2, C1). Lamin A/C is associated with mature differentiated cells, and lamin B1 and -B2 are constitutively expressed (Szeverenyi et al., 2008). Absence of lamina A/C softens the nucleus and leads to an irregular shape (e.g. invaginations and discontinuous nuclear envelope), whereas its overexpression results in a stiffer nucleus (Broers et al., 2004, Fidzianska et al., 1998, Lammerding et al., 2004, Sullivan et al., 1999, Swift et al., 2013). Lamin B1 and B2 are determinants of nuclear visco-elasticity (Lammerding et al., 2006, Pajerowski et al., 2007, Patwari et al., 2009, Swift et al., 2013). Lamin-associated proteins (LAPs) link to specific sites of chromatin forming a tether shown to cause gene silencing and physically connect the lamina to the INM (Tripathi and Prasanth, 2011).

The most abundant sub-nuclear component is the chromatin. Chromatin comprises long double stranded molecules of DNA wrapped around small globular proteins designated as histones. These are arginine and lysine rich, which are amino acids that bind to the negatively charged DNA molecules. There are five major types of histones (i.e. H1, H2A, H2B, H3, and H4), which assemble in three-dimensional complexes called nucleosomes. Compaction of nucleosome fibrils ultimately forms the chromosomes, as exemplified in Figure 2.6. The mass of chromatin becomes highly condensed during mitosis to form the compact metaphase chromosomes, 10,000- to 20,000-fold compacted.

During interphase, the condensed form of chromatin (heterochromatin) localises at the periphery of the nucleus, whereas the de-condensed and transcriptionally active form (euchromatin) remains dispersed within the nucleoplasm. Furthermore, there are two types of heterochromatin: the constitutive heterochromatin, which contains DNA sequences inherently not transcribed (e.g. satellite sequences present at the centromeres); and the facultative heterochromatin, which is silenced due to regulatory mechanisms, possibly reversible (Cooper and Hausman, 2004).

Interphase chromatin appears to be uniformly distributed, although the chromosomes are actually arranged in an organised fashion and divided into discrete functional domains. The non-random distribution of chromatin within the interphase nucleus was first suggested in 1885 by Rabl (Rabl, 1885) which introduced the relict telophase arrangement, organisation which is maintained throughout the interphase until the next prophase as shown subsequently (Comings, 1980, Avivi and Feldman, 1980). Individual chromosomes also occupy distinct territories within the nucleus of mammalian cells. The pioneer Thomas Cremer and co-workers first proposed the now well accepted model in which chromosomes occupy particular compartments within the nucleus, designated as chromosome territories (CT) (Cremer et al., 1982). These are spatially separated by inter-chromosomal domains where DNA transcription takes place (Cremer and Cremer, 2010). The functional repercussions of such spatial organisation within mammals remain unclear.

The rules that define or encode the principles of chromatin organisation have been extremely difficult to decipher in detail (van Holde and Zlatanova, 1995,

van Holde and Zlatanova, 2007). Isolated chromatin fibres were measured to be ~30nm in diameter in its early stage of compaction (Woodcock and Ghosh, 2010), however the arrangement of nucleosomes and linker DNA within this 30nm fibres have been difficult to study and remains controversial. Applying the concept of primary and secondary structures used for proteins, chromatin is thought to assemble in a bead-on-a-string fashion, ultimate forming a secondary structure of a fibre (Woodcock and Dimitrov, 2001). Such a model explains the rationale that the compaction of chromatin fibres is defined by steric interactions between the histones (the beads).

The accessibility of the DNA would be then defined by the distance between the histones. Currently, this is thought to occur via post-translational modifications (PTMs) of histone proteins at their N-terminal unstructured tails. Examples of such modifications are acetylation, methylation, ADP ribosylation, phosphorylation, SUMOylation and ubiquitination. Histone acetylation is associated with gene activation and, therefore, transcriptionally active genes. In contrast, methylation on a specific lysine (K) residue is correlated with either an active or a silent state of gene expression, depending on the residues being methylated. Moreover, each methylated lysine residue can exist in a mono-, di-, or tri-methylated state, further extending the indexing potential of this modification. In general, methylation on histone H3 lysine 4 (H3K4), 36 (H3K36), and 79 (H3K79) is linked to active gene expression (Krogan et al., 2002, Santos-Rosa et al., 2002), whereas di- and trimethylation on H3K9, H3K27, and H4K20 are associated with gene silencing and therefore used as heterochromatin markers (Cao et al., 2002, Johnson et al., 2002, Rice et al., 2003, Schotta et al., 2004). Nevertheless, histone lysine methylation modulates

other chromatin-related processes such as replication, recombination, and DNA repair. The enzymes that add or remove the methylation mark on lysine residues are named lysine methyltransferases (KMTs) and lysine demethylases (KDMs), respectively, for their broad or potentially broad spectra of protein substrates (Allis et al., 2007).

Gene expression occurs inside the nucleus and depends on the accessibility of DNA transcription machinery. Because of its organisation and dynamics, it has been speculated for decades chromatin organisation responds to mechanical forces (Shivashankar, 2011, Shivashankar, 2010, Martins et al., 2012). This is thought to happen via condensation/de-condensation impinged by forces transmitted by the cytoskeleton and LINC-complex proteins, which may

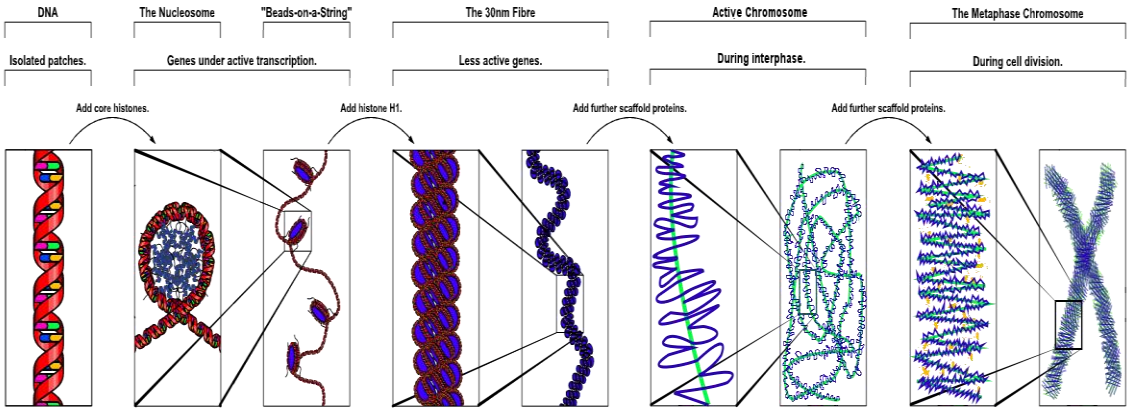

Figure 2.6 - Illustration of the hierarchical chromatin structure (Molecular Station).

From the left to the right: first illustration of double-stand DNA; second, monomeric unit of chromatin, the nucleosome; nucleosomes arranged as bead-on-a-string; next, two consecutive illustrations showing 30nm chromatin fibre; next, three illustrations of interphase higher-order chromatin, which arrangement may depend in several factors; finally, a representation of how higher-order chromatin condenses into chromosome in the metaphase for mitosis progression.

activate/deactivate mechano-sensitive genes.

2.4 Mechano-transduction

Cells respond to their mechanical surroundings. Mesenchymal stem cell (MSC) fate depends on substrate stiffness (Engler et al., 2006). When these stromal cells are seeded in substrates with equivalent stiffness to osteoid, they express osteogenic markers, whereas myogenesis is promoted in softer substrates (Engler et al., 2006, Rowlands et al., 2008). More recently, stiffness was shown to be involved in epithelial-mesenchymal transition (EMT), a process involved in tumour progression (Wei et al., 2015). Within the cell, numerous molecules and subcellular structures mediate force sensation and translate mechanical stimuli into biochemical signals. At a molecular level, mechanical forces may expose certain chemical groups and therefore alter their interactions with surrounding molecules. The arrangement of supramolecular structures may also be altered by exerting mechanical forces, leading to changes in molecular trafficking and possibly molecular-level deformations.

Classically, mechano-transduction consists of cascades of individual but integrated events triggered by an acting force (Hoffman et al., 2011). These happen in three phases: 1) mechano-sensitivity, 2) mechano-transmission and 3) mechano-response (Vogel and Sheetz, 2006). A first mechano-sensation triggers a stimulus, which is transmitted within the cell (mechano-transmission) and then converted at the effector structures which are able to react accordingly (mechano-response). The first line of mechano-sensation happens at the plasma membrane via cell-cell and cell-ECM receptors, followed by the

transmission of a relevant signal towards the responsive structures. This mechano-transmission depends significantly on the cytoskeleton, which may in turn deform the nucleus either passively or actively. Deformations imposed on the nucleus could alter chromatin structure or induce conformational changes in nuclear proteins, e.g. releasing transcriptional regulators or translocation of chromatin segments away for transcriptionally active repressive regions, thereby activating (or repressing) mechano-sensitive genes (Isermann and Lammerding, 2013). Yet, these are more of speculative hypotheses; as will be covered in section 2.4.2 (page 35) - there is limited data that proves that mechanical forces alone imposed upon the nucleus translate into biochemical signals.

2.4.1 The cytoskeleton in mechano-transduction

The cytoskeleton is a major component in force transmission within the cell. Maniotis and co-workers have elegantly shown the physical link between plasma membrane and the nucleus using a micro-needle apparatus (Maniotis et al., 1997). By pulling the micro-needle with an ECM-coated spherical bead at the tip, the authors were able to optically measure deformations at nuclear level. Upon the disruption of both F-actin and MT the position of the nucleus was affected, and upon application of external forces it was still able to deform. The authors proposed that the IF network alone does apply forces to the nucleus in order to deform it.

Recent studies have further demonstrated the importance of the cytoskeleton and its appendices in cellular biomechanics. Studies targeting the disruption of F-actin (e.g. cytochalasin D and latrunculin) report usually a decrease in nuclear

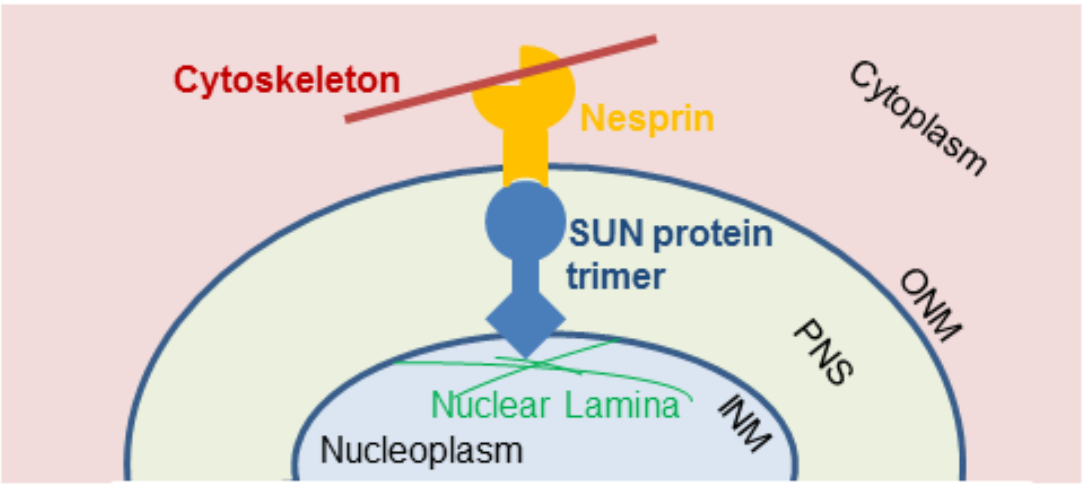

Figure 2.7 – Cytoskeleton-nucleus physical integration via LINC-complex proteins.

The LINC-complex is comprised of SUN-domain containing proteins, which exist as trimers, in the inner nuclear membrane (INM) and associate with the nuclear lamina. The KASH domains of full-length nesprins in the outer nuclear membrane (ONM) bind to the SUN domains of the SUN proteins within the luminal space (PNS), and serve to tether the nuclear envelope (NE) to cytoskeletal proteins.

size of adherent cells, whereas inhibiting microtubule polymerization by nocodazole leads to an increase in nuclear size (Mazumder et al., 2010, Mazumder and Shivashankar, 2010). As a result, F-actin is thought to impose tensile forces upon the nucleus, whereas MTs compression. This fits with the tensegrity model first proposed by Ingber (Ingber et al., 1981). Briefly, the tensegrity model consists of discontinuous compression-resistant members (*e.g.,* microtubules) interconnected directly or indirectly by a continuous series of tension elements (*e.g.* F-actin).

Cytoskeleton-nucleus physical contacts are conceivable to play an important role in force transmission and mechano-transduction in living cells.

Perturbations of LINC-complex proteins affect cell processes such as motility and cell polarity. As SUN proteins are a limiting factor in the recruitment of nesprins to the NE, overexpression of a KASH construct will lead to a displacement of nesprins from the NE (Ketema and Sonnenberg, 2011). This results in functional disruption of all endogenous LINC complexes. As a result, abnormal cytoskeletal architecture in cells overexpressing dominant-negative KASH (DN-KASH) constructs is observed at the perinuclear region (Lombardi et al., 2011). In this study, the close association of the vimentin network with the NE was partially lost, and actin stress fibres were fragmented in appearance around the nucleus (Lombardi et al., 2011). Reduced cytoplasm mechanical stiffness of these cells is observed when probed by ballistic intracellular nanorheology (Stewart-Hutchinson et al., 2008). Furthermore, the absence of lamin A/C also resulted in a redistribution of nesprin-3 from the NE to the ER and disrupted attachment of IF cytoskeletal components to the NE (Hale et al., 2008, Houben et al., 2009). The similarities in phenotype between LINC complex disruption and loss of lamin A/C corroborate the model that nesprins and lamin A/C are physically integrated, and that they contribute similarly for cell mechanics.

2.4.2 The Nucleus as mechano-sensor

The cell nucleus is highly organised, compartmentalised and dynamic (section 2.3.3). Many nuclear components occupy confined sub-regions within the nucleus, and the functional characterisation of each of these parts have received a lot of attention in the past years (Tripathi and Prasanth, 2011, Rajapakse and Groudine, 2011). As covered in the previous sections, mechanical stimuli are transmitted to the nucleus via the cytoskeleton network,

and these are able to mediate/alter its morphology and activity. Once the mechanical stimulus is imposed upon the nucleus, several events may happen such as: 1) chromatin re-arrangement; 2) chromosome-chromosome cross-talk; 3) inside-out nuclear trafficking; 4) assembly-disassembly of nuclear bodies.

Force transmission to the nucleus via the cytoskeleton is yet to be fully clarified. Lombardi et al. (2011) demonstrated that the ectopic expression of mini-nesprin-2 giant, a chimeric protein consisting of the N-terminal actin-binding domain of nesprin-2 giant and its C-terminal end with the KASH domain (Ostlund et al., 2009), enhanced the intracellular force transmission between the cytoskeleton and the nucleus. This suggests that a connection with the F-actin, as mediated via nesprin-1 and -2, plays a more prominent role in the establishment of mechanical integrity than the attachment of other cytoskeletal components to the NE. Although no study has addressed the implications of nesprin-1 and -2 in IFs architecture, some authors hypothesise that the localisation of IFs at the NE might not be solely dependent on nesprin-3 (Ketema and Sonnenberg, 2011). The simultaneous loss of IFs from the nuclear perimeter in *LMNA−/−* cells and those transfected with DN- KASH constructs is in accordance with what is observed in cells lacking in nesprin-3 (Postel et al., 2011). In addition, the loss of lamin A/C (*Lmna−/−*) in mouse embryonic fibroblasts (MEFs) led to the reduction of the overall cell stiffness as evaluated by compression and tensile testing, as well as by ballistic rheological testing (Broers et al., 2004, Lammerding et al., 2004, Lee et al., 2007). These studies corroborate the existence of cytoskeleton-nucleus physical integration, which is essential for IF network architecture. Further studies are needed to identify the

actual nesprin family members required for the maintenance of cellular stiffness and mechano-transduction.

The way mechanical forces are capable to alter nuclear activity and architecture is still unclear. Force-induced changes in nuclear rheology were examined by the use fluorescent fusion proteins binding ribosomal DNA and RNA, which yield punctate labels in the nuclear interior. In fact, a range of cell lines were subjected to compressive and shear forces over a period of time and fluctuations and movement of the punctuated labelled structures was observed, suggesting that external forces can indeed alter chromatin organisation and accessibility (Booth-Gauthier et al., 2012). Forces in the order of nano- to pico-Newtons are able to dissociate two major Cajal body proteins, coilin and SMN (survival motor neuro protein) in less than one second, and strikingly the disruption of F-actin or the depletion of lamin A/C abolished this response (Poh et al., 2012). The expression of lamin A/C scales with tissue stiffness, regulating the fate of human bone marrow–derived MSCs towards more osteogenic or adipogenic pathways when stem cells are seeded in stiff versus soft matrices, respectively (Swift et al., 2013). Overexpression of lamin A/C increased the probability of these cells to differentiate towards osteogenic lineages in soft matrices, similarly when cells are treated with an antagonist of retinoic acid pathway also in soft matrices. Furthermore, by depleting lamin A/C the authors observed that cells were not able to differentiate towards osteogenic lineages, which suggests that lamin A/C regulates stiffness-induced differentiation of MSCs (Swift et al., 2013). Both lamin A/C and emerin are determinants of nuclear mechanics, recently linked to coordinated actin-driven MKL1-SRF pathway (Ho et al., 2013, Lammerding et al., 2005, Rowat et al., 2006, Sullivan

et al., 1999). Force-induced unfolding of nuclear proteins may reveal cryptic binding sites, therefore promoting altered protein–protein interactions or phosphorylation of specific residues via nuclear kinases. This can happen either at the nuclear envelope or the nuclear interior. Phosphorylation of specific nuclear envelope components may further alter interaction with their binding partners or, in the case of lamins, trigger its partial depolymerisation as in mitosis (Kochin et al., 2014, Swift et al., 2013). In another study, isolated nuclei stiffen in response to cyclic force pulses, a phenomenon dependent on lamin A/C and emerin. The application of force on nesprin-1 activates Src, which in turn phosphorylates emerin by Src-family kinases (Guilluy et al., 2014).

Furthermore, Promyelocytic leukemia (PML) bodies contain nuclear matrix-associated domains and scaffolds for extracellular signal-regulated kinases 1 and 2 (ERK1/2) (Warren et al., 2010). This led some authors to speculate a role of PML in mechano-sensing and mechano-responsiveness. Structural filaments such as actin (Pederson and Aebi, 2005), myosin (Hofmann et al., 2006), spectrins (Young and Kothary, 2005) and lamin (both A and C type) (Broers et al., 2005) are also present throughout the nucleoplasm. Their connectivity with other structures as nuclear lamin and NPC have triggered the debate of whether the function of these subdomains may be influenced by mechanical stimuli, corroborating the hypothesis that the nucleus is also load-bearing (Misteli, 2007, Pederson and Aebi, 2005).

The direct mechanical regulation of chromatin remodelling is still to be proven. Shivashankar and co-workers have shown that the enlargement of the nucleus upon cytoskeleton-nucleus disruption via laser ablation or drug treatment

targeting F-actin and MTs results in the chromatin condensation of drosophila cells and fibroblasts, whereas disruption of tension generating F-actin leads to nuclear shrinkage (Mazumder et al., 2008, Mazumder et al., 2010, Mazumder and Shivashankar, 2010, Mazumder and Shivashankar, 2007). More recently, they have shown that external forces may affect chromatin structure using anisotropical correlative microscopy (Iyer et al., 2012, Li et al., 2011). These studies suggest that the nucleus is constantly under stress imposed by the cytoskeleton and that external imposed stress may alter the accessibility of DNA double strand to transcriptional complexes and, thus, activate/de-activate mechano-related genes.

Nuclear mechanics may be a level of regulation in cells by making them more or less responsive to external mechanical stress. In fact, the mechanics of the nucleus is consistently shown to change with differentiation: increased plasticity of stem cell nuclei in comparison to adult and differentiated cells (Banerjee et al., 2004, Banerjee et al., 2006, Bhattacharya et al., 2009, Pajerowski et al., 2007, Swift et al., 2013, Chalut et al., 2012). These reports suggest that indeed nuclear mechanics is important for overall cell behaviour.

2.4.3 Signalling pathways involved in mechano-transduction

Decades of research in this field have resulted in the recognition of signalling pathways influenced by mechanical cues, and several are common among different cell types. For instance, mitogen-activated protein kinase (MAPK) is mechanically activated in fibroblasts (Grinnell, 2003), keratinocytes (Reichelt, 2007), endothelial cells (Lehoux and Tedgui, 2003), smooth muscle cells (Li and Xu, 2007) and osteoblasts (Rubin et al., 2006). Heparin-binding epidermal

growth factor (EGF)-like growth factor (HB-EGF) is activated by reduced endothelial shear stress and stimulates smooth muscle cell proliferation *in vitro* (Zhang et al., 2008).

Cell contractility is essential for mechano-sensation in eukaryotic cells. Rho GTPases are signalling proteins often activated downstream of growth factors that regulate acto-myosin contractility through the activation of serine/threonine kinases and actin polymerisation factors (Hall and Nobes, 2000). The Rho GTPase that is most commonly associated with acto-myosin contractility is RhoA, although RhoC, Cdc42 and Rac1 can also be positive regulators of contractility; in the contrary, RhoE plays an inhibitory role. Several kinases are activated by the binding of active Rho GTPases and regulate myosin activity through phosphorylation. RhoA is known to activate ROCK and citron kinase, whereas the GTPase Cdc42 activates PAK and MRCK; Rac1 activates PAK, citron kinase and dystrophia myotonica protein kinase (DMPK) (Zaidel-Bar et al., 2015). The disruption of Rho-dependent contractility by the use of agents such as Y-27632 and blebbistatin lead to abnormal response to mechanical stress in several cell types, ultimately affecting their motility and fate. In fact, RhoA is dispensable for skin development, but crucial for cell contractility and migration of keratinocytes (Jackson et al., 2011), therefore showing that Rho–ROCK inhibition may not be sufficient for the observed phenotypes. This suggests that Rho-driven contractility may involve actions of unidentified targets such as those involved in the JNK and ERK signalling pathways (Gandham et al., 2013).

The intimate relationship between cell shape and cytoskeleton architecture is thought to regulate canonical signalling pathways involved in several cellular processes. Serum response factor (SRF) and yes-associated protein / transcriptional coactivator with PDZ-binding motif (YAP/TAZ) signalling pathways were recently linked with cell shape control and mechano-transduction (Miano et al., 2007, Connelly et al., 2010, Ho et al., 2013, Jain et al., 2013). SRF drives transcription with its co-factor MAL (also designated as MKL1) which interacts with G-actin (Miano et al., 2007). When substrate area is restricted, G-actin levels decrease, allowing SRF-MRTF to activate transcription and initiate terminal differentiation in human keratinocytes (Connelly et al., 2010). In spread cells, F-actin stress fibres formation causes YAP/TAZ activation and consequently YAP/TAZ becomes nuclear, promoting thus cell proliferation and inhibiting differentiation. In contrast, when ECM adhesive area is restricted (non-spread), YAP/TAZ gets excluded from the nucleus, their transcriptional properties are disabled, and cells undergo differentiation (Dupont et al., 2011).

Retinoic acid (RA) and Wnt signalling are other two signalling pathways involved in mechano-sensation (Fedorchak et al., 2014, Ivanovska et al., 2015). Retinoic acid receptor (RAR), RAR-α, RAR-β and RAR-γ, encoded respectively by the RARA, RARB, and RARG genes, bind to retinoid X receptors in the nucleus and regulate the transcription of many genes including *LMNA*. Lamin A/C expression is regulated by RARs, but the nuclear-to-cytoplasmic ratio of RARG also increases with matrix elasticity and lamin A/C overexpression. In MSCs, RAR antagonists increase lamin A/C levels and enhance osteogenesis on rigid substrates, but neither RA antagonist affects lamin A/C levels in cells on

soft substrates (Swift et al., 2013). Nevertheless, cell-cell junctions are also shown to be involved in force transmission via β-catenin, one of the most well-studied Wnt regulators. β-catenin interacts with chromatin remodelling proteins to orchestrate epigenetic modifications and therefore transcriptional activity of Wnt-responsive genes (Willert and Jones, 2006). The nuclear transport of β-catenin is dependent upon emerin and nesprin-2 (Fagotto et al., 1998, Neumann et al., 2010), which influences cell proliferation. Interestingly, mutations affecting emerin lead to a phenotype similar to nesprin-2 cells, also identical with *LMMA*-/-. The physical integrity of LINC-complex (including nuclear lamina) and emerin appears to be necessary for both RA- and Wnt-signalling mediated nuclear mechano-sensation and –responsiveness. Further studies combining live-cell high-resolution imaging with controlled mechanical stimuli may bring new insights into the field, and essentially, how the cross-talk between these different pathways dictates mechano-biology (Fedorchak et al., 2014).

2.5 The skin

Skin is the largest organ in the human body and possesses an incredible ability to respond to the external environment. Basic functions involve the protection of the body from insult and temperature regulation. Skin is a composite formed by three main layers: 1) the epidermis, a thin layer of stratified squamous epithelium that seats on top of a basement membrane rich in extracellular matrix components, followed by 2) the dermis within which the hair follicles and sweat glands extend, and 3) the subcutaneous tissue. The epidermis provides mechanical toughness and is able to withstand the physical and chemical

insults from the exterior. Keratinocytes, the main cell type in the epidermis, organise in four distinct stratums which are characterised by particular expression patterns: *stratum basale,* expressing keratin K14/5; *stratum spinosum*, rich in K10/1; *stratum granulosum* where cells flatten and initiate the formation of waterproof cornified envelope; and finally the *stratum corneum,* in which keratinocytes became apoptotic, producing degrading organelles and releasing lysosomal enzymes, which results in a tightly cross-linked cutaneous barrier. Terminally differentiated keratinocytes (also designated as corneocytes) are found in the cornified envelope (Rice and Green, 1977), embedded in an insoluble scaffold of proteins such as involucrin, filaggrin, and periplakin, as well as transglutaminase I cross-linked lipids (Segre, 2006). The dermis, on the other hand, does not undergo an obvious sequence of differentiation as the epidermis, although its structure and organisation is depth-dependent. Next to the basement membrane, the papillary side supplies blood vessels and nerve endings, followed by the reticular dermis that houses the hair follicles and sweat glands. Below is the subcutaneous tissue, also called hypodermis, containing adipocytes, lymphocytes and mast cells (Smith and Dean, 1998).

2.5.1 The cytoskeleton in skin homeostasis

Several signalling pathways and protein expression patterns are involved in skin homeostasis, which in the end relies on the proper balance and spatial arrangement of keratinocyte growth and differentiation in the epidermis (Fuchs and Raghavan, 2002). Proliferative keratinocytes seated on the basement membrane migrate upwards through the epidermis to replace cells shed from the surface of the skin (Barrandon and Green, 1987, Watt, 1998). For the formation and maintenance of epidermis barrier function, intercellular junctions

are essential, *e.g.* the desmosomes and the adherens junction (Green and Gaudry, 2000, Vasioukhin et al., 2000). Both F-actin and keratins are crucial in establishing these anchoring structures (Vasioukhin et al., 2000). Skin's physical integrity depends on these intercellular junctions and on the epidermis-dermis interface where basal keratinocytes adhere to underlying ECM-rich basement membrane through predominantly the integrins α6β4 and α3β1 (Carter et al., 1990).

Keratins are the major cytoskeleton of all epithelia and do contribute largely to the specialised keratinocyte functions, in particular in establishing desmosomal, hemidesmosomal, and cornified envelope proteins (Jones and Green, 1991, Kouklis et al., 1994, Candi et al., 1998, Hesse et al., 2004, Rogers et al., 2004, Schweizer et al., 2006, Kurokawa et al., 2011). As covered before (section 0), keratins are co-ordinately transcribed to allow the formation of keratin intermediate filaments from heterodimers of a type I and a type II protein. The epidermal type I keratin genes e.g. *KRT1*, *KRT2* and *KRT5*, each comprise 9 exons, whereas the genes coding for epidermal Type II keratins e.g. *KRT10* and *KRT14*, each consist of 8 exons (Szeverenyi et al., 2008). Proliferating basal cells express *KRT5*, *KRT14*, and *KRT15* (Nelson and Sun, 1983, Lloyd et al., 1995, Porter et al., 2000), and upon the switch to terminal differentiation, keratinocytes start to express *KRT1*, *KRT2e*, and *KRT10* (supra-basal cells). Disruption of epidermal homeostasis caused by inflammatory cues and tissue repair (e.g. wound healing) result in the transient expression of *KRT6*, *KRT16* and *KRT17* (Fuchs and Green, 1980, Byrne et al., 1994, Freedberg et al., 2001).

In skin, basal cells establish contacts with the basement membrane via integrin-based adhesions, which may be 1) focal adhesions (actin-dependent) and 2) hemidesmosomes (keratin-associated) (Figure 2.5). β1 containing integrins connect with F-actin through talin and vinculin, located around FAs and also at the apicolateral cell surface (Margadant et al., 2010). These integrins signal through focal adhesion kinase (FAK), integrin-linked kinase (ILK), kindlin-1 and CD151 to regulate several cell processes, such as motility and apoptosis, by activating with mitogen-activated protein kinase (MAPK) or phosphatidylinositol-3OH kinase (PI3K)/Akt pathways. Also, other actin-dependent pathways implicated in skin homeostasis have recently been described: serum response factor (SRF) and the YAP/TAZ (Connelly et al., 2010, Lee et al., 2014). In human keratinocytes, knockdown of SRF or its co-factor MAL inhibited differentiation, whereas overexpression of MAL stimulated SRF activity and involucrin expression. The downstream genes of *SRF*, *FOS* and *JUNB*, were involved in mechanically induced terminal differentiation. c-Fos mediated serum responsiveness, whereas JunB was regulated by actin and MAL (Connelly et al., 2010).

Intermediate filaments are finely regulated throughout the epidermis and are essential for skin's barrier function. In fact, keratins were recently proposed to regulate "inside-out" signalling involved in HD formation and organisation during keratinocytes migration and adhesion (Seltmann et al., 2015, Seltmann et al., 2013b). In mouse keratinocytes, loss of keratins led to an increased β4-integrin phosphorylation at Ser1354 and Ser1362 by PKCα and Erk1/2 kinase via plectin (Seltmann et al., 2015). The observed higher turnover of β4-integrins in the absence of plectin-keratin linkage is potentially caused by the two-fold

increase of EGF secreted by these cells. Further investigations are necessary to determine which mechanism underlies HDs formation and how this regulates the EGF signalling pathway.

The importance of HD formation and coupling with the keratin cytoskeleton via plectin in skin is notorious in blistering diseases such as epidermolysis bullosa simplex (EBS) and palmoplantar keratoderma (Fuchs and Raghavan, 2002). EBS affects individuals who suffer from trauma-induced blistering of skin with severity ranging from mild to lethal. Eighteen different genes affecting different proteins in the epidermis and BM have been identified in this class of skin disease (Fine et al., 2014). Basal EBS is commonly associated with four different genes: *KRT5*, *KRT14*, *BPAG1* and *PLEC*. Although recessively inherited, EBS caused by rare mutation in *PLEC* leads to generalised blistering and muscular dystrophy (Pfendner and Uitto, 2005). Plectin appears to be essential for cytoskeleton organisation of keratins and muscle cells.

2.6 Plectin and Plectinopathies

PLEC encodes the protein plectin, a high-molecular mass protein (~500 kDa) that is ubiquitously present in skin, mucous membranes, gut, muscle and heart tissue. At the moment, it is well established that plectin is a cytoskeletal cross-linker (Wiche et al., 2015). Its molecular structure (Figure 2.8) resembles that of desmoplakin, except its plakin domain is preceded by an N-terminal actin binding domain (ABD), consisting of a pair of calponin-homology (CH) subdomains arranged in tandem. Furthermore, plectin contains 6 plakin-repetitive domains (PRD), denoted B1-5 and C (Sonnenberg and Liem, 2007).

A cluster of basic residues located in the L sequence (connecting fourth and fifth PRDs) interacts with IFs (Nikolic et al., 1996).

Key functions of plectin isoforms have been revealed in detail in the past few years. It became clear that many of the functions provided by IFs are dependent on their proper cross-linking, site-specific targeting, and anchoring through accessory linkers such as plectin. Due to its universal IF-binding ability and unusual diversity provided by its numerous isoforms (Table 2.3), plectin is instrumental for the architecture and therefore function of IFs. In keratinocytes, plectin has high affinity to the quaternary structure of the heterodimeric K14/5 network (Bouameur et al., 2014) at hemidesmosomes (Gache et al., 1996, Koss-Harnes et al., 2002). Different isoforms confer different tethering properties. In skin, plectin 1, 1a and 1c are expressed. Inactivation of plectin gene in mice, similarly in humans, leads to skin blistering and myopathy with

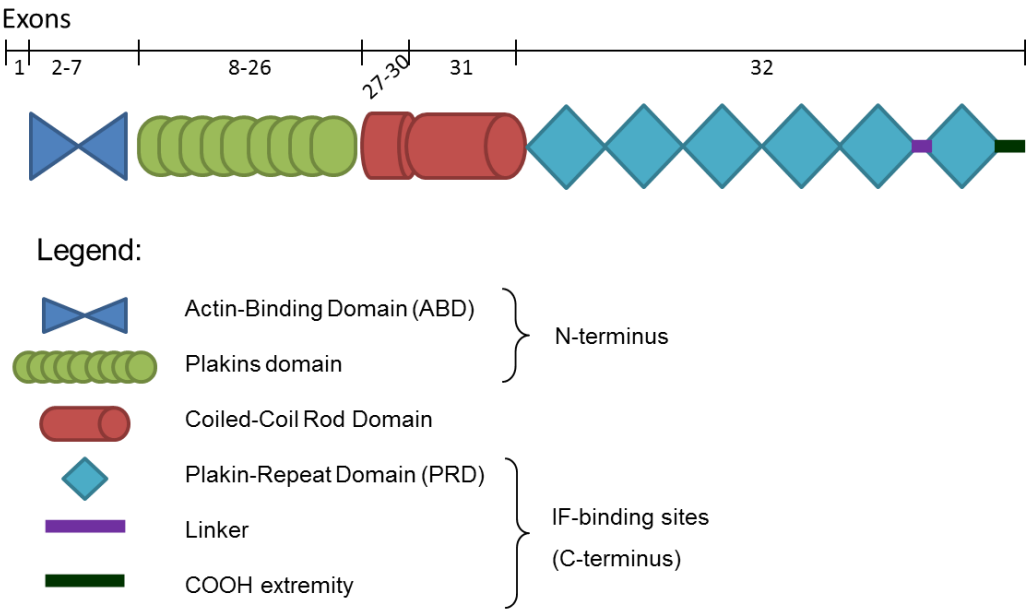

Figure 2.8 – Mammalian Plectin structure scheme.

necrotic muscle fibres, streaming of z-disks, focal rupture of sarcolemma and accumulation of mitochondria (Andra et al., 1997, Konieczny et al., 2008). The motility of plectin-deficient cells is also affected, although the end result is cell specific. For instance, *Plec* KO mouse keratinocytes are more motile, whereas plectin deficient fibroblasts are slower that the WT (Andra et al., 2003, Walko et al., 2011, Osmanagic-Myers et al., 2006). This reinforces the cell-type specificity of plectin, which may be attributed to the differential expression of its isomers.

Selective proteolysis of hemidesmosomal plectin 1a leads to EBS-Ogna a condition that affects skin only (Koss-Harnes et al., 2002, Walko et al., 2011, Gostynska et al., 2015, Andra et al., 2003). In comparison to the WT, plectin P1a mutant results in more fragile skin under mechanical insult (Koss-Harnes et al., 2002, Walko et al., 2011). In fact, the resulting reduction of integrin α4-mediated mediated clustering of the hemidesmosomes led to more motile cells

Table 2.3 – Human *PLEC* isoforms and transcript variants listed in NCBI RefSeq (Natsuga, 2015)

Isoform (RefSeq no)	Transcript variant (Tv) (RefSeq no)
Isoform 1 (NP_958782)	Tv 6 (NM_201380)
Isoform 1a (NP_958786)	Tv 11 (NM_20384)
Isoform 1b (NP_958784)	Tv 8 (NM_201382)
Isoform 1c (NP_00436)	Tv 1 (NM_00445)
Isoform 1d (NP_958783)	Tv 7 (NM_201381)
Isoform 1e (NP_201379)	Tv 3 (NM_201379)
Isoform 1f (NP_958780)	Tv 2 (NM_201378)
Isoform 1 g (NP_958785)	Tv 10 (NM_201383)

in EBS-Ogna cell model. Plectin interacts with the cytoskeleton in a tissue-specific way. Plectin-deficient fibroblasts possess an abnormal F-actin architecture and expression (Andra et al., 1998, Rezniczek et al., 2003). MTs get cross-linked to IFs via plectin P1c (Svitkina et al., 1996, Valencia et al., 2013). It appears that plectin further destabilises MTs via its interaction with MT-associated proteins.

Plectin may affect basic cellular processes such as glucose uptake, as in the case of myoblasts (Raith et al., 2013, Valencia et al., 2013). This is thought to be via mediation of the endocytosis and dynamics of adhesion complexes. In addition and the most important in the context of this thesis, loss of plectin has dramatic consequences in IFs dynamics, positioning of organelles and scaffolding of signalling cascades, which ultimately affect several cellular processes such as migration (Wiche et al., 2015). *In vivo* phenotypes associated with *PLEC* mutations are muco- cutaneous blistering, pyloric atresia, muscular dystrophy and cardiomyopathy (Table 2.4) (Charlesworth et al., 2013, Winter and Wiche, 2012). In 8% of EBS cases, *PLEC* is the mutated gene (Bolling et al., 2013).

2.6.1 Keratins and nuclear mechano-transduction in skin

Once terminal differentiation is initiated, keratinocytes migrate upwards towards the cornified envelope and their nucleus undergoes dramatic morphological changes. As previously noted, terminal differentiation in the epidermis involves a highly coordinated expression of keratins, lipids and other molecules (*e.g.* transglutamine) important for the barrier function and tissue homeostasis. This is thought to involve the regulation of higher-order chromatin remodelling and

proper spatial arrangements of the individual chromosomes, chromatin domains, and nuclear bodies (Hübner and Spector, 2010, Joffe et al., 2010, Schoenfelder et al., 2010). In differentiating cells, actively transcribed genes are spatially compartmentalised and frequently form intra- and inter-chromosomal topologically associated domains (or interactomes). Repressed genes, however, are spatially organised into inactive chromatin domains, typically lamin juxtaposed at the periphery of nucleoplasm (Misteli, 2007, Lieberman-Aiden et al., 2009, Schoenfelder et al., 2010, Nora et al., 2012). The spatial organisation of the transcriptionally active or silenced compartments in the nucleus is believed to depend on its size, shape, preferential arrangements of the chromosomes, number, and size of distinct nuclear bodies – all dramatically dynamic during differentiation (Dundr and Misteli, 2010, Joffe et al., 2010, Schoenfelder et al., 2010).

Gdula and co-workers have elegantly shown that morphological changes in the nucleus throughout the epidermis of mouse tissue was accompanied with an increase of nucleolus and heterochromatin markers (Gdula et al., 2013). Whether these are the cause or consequence of cytoskeleton remodelling provoked by alterations in integrin expression and adherens junctions is still unclear. The fine control of keratins throughout epidermis layers may explain the morphological changes throughout its thickness. A recent study has shown that the high levels of K5-K14 coiled-coil dimers in basal keratinocytes form parallel keratin bundles around the nucleus, a pattern that changes when cells undergo calcium driven terminal differentiation: trans-filament disulphide bonds are established via Cys367 and a perinuclear case around the nucleus leads to a rounded nucleus (Lee et al., 2012).

Table 2.4 - Subtypes of plectinopathies reported in literature, affected exons, inheritance, organs affected and severity of the conditions caused. Adapted from Gostynska et al. (2015)

Subtype	Exons affected	Inheritance	Organs affected	Severity
EBS-MD	9-32	AR	Skin,striated muscle, myocardium	Severe and progressive
EBS-MD-Mys	13,31,32	AR	Skin,striated muscle	Severe and progressive
EBS-PA	Distal	AR	Skin,pylorus	Lethal
EBS-Ogna	31	AD	Skin	Mild
EBS-plectin 1a	1a	AR	Skin	Moderate
LGMD2Q	1f	AR	Striated muscle	Severe and progressive

There is, therefore, the need to understand further how the cytoskeleton cooperates in nuclear mechano-transduction and establishment of its morphology. In the current work, it is envisaged the study of how actin and keratins cooperate in defining nuclear morphology in keratinocytes and its impact in cell's behaviour.

Chapter 3. Materials and Methods

In this section, the experimental tools utilised are thoroughly described, from the reagents used to the image processing algorithms developed. Firstly, the reagents and solutions utilised are described, following sample preparation techniques and protocols, finishing with the analytical methods (e.g. microscopy) and respective data processing and analysis.

3.1 Antibodies

A list of antibodies used are listed below (Table 3.1).

Table 3.1 – List of primary antibodies used for immunocytochemistry (ICC) or immunohistochemistry (IHC).

Antibodies	Species	Fixation	Dilution (ICC, IHC)	Source
Lamin A/C (clone 636)	Mouse	4% PFA	1:200	Santa Cruz
Keratin 14 (clone LL002)	Mouse	4% PFA	1:500	Abcam
HP1-alpha	Rabbit	4% PFA	1:200	Milipore
H3K27me3	Rabbit	4% PFA	1:200	Milipore
H3K4me3	Rabbit	4% PFA	1:200	Milipore
Involucrin (SY7)	Mouse	4% PFA	1:500	Cancer Research UK

RNA polymerase II (YSPTSPS repeat)	Mouse	4% PFA	1:500	Abcam
Plectin (10F6 clone)	Mouse	Methanol	1:200	Santa Cruz
H3K14ac	Rabbit	4% PFA	1:200	Milipore
H3K9me3 (6F12-H4)	Mouse	4% PFA	1:200	Milipore
Pan-Keratin (H-240)	Rabbit	4% PFA	1:500	Santa Cruz

Table 3.2 – List of secondary antibodies used for immunocytochemistry (ICC) or immunohistochemistry (IHC).

Antibodies	**Species**	**Dilution (ICC)**	**Source**
Alexa 488/568 Anti-Rabbit	Goat	1:1000	Molecular Probes
Alexa 488/555 Anti-Mouse	Donkey	1:1000	Molecular Probes
Phalloidin 488/555	Dye	1:1000-500	Invitrogen

3.2 Reagents and buffers

Table 3.3 – Solutions and buffers prepared. Throughout the thesis, all chemical were purchase from Sigma-Aldrich (USA), unless stated,

Buffer/Solution	Composition
Blocking buffer	10% Bovine Serum (Biosera), 0.25% Fish Gelatin in 1xPBS
4% (w/v) PFA	Paraformaldehyde in 1x PBS
FAD	10% FBS (Biosera), 1% Penicillin Streptomycin (Invitrogen), Insulin 5mg/mL, 10^{-10} M cholera toxin, 10 ng/mL EGF (Peprotech 100-15), and 0.5 ug/mL hydrocortisone (Fisher 35245-0010)
PB buffer	0.5% skim milk powder, 0.25% fish gelatin
Mowiol mounting media	Mowiol 40-88, Glycerol, 0.2 Tris-HCl (pH 8.5). Preparation protocol available at Cold Spring Harb Protoc (2006) doi:10.1101/pdb.rec10255

3.3 Tissue and cell isolation

3.3.1 Isolation of primary keratinocytes from neonatal human foreskin tissue

The isolation of epidermis cells, keratinocytes, is achieved by two consecutive enzymatic digestions: a first to dissociate the epidermis from the dermis; and a final trypsinization for the disruption of cell-cell contacts. Firstly, the foreskin samples were sterilised in 10% Betadine solution in water for 30s then washed twice in 70% ethanol for at least 10s each wash. Excess of connective tissue was removed mechanically and the skin cut small pieces of no more than $1cm^2$. This allows for more efficient and homogenous enzymatic digestion of the basement membrane once the area in contact with enzymatic solution is greater, which is achieved by incubating the tissue in dispase (Sigma) diluted in serum-free FAD (Table 3.3) at a final concentration of 2.5mg/mL overnight at 4^oC. The dispase was washed out with 1xPBS and subsequently twice in EDTA solution (Versene, Invitrogen). Epidermis was mechanically separated from dermis gently with pair of sterile tweezers and then incubated in pre-warmed 0.25% trypsin/EDTA (1x) at 37^oC for no longer than 30 minutes. Trypsin was blocked with FAD media in a ratio 1:2 (trypsin:FAD) and centrifuged for 5 minutes at 1200rpm. Cells were re-suspended in media, seeded on top of inactivated J2 monolayer and maintained as described in section 3.4.1

3.3.2 Mouse skin wholemount of plectin transgenic mice

Mouse tails of transgenic mice (*Plec* -/- and +/+), 2 days old, were kindly provided from Prof. Gerhard Wiche (Max F. Perutz Laboratories, University of Vienna, Austria). A superficial length-wise cut was performed with a scalpel and the skin was peeled gently. Following, 3-4 hours incubation with 5mM EDTA in

1xPBS at 37^{o}C, the epidermis was mechanically peeled off and immediately fixed in 4% formaldehyde in 1xPBS for 2 hours at room temperature. Finally, the tissue was washed with1x PBS three times and stored in 1xPBS + 0.2% sodium azide at 4^{o}C. The tissue was used for immunostaining and observation within 2 weeks.

3.4 Cell culture methods

3.4.1 Fibroblasts culture and feeder preparation

Fibroblast-keratinocyte co-culture of primary human keratinocytes *in vitro* was adopted (Rheinwald and Green, 1975, Rheinwald and Green, 1977). Briefly, a monolayer of fibroblasts is prepared, on top of which the keratinocytes will be accommodated. The fibroblastic cell line designated as J2-3T3 (kindly supplied by Fiona Watt, King's College London) was selected to provide optimal feeder support for human keratinocytes. These cells were cultured and maintained in Dulbecco's Modified Eagle Medium supplemented with 10% bovine serum (Biosera, UK) and 1 Penicillin Streptomycin. As these cells are highly proliferative in comparison to the keratinocytes, senescence is induced by treating the cells with Mitomycin C (0.4mg/mL final concentration in the media, for 2-3 hours). Cells are re-plated 24h before keratinocytes are seeded on top in a density of $4x10^{4}$ cells.cm^{-2}. Fresh cells J2 3T3 were thawed every 3 months, as with prolonged passaging the cells start to senesce or undergo spontaneous transformation.

3.4.2 Primary human keratinocytes culture onto monolayer of fibroblasts

After isolation (described in section 3.3.1), the primary human keratinocytes were seeded onto a dense monolayer of inactivated J2 clone of Swiss 3T3 cells

($4x10^4$ cells.cm^{-2}). Media was replaced every other day. After few days (2-3 days), keratinocyte colonies start to be noticeable. At a ~90% confluence (approx. every 5-7days), keratinocytes were passaged. Firstly, feeders are removed with 3-4 washes of EDTA solution (Versene, Invitrogen) for 5 minutes. After feeders de-attach, keratinocytes were treated with 0.05% trypsin/EDTA for 5 minutes, re-suspended in fresh FAD media (1:2) and centrifuged for 5mins at 1200rpm. The pallet is re-suspended in fresh media. Culture was continued (no further than passage 8) by re-platting the keratinocytes onto a previously senescent J2 monolayer or alternatively in bare plastic flask and kept in KSFM. Cells cultured in the absence of feeders were passaged only once.

3.4.3 Double KO for p53 and/or plectin mouse keratinocytes culture

Primary mouse keratinocytes *p53* KO + *Plec* +/+ (WT) and *p53* KO + *Plec* -/- (*Plec* KO) were maintained in EpiLife (Gibco, Life technologies, USA) media and supplemented with 1x Human Keratinocyte Growth Supplement (Gibco, Life technologies, USA) and 1% Penicillin Streptomycin. For passaging these cells, digestion was performed with 0.25% trypsin/EDTA (Gibco Life technologies, USA) for 10 minutes, re-suspended in EpiLife + 10% FBS and centrifuged at 1200 for 5mins. The pellet was homogenised using 1000µL and cells were re-plated in 1:5 dilutions (maximum).

3.4.4 HeLa, HaCats and J2 fibroblasts

HeLa cells are a cervical cancer cell line commonly used in research. They are spontaneously immortalised. HaCats are human keratinocyte cell line. J2 fibroblasts are the cell line utilised to support pHK culture as previously mentioned (section 3.4.1). These (HeLa, HaCats and J2 fibroblasts) were

commonly maintained in DMEM supplemented with 10% FBS (Biosera) and 1% Penicillin Streptomycin (Sigma-Aldrich, UK). At 90% confluence, they were treated with 0.05% trypsin/EDTA for 5 minutes, re-suspended in fresh DMEM and centrifuged at 1200rpm for 5 minutes. The pallet was re-suspended in DMEM and cells were typically plated in 1:10 ratio.

3.4.5 Cryopreservation of cells

For cryopreservation, confluent cells were detached from the dish using trypsin-EDTA digestion as described before, centrifuged and resuspended in 10% DMSO/media at $1x10^6$ cells per ml in a cryovial (Corning). Immediately after, cells were placed in a container with isopropanol at -80^oC overnight in order to allow a steady cooling velocity of -1^oC/min. The cryovials were then transferred to -180^oC bank (liquid nitrogen).

3.5 Cytoskeleton inhibitor treatment

Cells seeded onto glass coverslips or micro-patterned substrates were treated with cytoskeleton inhibitors at final concentrations according with Table 3.4.

Stock concentration of these reagents were diluted in DMSO and prepared at concentration normally 100-1000 times higher than final working concentration. This is to avoid any toxic effect resulting from DMSO. In order to account for eventual adverse effects, a carrier control was always used, which consists in adding DMSO at the same dilution as the one used for the treatment.

3.6 Transient transfection using small-interfering RNA (siRNA)

Small-interfering RNA consists of small sequence of RNA (20-25 base pairs

Table 3.4 – Cytoskeleton inhibitors treatment concentration.

Designation	Final Concentration (µM)	Solvent	Stock Concentration (mM)
Blebbistatin (Millipore)	50	DMSO	50
Latrunculin A (Millipore)	0.1	DMSO	0.1
Okadaic Acid	0.01-1 µg/ml	DMSO	0.1 µg/ml

long) which is currently routinely used in mammalians to reduce the expression of target genes (Elbashir et al., 2001). Plectin downregulation was achieved by siRNA as detailed below.

3.6.1 Transient transfection using a pool of human Plectin siRNA

Primary human keratinocytes (passage 2-5) were plated in 10cm plastic dishes (Corin) until 50-60% confluent. Human Plectin siRNA pool (ON-TARGET plus Human *PLEC* 5339 SMARTPool, Darmacon - GE healthcare, UK) was applied to the cells using Jet-Prime Transfection Reagent (PolyPlus, France). 40nM siRNA (final concentration) was used following manufacture's guidelines. Briefly, siRNA was mixed with Jet Prime buffer and 20µl/ml Jet Prime reagent was incubated for 10-15 minutes. This transfection cocktail was then added to the cells. After 4 hours, media was changed three times and cells were let to grow for 4 days prior to experiment.

3.7 Micro-contact imprinting – patterning ECM on glass substrates

Micro-engineering substrates were utilised to control the adhesion area for cells to adhere.

3.7.1 Glass cleaning and Chromium-Gold evaporation

For the fabrication of micro-engineered substrates, glass coverslips must be coated with gold (Au). Gold establishes weak adhesion to inert and commonly used glass and therefore oxidative metal, chromium, is used as intermediate layer in order to enhance gold adhesion. In addition, any impurities must be removed prior to metal deposition onto the glass to insure a homogenous and strong coating.

Glass slides were firstly washed by immersing them in deionised and distilled water and sonicated for 30 minutes. Slides were then rinsed with absolute ethanol, either dried with pressured nitrogen one by one or let to dry in a sterile hood. By thermal vapour deposition using Edwards Coating System E306A, sequential metal coating was performed onto the glass slide: a first layer of chromium (1.5-5nm thick) and 15nm gold. The rate and final thickness of evaporation was monitored by quartz balance Intellemetrics IL150.

3.7.2 Polymer brushes functionalisation

Patterned polyoligo(ethylene glycol methacrylate) (POEGMA) were generated as previously described (Brown et al., 2005, Ma et al., 2004). Briefly, master silicon moulds were created by photolithography and used to cast poly-dimethylsiloxane (PDMS) stamps. The micro-patterned stamps were inked with the thiol initiator, ω-mercaptoundecyl bromoisobutyrate (kindly provided by Dr

Julien Gautrot), and brought into conformal contact with gold-coated coverslips to deposit the initiator as a self-assembled monolayer for 15 seconds. Atom transfer radical polymerisation (ATRP) of the solution oligo(ethylene glycol) methacrylate (OEGMA; *Mn* 360 for –OH brushes) and oligo(ethylene glycol) methyl ether methacrylate *Mn* 300 for -CH_3 terminated ones, was carried out in a water/ethanol (4:1) solution of OEGMA (1.6 M), Cu(II)Br (3.3 mM), 2,2-bipyridine (82 mM) and Cu(I)Cl (33 mM). The reaction was performed at room temperature for 1h and 15 min for –OH and CH_3 brushes, respectively. The patterned substrates were rinsed with water and ethanol, dried, and stored at room conditions and used within 24 hours.

1.1.1.1.1 Peptide functionalisation of polymer brushes

POEGMA brushes were further functionalised for dynamic studies (Costa et al., 2014). To the previously prepared –OH terminated brushes, a solution of 0.2M *N,N'*-disuccinimidyl carbonate (DSC) and 0.2M 4-(dimethylamino) pyridine (DMAP) in *N*-(2,4-dimethylphenyl) formamide was let to react at RT overnight. After several washes in *N*-(2,4-dimethylphenyl) formamide and deionised water, propargylamine in *N*-(2,4-dimethylphenyl) formamide was furthermore let to react at RT overnight. Several washes in *N*-(2,4-dimethylphenyl) formamide water and absolute ethanol followed. Substrates were used within 1-3 days after preparation.

Following polymerisation, substrates were cut, sterilised in 70% ethanol for at least 10 minutes and incubated in serum containing media (10% FBS EpiLife, in the case of mouse keratinocytes) for at least 30 minutes. Cells were then seeded in a density of $225x10^3 cells.cm^{-2}$ (for 200µm diameter islands) and rinsed after 30 minutes. Cells were incubated overnight at 37^oC, 5% CO_2. *In situ*

functionalization of PEOGMA brushes with a desirable peptide is achieved via “click” chemistry (Costa et al., 2014). Directed migration of keratinocytes was achieved by functionalised micropatterned substrates with collagen type I peptide (Reyes and García, 2003) glycine-phenylalanine-hydroxyproline-glycine-glutamate-arginine ,GFOGER). Thiol–yne reaction was performed in the presence of a photoinitiator, Irgacure 2959 (2-hydroxy-40-(2-hydroxyethoxy)-2-methylpropiophenone, PI; Sigma–Aldrich, UK), and UV light(~23mWcm^{-2}, λ_{max} = 365 nm). Irgacure 2959 was re-suspended at 0.5% (w/v) in phenol-red and serum free DMEM (PSF-DMEM) and allowed to dissolve overnight at 37^{o}C. The coupling reaction was initiated by exposing the substrates to UV light from an LED array (Cetoni, Germany) for 1 minute. After exposure, substrates were immediately washed three times with fresh medium and incubated at 37^{o}C 5% CO_2 for the desirable time.

3.7.3 Seeding cells onto micro-patterned substrates – static model (-CH_3 terminated brushes)

Following sterilisation with 70% ethanol for at a minimum of 10 minutes, micro-patterned substrates were coated with 20 μg.ml^{-1} of rat type I collagen (BD Biosciences, UK) in PBS for 1 hour at 37 °C or overnight at 4°C. Substrates were rinsed three times with 1 mM HCl and twice with PBS. Prior to cell seeding, substrates were incubated for no longer than 1h in media supplemented with 10% FBS. Cell suspension was deposited in micro-patterned substrates at a variable concentration (50x10^3 for 20μm islands, and 25x10^3 for the other substrates). Cells were allowed to attach for 1-2 hours and, after washing with fresh medium, for another 2-3 hours to fully spread.

3.8 Immunostaining

3.8.1 Immunostaining of skin whole mounts

Following isolation and fixation as described in section 3.3.2 (page 56), the tissue was blocked and permeabilised in PB buffer (Table 3.3, page 55) for 30 minutes at room temperature. Primary antibodies were diluted in PB buffer in accordance with table (Table 3.1, page 53) and incubated at room temperature overnight with gentle agitation. Several washes in 1xPBS + 0.2% Tween 20 were performed over 4 hours with at least one rinse every hour (in total a minimum of 4 changes). This allows a more effective wash out of the primary antibody throughout the tissue mass and therefore avoiding non-specific binding and background fluorescence. Subsequently, fluorophore-conjugated antisera were incubated in the same fashion as the primary antibodies and washed in 1xPBS + 0.2% Tween 20 in the same manner as mentioned before for the primary. Tissue was mounted with Mowiol reagent and let drying at room temperature protected from the light. Mounted samples were kept at 4^{o}C and in the dark until imaging for no longer than 6 months in order to avoid fluorophore bleaching and fade overtime.

3.8.2 Immunostaining of cells

Fixed cells were and permeabilised with 0.2% Triton X-100 in PBS for 10 min at room temperature. Following at least three washes in PBS, samples were incubated with blocking solution. For keratinocytes, 10% bovine serum (BioSera, UK), 0.25% Fish gelatin in PBS was used for 30-60mins. For other cells, 0.2% bovine serum albumin in PBS was used for 10-30mins at room temperature. Subsequently, samples were incubated with primary antibody

diluted in respective blocking solution for either 1h at room temperature or overnight at 4^{o}C. Several washes in PBS followed. Fluorophore conjugated secondary antibodies, also diluted in blocking solution, were incubated for 1h at room temperature. The final dilutions and specificity of each antibody/dye used was as specified in section 3.1 in Table 3.1 and Table 3.2 (page 53-54). After washing three times in PBS and subsequently in deionised water, slides were mounted onto glass slides embedded in Mowiol solution and let to dry.

3.9 Optical microscopy

3.9.1 Fluorescence microscopy

For high-resolution analysis, fixed samples were analysed with either a Zeiss 510 or 710 laser-scanning confocal microscopes. 63x/1.4 Plan-APOCHROMAT- and 40x/1.30 EC-Plan-NEOFLUAR oil immersion objectives were used (model of objectives were common to both microscopes). Both microscopes are equipped with 405nm diode laser line (HXP120C Helium lamp), and 458nm, 477nm, 488nm, 514nm Argon laser lines (Lasos, Germany). This apparatus allows the imaging of blue, green and red channels at the same time. Typically, the blue channel was used to image the nuclei whereas the other two channels for the imaging of various desirable structures. For 3D imaging, Z-stacks were acquired with a z-spacing ranging from 0.28-1.5µm according with the sample and the ensuing purpose. For single cell quantification (e.g. determination of nuclei height), 0.28µm z-spacing was selected, whereas for qualitative and illustrative purposes 1-1.5µm z-spacing was chosen. Pixel depth of 16-bit was defined for intensity analysis; 8-bit was utilised for morphometric quantification or for illustrative purposes (e.g. representative images for figure display).

For low magnification epi-fluorescence microscopy, either Leica DMI4000 or Leica DMI5000 was used with the objectives 40x/0.7 PL FLUOTAR, 20x/0.4 CORR Ph1 and10x/0.30 Ph1 HC PL FLUOTAR.

3.9.2 Optical microscopy of living cells

Inverted optical microscope Nikon Eclipse TE2000-S coupled with mercury lamp Nikon C-SHG1 was routinely used to observe living cells in phase contrast mode or fluorescence. The objectives 5x, 10x, 20x and 40x were utilised according with the magnification intended. Nikon Digital Sight apparatus (including DS-Fi1 5MP coloured camera and DS-L2 standalone controller) allowed the digital capture of images.

3.9.3 Time-lapse phase contrast microscopy

Inverted optical microscope Zeiss Axiovert 200M with automatic positioning stage was used in order to perform live time-lapse microscopy. Objective 10x/NA 0.3 dry was utilised for phase contrast imaging. Temperature and CO_2 enrichment chambers (Solent Scientific, United Kingdom) were used in order to maintain cells at 37^{o}C and 5% CO_2. Each frame was imaged every 10 minutes for a total of 24 hours. Prior to imaging focusing plane and positions of the stage were set manually over regions of interest.

3.10 Image Analysis

Different analysis and processing routines were implemented using distinct software according with the desirable quantification. ImageJ was used for two dimensional data analysis of epi-fluorescent images; MatLab (MathWorks) was utilised for radial profiling of 2D confocal images, as well as for 3D quantification of nuclei height of single cell z-stacks. For the quantification of 3D geometry,

Imaris (Bitplane) was used. In the next sections it will be detailed how these different analyses were performed.

3.10.1 Morphometric analysis of high magnification confocal microscopy

Images acquired with LSCM microscope were used for quantitative analysis of nuclear morphology and keratin network architecture using either 630x or 1000x total magnification, respectively.

3.10.1.1 Keratin cytoskeleton architecture

BoneJ plug-in was utilised to analyse keratin network architecture imaged at total magnification of 1000x in LSCM (LSM 710, Zeiss, Germany). Images were firstly denoised by using the “despeckle” function, filtered (FFT bandpass, 50 and 5, 5% saturation) and manually threshold. Once as binary, the “thickness” function of BoneJ was chosen to analyse the thickness and spacing of keratin bundles of each frame.

3.10.1.2 Height and cross-sectional area of Z-stacks

The quantification of nuclear height was performed by using 3D confocal microscopy. A z-spacing of 0.28μm was selected for the acquisition of X-Y frame of DAPI signal. One cell per field was imaged (Figure 3.1 A). Each frame was threshold using histogram-based method, *i.e.* Otsu’s method. Binary morphometric filters were subsequently applied: firstly an open filter and then holes filling (Figure 3.1 B). As the pixel area throughout the z-stacks roughly follows of normal distribution, the height was determined by counting the frames within the range $\mu \pm \sigma^2$ of the

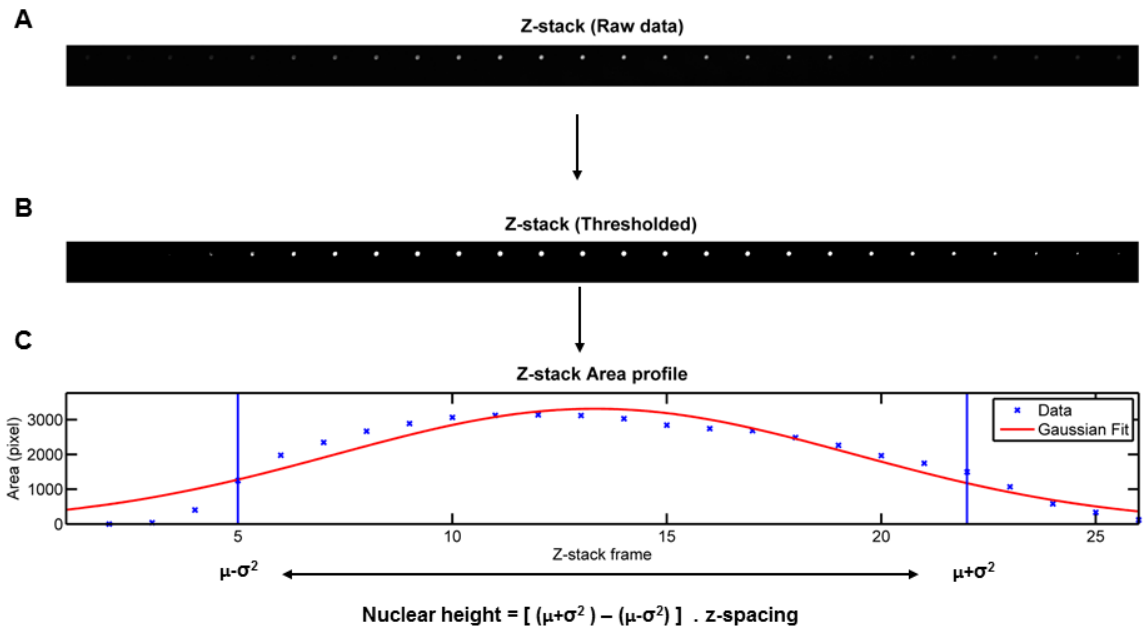

Figure 3.1 – Measuring of single cell nuclear height from confocal Z-stack using MatLab. A) Representative Z-stack of DAPI signal from a primary human keratinocyte. B) Same Z-stack after thresholding and binary filtering. C) Fitting Gaussian curve and determining the edges of the cell (represented by the blue vertical line in the graph).

fitted Gaussian curve (Figure 3.1). The maximum area was assumed to be the cross-sectional are of the profile. The algorithm is in Appendix I (page 180).

3.10.2 3D computational reconstruction and analysis (Imaris)

For the quantification of 3D geometry, 3D stacks acquired with confocal microscope (LSM 710) were processed using Imaris (Bitplane, Switzerland). Using Surpass module, a 3D ellipsoid was fit to the DAPI channel with a smoothing of 0.35μm and several characteristics of the object were extracted: volume, and geometry coefficients (*i.e.* ellipticity prolate and oblate), as well as XYZ axes length (both absolute and normalised). Validation of 3D reconstruction and accuracy of the methodology was performed by imaging 4

and 6m beads (Figure 4.3, page 86) using the same acquisition and processing parameters as for the cells.

With the intention to analyse the 3D directionality of the nucleus (crowding experiments, section 5.2.3 (page 105), the apical orientation of the nucleus was assessed by determining the sine of the longest axis of the fitted ellipsoid (*c* axis) with the X-Y plane – positive cells were assumed for angles above 45^{o} (sin (Ø) ≈ 0.71 of normalised vector).

3.10.3 Radial Profile of 2D confocal images

In order to investigate the distribution of particular markers throughout the nucleus, the radial analysis of its intensity was performed using MatLab (MathWorks, USA). This allows the analysis of the intensity distribution of a particular marker from the centre of the object (in this case the nucleus) towards its periphery. The outcome is a profile of the mean intensity (y) versus the distance from the interior of the circular object (centroid) towards the periphery (x). The validation of the algorithm (code in Appendix II, page 217), control images were generated with two different radial patterns and analysed using the script (Figure 3.2). The routine executes several steps of image processing: 1) Thresholding; 2) Filtering using binary morphometric operations; 3) determination of the centroid of the nucleus; 4) Radial analysis of the intensity and further radial averaging (*i.e.* at fixed distance from the centroid ρ, points are averaged in order to get a single value per distance); 4) Data averaging and analysis.

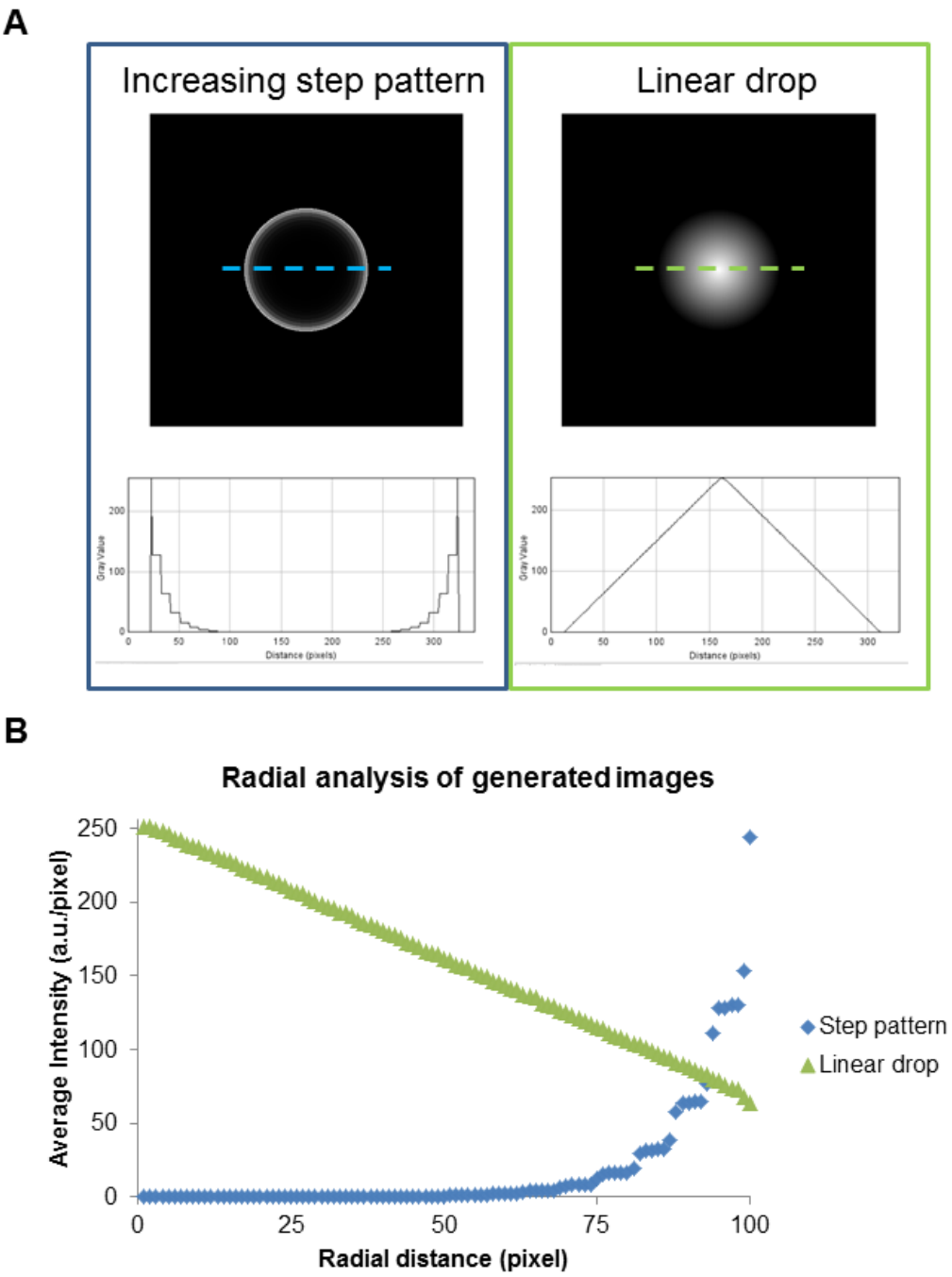

Figure 3.2 – Radial analysis algorithm validation.

1) Generated 8-bit images utilising MatLab with two distinct patterns: left, gradual step intensity pattern, right, linear increase pattern. 2) Outcome of the radial analysis algorithm developed in MatLab.

3.10.4 Manual quantification of nuclear morphology (epidermis wholemounts)

Epidermis wholemounts were imaged in confocal microscopy (LSM 710) using 400x total magnification. The quantification of 2D area of the nuclei in tissue wholemounts was performed by the “freehand selection” which allowed the delineation of each object and the extraction of its area. This approach was adopted when the distinction between objects is impossible such as in the tail skin of transgenic mouse tissue samples. Nuclei proximity does not allow a proper computational quantification as described above.

3.10.5 Morphometric analysis of low magnification

Images acquired with epi-fluorescent microscope used for quantitative analysis of nuclear morphology using 400x total magnification. For two-dimensional analysis, either ImageJ or MetaMorph software were used for the analysis of epi-fluorescent images. Both software packages allow the thresholding and subsequent filtering (binary morphometric operations), object detection and morphometric quantification. The later consisted in the measurement of each object’s area and shape descriptors (*i.e.* long and short diameter when an ellipsoid is fitted).

3.11 Atomic Force Microscopy for mechanical testing

Atomic force microscopy was used to investigate the mechanical properties of keratinocytes. This technique consists in the use of a soft cantilever with known spring constant (k) to impose a certain sample deformation (δ) and by monitoring the bending of the cantilever (d), the properties of the sample may be inferred (

Figure 3.3). Elasticity measurements are performed by pushing the cantilever into the sample and by acquiring force-distance curves (

Figure 3.3). With the intention of measuring the elastic modulus of keratinocyte's cytoplasm, JPK Nanowizard II (JPK, Berlin, Germany) was utilised. In this apparatus, the AFM is interfaced with an inverted microscope (IX-81, Olympus, Berlin, Germany), allowing the *in situ* testing of living cells.

3.11.1 Cantilever modification and calibration

MLCT triangular cantilevers were used with nominal spring constant k = 0.01N/m (Bruker, Manheim, Germany). Prior to each experiment, the cantilever spring constant was determined using thermal noise calibration. Firstly, the sensitivity of the photodiode (*i.e.* voltage-to-displacement conversion) was determined by pushing the cantilever against a hard sample (*i.e.* glass). As the cantilever is much softer than the glass, no indentation is assumed, allowing thus the conversion of the deflection (V) to distance (m). When not in contact with the sample, AFM tip oscillations are due to thermal fluctuations only, and by measuring the amplitude of these motions close to the resonance frequency it is possible to calculate its spring constant (k_c) (Hutter and Bechhoefer, 1993). The power spectral density of the fluctuations in the spring displacement has a Lorentzian line shape (Heer, 1972). The integral of power spectrum (*P*) equals the mean square of thermal fluctuations in the time-series data, and so the estimation of spring constant is determined by Hutter and Bechhoefer (1993):

$$\boldsymbol{k_c = \frac{k_B T}{P}} \qquad \textbf{Equation 3.1}$$

where k_B is the Boltzmann constant, $1.38 \times 10^{-16}\, erg.K^{-1}$ and *T* the temperature.

In order to minimise the invasiveness and plastic deformation induced by the sharp tip on living cells, a spherical coated cantilever was prepared by gluing a polystyrene bead (10μm diameter, PolySciences, France) to the very end of the tip. This is achieved by placing UV-curing glue onto a glass slide and gradually bringing the cantilever towards it, until it enters in contact with the glue. Immediately after contact, the cantilever is brought into contact with a PS bead (previously spread on another glass slide, or the same one used for the glue but away from it). Once the bead touches the glue, the cantilever is instantly lifted and let to cure under UV light for few minutes. This whole process is manually monitored by supervising the photodiode signal and the manual control of the Z-piezo.

3.11.2 Indentation testing and data acquisition

Living mouse keratinocytes were mechanically tested in normal EpiLife media (Invitrogen, UK) supplemented with 25mM HEPES buffer (final concentration) (Invitrogen, UK). Cantilever was landed on top of the cytoplasm of each cell by visual inspection and monitored using an optical microscope. Landing speed was set at 30.0μm/s and 1024 points per curve were collected, with the maximum force kept to a maximum of 2.5nN. Retraction curve was recorded with the same parameters (i*.e.* 30.0μm/s speed and 1024 sampling). Five curves were acquired per cell. At least 30 cells per condition were measured in a single experiment.

3.11.3 Data analysis

By pushing the cantilever into the sample and by monitoring cantilever deflection as the Z-piezo is moved towards the sample, it is possible to

determine sample's elastic modulus by recurring to contact mechanics principles (Figure 3.3).

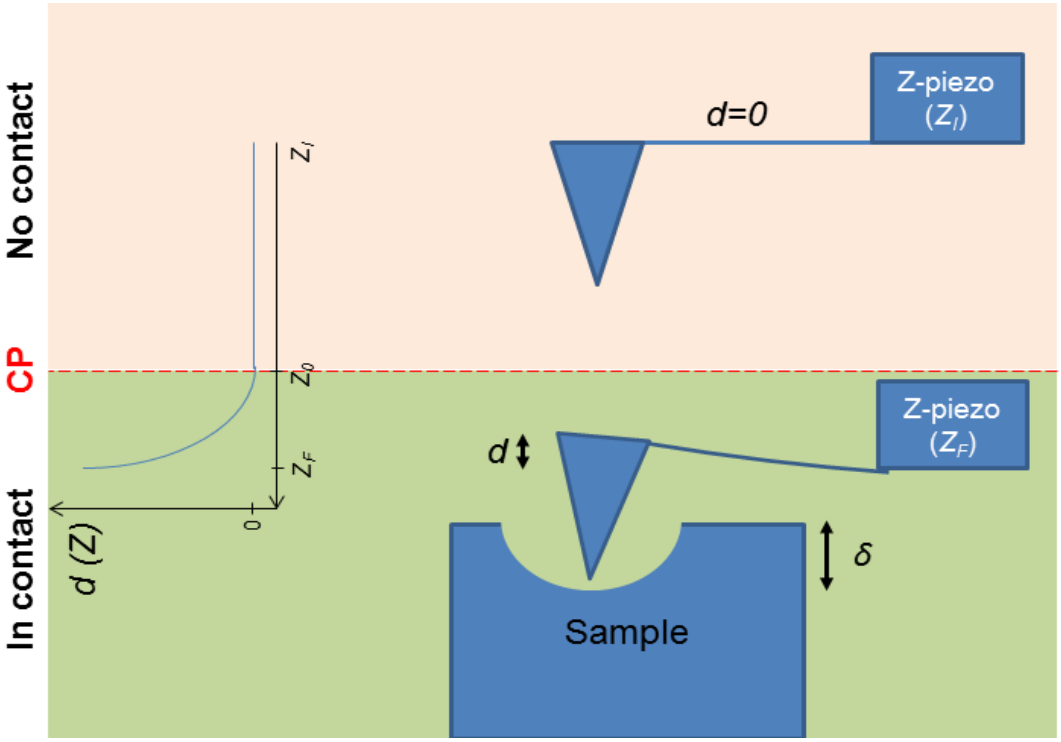

Figure 3.3 – Illustration showing the principles of AFM.

The size view of the cantilever connected to the remotely controlled Z-piezo is provided. Before contact the Z-piezo is at its initial position (Z_I). As no force is being applied to the tip at the end of the cantilever, no deflection is detected (d=0). As the Z-piezo is driven towards the sample and reaches the contact point (Z_{CP}), the static sample undergoes deformation (δ) and the cantilever bends (d>0) until a maximum depth is reached (Z_F). Illustration not drawn in scale.

The landing curve was used for the determination of elastic modulus (Vinckier and Semenza, 1998, Vinckier et al., 1996). The contact point was determined by implementing an error-based algorithm (Lin et al., 2007), consisting in several curve fittings and determination of the best fitting (minimum error).

Marching along the curve, the noncontact region is fit with a line while the latter portion is fit with a power function of the form (Equation 3.2).

$$\boldsymbol{d = d^i + b(w - w^i)^{3/2}} \qquad \textbf{Equation 3.2}$$

where *b* is the lone fitting parameter, *i* is the current iteration, and the exponent of 3/2 is characteristic of Hertzian indentation with a rigid sphere (Lin et al., 2007). The minimum sum of the mean square error (MSE) represents the best contact point and therefore used for the elastic modulus derivation. Next, sample indentation was determined by using $\boldsymbol{\delta = (z - z_0) - (d - d_0) = (z - d) - (z_0 - d_0) = w - w_0}$ Equation 3.3. and the elastic modulus derivate by$\boldsymbol{F = \frac{4ER^{1/2}}{3(1-\nu^2)}}$ Equation 3.4.

$$\boldsymbol{\delta = (z - z_0) - (d - d_0) = (z - d) - (z_0 - d_0) = w - w_0} \qquad \textbf{Equation 3.3}$$

where z_0 and d_0 represent the z-piezo position and deflection of the cantilever, respectively, at the contact point (CP).

$$\boldsymbol{F = \frac{4ER^{1/2}}{3(1-\nu^2)}} \qquad \textbf{Equation 3.4}$$

3.12 Focused ion beam cell preparation

Dual beam microscope (SEM/FIB) Quanta 3D ESEM (FEI, EU/USA) was used to mill through fixed cells for AFM imaging. Cells seeded in 20μm patterns were fixed with 4% PFA for 10 minutes and dehydrated by submersion once in gradual grades of ethanol/deionised water (*i.e.* 50,70, 90% v/v) and absolute ethanol (three times). Samples were further let to dry for a couple of minutes.

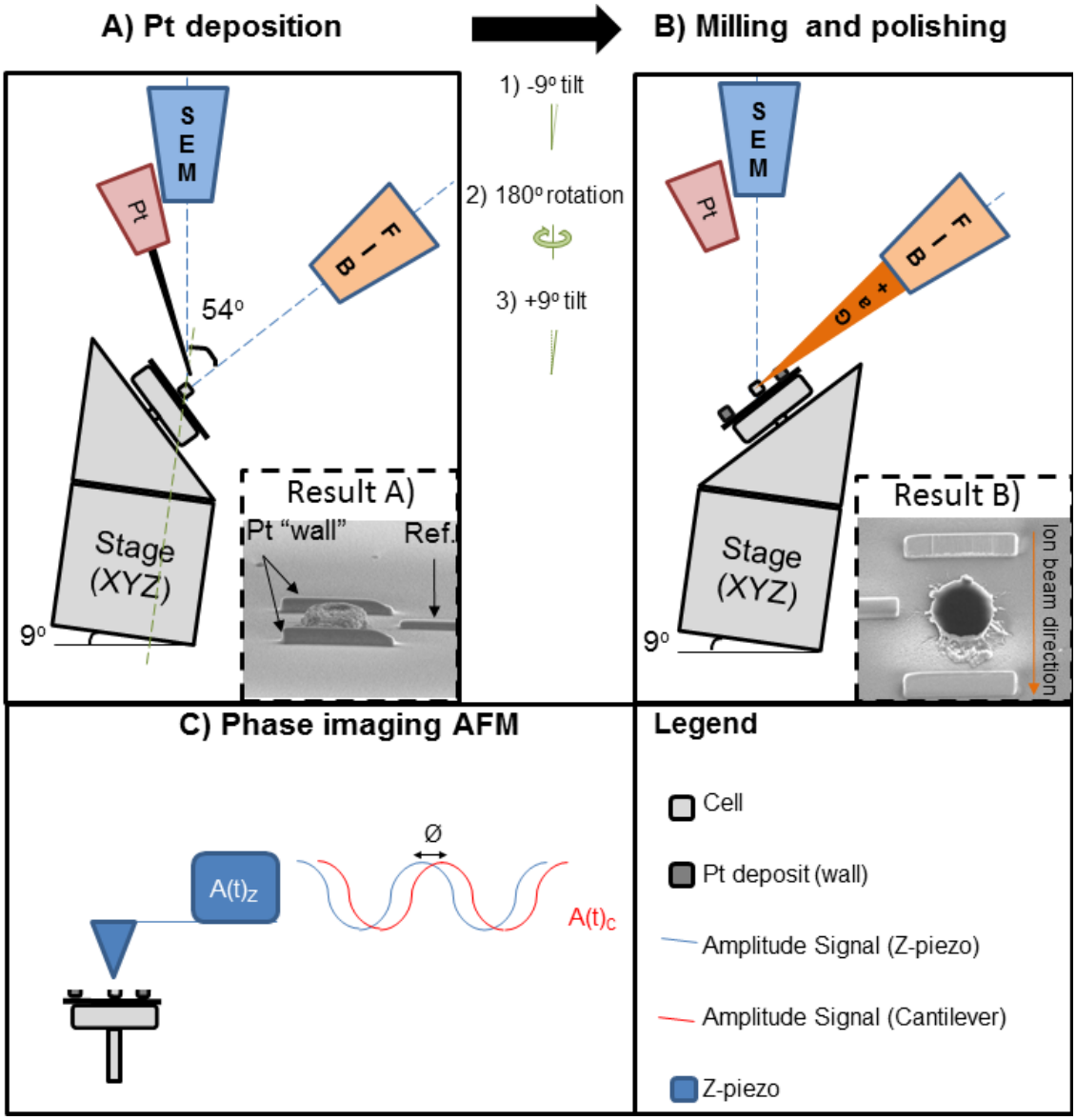

Figure 3.4 – Schematic of SEM/FIB cell preparation for phase imaging AFM.

A) **For platinum deposition of aligning and reference walls, cell is positioned to the eucentric height (10mm away from electron beam) and tilted further 9° degrees. After Pt deposition (inset image in A), sample re-tilted for original position (1), concentrically rotated 180° (2) and further tilted 9° (3). B) Milling and polishing was then performed using varying intensities. Representative result as inset image. C) Sample was then transferred to AFM and imaged in tapping mode. The phase lag [continues next page] (Ø) was recorded and used to qualitatively evaluate the roughness of the sample. Illustration is not drawn to scale.**

Using double sized carbon tape, the substrate was fixed on 12.5 mm aluminium stub (Agar Scientific) and gold-coated (CED030, Leica, Germany). The sample was then placed in a 45^{o} pre-tilted stage, loaded SEM/FIB chamber and brought to high vacuum (~5.25×10^{-4} Pa). Electron acceleration was kept as 10kV at all times in order to avoid sample heating, and the ion beam was set to 16kV for milling. The eucentric point was firstly found, consisting on the height at which the focused feature within the sample does not move as the stage is tilted. This is achieved by firstly bringing the cell to 10mm away from the electron beam and by focusing in a particular region of interest. Gradually, the tilting angle was increased and the moved feature is brought again to the original position by adjusting the Z (height) of the stage (only).

Once the eucentric point is found, the stage can be set in two different positioning essential for A) Pt deposition and B) milling and polishing (Figure 3.4). The first is a critical step for successful milling with two purposes: importantly, shields the sample (the Pt “walls”), and secondly may be used for location (Pt “reference”) - Figure 3.4 A inset. Pt deposition was achieved by landing the pre-warmed gas needle and performing the ion beam patterning of the desired features (Figure 3.4 A). It is important the current of ion beam to be kept within 2-6 nA/cm^2 for good deposition. By creating the protective Pt walls, a more precise milling is insured, and also helps the alignment of the stage tangent to the cell as they are the same height. As the cell is incredibly soft, the attempt to focus on it without the Pt walls, even for few seconds, would cause its damage. On the other hand, the Pt reference allows focusing the beam right on the cells, as the Pt walls are quite far it, another essential step for an accurate and clean milling.

Several milling conditions were experimented, as well as polishing runs. After milling, using FIB, labelling features in the pattern were performed to identify the cell. The sample was transferred to AFM for imaging within few days after milling.

3.13 Phase imaging AFM

Ntegra Spectra (NT-MDT, Russia) AFM was used to image cross-sectioned cells section 3.12. For imaging, the instrument was operated in tapping mode using 3 $N.m^{-1}$ (RFESPA-75, Bruker, USA) nominal spring constant cantilever. A 5x5µm window (256x256 resolution) was imaged per cells in order to assess its root mean square (RMS) from the topography image (height). For image analysis, NOVA (NT-MDT, Russia) software was utilised.

3.14 Statistical Analysis

All data were analysed by T-test, one- or two-factor ANOVA and Tukey's test for posthoc analysis. Significance was determined by $P < 0.05$.

Chapter 4. Actomyosin independent nuclear deformations in response to cell shape

4.1 Introduction

The shape and appearance of the nucleus is one of the main features that define its function. In histopathology, aberrant nuclei with abnormal shape and size are markers for tumour cells, a phenomenon called pleomorphism (Dey and Baloch, 2009). Within the cell, the nucleus is physically integrated with the cytoskeleton via linkage to LINC proteins and, at the plasma membrane the cytoskeleton is able to bind to the focal adhesion. This membrane-cytoskeleton-nucleus physical integration constitutes the foundation of current models in mechano-biology, which attempt to explain the ability of cells to respond to environmental cues. In such models, the nucleus is thought to respond to mechanical forces transmitted via the cytoskeleton by adapting gene expression (Costa et al., 2012, Hoffman et al., 2011, Dahl et al., 2010, Dahl et al., 2008, Ingber et al., 2014, Mammoto et al., 2012, Wang et al., 2010, Mammoto and Ingber, 2010, Mammoto and Ingber, 2009). Numerous studies have examined mechano-transduction phenomena, e.g. focusing at genetic and protein expression in response to particular mechanical stimuli, but only a few studies characterised morphological changes that the nuclei undergoes in response to cytoskeletal remodelling, in particular in human keratinocytes.

The re-organisation of the cytoskeleton is a key regulatory process in the cell. The cytoskeleton itself may form a variety of architectures within a cell, depending on its activity. Actin, one of the most investigated cytoskeletal proteins, is a key protein in several cellular processes such as differentiation, proliferation, motility and apoptosis (Brock and Ingber, 2005, Chen et al., 2003, Dike et al., 1999, Ikeda et al., 2003, McBeath et al., 2004, Straight et al., 2003,

Abu Shah and Keren, 2013, Vaezi et al., 2002). Importantly, due to its ability to polymerise and form thick and long filaments throughout the cell, it has been associated with the generation of intracellular tension and overall cell mechanics (Blanchoin et al., 2014). As these filaments may bind the membrane to the nucleus via LINC complex of proteins, some authors have rationalised that actin stress fibres may pull the nucleus laterally, causing therefore its expansion (Shivashankar, 2011). Other than pulling the nucleus, it seems that F-actin exerts compression upon the nucleus by apical F-actin. These work as cables going over the nucleus, which under tension push the nucleus towards the substrate (Khatau et al., 2009, Li et al., 2014).

Amongst tissues and cell types, the expression of cytoskeleton proteins may vary. Contrarily to F-actin and microtubules, the intermediate filaments expression depends on cell type (e.g. fibroblasts express vimentin, whereas muscle cells desmin). In keratinocytes, keratins (the most abundant IF expressed in epithelial cells) form a thick cytoplasmatic network, which contributes remarkably to their resiliency and strength (Fudge et al., 2008, Ramms et al., 2013, Seltmann et al., 2013a). Recent studies suggest a role of K14/5 structure in defining nucleus morphology throughout the epidermis (Lee et al., 2012).

Regardless of the specific mechanism, re-organisation of cytoskeleton ought to translate into nuclear deformations. To date, few studies have examined how different structures of the cytoskeleton translate into micro-scale deformations in cell shape to the nucleus. Therefore, by controlling cell shape using micro-engineered substrates and hence inducing controlled cytoskeleton re-

organisation, it is possible to precisely measure the three-dimensional nuclear morphology and the role of specific cytoskeletal components. In the current chapter it is aimed to:

1) Characterise nuclear deformations in response to adhesive area control
2) Mechanistically investigate how actin and contractility affect nuclear deformations
3) Mechanistically investigate how IF integrity affects nuclear deformations

4.2 Results

4.2.1 Adhesive area and geometry pattern regulates nuclear morphology

In both the epidermis of the skin and *in vitro* culture, individual primary human keratinocytes display a heterogeneous mixture of different cell shapes and sizes. In order to control these shapes independently of other factors and investigate directly the impact on nuclear mechano-transduction, micro-engineered substrates were used. Throughout this chapter, four different patterns were used for the purpose: circular islands of 20, 30 and 50 μm diameter, and Shape Factor 8 (SF8). The latter is an ellipse with a ratio between the large and the small axis (L/l) equal to eight, with the equivalent area of 30μm circles. Primary human keratinocytes were seeded onto micro-patterned substrates. Paraformaldehyde fixation and immunostaining followed, and individual cells were imaged by laser scanning confocal microscopy (LCSM). By looking at the DAPI channel it is evident that with the increase in pattern area the cross-sectional area of the nucleus also increases (Figure 1.1). This effect is seen in both HeLa and primary human keratinocyte cells (Figure 4.1).

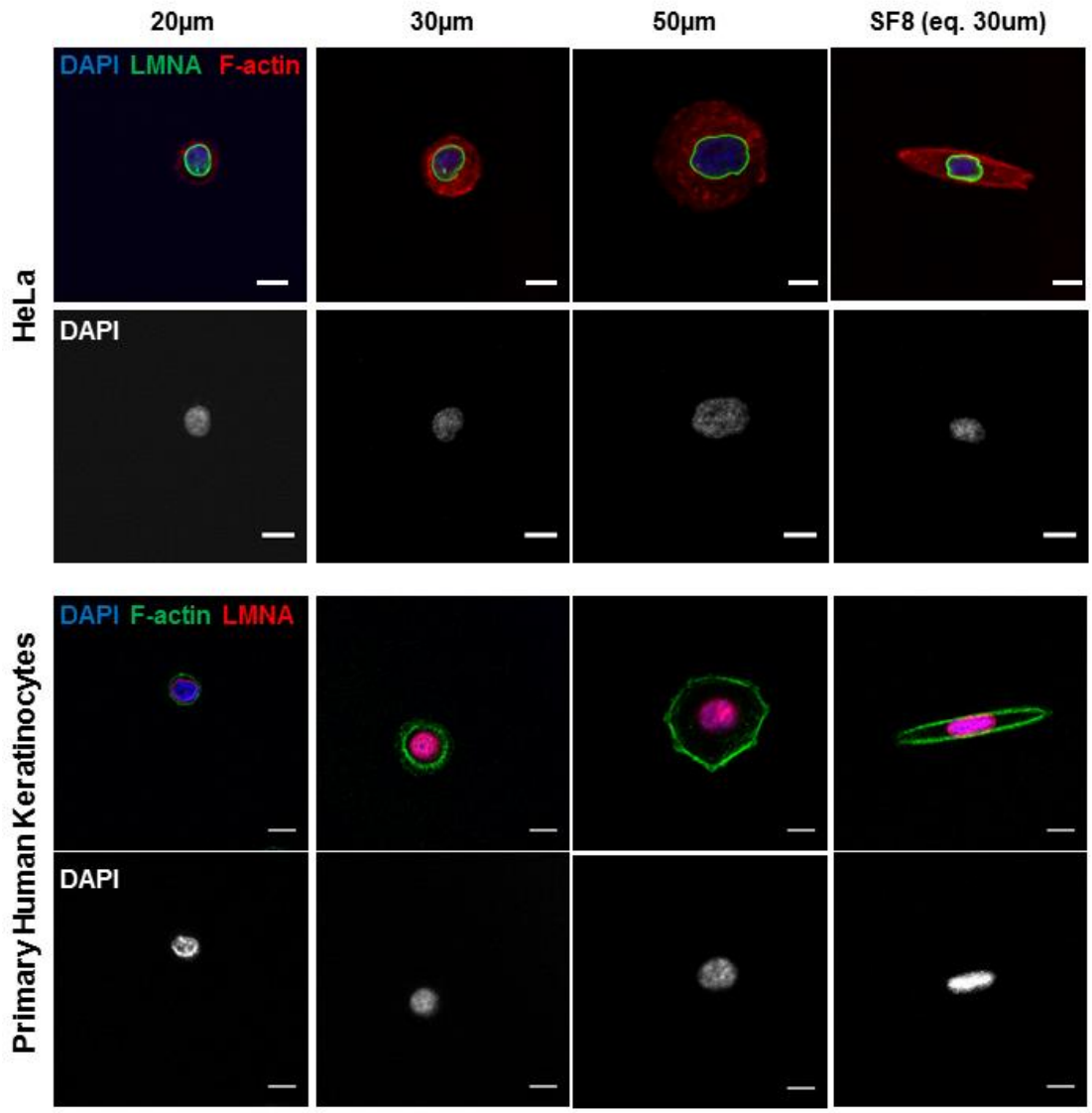

Figure 4.1. - Representative LSCM images of cells seeded onto micro-patterned substrates.

First two rows: HeLa cells labelled for DNA (DAPI dye, blue channel), nuclear lamina (Lamin A/C, green channel) and F-actin filaments (Phalloidin, red channel). Corresponding DAPI channel is shown alone in the second row in order to display the changes of nuclear cross-sectional area. Last two rows: primary human keratinocytes (pHK) cells labelled for DNA (DAPI dye, blue channel), F-actin filaments (Phalloidin, green channel) and nuclear lamina (Lamin A/C, red channel). Correspondent DAPI channel is shown alone in the second row in order to display the changes of nuclear cross-sectional area. Scale bars = 10µm.

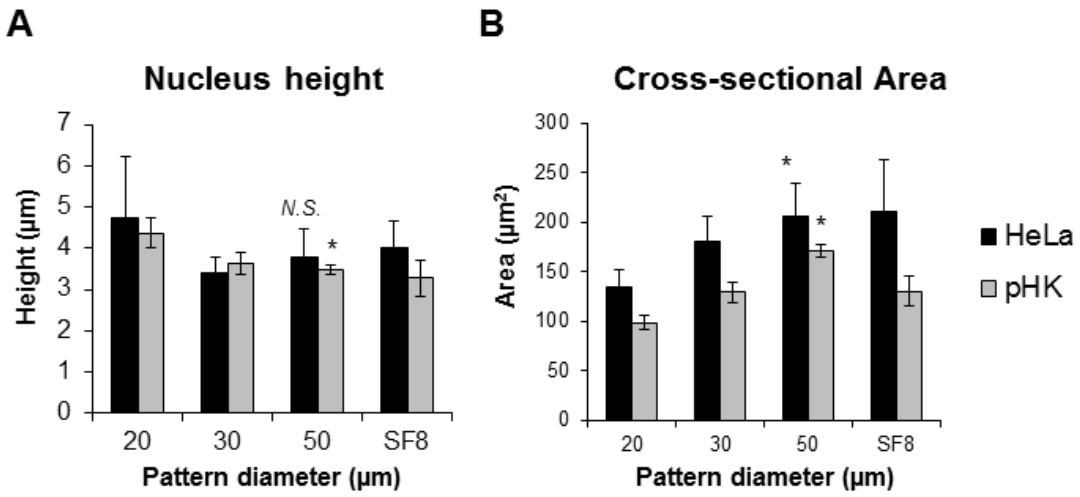

Figure 4.2. – Nuclear cross-sectional area increases dramatically in response to larger islands.

Two-dimensional quantification of HeLa and pHK nuclear morphology seeded onto micro-patterned substrates. A) Height measurements of HeLa and primary human keratinocytes using developed routine written in MatLab. (B) Quantification o the cross-sectional area. In both cases, DAPI channel was the one used for the measurements. Data represents the mean ± SEM over all measurements. * P<0.05 (Two-tail T-test, unequal variance assumed). N = 3 experiments, (37 <n < 76 cells analysed).

Nuclear height, measured by analysing z-stacks, in both cell types does not decrease dramatically from cells seeded in 20 µm islands in comparison to the 50 µm, although the cross-sectional are does increase up to approximately 40% and 60% for HeLa and pHK, respectively. This explains the increase of nuclear volume, by ~30%, in spread cells (50 µm) when compared with 20 µm (Figure 4.3. B). Furthermore, the geometry of the nucleus was assessed by fitting an ellipsoid to the entire stack (previously threshold) as exemplified in Figure 4.3. (panel A) and the ellipticity coefficients for prolate and oblate geometries were

analysed. In elongated cells (seeded on SF8 patterns) there is a significant shift from an oblate to a prolate ellipse Figure 4.3. (panel C). This result indicates that the nucleus changes from a disk-like shape towards a zeppelin-like shape when cells are forced to elongate. Furthermore, this finding confirms that the nucleus is spatially integrated within the cell, and by controlling cell spreading area *in vitro* (in a 2D substrate) it is possible to induce defined nuclear deformations.

As mentioned before, actin is one of the most studied cytoskeletal proteins in current research. Previous work, for instance in fibroblasts and endothelial cells, show that by inhibiting actin polymerisation the physical integration of the nucleus is lost, at least partially (Mazumder et al., 2010, Mazumder and Shivashankar, 2007, Versaevel et al., 2012). To determine the role of the F-actin cytoskeleton in the deformation human keratinocyte nuclei, cells were treated with two different actin-associated inhibitors: latrunculin A and blebbistatin. Prior to the experiments, different concentrations of latrunculin A and blebbistatin were tested (data not shown) and the lower concentration to cause the predicted disruption was chosen. The doses in the end chosen were coincident with those reported in the literature: 10nM for latrunculin and 50µM for Blebbistatin. Latrunculin A, which causes total disruption of F-actin polymerisation, resulted in a “collapse” of the cellular body (Figure 4.5). Cells treated with latrunculin A lacked phalloidin staining, (Figure 4.5) which indicates total depolymerisation of actin filaments. On the other hand, blebbistatin caused a total loss of stress-fibres (Figure 4.5) as qualitatively assessed by

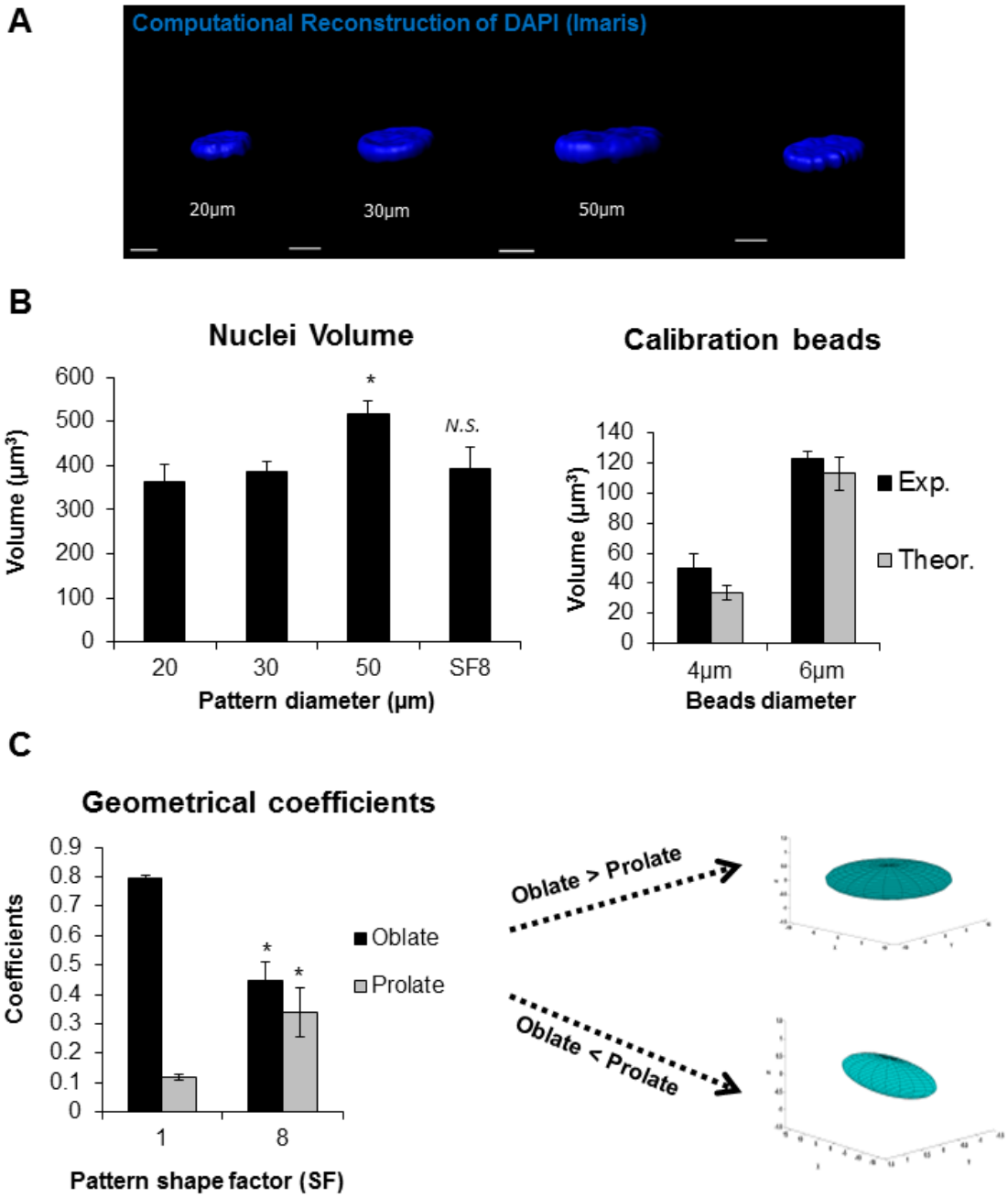

Figure 4.3. – Three-dimensional analysis of nuclei of primary human keratinocytes on micro-patterned substrates.

Cells were let to adhere and spread for approximately 4 hours and immuno-labelled for 3D confocal microscopy. A) Representative 3D reconstruction of single nucleus using Imaris (Bitplane) of cells seeded in micropatterns. B) Quantification of nuclear volume (left) and validation using polystyrene beads (right). C) Quantification of the geometrical coefficients for ellipsoid fitting using Imaris of circular patterns (SF1 = 20, 30 and 50µm) versus SF8. The bigger the prolate over oblate, the more cigar-like [continues next page]

the nuclei gets, as represented by the blue coloured 3D reconstruction (right). Data represent average of three independent experiments (N=3, 9 < n < 17 cells per experiment). Error bars represent standard error means. Levels of significance indicated with * represent *p*<0.05 of One Way ANOVA testing: in panel B, 20µm versus 50µm and in panel C, SF=1 versus SF=8.

fluorescence microscopy, although this was not sufficient to disturb nuclear deformations in spread cells as compared with control. This suggests that F-actin is required for nuclear mechano-transduction, but acto-myosin contractility is dispensable for maintaining nuclear morphology. Therefore, other structures are likely also involved in nuclear integration within keratinocytes.

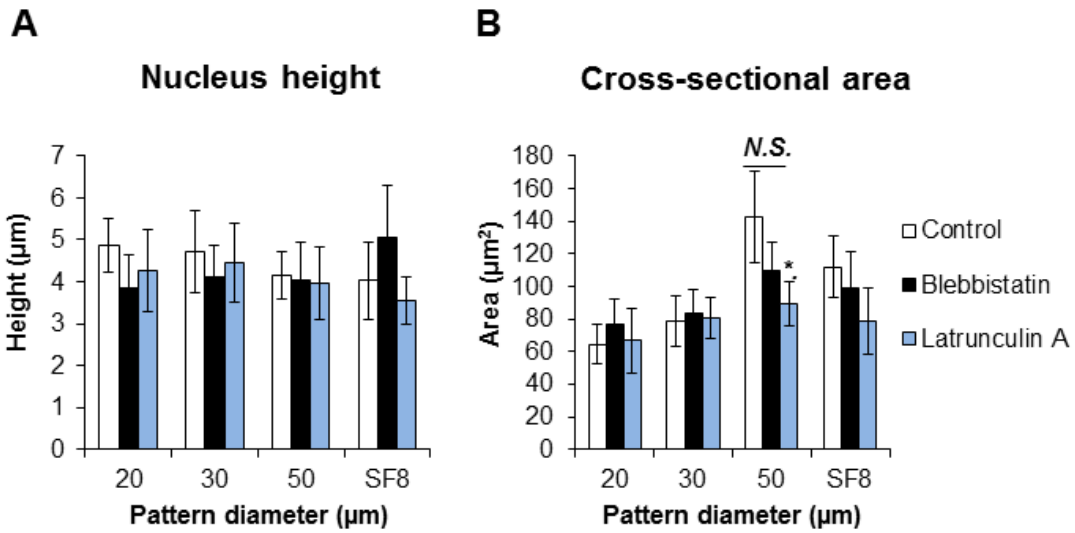

Figure 4.4. - Nuclear morphology of primary human keratinocytes depends partially of acto-myosin contractility.

Cells were seeded onto micropatterns and let to adhere for 1 h, following 3 h treatment with different cytoskeleton inhibitors: blebbistatin (50µM) and latrunculin (0.1µM). A) Nuclear height and B) cross-sectional area were quantified using LSCM. Data epresents the mean ± SEM. N=3 independent experiment,23 < n < 32 measured cells; *p<0.05.

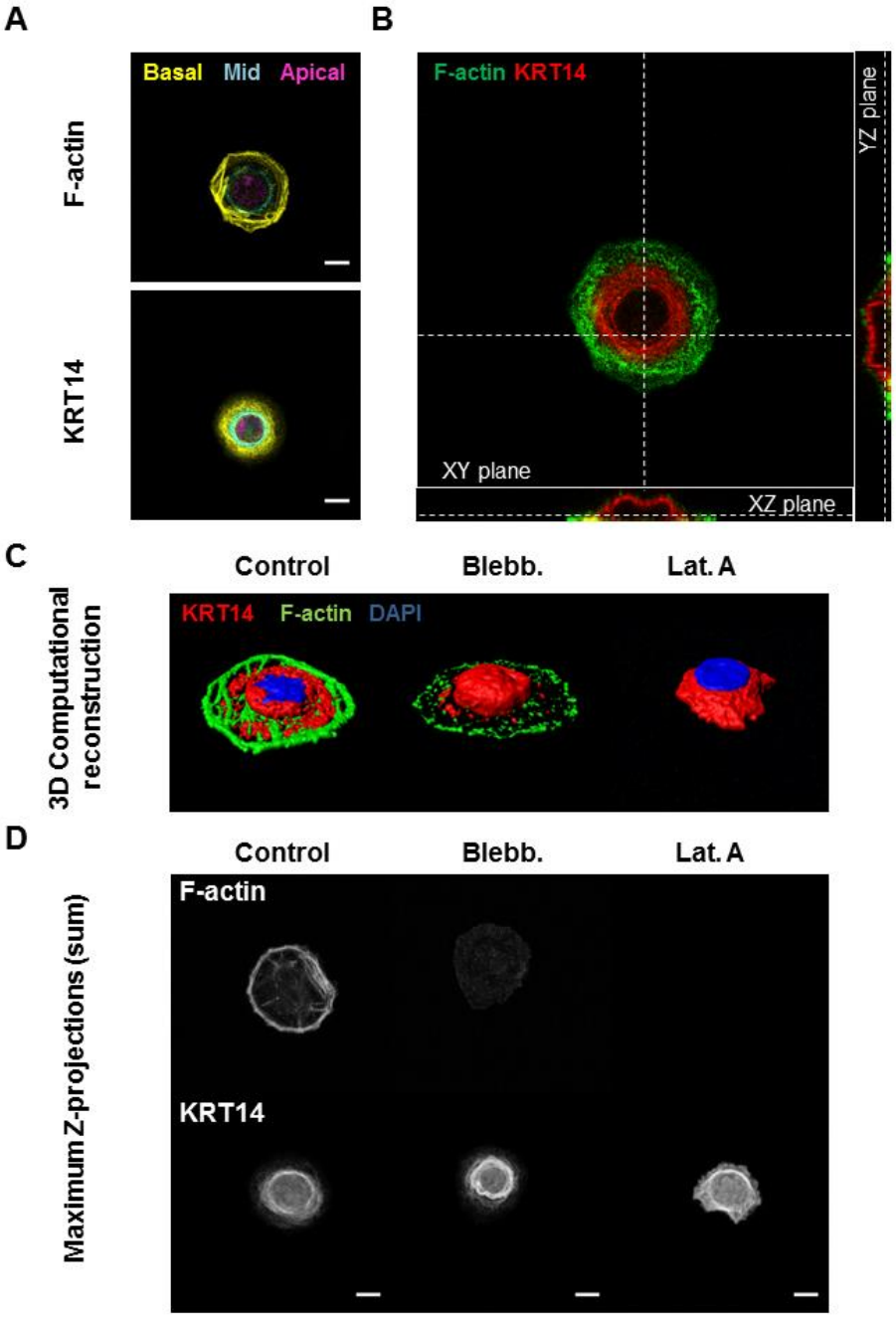

Figure 4.5. - Mechanistic analysis of 3D actin cytoskeleton and keratin 14 in human keratinocytes seeded on 50µm patterns.

A) Organisation of actin and K14 cytoskeleton throughout cell's height. B) Orthogonal view of F-actin and K14. C) 3D visualisation of F-actin, K14 and DAPI in cells treated with cytoskeleton inhibitors treatment for 3h. D) Sum Z-projections of F-actin and K14. Z-spacing = 0.28 µm. Scale bar = 10µm

The intermediate filament network of keratins is abundantly expressed in keratinocytes and important structures in mechano-transduction. Despite their role in maintaining cell mechanics, whether keratins regulate nuclear mechano-transduction is still unclear. Keratin forms a dense network around the nucleus Figure 4.5 even in the presence of actin-associated inhibitors.

Okadaic acid, a potent inhibitor of protein phosphatases (PP1 and PP2) was previously used to disrupt keratins in mouse keratinocytes (Osmanagic-Myers et al., 2006). In spontaneously immortalized human keratinocytes (HaCaT cell line), treatment with okadaic acid led to dramatic “collapse” of cells (Figure 4.6), similarly to Latrunculin A treatment, as assessed by fluorescence microscopy. Several doses and exposure times were experimented. Above a concentration of 0.25ug/mL, reduction of nuclear cross-section was observed after 4h treatments, which was accompanied by a breakdown of keratin network (Figure 4.6). Treatment of 2 hours did not cause a disruption of K14 at any of the tested concentrations. It is important to also mention that the spreading area did increased dramatically, as evident from the representative images (parameter not assessed). It is therefore concluded that hyperphosphorylation of keratins leads to a dramatic reduction of nuclear morphology and overall cell spreading as assessed by immunofluorescence. These results suggest the importance of keratins in maintaining cell integrity in keratinocytes, which consequently affects the transmission of forces to the nucleus. However, the effects of okadaic acid may be unspecific, as seronine/thyrosine phosphatases are upstream of several other cellular processes (Kiely and Kiely, 2015).

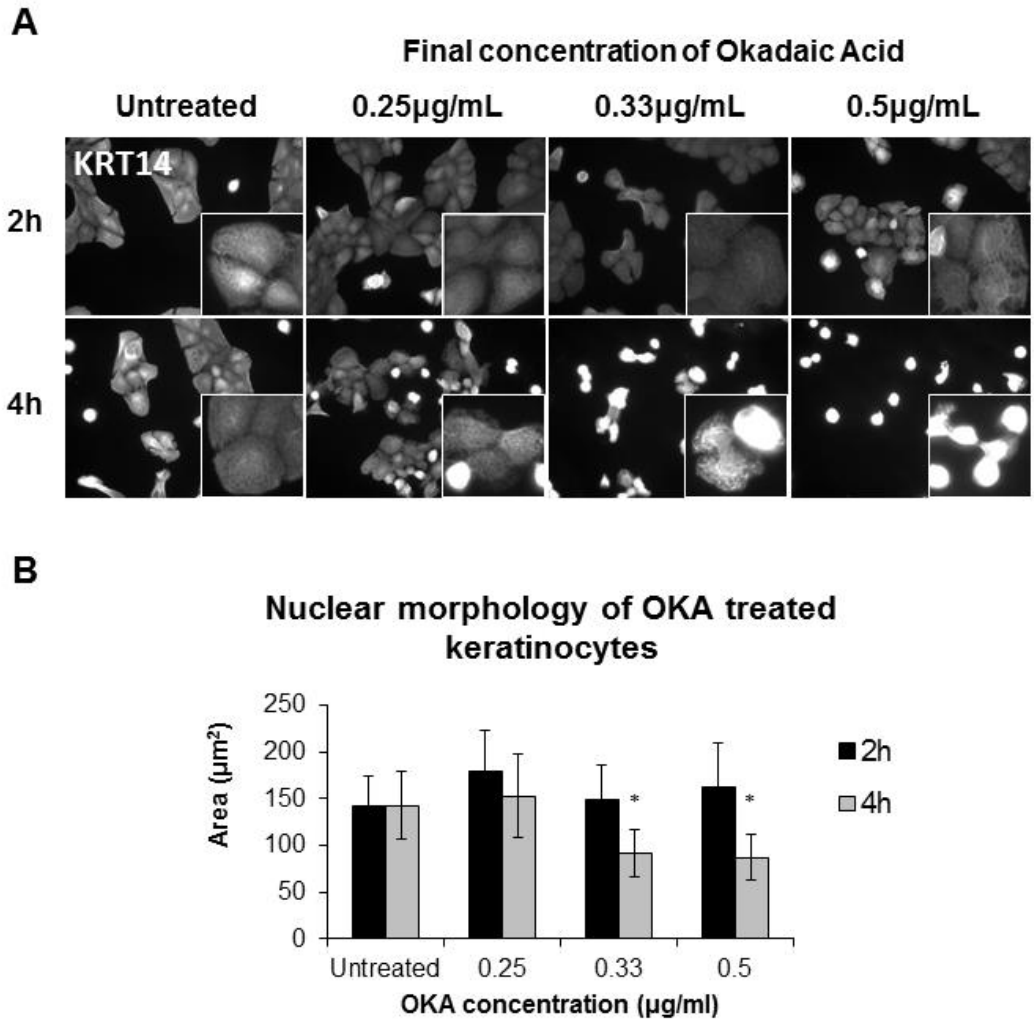

Figure 4.6. – The effects of okadaic acid (OKA) on nuclear morphology of HaCaTs.

Cells seeded onto glass coverslips were treated with OKA for 2 or 4 hours at several concentrations. A) Representative images of K14 cytoskeleton by fluorescence microscopy; zoom-in as insets. Total magnification of 400x was used for the imaging. B) Nuclear morphology (cross-sectional area) of imaged cells. Data represent the mean ± SD, 109 < n < 393 ; p<0.05 (T-test, two-tail, unequal variance assumed).

4.3 Discussion

The translation of mechanical cues into specific biological response remains poorly understood in current cellular biology. Current models in mechano-biology consider the nucleus as a central mechano-effector, *i.e.* a structure that

translates mechanical stimuli into a specific biochemical response. Deformations imposed upon the nucleus may lead to localised structural changes and therefore alter interactions between molecules. Utilising micro-patterned substrates, it was hypothesised that the control of cell shape would control nuclear morphology. Indeed, the nucleus in spread keratinocytes (seeded on 50μm islands) is bigger when compared with confined cells, and a substantial increase of ~30% volume is observed. Other authors have reported similar responses in NIH 3T3 fibroblasts, with an increase of volume as a consequence of an increase of adhesive area regardless of cell shape (Jain et al., 2013). In smooth muscle cells, both area and shape appears to affect nuclear volume (Thakar et al., 2009). In the case of keratinocytes, the nuclear volume is determined exclusively by the spreading area other than the shape of the adhesive pattern as examined by comparing round versus elongated cells with constant area.

Forces within the cell are regulated by the cytoskeleton, but the way the morphology of the nucleus is regulated is still unclear. The F-actin cytoskeleton, involved in nuclear positioning (Huelsmann and Brown, 2014), rotation (Brosig et al., 2010, Kumar et al., 2014) and division (Chircop, 2014), is thought to be the principal generator of tension upon the nucleus of eukaryotes. In the present study, with the purpose of dissecting the involvement of the actin cytoskeleton in keratinocyte nuclear mechano-transduction, different chemical agents were used eliciting distinct degrees of effects. Latrunculin was the most potent tested agent, which resulted in the structural collapse of treated cells. These cells were unable to spread and consequently the shape of the nucleus was unaffected in the testing conditions. Latrunculin depolymerizes actin filaments by binding

specifically to G-actin (the monomeric form of actin) in a molar ratio of 1:1 (Coue et al., 1987), and it is extensively used in literature (Peterson and Mitchison, 2002). The use of latrunculin lead to a complete disruption of F-actin, resulting a cell's body collapse: cells lost the ability to spread. On the other hand, the inhibition of myosin II-driven contractility (Straight et al., 2003) had no significant effect in nuclear deformation. In blebbistatin and cytochalasin D treated fibroblasts, the nuclear area and volume decreases dramatically (Mazumder et al., 2010), although in this study the authors do not account for cell spreading area. Importantly, the inhibition of F-actin alone is not enough to fully disrupt the transmission of forces to the nucleus as observed in fibroblasts (Maniotis et al., 1997). In endothelial cells, F-actin was shown to regulate lateral compression when cells are elongated in high aspect ratio patterns (Versaevel et al., 2012). Alternatively to disrupting the cytoskeleton chemically, laser ablation was utilised in another study in order to achieve a total the transmission of forces to the nucleus by shinning a high power laser over cells transfected with gold nanoparticles (Mazumder and Shivashankar, 2007). In this study, a dramatic shrinkage of the nucleus was achieved using this technique after 20 minutes of laser exposure and the structure of all cytoskeleton proteins was crudely disrupted. This technique needs further validation as possible stress to the cells due to high power laser and eventual thermal excitation may be induced, and the observed results being in reality due to cell stress.

Although the synergistic interactions between F-actin and IFs remain unclear, there is an agreement that actin and intermediate filaments are important biomechanical determinants in keratinocytes (Bordeleau et al., 2012, Ramms et al., 2013, Seltmann et al., 2013a). Interestingly, treating these cells with

calyculin A or acrylamide, analogous to OKA treatment, caused an opposite response to any of the F-actin inhibitors: in cells seeded in elongated patterns, the elongation of the nucleus was even more pronounced than untreated cells (Versaevel et al., 2012). This shows that IFs are likely to be involved in the transmission of forces towards the nucleus, as earlier defended by Maniotis et al. (1997). The disruption of F-actin by the use of cytochalasin D in combination with nocodazole (MT disrupting agent) did not block the transmission of forces towards the nucleus. Using AFM and optical trap, the authors investigated the mechanical implications of the loss of keratins in mouse keratinocytes by measuring the elastic modulus of keratins mutant cells. In keratinocytes lacking all keratins (*KtyI*$^{-/-}$), decreased elastic modulus was measured when compared with WT cells (Ramms et al., 2013, Seltmann et al., 2013a). In addition, the relative decrease of cell stiffness upon latrunculin A was the same between WT and *KtyI*$^{-/-}$ (Seltmann et al., 2013a). This suggests that F-actin and keratins are mechanically distinct and that cells overall stiffness is defined by the sum of the two. However, judging by the figures provided, the authors did not achieve total actin depolymerisation. A better disruption of F-actin would be ideal in order to prove the effects of latrunculin in cell mechanics, and the actin levels proven by immunocytochemistry or Western immunoblotting. In fibroblasts, vimentin contributes mainly to cytoplasmic stiffness, whereas actin dominates cortical stiffness (Guo et al., 2013). The simplistic model proposed by Ramms et al. (2013) and Seltmann et al. (2013) does not account for the special organisation of keratins and actin, nor the volume fraction of these. Importantly, most of these studies do not account for the viscoelastic behaviour of these structures, which may naturally lead to measuring errors and unrealistic observations.

Actin is necessary for cell integrity and nuclear deformation, although myosin II contractility appears to not have an effect, which suggests that the generation of tension is not required for nuclear deformations in keratinocytes. As there is a fine interdependent cross-talk between various cytoskeleton structures (Huber et al., 2015), it is hypothesised in the current study that IFs are also involved in the generation of forces towards the nucleus. In fact, upon actin disruption, both latrunculin and blebbistatin treatment led to changes in K14 architecture. A recent study has shown that keratins are up-regulated upon actin disruption via latrunculin treatment in MSCs in a matter of minutes (Chang et al., 2014), although this could be due to the activation of several different signalling pathways which are possibly affected e.g. SRF. This may consist of a biomechanical compensatory pathway, in which cells upon absence of a particular cytoskeleton protein may express another in order to ensure its mechanical integrity. Naturally, further investigations are required in order to assess such speculation. Nevertheless, it would be interesting the use of super-resolution image analysis and advanced imaging techniques for a closer inspection keratins organisation upon actin disruption (Portet et al., 1999, Vassy et al., 1996).

In order to perturb keratins, okadaic acid (OKA) treatment in keratinocytes was performed, which caused a complete collapse of cell body and loss of cell adhesions: evident reduction of spreading area and nuclear cross-sectional area. In accordance with the present results, hyperphosphorylation leads to drastic morphological changes in keratinocytes, which is marked by an accumulation of keratins around the nucleus (Kasahara et al., 1993). OKA treatment was also used in wound healing experiments *in vitro* with HaCats (i.e.

scratch assay). This treatment affected drastically cell morphology, migration and proliferation (Ruzsnavszky et al., 2013). In fact, protein phosphatase 2A (PP2), one of the targets of OKA, is involved in a plethora of signalling pathways, affecting numerous cell processes. Together with PP1, PP2 is responsible for up to 90% of all serine/threonine activity in a cell, including those that regulate the cell cycle, cell metabolism, cell migration and cell survival (Arroyo and Hahn, 2005, Eichhorn et al., 2009, Westermarck and Hahn, 2008, Janssens and Goris, 2001, Kalev and Sablina, 2011, Perrotti and Neviani, 2013, Schonthal, 2001, Seshacharyulu et al., 2013).

In summary, utilising micro-patterned substrates it was possible to control nuclear morphology of keratinocytes in a reproducible manner, which allowed us to dissect how specific cytoskeletal components regulate nuclear deformation. F-actin is required for cell spreading and maintenance of nuclear morphology, but acto-myosin contractility is dispensable. The disruption of keratins was achieved via OKA treatment, which also hampered cell spreading and nuclear expansion. This inhibitor, however, is likely to target several other signalling pathways within the cell. Alternative strategies to more specifically target keratins are next employed in order to investigate their role in nuclear mechano-transduction.

Chapter 5. Plectin regulates keratin network architecture and nuclear mechano-transduction

5.1 Introduction

While the actin cytoskeleton and LINC complex control nuclear mechano-transduction for some cell types (Li et al., 2014; Versaevel et al., 2012), the role of intermediate filaments in force transmission to the nucleus is less clear. In epidermal keratinocytes, the keratin cytoskeleton contributes significantly to overall cell rigidity and could potentially influence nuclear mechano-transduction (Kröger et al., 2013; Ramms et al., 2013; Seltmann et al., 2013). Mutations in keratins lead to a range of phenotypes affecting the physical integrity of epithelial tissues, one of the most common diseases being epidermolysis bullosa simplex (EBS). EBS is associated with four different genes: *KRT5*, *KRT14*, *BPAG1* and *PLEC*. In vivo phenotypes associated with *PLEC* mutations are similar to those observed in K14/5 mutations, consisting of 8% of EBS cases (Bolling et al., 2013).

Plectin has a great affinity to the heterodimeric K14/5 quaternary structure (Bouameur et al., 2014) and stabilises hemidesmosomes in a calcium-calmodulin dependent fashion (Litjens et al., 2006, Song et al., 2015). The loss of plectin in keratinocytes affects their keratin network architecture, which impacts other processes such as motility (Osmanagic-Myers et al., 2006). Although, how these structural changes define the mechanics of living cells is still unclear. A recent study has shown that *Plec* KO cells are stiffer than WT in keratinocytes, whereas in myoblasts WT cells are stiffer than *Plec* KO (Bonakdar et al., 2015). In the same study, the authors demonstrate that the forces imposed to the underlying substrate follows the same trend and stiffer *Plec* KO cells have accelerated motile velocity, in agreement with previous

wound healing experiments (Osmanagic-Myers et al., 2006). Further mechanical characterisation of cytoplasm properties of plectin mutant cells would help understanding the role of plectin in the overall mechanics of the cell, information that can be useful to understand nuclear mechano-transductive events.

As previously shown (Chapter 4), the nuclear morphology of pHK is dependent on actin polymerisation, although not on actomyosin contractility (Figure 4.4). On the basis that keratins do also contribute to keratinocytes mechanics, it is herein hypothesised that structural changes introduced by the loss of plectin in keratin network alter the transmission of forces to the nucleus and consequently its morphology. To experimentally test this hypothesis, the *Plec* KO model is used in the following studies:

1) Investigate the impact of plectin on keratin structure.
2) Understand how the disruption of keratins affects nuclear mechano-transduction and single cell mechanics, as well as how nuclear morphology in multi-cellular context is determined by plectin.
3) Study how the establishment of calcium-dependent junctions regulates nuclear morphology in cell monolayers.
4) Examine the nuclear morphology in migrating cells
5) Determine the role of plectin in regulating nuclear morphology in vivo

Furthermore, the replication of *Plec* KO phenotype is attempted in pHK by transient transfection with plectin small-interfering RNA pool. Following the seeding of single siRNA knockdown cells on micro-patterned substrates, the nuclear morphology and keratin structure were assessed.

5.2 Results

5.2.1 Plectin regulates K14 architecture in mouse keratinocytes

Keratin 14 is abundantly expressed in basal keratinocytes. Mutations in plectin are known to affect keratin architecture in keratinocytes, although impact of the absence of plectin upon keratin network has not been quantified. At high magnification (total of 1000x), K14 network assembles into a trabecular-like lattice (Figure 5.1). Qualitatively, *Plec* KO mouse keratinocytes possess a more open network with wider spacing between bundles in comparison with WT cells, as assessed by confocal microscopy. In order to characterise these changes in morphology, “thickness” analysis was performed using BoneJ (Doube et al., 2010) plug-in for ImageJ on high magnification images (Figure 5.2) following a pre-processing routine (i.e. de-noising, filtering and thresholding), as illustrated in Figure 5.2 A. The K14 network in WT forms is denser (smaller spacing) than *Plec* KO, although the thickness of the bundles is similar. Plectin therefore regulates the architecture of K14 in mouse keratinocytes.

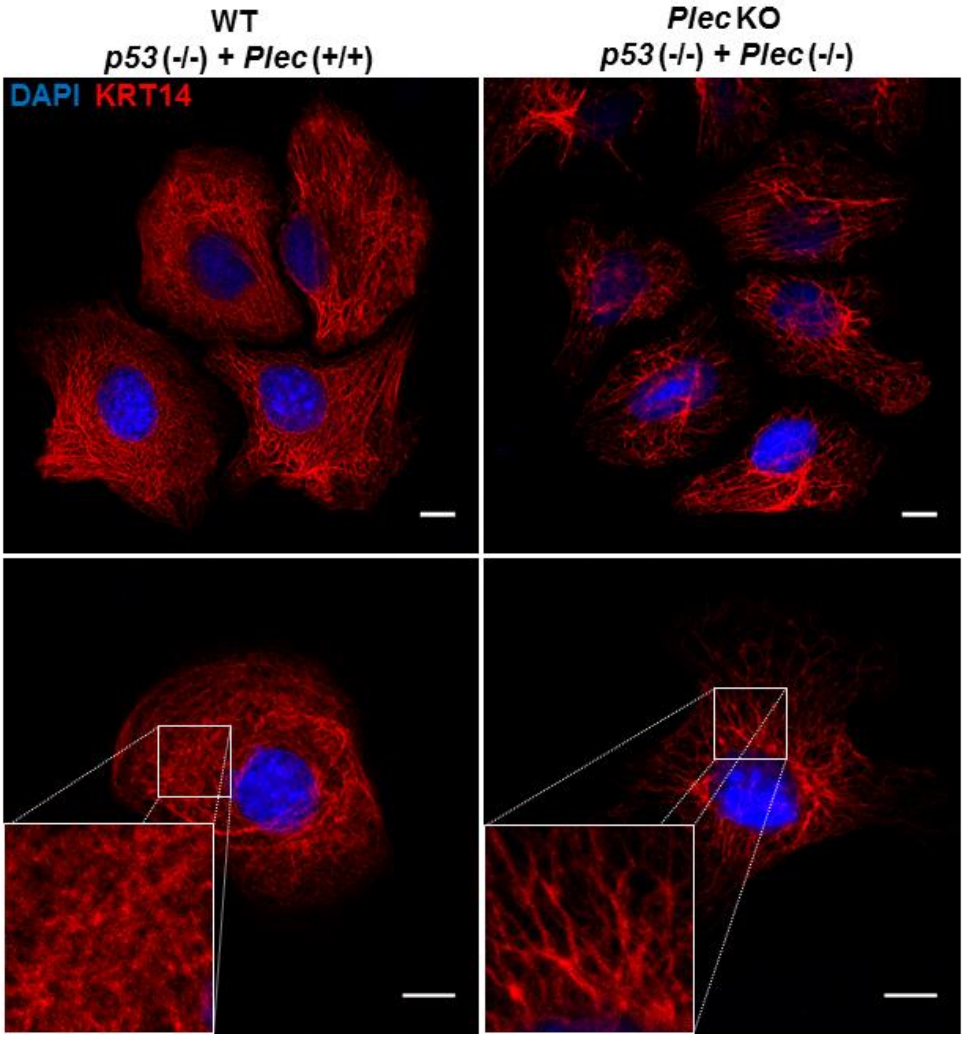

Figure 5.1 – Plectin regulates K14 architecture in mouse keratinocytes.

Representative images of mouse keratinocytes isolated from transgenic mice (p53 -/-) seeded in collagen type I coated glass substrate. Left column: in upper panel, colony of WT cells (*Plec* +/+) and bellow a high magnification of single cells; Right column: colony of *Plec* KO cells and bellow a high magnification of single *Plec* KO cells. Inset is displayed for closer inspection of trabecular-like K14 architecture. Scale bar: 10µm).

Whether these structural differences define keratinocyte mechanics is still controversial. Therefore, Atomic Force Microscopy (AFM) was utilised in order to characterise the mechanics of these cells. The deflection of the cantilever is

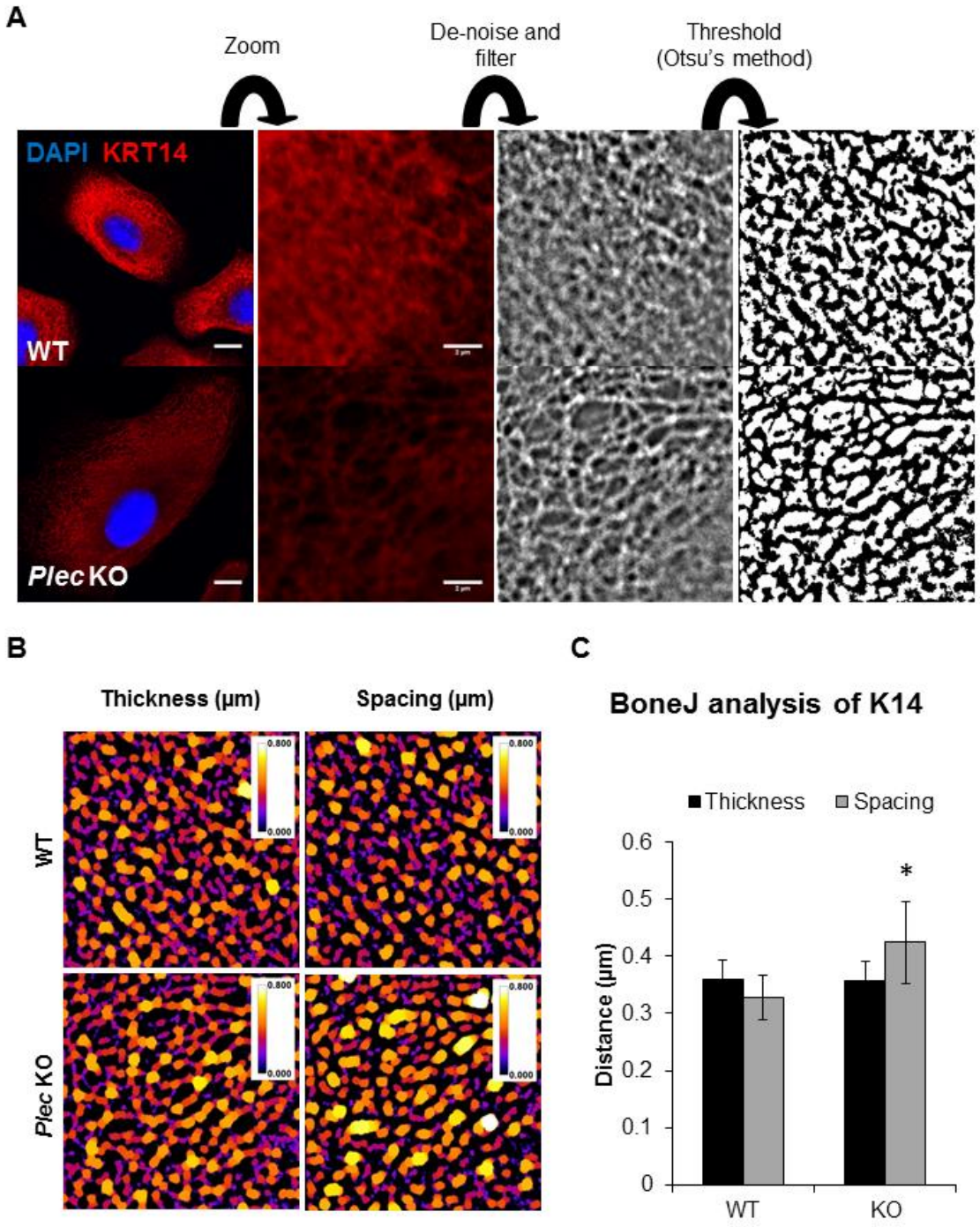

Figure 5.2 – Plectin cross-links K14 network.

A) Step-by-step image processing performed before "Thickness" analysis using BoneJ software (Doube et al. 2010), which returns two distinct parameters of the trabecular-like pattern: thickness and spacing. B) Output map of K14 thickness and spacing between bundles of the above cells. C) Quantification of thickness and spacing parameters returned by BoneJ. Data represents mean ± standard deviations. * represents significance of $p<0.05$ (two-tail T-test, unequal variance assumed, n=10 cells).

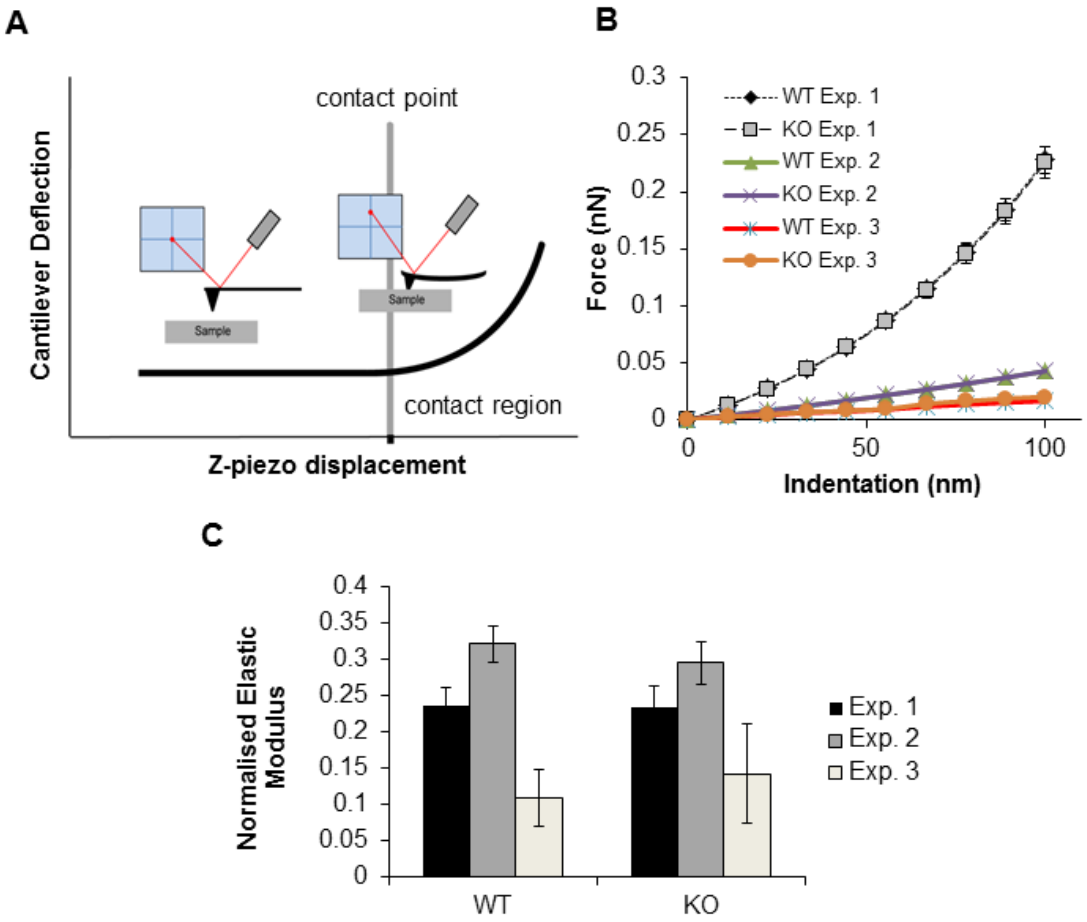

Figure 5.3 – Cytoplasm mechanics using AFM led to unreproducible results.

A) Illustrative scheme of a characteristic force-displacement curve utilised to prove the mechanics of keratinocytes cytoplasm. The bending of the cantilever is proportional to the force applied to the sample and therefore used to determine the elastic modulus. B) Average of interpolated force-indentation curve of WT and *Plec* KO keratinocytes as proved in three independent experiments. C) Average of normalised elastic modulus of WT and *Plec* KO cells demonstrating measurements variability. Experiment-to-experiment variations overcome the differences between WT and *Plec* KO. Data represents the mean ± SEM over all measurements.

recorded as the Z-piezo displacement is accurately controlled, being possible to calculate the elastic modulus of the sample as the contact area may be predicted. The variability from experiment to experiment was higher than the differences between WT versus *Plec* KO cells (Figure 5.3 B). Overall, there

were no significant differences in the normalised elastic modulus (normalised by the maximum modulus of each independent experiment), between WT and *Plec* KO keratinocytes (Figure 5.3 C), suggesting that the mechanics of the cytoplasm of these cells is similar.

5.2.2 Plectin regulates nuclear morphology

Next, the implications of the abnormal K14 network in defining nuclear morphology were assessed. As before, cells were seeded in collagen type I micro-patterned islands of 20, 30, 50μm diameter, as well as SF8. Using the DAPI staining for quantification of nuclear morphology after 4h seeding, 2D and 3D analysis was performed, in accordance with the methodology (section 3.10.2,page 68). When spread, *Plec* KO cells possessed larger nuclei when compared with the WT cells, and when elongated the longest axis of the nucleus was significantly larger (Figure 5.4 B and C). This suggests that the nucleus of *Plec* KO is more deformable when compared with the WT.

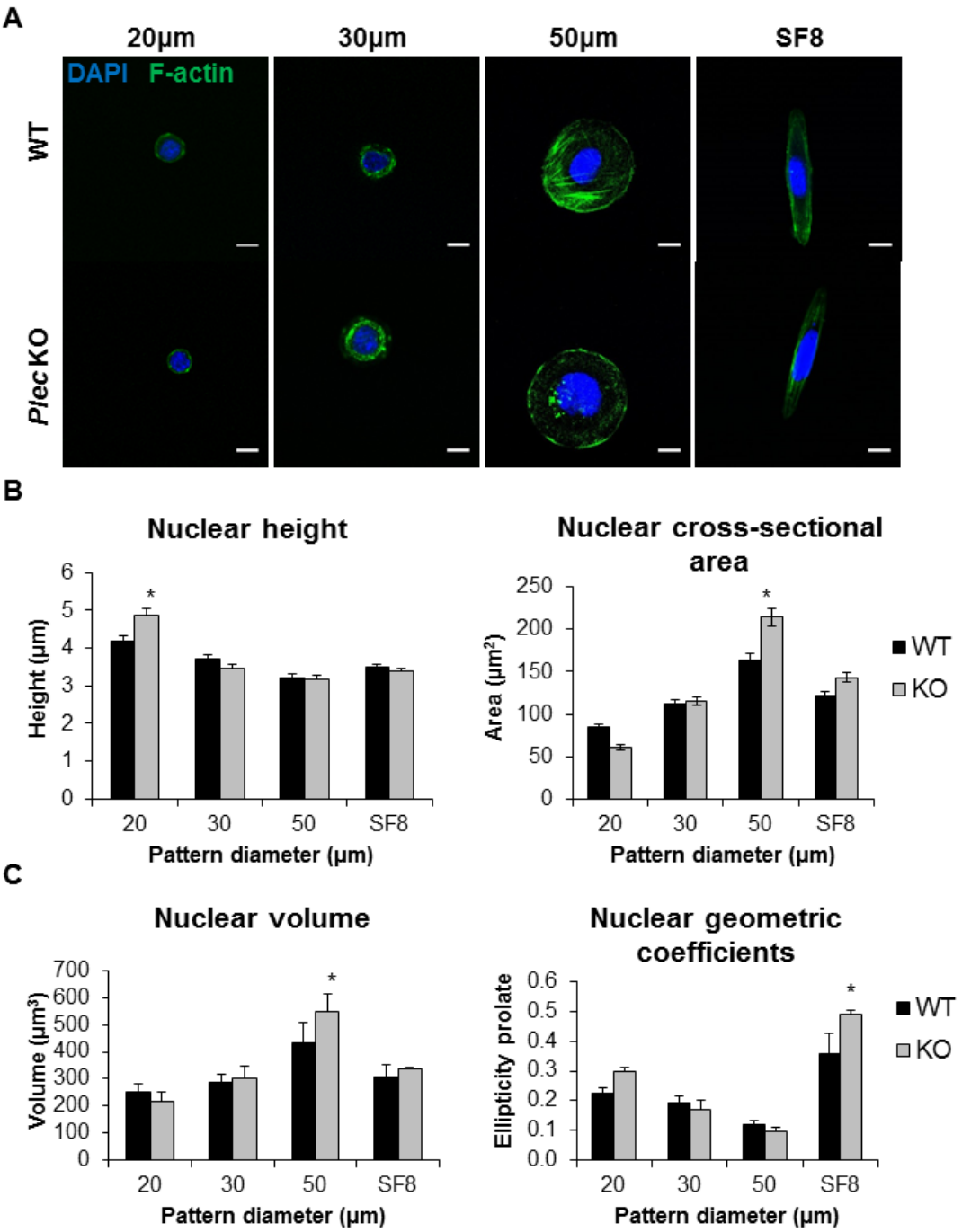

Figure 5.4 – Plectin regulates nuclear morphology of single keratinocytes.

DAPI and F-actin visualisation of A) WT (first row) and *Plec* KO (second row). Scale bar 10µm. B) WT and *Plec* KO nuclear height on the right; cross-section on the left. C) WT and *Plec* KO nuclear volume and geometric coefficients. Data represents the mean ± SEM of all measurements;* represents significance of $p<0.05$ (two-tail T-test, unequal variance assumed). $N=3$ (independent experiments), n≥10 cells per experiment.

5.2.3 Plectin influences cell crowding and nuclear morphology in cell aggregates

In vivo, keratinocytes form a continuous stratified epithelium in which cells are connected to each other via cell-cell adhesions. In addition to single cell adhesion and spreading, the role of plectin in regulating nuclear morphology in multi-cellular structures was investigated. The rationale behind it was to create a micro-environment with controlled ECM area that would accommodate variable number of cells and test the ability of these cells to compact together. 200 μm islands were chosen for the purpose as they may accommodate duzens of cells and were easy to fabricate. WT and *Plec* KO cells were seeded onto these 200 μm islands at either low (37,500 per cm^2) or high (225,000 per cm^2) densities, given 2 hours to adhere to the substrates, plus 3-4 more hours to spread. At low density (minimum to completely cover the micro- pattern), similar number of cells per micro-patterned were observed, whereas at higher density there were significantly more *Plec* KO cells per pattern (Figure 5.5 B).

The 3D nuclear morphology was further assessed by fitting an ellipsoid in 3D (Figure 5.5). Both the volume and the orientation of the nucleus were determined in the cluster of cells. The nuclear volume of *Plec* KO cells at high density was also significantly smaller than at low density. The density had no effect on the nuclear volume of WT cells (Figure 5.6 A). Intriguingly, the nuclei of *Plec* KO cells were more elongated in the apical direction (Z axis) compared to the WT cells at both densities (Figure 5.6 B). These results indicate that plectin is indeed important for cell density sensing. In the absence of plectin, keratinocytes are more sensitive to cell crowding, which in turn affects cell

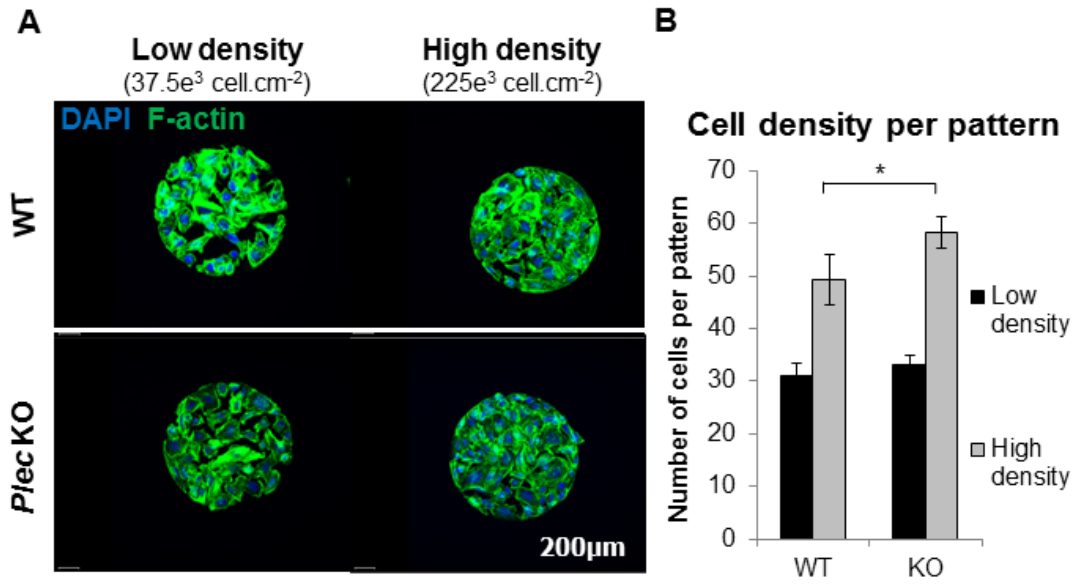

Figure 5.5 – Colony of mouse keratinocytes seeded in large micro-patterns at low and high density.

A) DNA and F-actin visualisation of WT (top row) and *Plec* KO (bottom row) at low (37,500 cells per cm^2) and high density (225,000 per cm^2). B) Quantification of the number of cells per 200µm island (200µm in diameter). Bars represent means and error bars the standard error mean of all measurements;* represents significance of $p<0.05$. $N=3$ (independent experiments). Scale bar 30µm.

packing and nuclear deformation, and may reflect defects in the keratin cytoskeleton and cellular mechanics.

5.2.4 The formation of cell-cell junctions restores nuclear morphology of *Plec* KO keratinocytes

In vivo, keratinocytes form cell-cell junctions, such as adherens junctions and desmosomes, which regulate cell shape and cytoskeleton architecture. By adding 1.8mM calcium to the media of confluent monolayer of keratinocytes, the nuclear morphology was quantified in *Plec* KO and WT. Interestingly, the recruitment of E-cadherin to the cell periphery and formation of cell-cell

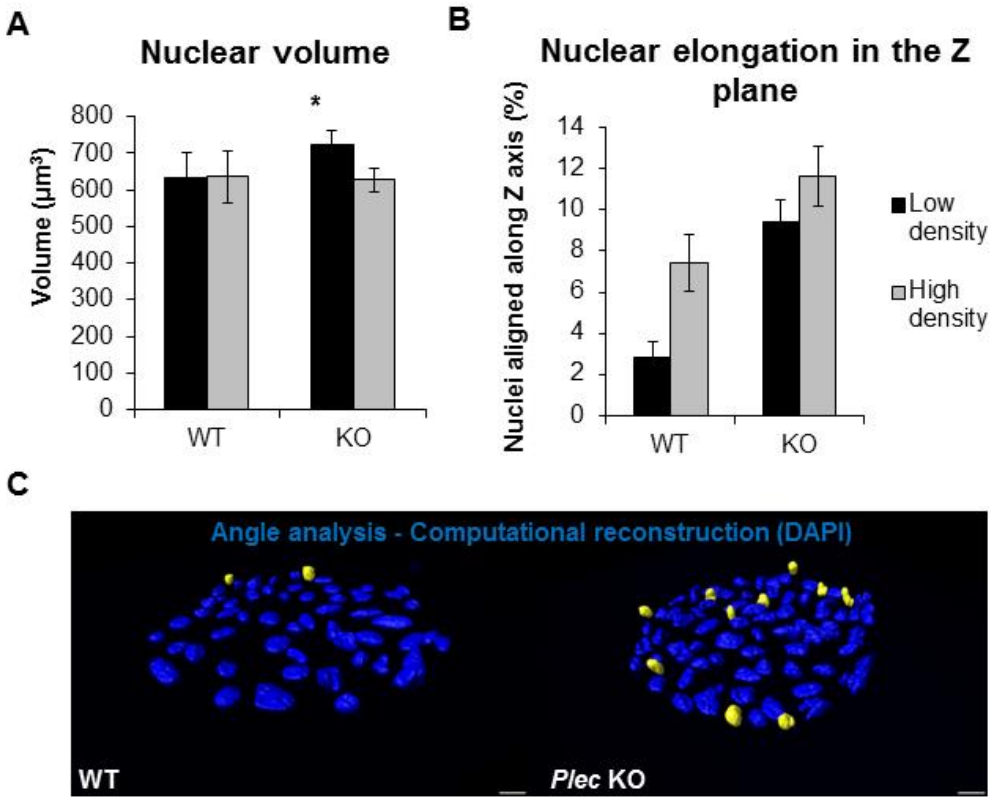

Figure 5.6 – Plectin regulates 3D morphology and orientation of mouse keratinocytes colonies.

A) **Quantification of nuclear volume. B) The percentage of nuclei preferentially elongated in the Z-axis (angle of major axis 45^{o} above XY plane). C) Representative 3D reconstruction of DAPI stained nuclei. Yellow nuclei show those preferentially aligned with Z-axis. Data represent mean ± SEM. N=3 experiments, n ≥ 300 cells per experiment. *P < 0.05 comparing WT versus *Plec* KO at particular density. Scale bar 30µm.**

junctions after 24h led to the loss of differences between *Plec* KO and WT cells, as maintained in the controls (Figure 5.7). This suggests that the phenotype observed in *Plec* KO keratinocytes seeded in planar substrates is dependent on the dissociation of cell-cell junctions.

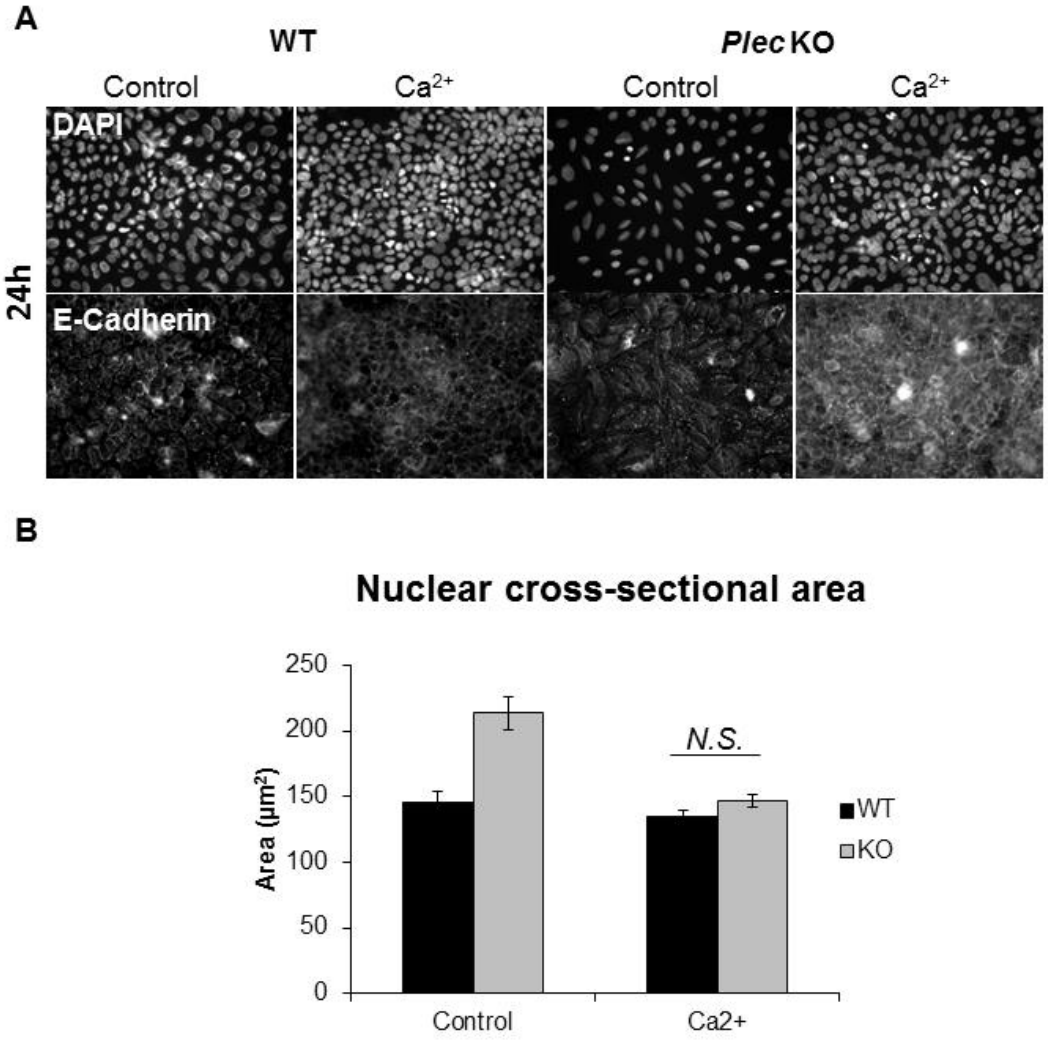

Figure 5.7 – Formation of calcium-dependent junctions restores nuclear morphology in *Plec* KO mouse cells.

A) Representative images of WT and *Plec* KO monolayer of cells treated 1.8mM of calcium for 24h and control. Formation of adherens junctions were monitored by immuno-labelling against E-cadherin (lower row). B) Quantification of nuclear cross-sectional area. Data represents mean values ± SEM. *N.S.* represents significance levels $p>0.05$ (two-tail T-test, unequal variance assumed). $274<n<920$ cells measured. Total magnification 200x.

To investigate the plasticity and dynamics of nuclear deformation, the previously developed dynamically adhesive micro-patterns were used (Costa et al., 2014). This technology consists in an *in vitro* wound healing assay. Keratinocytes were seeded in 200µm clusters (as before) and released from the micro-patterns. The migration was induced by functionalising the surrounding brushes with collagen type I mimetic peptide (*i.e*. GFOGER) (Reyes and García, 2003) using the thiol-yne coupling reaction (Costa et al., 2014). Cells migrated outwards from the pattern and as they spread, the expansion of the nucleus was analysed (Figure 5.8). Nuclear cross-sectional area remained relatively constant in WT cells migrating onto the functionalised surface, in agreement with the static crowding experiment (section 5.2.3), showing that in WT cells the nuclei are less susceptible to deformation. In contrast, *Plec* KO nuclei expanded as cells migrated. After 6 hours from GFOGER activation, the nuclei of *Plec* KO cells were significantly larger than the WT cells (Figure 5.8 B). These results indicate that reduced nuclear area caused by cell crowding in *Plec* KO cells (time 0h, where cross-sectional area of WT and *Plec* KO are equal) is reversible (Figure 5.8 B).

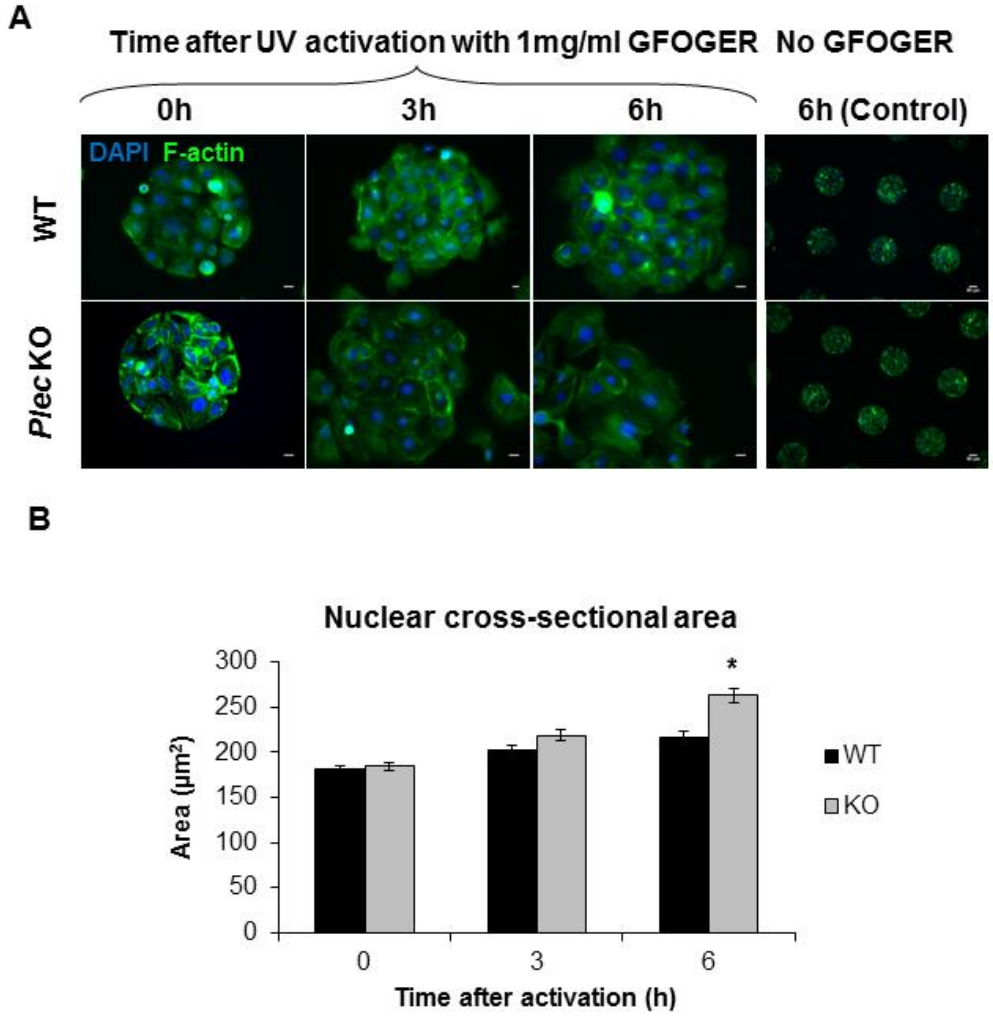

Figure 5.8 – Plectin determines nuclear plasticity in migrating keratinocytes.

A) Representative fluorescence images of F-actin and DNA of WT and *Plec* KO cells before (0 hours), 3 and 6 hours after photo-activated coupling of the collagen-mimetic peptide (GFOGER) to the surrounding polymer surface. Scale bar = 10µm (GFOGER activated images); total magnification 10x for 6h Control. Scale bar = 50µm. B) Quantification of leading edge cells nuclear morphology at times 0, 3, and 6 hours after activation with the GFOGER peptide. Data represent the mean ± SEM (156<n<245 leading edge cells quantified, N=2 experiments). *P < 0.05 comparing WT and *Plec* KO at 6 hours (two-tail T-test, unequal variance assumed).

5.2.5 Nuclear morphology is perturbed in plectin deficient epidermis

To investigate whether plectin also influences nuclear mechanics *in vivo*, nuclear morphology of *Plec* KO mouse model (2 days old litter) were analysed in whole-mount preparations of the tail skin (Jensen et al., 1999, Braun et al., 2003). The epidermis was immuno-labelled for keratin 14 and DNA (DAPI),

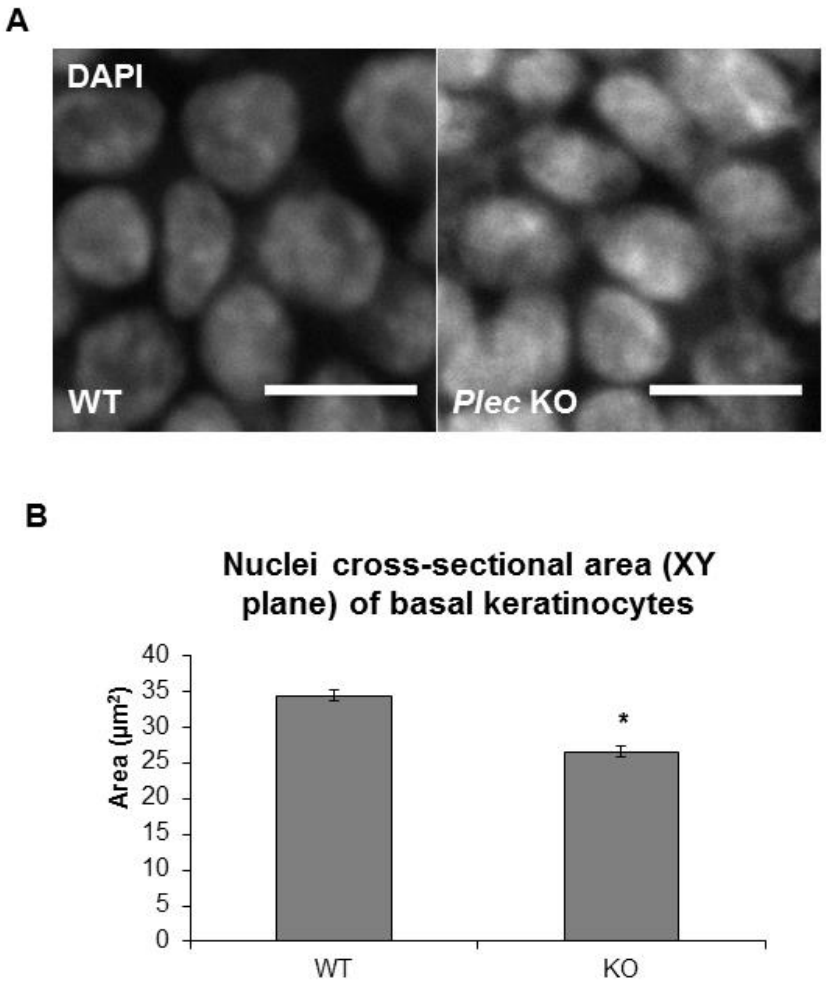

Figure 5.9 – Nuclear morphology of Plectin KO epidermis of neonatal mice is perturbed. A) Representative image of DNA of WT and KO whole-mounts of isolated epidermis. (B) Quantification of nuclear area. Data represent the mean ± SEM (n>50 cells per tail, at least two animals per condition were images). *P < 0.05 comparing WT and KO (two-tail T-test, unequal variance assumed). Scale bar 10µm.

followed by manual nuclear morphology quantification (cross-sectional area). Compared to normal epidermis, the nuclei of basal keratinocytes (located by K14 co-staining, data not shown) were significantly smaller (Figure 5.9). This suggests that plectin leads to abnormally smaller nuclei in epidermis. These results are consistent with human skin samples from EBS-MD patients, which possess an abnormal nuclear morphology (Almeida et al., 2015) (in Appendix I, page 180). Altogether, these data demonstrate that plectin also regulates nuclear morphology *in vivo*.

5.2.6 Transient knockdown of plectin leads to abnormal nuclear mechano-transduction of primary human keratinocytes but not evident K14 perturbations

The effects of plectin in defining nuclear morphology in primary human keratinocytes (pHK) are yet to be elucidated. In order to knockdown plectin expression in pHK and see if the phenotype of mouse keratinocytes can be replicated, transient transfection of *PLEC* small-interfering RNA (siRNA) was performed. After 4 days from transfection, cells were seeded onto single cell micro-patterns and treated with blebbistatin. Transfection efficiency was qualitatively confirmed by fluorescence microscopy (Figure 5.10 A) and the nuclear morphology assessed in 2D. Unexpectedly in all conditions, spread cells (50µm) had equal nuclear cross-sectional area (Figure 5.8) - no statistically significant differences were detected. Both *PLEC* siRNA and blebbistatin treatment affected the elongation of the nucleus in the SF8 patterns. *PLEC* siRNA nuclei were less elongated than the control, whereas *PLEC* siRNA treated with blebbistatin were still able to elongate but not as much as *PLEC*

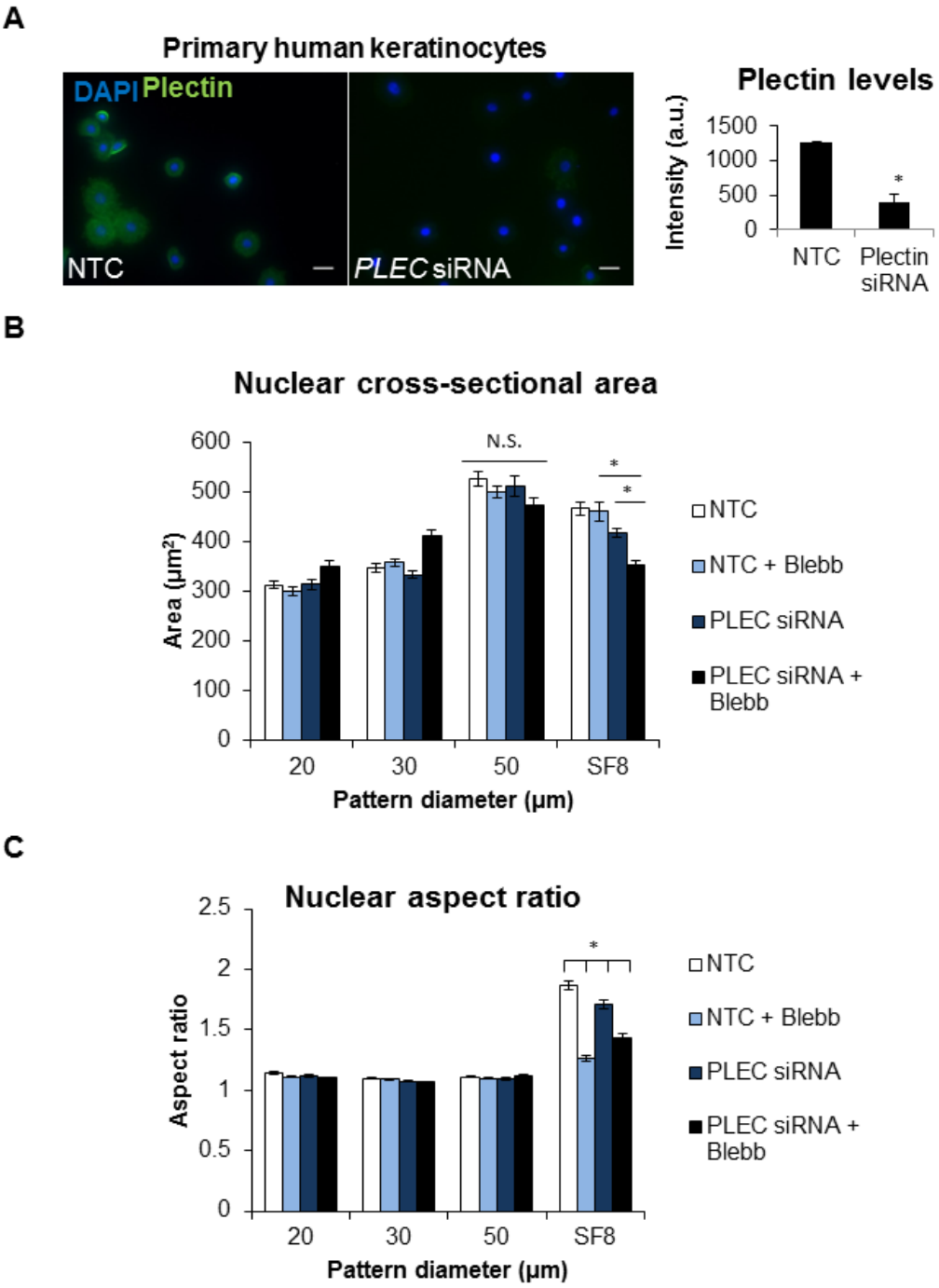

Figure 5.10 – *PLEC* siRNA in pHK leads to an abnormal actomyosin-dependent nuclear mechano-transduction.

A) Representative images of pHK seeded on collagen type I coated glass coverslips immuno-labelled against plectin; quantification of fluorescence levels quantified on the right graph (n>15 cells, N=2 independent experiments). Quantification of nuclear cross-sectional area (B) and nuclear aspect ratio (C) of Plectin siRNA [continues next page]

transfected cells seeded on 50µm and further treated with blebbistatin. * represents significance values P < 0.05, *N.S.* = P > 0.05 (two-tail T-test, unequal variance assumed). For quantification in A), N=2 independent experiments, n≥30 cells; B) and C) N=3 experiments, n≥30 per experiment. Scale bar 100µm.

siRNA and the control. This demonstrates that normal levels of plectin in pHK are essential for actomyosin-driven elongation of the nucleus.

In order to gain insights on the basis for this behaviour, these cells were co-stained against keratin 14. *PLEC* siRNA cells did not possess the same features of *Plec* KO mouse cells (Figure 5.11). Instead, K14 bundles appeared enriched, possibly thicker, judging by the brightness of the image over qualitative analysis. Altogether, these data show that plectin influences pHK nuclear mechano-transduction, although the phenotype upon transient knockdown is different from the complete *Plec* KO observed in mouse keratinocytes.

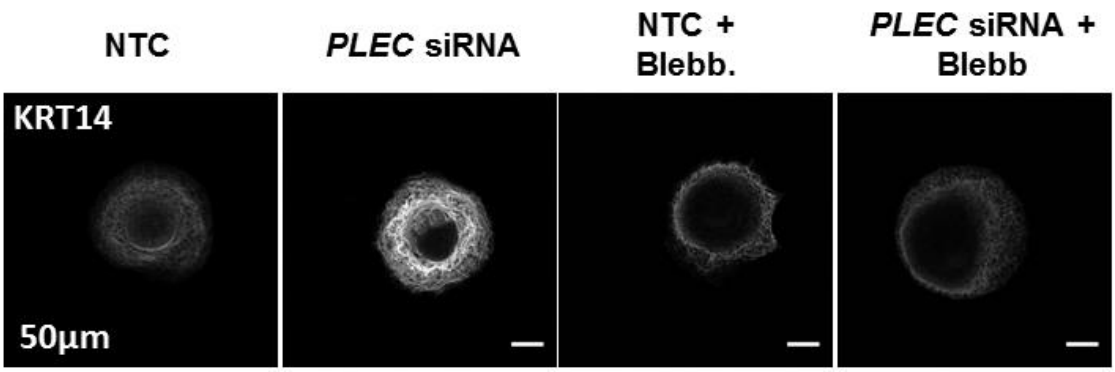

Figure 5.11 – Plectin siRNA does not cause dramatic changes in K14 network of pHK. Representative images of keratin 14 of Plectin siRNA pHK and NTC seeded in 50µm patterns with and without blebbistatin treatment. Scale bar = 10µm.

5.3 Discussion

In this chapter the mechanisms of force transmission from external adhesive cues to the nucleus of epidermal keratinocytes were examined. Micro-patterned collagen substrates were utilised to precisely control the adhesion and spreading of single cells, as well as crowding in cell colonies. The results demonstrate that in keratinocytes, the size and shape of the nucleus changes in response to defined biophysical cues, and the extent of this deformation is controlled by the cytolinker plectin and F-actin contractility. Plectin is required for maintaining a dense keratin network and dampens nuclear deformation induced by either cell spreading or crowding. Interestingly, the effect of plectin in promoting excessive nuclear deformation appears to depend on F-actin contractility and on the direct linkage of the cytoplasm to the nuclear membrane via nesprins (Almeida et al., 2015) (in Appendix I, page 180). Based on these findings, it is proposed further on section 7.2.1 (page 142) a model in which the keratin cytoskeleton protects the nucleus from forces generated by F-actin as cell spreads.

Plectin is a well-established regulator of cytoskeletal architecture across different cell types. The complete loss of full-length plectin in mouse leads to EBS with muscle dystrophy (EBS-MD) (Andrä et al., 1997). In this study, several resemblances between EBS-MD human patients and mice model were observed, including abnormal architecture of muscle fibres and higher necrotic cells in smooth muscle, as well as skin blistering. Plectin (-/-) mice died only a few days after birth, most likely from the loss of body fluid and proteins as a consequence of skin blistering, possibly combined with malfunction of the heart

and vascular endothelial system. Although the architecture of the skin appeared to be normal in plectin (-/-) mice, we looked into more detail at the morphology of the nuclei in basal keratinocytes. *Plec* KO basal cell have a reduced area in the XY plane (being Z the thickness axis), in agreement with this, basal keratinocytes in EBS-MD patients do also possess an abnormal morphology (Almeida et al. 2015). This suggests that the mechanics of these cells is in fact different, so that the absence of plectin leads to reduced nuclei in basal cells.

Cellular studies potentially may elucidate how nuclear morphology is regulated by plectin and other cytoskeleton proteins *in vivo*. The absence of plectin in keratinocytes induces the formation of thicker keratin filament bundles, with larger voids within the meshwork (Osmanagic-Myers et al., 2006). In fact, in the present work, utilising image processing techniques, it is shown that plectin works as a K14 bundle cross-linker. The spacing between bundles is increased in the absence of plectin. To check such measurements, transmission electron microscopy (TEM) could be used once allows higher magnification imaging. In human keratinocytes, the down regulation of plectin (*PLEC* siRNA) does not perturb K14 architecture to the same extent, leading to a normal nuclear deformation in spread cells (50μm islands). The residual levels of plectin still expressed, may be enough to not cause the disruption of keratin network, and therefore explaining why the human keratinocytes behave differently to the mouse KO cells. In human EBS patients (with mutation in *PLEC* gene), dramatic morphological changes were observed in basal cells (Almeida et al., 2015) (in Appendix I, page 180).

The effects of plectin appear to be cell-type specific. In fibroblasts, plectin is necessary for localisation of vimentin intermediate filaments to focal adhesions at the cell periphery (Burgstaller et al., 2010, Spurny et al., 2008) and inhibits cell motility (Gregor et al., 2014). MCF-7 breast cancer cells similarly acquire a slower, less protrusive phenotype in the absence of plectin (Boczonadi et al., 2007). Plectin also impacts the organisation of the intermediate filament protein glial fibrillary acidic protein (GFAP) in astrocytes, and contributes to the fibrotic phenotype of R239C GFAP mutant cells (Tian et al., 2006). The altered IFs architecture affects the mechanics of cells, which appears to also be cell specific. The loss of plectin reduces fibroblast and myocytes cytoplasm stiffness and impairs force transmission (Na et al., 2009, Bonakdar et al., 2015), whereas keratinocytes were proved to be stiffer (Bonakdar et al., 2015). Using AFM, the elastic modulus of mouse keratinocytes was determined, although the data was not reproducible therefore inconclusive. Within each individual experiment, differences between *Plec* KO and WT were not detected. The elastic modulus from experiment to experiment varied dramatically. In order to analyse in more detail the causes of such disparity of results, more time and an increased number of measurements required would be. Nevertheless, the data here presented shows that plectin is a key regulator of cellular architecture, and the data here reported add a new dimension to this function, specifically in the control of nuclear morphology. Given the cell type-specific function of plectin in cytoskeletal organisation and migration, its role in force transmission to the nucleus for other cell types will be an important area of investigation in future studies.

Plectin indirectly protects the nucleus from deformation via keratin filament cross-linking rather than direct linkage to the nuclear membrane, as the expression of dominant negative-KASH nesprin did not affect nuclear deformations on the WT (Almeida et al., 2015) (in Appendix I, page 180). Consistent with this result, crystallographic characterisation of keratin filament bundles recently revealed that the disulphide bond responsible for the X-shaped coiled-coil heterodimers is enriched in the perinuclear region of basal keratinocytes of the epidermis, where it is thought to stabilise a cage of keratin around the nucleus and provide mechanical support in early stages of differentiation (Lee et al., 2012). In other studies, epidermal specific overexpression of mutant Lamin A/C (progerin) led to abnormal nuclear morphology in keratinocytes (Wang et al., 2008), and in some instances progerin overexpression promoted hyperproliferation and hair loss (Sagelius et al., 2008). In addition, lamin-associated proteins (LAP) 2α, a chromatin binding protein is essential for epidermis homeostasis (Naetar et al., 2008). The loss of LAP-2α leads to hyperproliferation of progenitor keratinocytes, resulting thus in tissue hyperplasia. These findings demonstrate that, in addition to the keratins, the nuclear lamina and associated proteins are important for maintaining keratinocyte nuclear morphology, and further suggest that disruption of nuclear mechanics does indeed influence epidermal cell function. The functional implications of nuclear morphology in cell behaviour are explored in the next section.

Clinically, mutations in plectin (plectinopathies) manifest into different symptoms according to the missing isoforms (Winter and Wiche, 2013), while keratin 14 mutations themselves disrupt keratin filament mechanics (Russell et al., 2004)

and lead to distinct forms of EBS (Coulombe et al., 1991). In future studies, investigation of how other types of plectin mutations, such as in EBS Ogna (Walko et al., 2011), and EBS caused by keratin mutations may affect nuclear morphology will be of great importance. Moreover, identifying a potential role for nuclear mechanics in the pathophysiology of blistering skin diseases could shed new light on our understanding and treatment of these complex and painful conditions.

Chapter 6. Chromatin remodelling is regulated by cell shape in keratinocytes

6.1 Introduction

Studies in the previous chapters demonstrated that cell shape regulates keratinocyte nuclear morphology and that this response depends on the cytolinker plectin. Changes in the size and shape of the nucleus could potentially affect chromatin structure and gene expression. This implies that mechanical forces are capable of altering the interactions and/or kinetics of regulatory pathways for DNA transcription, which may involve: 1) chromatin remodelling; 2) chromosome-chromosome cross-talk; 3) nuclear trafficking; or 4) assembly-disassembly of nuclear bodies.

DNA transcription involves the recruitment of RNA polymerases at the promoter region of the gene. The initiation of transcription by RNA pol II is controlled at three different levels (Koster et al., 2015). First, gene-specificity is achieved through DNA-sequence-specific binding by activator and repressor proteins (gene-specific transcription factors, GSTFs), which serve as an initiation flag for promoter or enhancer activity. The second level of control is exerted by transcriptional co-activator and co-repressor complexes, which often act through chromatin structures and modifications. These complexes are recruited to specific genomic elements by GSTFs, by chromatin modifications, by DNA, and in some cases by regulatory RNAs. The third level is formed by the RNA Pol II pre-initiation complex (PIC) (Vannini and Cramer, 2012, Vannini, 2013, Thomas and Chiang, 2006).

While there is a strong association between nuclear deformation, chromatin remodelling, and cell behaviour, a definitive causative relationship is yet to be established. Supportive of the hypothesis that chromatin may consist of a

mechano-sensor within the nucleus, direct mechanical stimulation of HeLa cells caused rapid de-compaction of chromatin (Iyer et al., 2012), and in isolated nuclei, cyclic forces promote overall nuclear stiffening (Guilluy et al., 2014). The application of force on nesprin-1 activates Src, which in turn phosphorylates emerin by Src-family kinases (Guilluy et al., 2014). Phosphorylation of specific nuclear envelope components may further alter interaction with their binding partners or, in the case of lamins, may trigger its partial depolymerisation (Kochin et al., 2014, Swift et al., 2013). How these events alter the higher-order structure of chromatin and ultimately regulate gene expression is still to be unravelled.

Chromatin is hierarchically organised (section 2.3.3). Epigenetic regulatory mechanisms control covalent DNA and histone modifications, ATP-dependent chromatin remodelling, higher-order chromatin folding and the specific arrangement of genes and distinct chromatin domains within the nuclear space (Hübner and Spector, 2010, Naumova and Dekker, 2010, Rando and Chang, 2009, Wang et al., 2009). The four core histones — H2A, H2B, H3 and H4 — that make up the nucleosome are subject to numerous modifications, including phosphorylation, ubiquitylation, sumoylation, acetylation and methylation (Strahl and Allis, 2000, Greer and Shi, 2012). Histone methylation and acetylation affect the structure of chromatin by mediating the accessibility of DNA transcriptional machinery and thereby gene expression (Mozzetta et al., 2015). Lysine methylation is associated with either activation or repression of gene expression, depending on the location and degree of methylation (Greer and Shi, 2012, Zhou et al., 2011, Berger, 2007, Barski et al., 2007, Cao et al., 2002, Esteller, 2007, Fuks, 2005, Paik et al., 2007). For example, genes marked by

histone H3K9, H3K27 or H4K20 methylation are usually repressed, whereas those associated with H3K4 and H3K36 methylation are generally activated (Barski et al., 2007). At the chromatin level, euchromatin is typically enriched with transcriptionally active genes markers e.g. H3K4me3, whereas facultative and constitutive heterochromatin is rich in H3K27me3 and H3K9me3, respectively. Constitutive heterochromatin formation involves the recruitment of heterochromatin protein 1 (HP1), which recognises H3K9me3 (Lachner et al., 2001). Defective nuclear lamina leads to the loss of H3K9me3 and HP1 (Shumaker et al., 2006). The lack of heterochromatin as a result of progeria overexpression in embryonic stem cells similarly causes chromatin de-condensation (Chalut et al., 2012). Not only in the context of disease, chromatin compaction impairs the differentiation of stem cells: as stem cells commit to differentiation, their nucleus stiffens, which is thought to occur due to gene silencing and heterochromatin formation (Pajerowski et al., 2007, Swift et al., 2013, Chalut et al., 2012). Other than providing physical support to the nucleus, lamin A/C and associated proteins (e.g. LBR), play a role in heterochromatin organisation (Solovei et al., 2013) and therefore gene silencing.

In the skin, increased clusters of heterochromatin accompany decreased nuclear volume (Gdula et al., 2013). In this same study, DNA transcription was reduced as terminal differentiation occurs, which is marked by the decrease of RNA polymerase II down-regulation, as well as the drop of levels in euchromatin markers such as H3K4me3 (Gdula et al., 2013). Utilising micro-patterned substrates, it has been shown that histone deacetylation occurs with cell rounding due to limited cell adhesion area (Lebeyec et al., 2007, Connelly

et al., 2011, Jain et al., 2013). Whether mechanical cues mediate chromatin mechanics and organisation is still unclear.

Currently, one of the main challenges in mechano-biology is the limited number of tools to accurately investigate the mechanical properties of soft materials such as cells. Micro-pipette aspiration, atomic force microscopy, optical and magnetic tweezers are the standard goal techniques utilised in cellular mechanics, each of them having different modes and principal of operation. AFM is one of the most versatile techniques for both imaging and mechanical testing of synthetic materials, and recent AFM microscopes allow the *in situ* mapping of structural and mechanical properties of living cells. The quantitative mechanical mapping using AFM inside the cell may bring novel insights into native structural information.

Widely used in nano- and micro-electronics, FIB allows the milling of several different materials. The small dual beam system, combines FIB and SEM in a single instrument, which allows simultaneous high-resolution imaging using SEM with FIB milling or chemical vapour deposition and etching (Bailey et al., 2013). Series of thin millings allow the capture of the exposed sample throughout its volume, a technique designated as “Slice and View”, which have been particularly attractive for the 3D imaging of biological materials (Heymann et al., 2009, Bushby et al., 2011, Kamino et al., 2004). Instead of structural contrast of cellular architecture, the mechanical properties of biological materials may be investigated using SEM/FIB preparation to create geometrically defined structures in the material and prove its mechanics. By inserting a small AFM cantilever inside SEM/FIB chamber, nano-tensile testing

in mineralised collagen fibrils and nanofibers has been elegantly performed, as well as bending test on cortical bone and limpet teeth (Jimenez-Palomar et al., 2012, Lu and Barber, 2012, Hang and Barber, 2010, Hang et al., 2011, Hang et al., 2014). In the present work, it is intended the use of SEM/FIB to mill through a keratinocytes on micro-patterns and investigate the spatial mechanical properties of cell's interior.

For mechanical mapping, the roughness of the surface ought to be minimised. Conventional quantitative mechanical information on materials surfaces may be obtained by nanoindentation and force volume AFM imaging (Reynaud et al., 2000, Butt et al., 2005, Tranchida et al., 2006, Schönherr et al., 2005). Phase contrast imaging may, in theory, also be used for purpose. The phase lag between the drive signal and the response of the cantilever while the AFM tip scans over a surface is then used to give a phase contrast signal. Phase contrast is due to energy dissipation at tip-sample interaction, which should be more accurately described as an elastic recovery rate, in order to elucidate the surface mechanical properties at high spatial resolution (Nicolás and Ricardo, 2006, Bailey et al., 2013). In addition, PeakForce^{TM} and HarmonicX^{TM} AFM may be used for fast scan and mechanical mapping of soft samples (Sahin et al., 2007, Sahin and Erina, 2008). Studies combining *in situ* AFM mechanical testing with SEM/FIB preparation will allow the study of biological phenomena such as chromatin remodelling in high-resolution.

In the present study, it is hypothesised that cell shape, which controls terminal differentiation in keratinocytes, influences chromatin remodelling. In order to

provide evidence to support this hypothesis, the following aims were investigated:

1) The characterisation of the levels and distribution of chromatin epigenetic markers for euchromatin and heterochromatin in response to adhesion area.
2) The study of whether the absence of plectin leads to abnormal chromatin remodelling.
3) To explore how lamin A/C structure changes in response to adhesion area.

In addition, a novel approach to map the mechanical properties of keratinocyte's nucleus was developed utilising SEM/FIB and AFM phase imaging. This may provide useful for future studies in nuclear mechano-transduction and biophysics.

6.2 Results

6.2.1 Adhesion area regulates terminal differentiation and H3K4me3 levels

Cell-ECM adhesions are key regulators of keratinocyte growth and differentiation, which is marked by the expression of high levels of several genes, such as involucrin (*IVL*). In order to assess how IVL is regulated by adhesive area over time, primary human keratinocytes (pHK) were seeded in 20 and 50μm islands for 1, 4 and 24hrs. After 24 hours, pHK seeded in

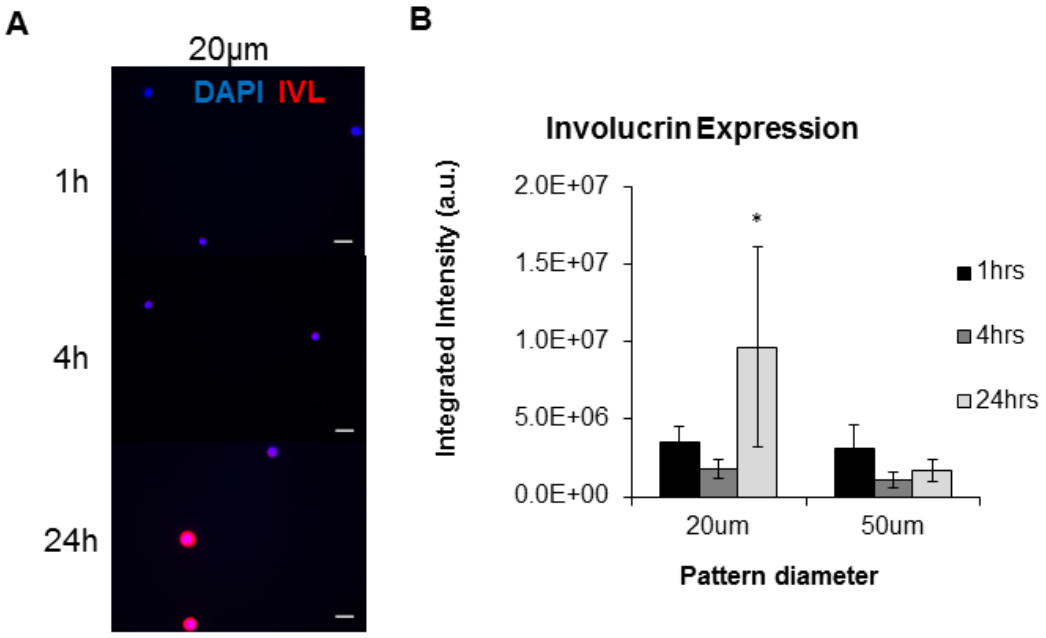

Figure 6.1 – Small adhesive area induces terminal differentiation after 24h seeding.

A) DAPI and involucrin (IVL) representative images using epi-fluorescent microscope of pHK seeded on 20μm islands. B) Average intensity (normalised) of IVL fluorescence of cells seeded on 20 and 50μm islands at 1, 4 and 24 hours after seeding. * P<0.05 comparing 1h versus 24h time-point (two-tailed T-test, unequal variance assumed). N=3 experiments.

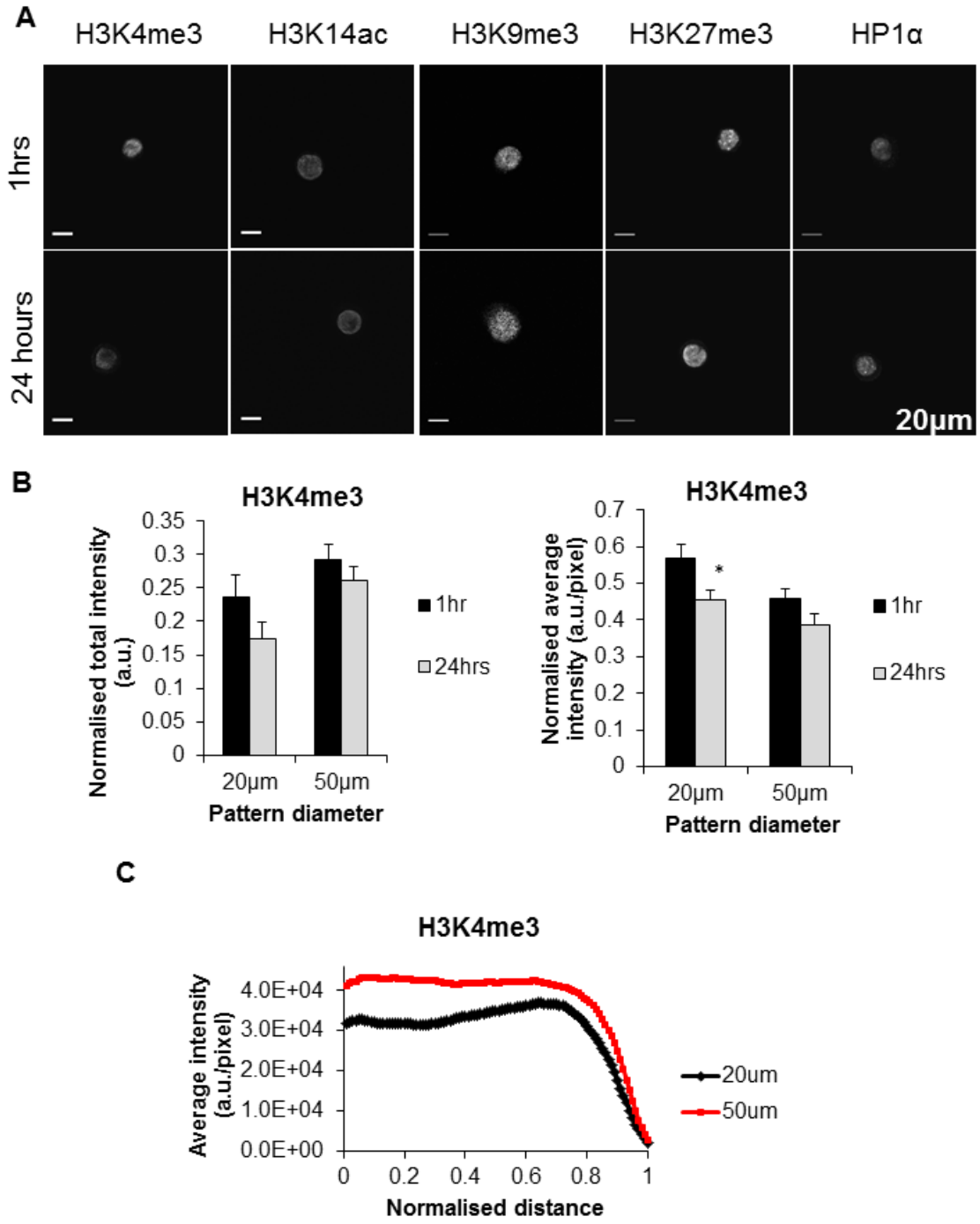

Figure 6.2 – Cell shape regulates epigenetic markers in a time-dependent manner.

A) LSCM images for several epigenetic markers of primary human keratinocytes (pHK) seeded in 20µm islands 1 and 24 hours after seeding. From left to right column: trimethylated histone 3 lysine 4 residue (H3K4me3), acetylated histone 3 lysine 14 (H3K14ac), trimethylated histone 3 lysine 9 residue (H3K9me3), trimethylated histone 3 lysine 27 residue (H3K27me3), heterochromatin protein 1-alpha [continues next page]

(HP1α). B) Quantification of H3K4me3 intensity levels. C) Radial distribution of H3K4me3, representing the average intensity of 15 cells out of a one representative experiment. * P<0.05 comparing 1h versus 24h time-point (two-tailed T-test, unequal variance assumed). N=3 experiments. Scale bar = 10μm.

20μm, islands express high levels of IVL, indicating that these cells were undergoing terminal differentiation (Figure 6.1), while cells on 50μm islands remained IVL negative. Furthermore, to investigate how the levels of euchromatin and heterochromatin change with differentiation in keratinocytes, a screening of several markers for these two distinct forms of chromatin was performed by immunocytochemistry (Figure 6.2 A). No striking differences were seen in any of the markers in cells seeded on 20m islands at 1 and 24h, apart from H3K4me3, in which the intensity appears to drop after 24h in comparison with 1 h time point. To investigate this further, the level of total intensity and brightness (average intensity) was measured (Figure 6.2 B). There is indeed a decrease of both overall levels (total intensity) and average intensity of H3K4me3 after 24h in 20μm seeded cells ($p<0.05$, two-tailed T-test, unequal variance assumed). The radial distribution of H3K4me3 does not change with cell spreading, being quite homogenously distributed throughout the nucleus in both cases (Figure 6.2 C). This shows that cell shape regulates the levels of H3K4me3 without affecting its distribution throughout the nucleus.

6.2.2 Cell spreading regulates heterochromatin and nuclear lamina distribution

Actively transcribed genes are typically in the centre of the nucleus, whereas regions near the nuclear lamina are associated with repressed and silent

chromatin (Rajapakse and Groudine, 2011). Next, it was investigated how the formation heterochromatin occurs at longer time scales and how this correlates with DNA transcription. Cells were seeded again in 20 and 50μm islands for 4, 24 and 48h after seeding and immunostained for H3K27me3 and RNA polymerase II (RNAP II). The total levels of H3K27me3 intensity (a marker for heterochromatin) were unchanged with time in both 20 and 50μm (Figure 6.3). Strikingly, the ring-like pattern close to nuclear envelope characteristic of heterochromatin is almost absent in 50μm cells, whereas in the confined 20μm cells is maintained (Figure 6.3. C). Also, the distribution of RNAPII appears to be affected, changing from more central at 4h to become homogenous throughout the nucleus with time (Figure 6.3. C).These results shows that adhesive area regulates chromatin remodelling in a complex way either by affecting the overall levels of methylation at particular Lys (as the case of H3K3me4), or by inducing spatial re-distribution. Interestingly, in pHK, the latter appear to occur in short time-frames (within 4h), whereas Lys modifications take longer (24h).

Perinuclear chromatin is typically rich in silenced genes. Lamin A/C is thought to play a role in the creation of this repressive environment. Following H3K27me3 re-arrangement, it was next investigated how lamin A/C responds to adhesive area. Therefore, cells seeded in 20 and 50μm were immunostained for lamin

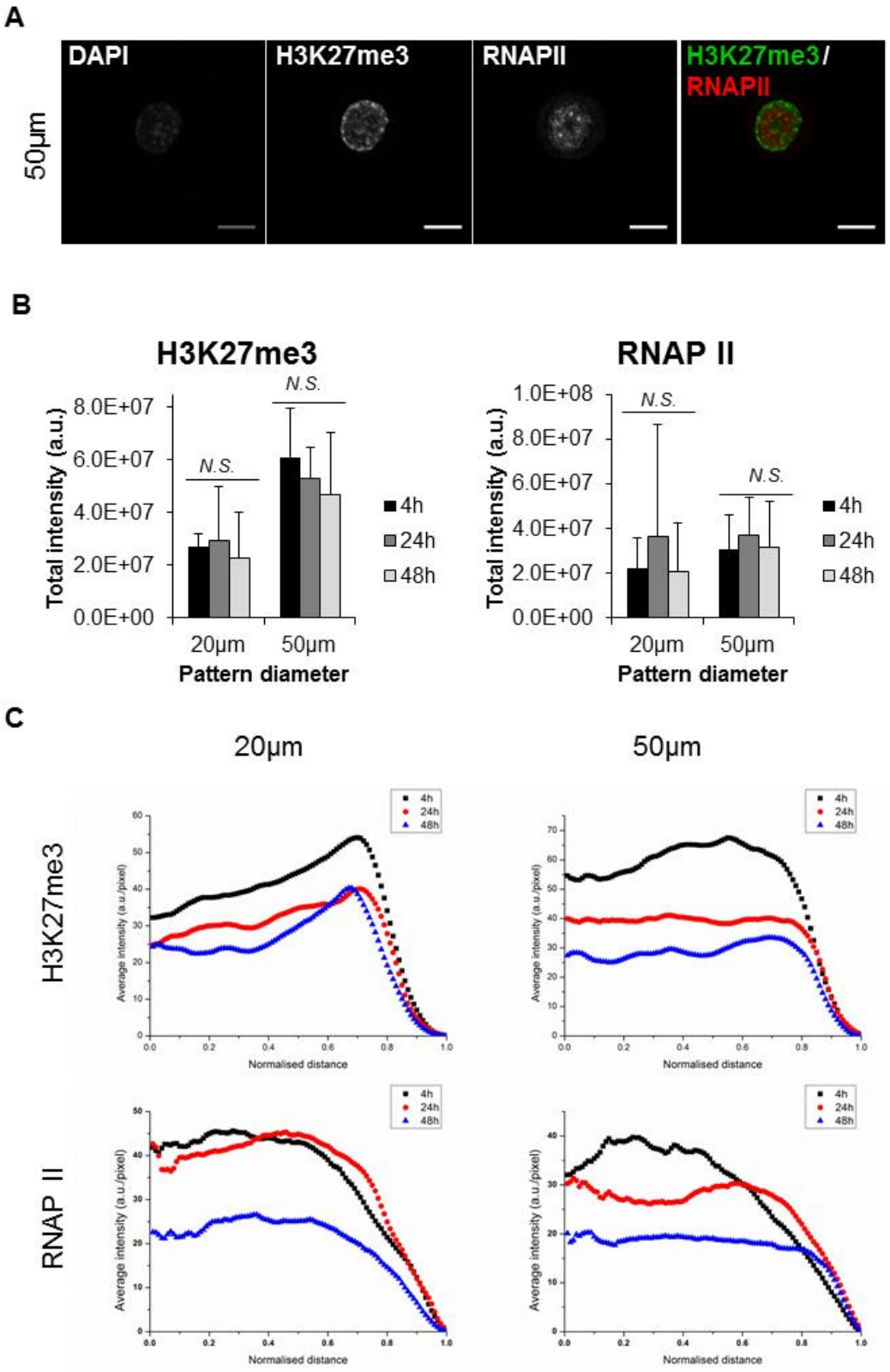

Figure 6.3 – Distribution of heterochromatin marker is regulated by cell shape.

A) Intensity levels of H3K27me3 and RNA polymerase II in pHK [Continues next page]

seeded on 20 and 50 µm islands. B) Radial profile for H3K27me3 (top row) and RNA pol. II (bottom row).* P<0.05 comparing 4h versus 24 and 48h time-point (One-way ANOVA, Tukey mean comparison test), n=15 cells, N.S. No Significance (P>0.05).

A/C and the radial profiling algorithm was used to investigate its distribution Figure 6.4. With the increase of nuclear volume (in 50µm cells) the

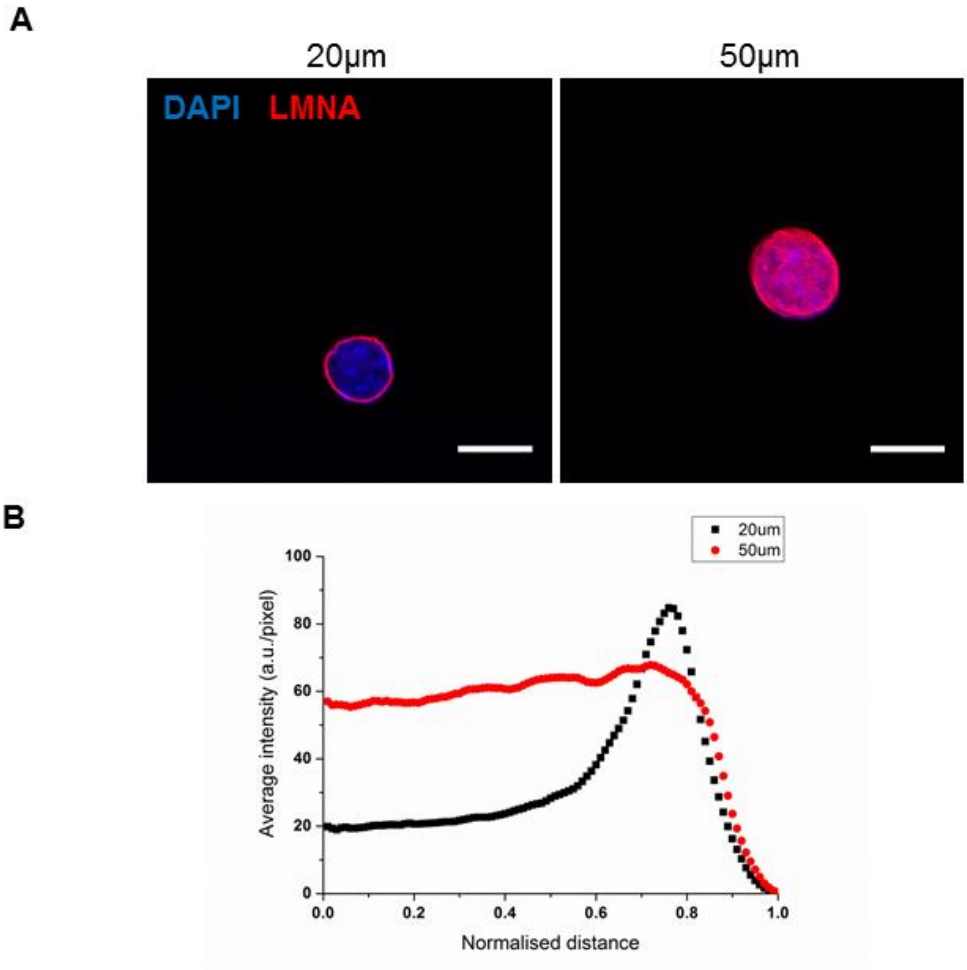

Figure 6.4 – Nuclear lamina structure is defined by cell shape.

A) DAPI and lamin A/C representative images of pHK seeded on 20 and 50 µm islands. B) Radial distribution of average intensity of lamin A/C channel. n = 15 cells. No statistical analysis performed.

characteristic ring-like pattern is attenuated and almost unnoticeable after 4hrs, contrarily with 20μm cells which form well delimited ring-like pattern. This transduces into a sharp distal peak in the confined cells, which is not seen in the spread cells (

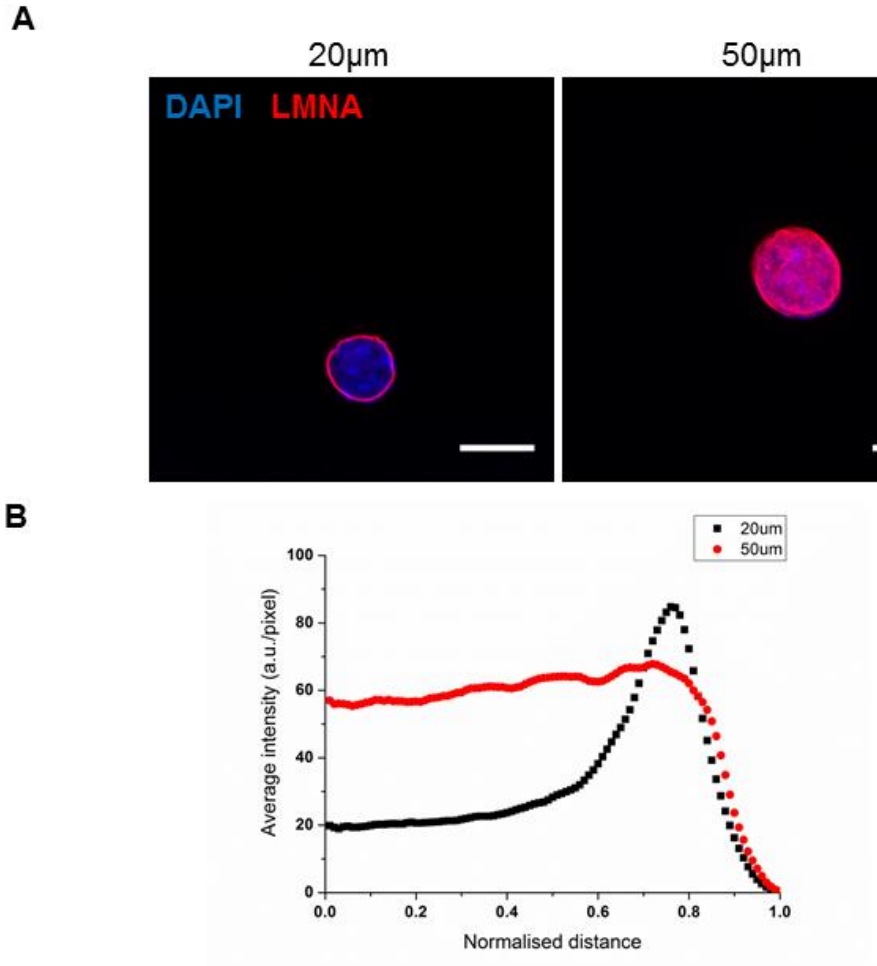

Figure 6.4).

6.2.3 Ring-like heterochromatin distribution is maintained in spread *Plec* KO keratinocytes

The nucleus of *Plec* KO keratinocytes deforms greater than the WT, as it was explored in detail in the previous chapter (section 5.2.2). It was next investigated whether the response noticed with pHK regarding the H3K27me3 re-arrangement Figure 6.3 is observed in mouse keratinocytes. The

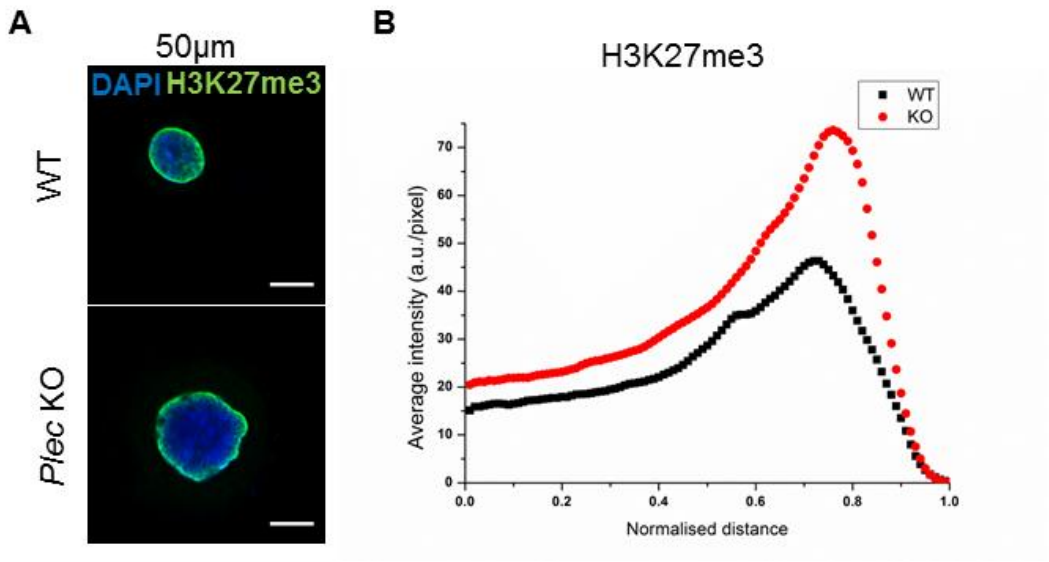

Figure 6.5 – Ring-like distribution of heterochromatin marker is maintained in mouse keratinocytes.

A) Representative DAPI and H3K27me3 images of WT and *Plec* KO mouse keratinocytes.

B) Radial distribution of average intensity of H3K27me3 channel. n=15 cells. No statistical analysis performed

ring-like pattern of H3K27me3 in the nuclei of mouse cells seeded on 50µm islands was more pronounced than human cells (Figure 6.3), and 4 hours after spreading, there were no measurable differences between *Plec* KO and WT cells (Figure 6.5), demonstrating that the mouse keratinocytes behave differently than the human cells.

6.2.4 Development of a novel sample preparation approach to investigate chromatin condensation

The mapping of mechanical properties of cells interior would be highly advantageous for mechano-biology research and would allow the study of key bio-mechanical events so far impossible. In order to map the mechanical properties of a sample utilising any AFM mode (e.g. phase imaging or PeakForce), roughness effects must be reduced. Dual-beam microscope

integrating electron gun (for SEM imaging) with focused ion beam (FIB) allows the sputtering of most matter, including soft materials as polymers and cells. SEM is used to image the spot of interest and FIB to mill through the sample. Fixed pHK were successfully cross-sectioned using this apparatus (Figure 6.6 A3). This involved the creation of at least one Pt wall placed between the beam and the cell that worked as a shield (illustrated in Figure 6.6 A top). Atomic force microscopy (AFM) was then used to analyse the topography of the milled cell. The instrument was operated in semi-contact mode (also known as tapping imaging), and both height (topography) and phase were recorded and analysed (Figure 6.6B).

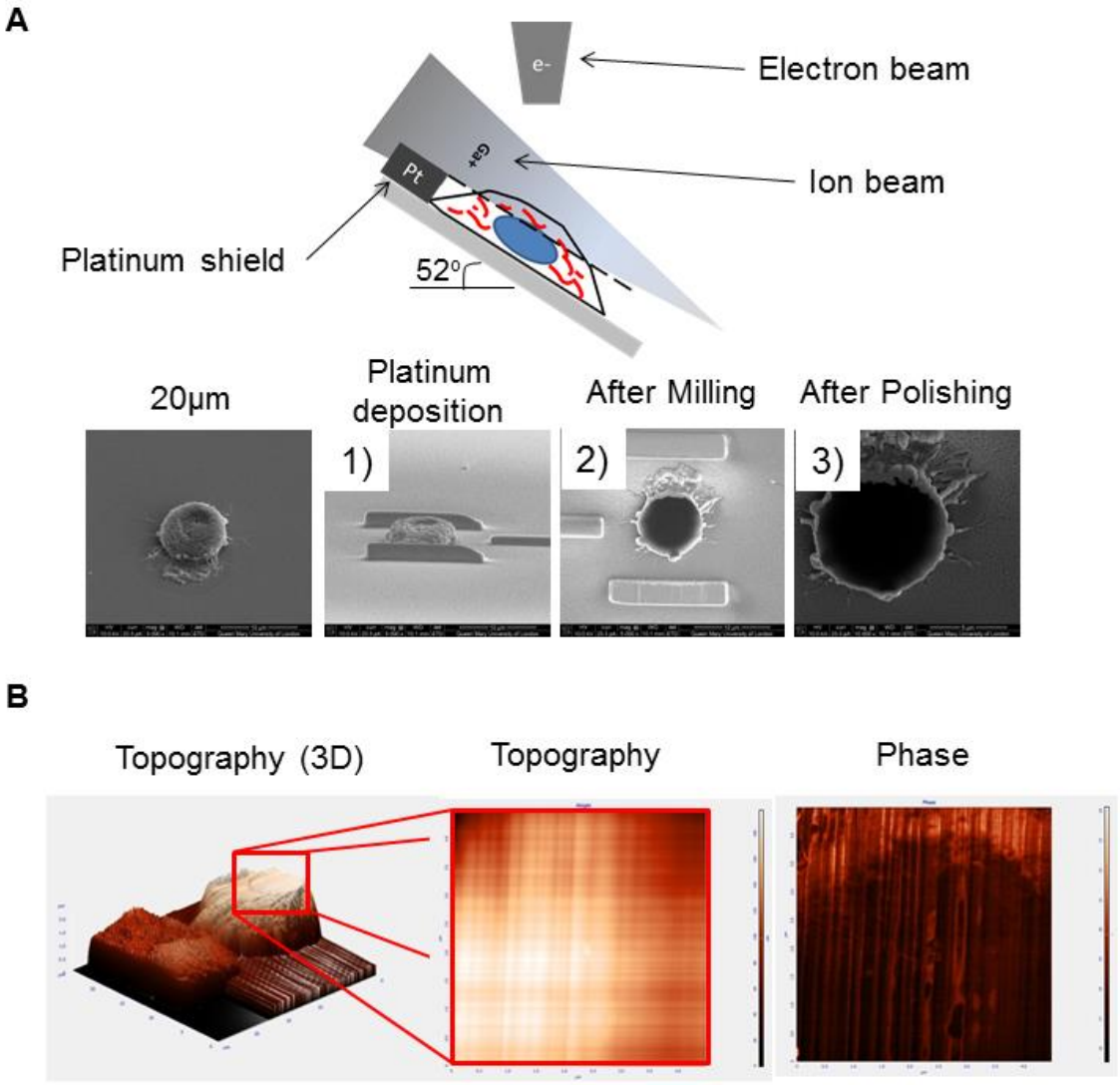

Figure 6.6 – SEM/FIB sample preparation and AFM microscopy for high-resolution of fixed cells seeded on 20 µm islands.

A) Step-by-step illustration of SEM/FIB sample preparation with representative images using SEM. A platinum wall is deposited to shield the cell and narrow the ion beam(1) before milling (2). After milling, polishing step(s) may follow in order to flatten the surface (3). B) Representative imaging using AFM: left, 3D visualisation of the height of the cell (topography); right-top, 5x5µm height (topography) image of cell interior; with respective phase image on the right-bottom.

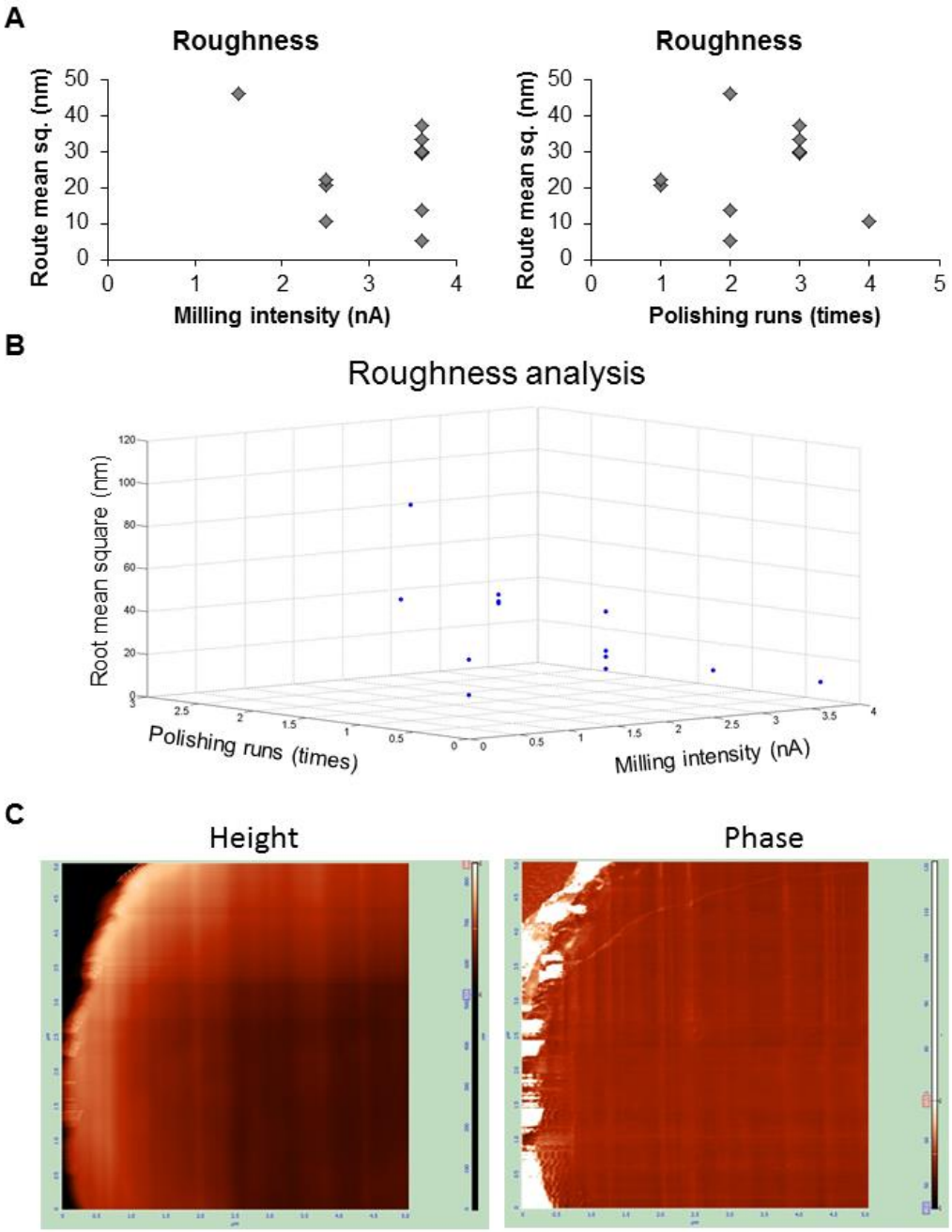

Figure 6.7 – Optimisation of SEM/FIB cell milling.

A) Roughness analysis (root mean square of height image, nm) of cross-sectioned cells using different milling intensities (left) and polishing runs (right). B) 3D plotting of root mean square for all the cells tested. C) 5x5µm height and phase image of the cell with the lowest RMQ value.

As the aim is to produce the flattest surface possible, several milling intensities and polishing was performed: milling intensity ranged from 1.5 to 3.6nA (acceleration kept constant at 16 KeV); 1-4 polishing runs were performed in a single cell after milling with low beam intensities ranging from 0.15 to 1.5nA (acceleration also kept constant at 16 KeV). After SEM/FIB preparation, the outcome roughness was assessed using AFM (Figure 6.6 B) by measuring the root mean square (RMS) of the height images (window of 5x5µm) utilising Nova^{TM} software (NT-MDT, Russia). Out of 11 analysed different cells (Figure 6.7), 3.6nA milling intensity with two consecutive polishing runs appears to be more effective in producing flat surfaces (Figure 6.7B). These data demonstrates that SEM/FIB cutting can be utilised to produce flat cross-sections of fixed cells (Figure 6.7 C). Altogether, within this chapter the results demonstrate that the dynamics of chromatin remodelling is influenced by cell shape in a time-dependent fashion and that new techniques for cell preparation could be employed to explore even further the mechanics of the nucleus.

6.3 Discussion

6.3.1 Limited adhesive area induces terminal differentiation and reduced euchromatin levels in pHK, while cell spreading causes heterochromatin and lamin A/C re-distribution

Lineage-specific differentiation programs in progenitor cells require a high degree of coordination in chromatin organisation (Lanctôt et al., 2007, Joffe et al., 2010, Schoenfelder et al., 2010). In agreement with previous studies (Connelly et al., 2010, Connelly et al., 2011), the reduction of ECM-cell contacts forced keratinocytes to differentiate *in vitro*. This response correlated with a decrease of H3K4me3, whereas cell spreading led to quick redistribution of both

lamin A/C and H3K27me3-enriched chromatin. The pronounced peripheral staining of H3K27me3 seen in the nuclei of confined cells was almost lost in cells spread on 50 μm islands, which interestingly correlated with a more homogenous staining of lamin A/C throughout the nucleus. In other studies, the inactivation of H3K27me3 demethylase JMJD3 led to blockage of progenitor cell differentiation (Sen et al., 2008), which is in agreement with the overall decrease of H3K27me3 intensity levels in spread cells (50μm). In adult epidermal stem cells, actively transcribed genes important for the maintenance of the stem cell phenotype show both H3K4me3 and H3K79me2 histone marks, while repressed non-epidermal genes and genes activated during cell differentiation are enriched by H3K27me3 (Lien et al., 2011). Consistent with our results, upper layers of the mouse epidermis have much lower levels of euchromatin marks and transcriptionally active genes (i.e. H3K4me3, H3K56ac and RNA Pol II), while H3K9me3 and H3K27me3 increase (Gdula et al., 2013). Altogether, the data here indicate that mechanically induced terminal differentiation in keratinocytes is accompanied of down regulation of euchromatin markers and redistribution of heterochromatin and lamin A/C, which suggests that nuclear morphology potentially regulates chromatin remodelling. It is also pertinent to note that cell cycle-regulating genes, which are typically thought to be silenced upon differentiation, are in fact enriched in H3K4me3 without detectable H3K27me3 (Lien et al., 2011). These data suggest that more complex regulatory mechanisms are involved in the repression of cell cycle–associated genes in stem cells, which may include the activity of anti-proliferative or lack of pro-proliferative signalling pathways (Botchkarev et al., 2012).

6.3.2 *In situ* mechanical mapping of nuclear interior

Heterochromatin is a dense form of chromatin, where complexes of proteins tightly bind histones to each other and limit the access of DNA transcriptional machinery. On the other hand, euchromatin has a more open structure due to repulsive steric forces caused by overall acetylation of histones. In solid physics, denser matter is generally stiffer. Therefore, if within the nucleoplasm there are zones with distinct densities, the mapping of mechanical properties (e.g. elastic modulus) would allow a new avenue of research into the relationship between mechanics and chromatin remodelling. Atomic force microscopy is a high-resolution technique that allows the mechanical mapping of various types of samples.

The development of a novel technique for mechanical mapping of single cell interiors using a combination of SEM/FIB preparation and AFM imaging was performed. SEM/FIB preparation was utilised to minimise the roughness of the cell interior for mechanical mapping. A range of different studies could be performed from this approach. For instance, it would be interesting to use different fixative agents in order to investigate the effects of fixation in structural-mechanical properties of cells, as well as hydration. Embedding materials may also be considered, and the use of gold-immunolabelling would allow the specific labelling of particular structures within the cell, which could be used for identification/enhancement purposes. For instance, in order to enhance the nuclear envelope, anti-lamin A/C antibodies coupled with solid bead (e.g. polystyrene or gold) could be used. In principal these would show up clearly upon imaging/mechanical testing as the beads possess higher elastic modulus than the surrounding cellular milieu.

Importantly, further optimisation of the technique is necessary regarding the inclusion of gallium ions in response milling intensity and acceleration voltage. In silicon, higher acceleration voltage lead to higher inclusion of Ga+ and result in materials stiffening due to the generation of free-radicals which promote cross-linking (Brezna et al., 2003b, Brezna et al., 2003a, Rubanov and Munroe, 2004, Miroslav et al., 2011). In polycarbonate, high currents lead to degradation of polymeric chains and drop in the elastic modulus as measured by the phase shift, whereas extremely low currents introduce topographical artefacts which are also not ideal for mechanical mapping (Bailey et al., 2013). Commercially available incorporated SEM/FIB/AFM such as BRR^{TM} (Zeiss, Germany) and MV-SEMView^{TM} (Nanonics Imaging Ltd, Israel) are the future of 3D *in situ* high-resolution imaging and mechanics, which may bring new insights into still unanswered questions such as in the actual structure of chromatin fibres inside the cell.

Chapter 7. Discussion

7.2 Background

The importance of mechanics in biology has been recognised for centuries, firstly by Wilhelm His in the late 1800s (His, 1874, Paluch et al., 2015). Forces are crucial in development and tissue morphogenesis, as well as in cell differentiation, motility and disease progression. Current models in mechano-transduction place the nucleus as a central entity able to translate physical information into biochemical responses (Wang et al., 2010, Vogel and Sheetz, 2006, Shivashankar, 2011, Shivashankar, 2010). This is thought to happen via the cytoskeleton, as cytoskeletal proteins form filamentous structures that span throughout the cell cytoplasm and integrate with the nucleus. Ultimately, forces imposed on the nucleus may alter its activity. In the present thesis, utilising controlled adhesive cues, it was examined how the cytoskeleton defines nuclear morphology, and how this impacts subnuclear structures with a particular focus on chromatin remodelling.

7.2.1 The cytoskeleton regulates nuclear morphology

In chapter 4, the morphology of the nucleus was investigated in detail. When cultured on 2D substrates with controlled adhesive areas of increasing sizes, spread keratinocytes acquired a larger nucleus when compared with cells that have limited ECM on which to adhere. Surprisingly, the blockage of actomyosin contractility had no effect in the ability of the nucleus to deform in keratinocytes, in contrast to other cells, *e.g.* endothelial cells, fibroblast, smooth muscle cells. Reports in literature show that in response to blebbistatin nuclear morphology is drastically affected (Versaevel et al., 2012, Thakar et al., 2009, Lebeyec et al., 2007, Li et al., 2014, Jain et al., 2013). Latrunculin A, which binds in a 1:1 ratio

to G-actin (Coue et al., 1987), caused a drastic shrinkage of nuclear morphology, which is likely to be due to the failure of keratinocytes to spread. F-actin is therefore essential for keratinocytes shape control and therefore nuclear mechano-transduction in an actomyosin independent way.

Early studies using cytoskeleton inhibitors have shown that the transmission of forces towards the nucleus is dependent on more than one cytoskeletal protein (Maniotis et al., 1997). Some authors have proposed that F-actin exerts lateral tension to the nucleus towards expansion and the MT compression (Mazumder and Shivashankar, 2010, Mazumder et al., 2010). Laser ablation of the cytoskeleton using of gold particles was attempted (Mazumder and Shivashankar, 2007), which led to a dramatic shrinkage of the nuclear morphology and EGF-H2B in HeLa cells. In this study, all the cytoskeleton proteins (MT, F-actin and IF) suffered massive disruption, which may explain the shrinkage of the nucleus within 20 minutes. Although heating caused by the laser ablation may have caused degradation of several other proteins and induced stress in the cells. In fact, it is still a challenge to isolate the effects of specific cytoskeletal proteins as they each cross-talk with other and affect diverse cell functions.

Basal keratinocytes express high levels of K14, which forms a dense network throughout the cytoplasm of these cells and proved to be a major determinant of cells mechanics (Ramms et al., 2013, Seltmann et al., 2013a). Okadaic acid treatment (serine/threonine phosphatase PP1 and PP2 inhibitor) decreased nuclear cross-sectional area and disrupted cell shape and spreading, a similar response to latrunculin A treatment. This demonstrates that keratin network is

also essential for cell shape maintenance and therefore nuclear mechano-transduction. Reports have shown that OKA causes specific hyperphosphorylation of intermediate filaments (Kasahara et al., 1993, Osmanagic-Myers et al., 2006), although due to the central role of PP1 and PP2 in phosphorylation of several other molecules in the cell, non-specific effects may underlie this response. Therefore, a better model that might introduce specific disruption in the keratin network was sought, in this case *Plec* KO keratinocytes.

The *Plec* KO mouse keratinocyte model (kindly provided by Prof. Gerard Wiche, Austria) was adopted in the present thesis as they possess abnormal keratin network architecture (Osmanagic-Myers et al., 2006). These cells lack the cytolinker plectin which is essential for keratin cross-linking (Andra et al., 2003, Andrä et al., 1997, Castañón et al., 2013, Wiche et al., 2015, Winter and Wiche, 2012) and therefore used to understand how irregular keratin networks regulate nuclear mechano-transduction in response to adhesive cues. Although the abnormalities in keratin network have been appreciated (Osmanagic-Myers et al., 2006), no quantitative analysis of its architecture is available in the literature. The K14 network of *Plec* KO keratinocytes was here characterised using high magnification LSCM and compared to the WT. Interestingly, keratin bundles formed a less dense network in comparison with WT, although the measurable bundle thickness was unchanged. The first parameter is in agreement with Osmanagic-Myers et al. (2006), although bundle thickness was reported to be higher in this early study although no quantification and statistical was adopted to support such observations. The data here presented (Chapter 5) show that plectin works as a cross-linker of keratin network in keratinocytes: it regulates

the spacing between the bundles. This could be further confirmed by the use of TEM and measurement of the thickness of keratin bundles. The molecular mechanism that explains how plectin may intervene in the assembly of keratins network is yet to be characterised.

Next, after seeding *Plec* KO on micropatterns a more deformable nucleus was observed in spread cells (50μm). Importantly, the enlarged nucleus in *Plec* KO was dependent on the actomyosin contractility (Almeida et al., 2015) (in Appendix I, page 180). The expression of DN-KASH, which disrupts the physical linkage between the cytoskeleton and the nucleus, did not affect nuclear morphology in WT cells, which suggests that keratin normally protects the nucleus from lateral deformation independently of cytoskeleton-nucleus linkage (Figure 7.1). When the full-length plectin is not present, keratin structure gets less dense and the nucleus has space to expand in response to actomyosin-driven cell spreading (Figure 7.1). It is, therefore, reasonable to state that keratin network impacts cell mechanics in a way that regulates the generation of internal forces.

Furthermore, plectin may play an important role in post-translational modifications of keratins and the ability to respond to stress. In the case of hepatocytes, K8 phosphorylation acts as a phosphate “sponge” against stress (Snider and Omary, 2014, Omary et al., 2006, Ku and Omary, 2006). The same phosphorylation motif identified in K8 is conserved in several type II IFs, including K4, K5 and K6, in which the phosphorylated residue is a Thr (LLTPL) (Snider and Omary, 2014). K4, K5 and K6 also undergo phosphorylation in response to stress (e.g. ultraviolet radiation and apoptosis) or disease (e.g.

psoriasis and squamous cell carcinoma) (Toivola et al., 2002). Phosphorylation of K8 is mediated by p38 and JUN kinases, which are rapidly activated and recruited to keratin IFs during stress (Wöll et al., 2007, He et al., 2002, Ku et al., 2002). Following phosphorylation by p38, keratin IFs are disassembled into granules, and this reversible event seems to be necessary for the short-term

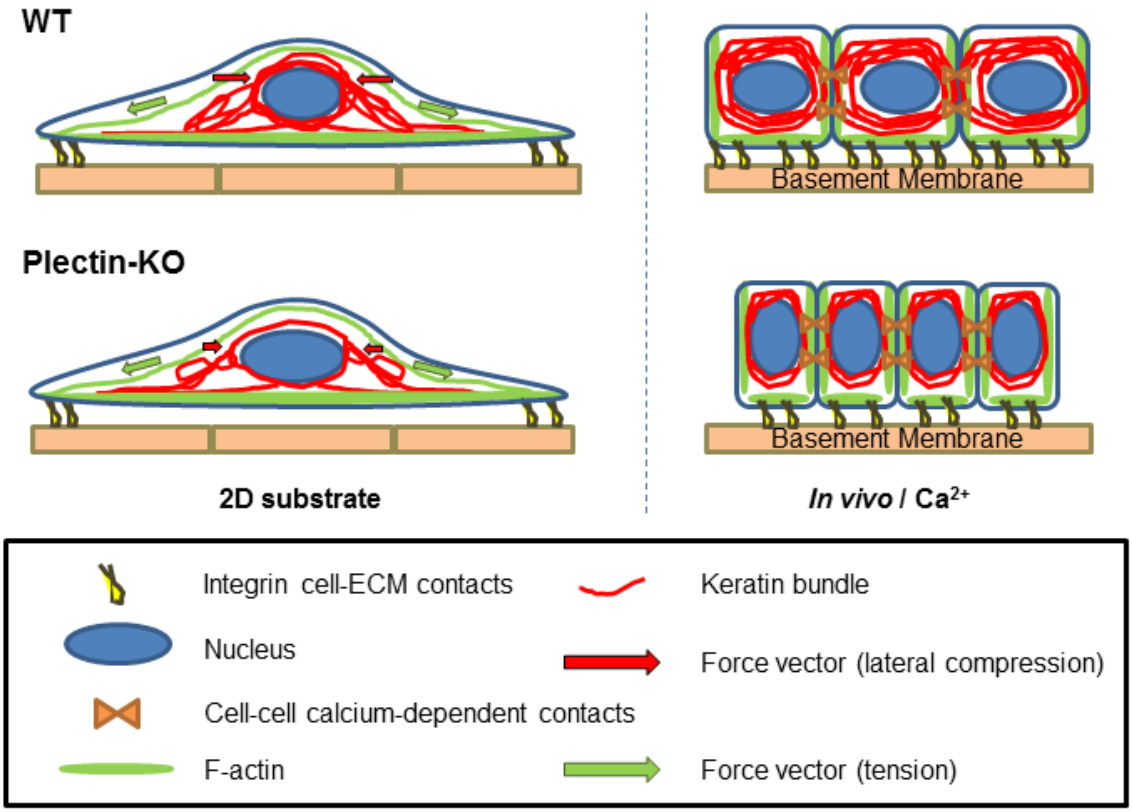

Figure 7.1 – Illustrative model of the effects of plectin in nuclear mechano-transduction. The balance of internal forces that regulate the nucleus are determined by 1) F-actin, which exerts compression on the apical side of the nucleus by generating tension as the cell spreads (green arrows), and 2) by keratin network, which architecture is defined, in its turn, by plectin. The *Plec* KO cells possess a more open K14 network, as illustrated above in red, and as result this network exerts possibly lower lateral force that opposes

F-actin driven compression and hence expansion. When cells are compacted and establish cell-cell contacts, this exacerbated nuclear morphology seen in *Plec* KO is lost.

regulation of epithelial cell plasticity (Fois et al., 2013). In fact, keratin re-arrangement and K18 phosphorylation at cell-cell contacts was detected in keratinocytes after mechanical stress. It would be interesting to investigate further how plectin is involved in this mechanically induced response, and ultimately how the nucleus is affected by different forms of cellular stress.

Plectin deficiency affects also the migration of keratinocytes *in vitro*. *Plec* KO keratinocytes migrate faster than WT (Osmanagic-Myers et al., 2006), which is accompanied by larger deformations of the nucleus as shown here. This could potentially have implications in the wound healing. The impact of IFs in cell growth and migration, both essential for re-epithelialisation is still not completely understood and follows complex expression patterns in humans (Patel et al., 2005). Vimentin promotes migration, whereas keratins attenuate the invasive properties of tumour cells (Snider and Omary, 2014, Chung et al., 2013, Seltmann et al., 2013a). Further investigations looking at how keratin integrity and structure change in migrating cells, both *in vitro* and *in vivo*, would help to understand the dynamics of these key proteins in epithelial tissues. Live 4D imaging would definitely be helpful to understand to a greater extent these phenomena, and further down the line this knowledge would contribute for regenerative medicine and tissue engineering applications.

To gain further insight into more physiologically relevant events the behaviour of *Plec* KO cells was assessed in multi-cell clusters. Seeding *Plec* KO cells in high

density on large patterns led to higher degrees of cell compaction when compared with WT. This result is in agreement with the *in vivo* observations where *Plec* KO basal cells in the epidermis are smaller. These findings suggest that cellular mechanics, dictated in this case by keratin cytoskeleton, affects nuclear morphology and distribution at tissue level. Indeed, the role of the cytoskeleton composition and architecture in regulating epidermis nuclear morphology only recently has been appreciated (Lee et al., 2012, Pan et al., 2013, Wallace et al., 2012). Double-null KO (*K10$^{-/-}$/K1$^{-/-}$)* mice lose their nucleus prematurely in the suprabasal layer of epidermis, along with low levels of emerin and lamin A/C (Wallace et al., 2012). Also, the establishment of disulfide bonds, at an early stage of differentiation, is shown to stabilise a cage of keratin IFs that may impact the size and shape of the nucleus in a calcium-dependent fashion (Lee et al., 2012). Furthermore, nuclear morphology in human EBS patients is affected, resulting a more elongated nuclei (higher aspect ratio) and smaller cross-sectional area (Almeida et al., 2015) (in Appendix I, page 180). This condition leads to blistering patient's skin under stress and *PLEC* mutations represent 8% of EBS cases (Bolling et al., 2013). With the gradual increase of reports in EBS (Charlesworth et al., 2013, Chamcheu et al., 2011) the results of this thesis could bring new insights into the effects of plectin in skin disease progression and will be an important area of investigation in the future.

7.3 Adhesive cues control nuclear architecture in primary human keratinocytes

In chapter 5, the analysis of chromatin remodelling in response to adhesive cues was investigated. Confined cells (seeded on 20μm islands) undergo

terminal differentiation after 24 hours, which was accompanied by a drop of euchromatin levels, measured using H3K4me3 marker. In spread cells, a rapid heterochromatin re-distribution (H3K27me3 signal) was observed. Chromatin is recently shown to affect overall nuclear stiffness. Chromatin de-condensation leads to the softening of the nucleus (Chalut et al., 2012), whereas heterochromatin is thought to be responsible for its stiffening (Banerjee et al. 2006, Bhattacharya et al., 2012). Further evidence are necessary in looking how chromatin condensation state influences overall nuclear mechanics.

The peripheral nuclear staining of lamin A/C was much more pronounced in confined cells (20μm). Nuclear lamina is classically associated with nuclear mechanics (Rowat et al., 2006, Rowat et al., 2005, Broers et al., 2005, Broers et al., 2004) and nuclear envelope physical integrity (Jung et al., 2014). Lamin A/C is shown to contribute to the visco-elasticity of the nucleus, whereas lamin B its elasticity (Swift et al. 2013). Its functional role, although, is not fully understood. Lamins have the ability to interact with many nuclear molecules (Wilson and Berk, 2010, Wilson and Foisner, 2010), including the DNA itself and lamin-binding proteins, which in turn bind to heterochromatin (Wagner and Krohne, 2007), suggesting its role in chromatin silencing. Unfortunately, few studies have addressed, other than overall levels of expression of nuclear lamins, structural changes on the meshwork which may possibly alter its interaction with proteins in the nucleoplasm such as actin, emerin (Sakaki et al., 2001), or even transcription factors such as Oct-1 (Malhas et al., 2009). Altogether, chromatin silencing and nuclear lamina are possibly regulated (at certain extent) by mechanical cues, which may dictate keratinocyte's mechano-responses. Future studies addressing conformational studies in response to mechanical cues are

needed to understand its impact in cell fate and epidermal homeostasis. It would be of particular interest to study how different genes of the EDC loci (Epidermal Differentiation Complex) are mediated by adhesive cue, as well as Satb1 and Brg1, as these have been shown to be key regulators of keratinocyte's higher-order structure of chromatin during differentiation (Mardaryev et al., 2014, Botchkarev et al., 2012, Fessing et al., 2011). Furthermore, gene expression profiling using (e.g. microarray technology) in *Plec* KO mouse keratinocytes seeded in different micropatterns would provide essential information of the genes that are regulated directly or indirectly by plectin under particular mechanical cues.

7.4 New approaches, new insights into mechano-transduction

Typically, techniques used to measure the mechanics of biological materials lack in spatial resolution. A novel method that allows the imaging of cell's interior was developed. The technique consists in the use of dual beam microscopy (SEM/FIB) to mill through single cells, which allows the subsequent mechanical testing of cell interior utilising atomic force microscopy (AFM). SEM/FIB has been applied in for high resolution imaging of biological materials (Kamino et al., 2004, Milani and Drobne, 2006, Grandfield and Engqvist, 2012). Also, this apparatus was utilised to perform nano-scale mechanical testing by incorporating an AFM into the dual beam chamber (Hang and Barber, 2010, Hang et al., 2011, Jimenez-Palomar et al., 2012). The same rationale was followed in the present work, although the ultimate goal is to perform *in situ* mechanical mapping inside the cell. Successful milling and polishing was achieved, and the next step would be to analyse the spatial mechanics inside the cell. Future work recommendations include: the use of different fixative agents in order to minimise the cross-linking induced by aldehyde-based fixatives (e.g. paraformaldehyde and glutaraldehyde); the use of beads tagged with antibodies (e.g. anti-lamin A/C-Au) to label particular structures inside the nucleus and obtain reasonable mechanical contrast as a positive control; possibly the use of chemical inhibitors or osmolalities to induce either condensation or decondensation of chromatin as controls; among others.

7.5 Conclusions and Final Remarks

The work presented in this thesis demonstrates that nuclear mechano-transduction in keratinocytes is dictated (at least partly) by the complex network of keratin intermediate filaments, which the structure is regulated by the cross-linker protein plectin. The study here reported brings new insights into the role of plectin in regulating the mechanics of keratinocytes and nuclear mechano-transduction. It is demonstrated that plectin cross-links keratin network and that this is important in protecting the nucleus against actomyosin-dependent deformation, impacting ultimately the morphology of the nucleus *in vivo*. Furthermore, it is shown that nuclear deformations causes rapid re-distribution of heterochromatin markers in human keratinocytes. Also, reduced euchromatin levels correlate with terminal differentiation upon loss of ECM-cell contacts. These findings suggest that mechanical cues orchestrate the epidermal terminal differentiation programme in a complex time-dependent fashion. In summary, the present work supports the idea that the nucleus itself is a mechano-sensor, and that the mechano-sensitivity of cells depend upon the intermediate filament network and actomyosin contractility. In addition, a novel technique for investigations into the mechanical properties of cells is presented with the intention to provide guidance for future studies. It is provided details on how focused ion beam technology combined with atomic force microscopy could be utilised to instigate nano-scale mechanics of the cell's interior.

7.6 Bibliography

ABU SHAH, E. & KEREN, K. 2013. Mechanical forces and feedbacks in cell motility. *Curr Opin Cell Biol,* 25**,** 550-7.

ACHARD, V., MARTIEL, J. L., MICHELOT, A., GUERIN, C., REYMANN, A. C., BLANCHOIN, L. & BOUJEMAA-PATERSKI, R. 2010. A "primer"-based mechanism underlies branched actin filament network formation and motility. *Curr Biol,* 20**,** 423-8.

AKIN, O. & MULLINS, R. D. 2008. Capping protein increases the rate of actin-based motility by promoting filament nucleation by the Arp2/3 complex. *Cell,* 133**,** 841-51.

ALLIS, C. D., BERGER, S. L., COTE, J., DENT, S., JENUWIEN, T., KOUZARIDES, T., PILLUS, L., REINBERG, D., SHI, Y., SHIEKHATTAR, R., SHILATIFARD, A., WORKMAN, J. & ZHANG, Y. 2007. New nomenclature for chromatin-modifying enzymes. *Cell,* 131**,** 633-6.

ALMEIDA, F. V. M., WALKO, G., MCMILLAN, J. R., MCGRATH, J. A., WICHE, G., BARBER, A. H. & CONNELLY, J. T. 2015. The cytolinker plectin regulates nuclear mechanotransduction in keratinocytes. *Journal Cell Science,* Under revision.

ANDRA, K., KORNACKER, I., JORGL, A., ZORER, M., SPAZIERER, D., FUCHS, P., FISCHER, I. & WICHE, G. 2003. Plectin-isoform-specific rescue of hemidesmosomal defects in plectin (-/-) keratinocytes. *J Invest Dermatol,* 120**,** 189-97.

ANDRÄ, K., LASSMANN, H., BITTNER, R., SHORNY, S., FÄSSLER, R., PROPST, F. & WICHE, G. 1997. Targeted inactivation of plectin reveals essential function in maintaining the integrity of skin, muscle, and heart cytoarchitecture. *Genes & Development,* 11**,** 3143-3156.

ANDRA, K., NIKOLIC, B., STOCHER, M., DRENCKHAHN, D. & WICHE, G. 1998. Not just scaffolding: plectin regulates actin dynamics in cultured cells. *Genes Dev,* 12**,** 3442-51.

ARROYO, J. D. & HAHN, W. C. 2005. Involvement of PP2A in viral and cellular transformation. *Oncogene,* 24**,** 7746-55.

AVIVI, L. & FELDMAN, M. 1980. Arrangement of chromosomes in the interphase nucleus of plants. *Hum Genet,* 55**,** 281-95.

BAI, M., MISSEL, A. R., KLUG, W. S. & LEVINE, A. J. 2011. The mechanics and affine-nonaffine transition in polydisperse semiflexible networks. *Soft Matter,* 7**,** 907-914.

BAILEY, R. J., GEURTS, R., STOKES, D. J., DE JONG, F. & BARBER, A. H. 2013. Evaluating focused ion beam induced damage in soft materials. *Micron,* 50**,** 51-56.

BANERJEE, B., BALASUBRAMANIAN, S., ANANTHAKRISHNA, G., RAMAKRISHNAN, T. V. & SHIVASHANKAR, G. V. 2004. Tracking operator state fluctuations in gene expression in single cells. *Biophys J,* 86**,** 3052-9.

BANERJEE, B., BHATTACHARYA, D. & SHIVASHANKAR, G. V. 2006. Chromatin structure exhibits spatio-temporal heterogeneity within the cell nucleus. *Biophys J,* 91**,** 2297-303.

BARRANDON, Y. & GREEN, H. 1987. Three clonal types of keratinocyte with different capacities for multiplication. *Proc Natl Acad Sci U S A,* 84**,** 2302-6.

BARSKI, A., CUDDAPAH, S., CUI, K., ROH, T. Y., SCHONES, D. E., WANG, Z., WEI, G., CHEPELEV, I. & ZHAO, K. 2007. High-resolution profiling of histone methylations in the human genome. *Cell,* 129**,** 823-37.

BERGER, S. L. 2007. The complex language of chromatin regulation during transcription. *Nature,* 447**,** 407-12.

BERIAULT, D. R., HADDAD, O., MCCUAIG, J. V., ROBINSON, Z. J., RUSSELL, D., LANE, E. B. & FUDGE, D. S. 2012. The mechanical behavior of mutant K14-R125P keratin bundles and networks in NEB-1 keratinocytes. *PLoS ONE,* 7**,** e31320.

BERNHEIM-GROSWASSER, A., WIESNER, S., GOLSTEYN, R. M., CARLIER, M. F. & SYKES, C. 2002. The dynamics of actin-based motility depend on surface parameters. *Nature,* 417**,** 308-11.

BERTAUD, J., QIN, Z. & BUEHLER, M. J. 2010. Intermediate filament-deficient cells are mechanically softer at large deformation: A multi-scale simulation study. *Acta Biomaterialia,* 6**,** 2457-2466.

BHATTACHARYA, D., TALWAR, S., MAZUMDER, A. & SHIVASHANKAR, G. V. 2009. Spatio-temporal plasticity in chromatin organization in mouse cell differentiation and during Drosophila embryogenesis. *Biophys J,* 96**,** 3832-9.

BLANCHARD, G. B., KABLA, A. J., SCHULTZ, N. L., BUTLER, L. C., SANSON, B., GORFINKIEL, N., MAHADEVAN, L. & ADAMS, R. J. 2009. Tissue tectonics: morphogenetic strain rates, cell shape change and intercalation. *Nat Methods,* 6**,** 458-64.

BLANCHOIN, L., BOUJEMAA-PATERSKI, R., SYKES, C. & PLASTINO, J. 2014. *Actin Dynamics, Architecture, and Mechanics in Cell Motility*.

BOCZONADI, V., MCINROY, L. & MAATTA, A. 2007. Cytolinker cross-talk: periplakin N-terminus interacts with plectin to regulate keratin organisation and epithelial migration. *Exp Cell Res,* 313**,** 3579-91.

BOLLING, M. C., JONGBLOED, J. D. H., BOVEN, L. G., DIERCKS, G. F. H., SMITH, F. J. D., MCLEAN, W. H. I. & JONKMAN, M. F. 2013. Plectin Mutations Underlie Epidermolysis Bullosa Simplex in 8% of Patients. *Journal of Investigative Dermatology,* 134**,** 273-276.

BONAKDAR, N., SCHILLING, A., SPÖRRER, M., LENNERT, P., MAINKA, A., WINTER, L., WALKO, G., WICHE, G., FABRY, B. & GOLDMANN, W. H. 2015. Determining the mechanical properties of plectin in mouse myoblasts and keratinocytes. *Experimental Cell Research,* 331**,** 331-337.

BOOTH-GAUTHIER, ELIZABETH A., ALCOSER, TURI A., YANG, G. & DAHL, KRIS N. 2012. Force-Induced Changes in Subnuclear Movement and Rheology. *Biophysical Journal,* 103**,** 2423-2431.

BORDELEAU, F., MYRAND LAPIERRE, M.-E., SHENG, Y. & MARCEAU, N. 2012. Keratin 8/18 Regulation of Cell Stiffness-Extracellular Matrix Interplay through Modulation of Rho-Mediated Actin Cytoskeleton Dynamics. *PLoS ONE,* 7**,** e38780.

BOTCHKAREV, V. A., GDULA, M. R., MARDARYEV, A. N., SHAROV, A. A. & FESSING, M. Y. 2012. Epigenetic Regulation of Gene Expression in Keratinocytes. *Journal of Investigative Dermatology*.

BOUAMEUR, J. E., FAVRE, B., FONTAO, L., LINGASAMY, P., BEGRE, N. & BORRADORI, L. 2014. Interaction of plectin with keratins 5 and 14: dependence on several plectin domains and keratin quaternary structure. *J Invest Dermatol,* 134**,** 2776-83.

BOUKELLAL, H., CAMPAS, O., JOANNY, J. F., PROST, J. & SYKES, C. 2004. Soft Listeria: actin-based propulsion of liquid drops. *Phys Rev E Stat Nonlin Soft Matter Phys,* 69**,** 061906.

BRANGWYNNE, C. P., MACKINTOSH, F. C., KUMAR, S., GEISSE, N. A., TALBOT, J., MAHADEVAN, L., PARKER, K. K., INGBER, D. E. & WEITZ, D. A. 2006. Microtubules can bear enhanced compressive loads in living cells because of lateral reinforcement. *J Cell Biol,* 173**,** 733-41.

BRAUN, K. M., NIEMANN, C., JENSEN, U. B., SUNDBERG, J. P., SILVA-VARGAS, V. & WATT, F. M. 2003. Manipulation of stem cell proliferation and lineage commitment: visualisation of label-retaining cells in wholemounts of mouse epidermis. *Development,* 130**,** 5241-55.

BRENNICH, M. E., NOLTING, J.-F., DAMMANN, C., NODING, B., BAUCH, S., HERRMANN, H., PFOHL, T. & KOSTER, S. 2011. Dynamics of intermediate filament assembly followed in micro-flow by small angle X-ray scattering. *Lab on a Chip,* 11**,** 708-716.

BREZNA, W., WANZENBÖCK, H., LUGSTEIN, A., BERTAGNOLLI, E., GORNIK, E. & SMOLINER, J. 2003a. Focussed ion beam induced damage in silicon studied by scanning capacitance microscopy. *Semiconductor Science and Technology,* 18**,** 195.

BREZNA, W., WANZENBÖCK, H., LUGSTEIN, A., BERTAGNOLLI, E., GORNIK, E. & SMOLINER, J. 2003b. Scanning capacitance microscopy investigations of focused ion beam damage in silicon. *Physica E: Low-Dimensional Systems and Nanostructures,* 19**,** 178-182.

BROCK, A. L. & INGBER, D. E. 2005. Control of the direction of lamellipodia extension through changes in the balance between Rac and Rho activities. *Mol Cell Biomech,* 2**,** 135-43.

BROERS, J. L., KUIJPERS, H. J., OSTLUND, C., WORMAN, H. J., ENDERT, J. & RAMAEKERS, F. C. 2005. Both lamin A and lamin C mutations cause lamina instability as well as loss of internal nuclear lamin organization. *Exp Cell Res,* 304**,** 582-92.

BROERS, J. L., PEETERS, E. A., KUIJPERS, H. J., ENDERT, J., BOUTEN, C. V., OOMENS, C. W., BAAIJENS, F. P. & RAMAEKERS, F. C. 2004. Decreased mechanical stiffness in LMNA-/- cells is caused by defective nucleo-cytoskeletal integrity: implications for the development of laminopathies. *Hum Mol Genet,* 13**,** 2567-80.

BROSIG, M., FERRALLI, J., GELMAN, L., CHIQUET, M. & CHIQUET-EHRISMANN, R. 2010. Interfering with the connection between the nucleus and the cytoskeleton affects nuclear rotation, mechanotransduction and myogenesis. *The International Journal of Biochemistry & Cell Biology,* 42**,** 1717-1728.

BROWN, A. A., KHAN, N. S., STEINBOCK, L. & HUCK, W. T. S. 2005. Synthesis of oligo(ethylene glycol) methacrylate polymer brushes. *European Polymer Journal,* 41**,** 1757-1765.

BRUCE ALBERTS, ALEXANDER JOHNSON, JULIAN LEWIS, DAVID MORGAN, MARTIN RAFF, KEITH ROBERTS & WALTER, P. 2015. The

Cytoskeleton. *Molecular Biology of the Cell.* New York: Garland Science, Taylor & Francis Group, LLC.

BURGSTALLER, G., GREGOR, M., WINTER, L. & WICHE, G. 2010. Keeping the Vimentin Network under Control: Cell-Matrix Adhesion-associated Plectin 1f Affects Cell Shape and Polarity of Fibroblasts. *Molecular Biology of the Cell,* 21**,** 3362-3375.

BURNETTE, D. T., SHAO, L., OTT, C., PASAPERA, A. M., FISCHER, R. S., BAIRD, M. A., DER LOUGHIAN, C., DELANOE-AYARI, H., PASZEK, M. J., DAVIDSON, M. W., BETZIG, E. & LIPPINCOTT-SCHWARTZ, J. 2014. A contractile and counterbalancing adhesion system controls the 3D shape of crawling cells. *The Journal of Cell Biology,* 205**,** 83-96.

BUSHBY, A. J., P'NG, K. M. Y., YOUNG, R. D., PINALI, C., KNUPP, C. & QUANTOCK, A. J. 2011. Imaging three-dimensional tissue architectures by focused ion beam scanning electron microscopy. *Nat. Protocols,* 6**,** 845-858.

BUTT, H.-J., CAPPELLA, B. & KAPPL, M. 2005. Force measurements with the atomic force microscope: Technique, interpretation and applications. *Surface Science Reports,* 59**,** 1-152.

BYRNE, C., TAINSKY, M. & FUCHS, E. 1994. Programming gene expression in developing epidermis. *Development,* 120**,** 2369-83.

CAMERON, L. A., FOOTER, M. J., VAN OUDENAARDEN, A. & THERIOT, J. A. 1999. Motility of ActA protein-coated microspheres driven by actin polymerization. *Proc Natl Acad Sci U S A,* 96**,** 4908-13.

CANDI, E., TARCSA, E., DIGIOVANNA, J. J., COMPTON, J. G., ELIAS, P. M., MAREKOV, L. N. & STEINERT, P. M. 1998. A highly conserved lysine residue on the head domain of type II keratins is essential for the attachment of keratin intermediate filaments to the cornified cell envelope through isopeptide crosslinking by transglutaminases. *Proc Natl Acad Sci U S A,* 95**,** 2067-72.

CAO, R., WANG, L., WANG, H., XIA, L., ERDJUMENT-BROMAGE, H., TEMPST, P., JONES, R. S. & ZHANG, Y. 2002. Role of histone H3 lysine 27 methylation in Polycomb-group silencing. *Science,* 298**,** 1039-43.

CARTER, W. G., KAUR, P., GIL, S. G., GAHR, P. J. & WAYNER, E. A. 1990. Distinct functions for integrins alpha 3 beta 1 in focal adhesions and alpha 6 beta 4/bullous pemphigoid antigen in a new stable anchoring contact (SAC) of keratinocytes: relation to hemidesmosomes. *J Cell Biol,* 111**,** 3141-54.

CASTAÑÓN, M. J., WALKO, G., WINTER, L. & WICHE, G. 2013. Plectin–intermediate filament partnership in skin, skeletal muscle, and peripheral nerve. *Histochemistry and Cell Biology,* 140**,** 33-53.

CHALUT, K. J., HOPFLER, M., LAUTENSCHLAGER, F., BOYDE, L., CHAN, C. J., EKPENYONG, A., MARTINEZ-ARIAS, A. & GUCK, J. 2012. Chromatin decondensation and nuclear softening accompany Nanog downregulation in embryonic stem cells. *Biophys J,* 103**,** 2060-70.

CHAMCHEU, J. C., SIDDIQUI, I. A., SYED, D. N., ADHAMI, V. M., LIOVIC, M. & MUKHTAR, H. 2011. Keratin gene mutations in disorders of human skin and its appendages. *Archives of Biochemistry and Biophysics,* 508**,** 123-137.

CHANG, T.-H., HUANG, H.-D., ONG, W.-K., FU, Y.-J., LEE, O. K., CHIEN, S. & HO, J. H. 2014. The effects of actin cytoskeleton perturbation on keratin intermediate filament formation in mesenchymal stem/stromal cells. *Biomaterials,* 35**,** 3934-3944.

CHARLESWORTH, A., CHIAVERINI, C., CHEVRANT-BRETON, J., DELRIO, M., DIOCIAIUTI, A., DUPUIS, R. P., EL HACHEM, M., LE FIBLEC, B., SANKARI-HO, A. M., VALHQUIST, A., WIERZBICKA, E., LACOUR, J. P. & MENEGUZZI, G. 2013. Epidermolysis bullosa simplex with PLEC mutations: new phenotypes and new mutations. *Br J Dermatol,* 168**,** 808-14.

CHEN, C. S., ALONSO, J. L., OSTUNI, E., WHITESIDES, G. M. & INGBER, D. E. 2003. Cell shape provides global control of focal adhesion assembly. *Biochem Biophys Res Commun,* 307**,** 355-61.

CHIRCOP, M. 2014. Rho GTPases as regulators of mitosis and cytokinesis in mammalian cells. *Small GTPases,* 5.

CHOI, C. K., VICENTE-MANZANARES, M., ZARENO, J., WHITMORE, L. A., MOGILNER, A. & HORWITZ, A. R. 2008. Actin and alpha-actinin orchestrate the assembly and maturation of nascent adhesions in a myosin II motor-independent manner. *Nat Cell Biol,* 10**,** 1039-50.

CHUNG, B.-M., ROTTY, J. D. & COULOMBE, P. A. 2013. Networking galore: intermediate filaments and cell migration. *Current Opinion in Cell Biology,* 25**,** 600-612.

COMINGS, D. E. 1980. Arrangement of chromatin in the nucleus. *Hum Genet,* 53**,** 131-43.

CONNELLY, J. T., GAUTROT, J. E., TRAPPMANN, B., TAN, D. W.-M., DONATI, G., HUCK, W. T. S. & WATT, F. M. 2010. Actin and serum response factor transduce physical cues from the microenvironment to regulate epidermal stem cell fate decisions. *Nature Cell Biology,* 12**,** 711-718.

CONNELLY, J. T., MISHRA, A., GAUTROT, J. E. & WATT, F. M. 2011. Shape-Induced Terminal Differentiation of Human Epidermal Stem Cells Requires p38 and Is Regulated by Histone Acetylation. *PLoS ONE,* 6**,** e27259.

COOPER, G. M. & HAUSMAN, R. E. 2004. *The Cell - A molecular approach,* Washington D.C., ASM Press.

COSTA, P., ALMEIDA, F. V. M. & CONNELLY, J. T. 2012. Biophysical signals controlling cell fate decisions: How do stem cells really feel? *The International Journal of Biochemistry & Cell Biology,* 44**,** 2233-2237.

COSTA, P., GAUTROT, J. E. & CONNELLY, J. T. 2014. Directing cell migration using micropatterned and dynamically adhesive polymer brushes. *Acta Biomaterialia,* 10**,** 2415-2422.

COUE, M., BRENNER, S. L., SPECTOR, I. & KORN, E. D. 1987. Inhibition of actin polymerization by latrunculin A. *FEBS Lett,* 213**,** 316-8.

COURSON, D. S. & ROCK, R. S. 2010. Actin cross-link assembly and disassembly mechanics for alpha-Actinin and fascin. *J Biol Chem,* 285**,** 26350-7.

CREMER, T., CREMER, C., BAUMANN, H., LUEDTKE, E. K., SPERLING, K., TEUBER, V. & ZORN, C. 1982. Rabl's model of the interphase chromosome arrangement tested in Chinise hamster cells by premature

chromosome condensation and laser-UV-microbeam experiments. *Human Genetics,* 60**,** 10.
CREMER, T. & CREMER, M. 2010. Chromosome Territories. *Cold Spring Harbor Perspectives in Biology,* 2:a003889.
CRISP, M., LIU, Q., ROUX, K., RATTNER, J. B., SHANAHAN, C., BURKE, B., STAHL, P. D. & HODZIC, D. 2006. Coupling of the nucleus and cytoplasm: role of the LINC complex. *J Cell Biol,* 172**,** 41-53.
CUCCI, R. A., PRASAD, S., KELLEY, P. M., GREEN, G. E., STORM, K., WILLOCX, S., COHN, E. S., VAN CAMP, G. & SMITH, R. J. 2000. The M34T allele variant of connexin 26. *Genet Test,* 4**,** 335-44.
DAHL, K. N., BOOTH-GAUTHIER, E. A. & LADOUX, B. 2010. In the middle of it all: Mutual mechanical regulation between the nucleus and the cytoskeleton. *Journal of Biomechanics,* 43**,** 2-8.
DAHL, K. N., RIBEIRO, A. J. S. & LAMMERDING, J. 2008. Nuclear Shape, Mechanics, and Mechanotransduction. *Circulation Research,* 102**,** 1307-1318.
DAS, M., LEVINE, A. J. & MACKINTOSH, F. C. 2008. Buckling and force propagation along intracellular microtubules. *EPL (Europhysics Letters),* 84**,** 18003.
DAYEL, M. J., AKIN, O., LANDERYOU, M., RISCA, V., MOGILNER, A. & MULLINS, R. D. 2009. In silico reconstitution of actin-based symmetry breaking and motility. *PLoS Biol,* 7**,** e1000201.
DEY, P. & BALOCH, Z. 2009. Cancer nucleus: Morphology and beyond. *Diagnostic Cytopathology***,** NA-NA.
DIKE, L. E., CHEN, C. S., MRKSICH, M., TIEN, J., WHITESIDES, G. M. & INGBER, D. E. 1999. Geometric control of switching between growth, apoptosis, and differentiation during angiogenesis using micropatterned substrates. *In Vitro Cell Dev Biol Anim,* 35**,** 441-8.
DOUBE, M., KŁOSOWSKI, M. M., ARGANDA-CARRERAS, I., CORDELIÈRES, F. P., DOUGHERTY, R. P., JACKSON, J. S., SCHMID, B., HUTCHINSON, J. R. & SHEFELBINE, S. J. 2010. BoneJ: Free and extensible bone image analysis in ImageJ. *Bone,* 47**,** 1076-1079.
DUNDR, M. & MISTELI, T. 2010. Biogenesis of nuclear bodies. *Cold Spring Harb Perspect Biol,* 2**,** a000711.
DUPONT, S., MORSUT, L., ARAGONA, M., ENZO, E., GIULITTI, S., CORDENONSI, M., ZANCONATO, F., LE DIGABEL, J., FORCATO, M., BICCIATO, S., ELVASSORE, N. & PICCOLO, S. 2011. Role of YAP/TAZ in mechanotransduction. *Nature,* 474**,** 179-183.
EICHHORN, P. J., CREYGHTON, M. P. & BERNARDS, R. 2009. Protein phosphatase 2A regulatory subunits and cancer. *Biochim Biophys Acta,* 1795**,** 1-15.
ELBASHIR, S. M., HARBORTH, J., LENDECKEL, W., YALCIN, A., WEBER, K. & TUSCHL, T. 2001. Duplexes of 21-nucleotide RNAs mediate RNA interference in cultured mammalian cells. *Nature,* 411**,** 494-498.
ENGLER, A. J., SEN, S., SWEENEY, H. L. & DISCHER, D. E. 2006. Matrix elasticity directs stem cell lineage specification. *Cell,* 126**,** 677-89.
ESTELLER, M. 2007. Cancer epigenomics: DNA methylomes and histone-modification maps. *Nat Rev Genet,* 8**,** 286-98.

FAGOTTO, F., GLUCK, U. & GUMBINER, B. M. 1998. Nuclear localization signal-independent and importin/karyopherin-independent nuclear import of beta-catenin. *Curr Biol,* 8**,** 181-90.

FALZONE, T. T., LENZ, M., KOVAR, D. R. & GARDEL, M. L. 2012. Assembly kinetics determine the architecture of alpha-actinin crosslinked F-actin networks. *Nat Commun,* 3**,** 861.

FEDORCHAK, G. R., KAMINSKI, A. & LAMMERDING, J. 2014. Cellular mechanosensing: getting to the nucleus of it all. *Prog Biophys Mol Biol,* 115**,** 76-92.

FESSING, M. Y., MARDARYEV, A. N., GDULA, M. R., SHAROV, A. A., SHAROVA, T. Y., RAPISARDA, V., GORDON, K. B., SMORODCHENKO, A. D., POTERLOWICZ, K., FERONE, G., KOHWI, Y., MISSERO, C., KOHWI-SHIGEMATSU, T. & BOTCHKAREV, V. A. 2011. p63 regulates Satb1 to control tissue-specific chromatin remodeling during development of the epidermis. *The Journal of Cell Biology,* 194**,** 825-839.

FIDZIANSKA, A., TONIOLO, D. & HAUSMANOWA-PETRUSEWICZ, I. 1998. Ultrastructural abnormality of sarcolemmal nuclei in Emery-Dreifuss muscular dystrophy (EDMD). *J Neurol Sci,* 159**,** 88-93.

FINE, J. D., BRUCKNER-TUDERMAN, L., EADY, R. A., BAUER, E. A., BAUER, J. W., HAS, C., HEAGERTY, A., HINTNER, H., HOVNANIAN, A., JONKMAN, M. F., LEIGH, I., MARINKOVICH, M. P., MARTINEZ, A. E., MCGRATH, J. A., MELLERIO, J. E., MOSS, C., MURRELL, D. F., SHIMIZU, H., UITTO, J., WOODLEY, D. & ZAMBRUNO, G. 2014. Inherited epidermolysis bullosa: updated recommendations on diagnosis and classification. *J Am Acad Dermatol,* 70**,** 1103-26.

FLETCHER, D. A. & MULLINS, R. D. 2010. Cell mechanics and the cytoskeleton. *Nature,* 463**,** 485-492.

FOIS, G., WEIMER, M., BUSCH, T., FELDER, E. T., OSWALD, F., VON WICHERT, G., SEUFFERLEIN, T., DIETL, P. & FELDER, E. 2013. Effects of keratin phosphorylation on the mechanical properties of keratin filaments in living cells. *FASEB J,* 27**,** 1322-9.

FONTAO, L., STUTZMANN, J., GENDRY, P. & LAUNAY, J. F. 1999. Regulation of the type II hemidesmosomal plaque assembly in intestinal epithelial cells. *Exp Cell Res,* 250**,** 298-312.

FREEDBERG, I. M., TOMIC-CANIC, M., KOMINE, M. & BLUMENBERG, M. 2001. Keratins and the keratinocyte activation cycle. *J Invest Dermatol,* 116**,** 633-40.

FUCHS, E. 1995. Keratins and the skin. *Annu Rev Cell Dev Biol,* 11**,** 123-53.

FUCHS, E. & GREEN, H. 1980. Changes in keratin gene expression during terminal differentiation of the keratinocyte. *Cell,* 19**,** 1033-42.

FUCHS, E. & RAGHAVAN, S. 2002. Getting under the Skin of Epidermal Morphogenesis. *Nature Reviews Genetics,* 3**,** 199-209.

FUDGE, D., RUSSELL, D., BERIAULT, D., MOORE, W., LANE, E. B. & VOGL, A. W. 2008. The Intermediate Filament Network in Cultured Human Keratinocytes Is Remarkably Extensible and Resilient. *PLoS ONE,* 3**,** e2327.

FUKS, F. 2005. DNA methylation and histone modifications: teaming up to silence genes. *Curr Opin Genet Dev,* 15**,** 490-5.

GACHE, Y., CHAVANAS, S., LACOUR, J. P., WICHE, G., OWARIBE, K., MENEGUZZI, G. & ORTONNE, J. P. 1996. Defective expression of plectin/HD1 in epidermolysis bullosa simplex with muscular dystrophy. *J Clin Invest,* 97**,** 2289-98.

GANDHAM, V. D., MADDALA, R. L., RAO, V., JIN, J. Y., EPSTEIN, D. L., HALL, R. P. & ZHANG, J. Y. 2013. Effects of Y27632 on keratinocyte procurement and wound healing. *Clin Exp Dermatol,* 38**,** 782-6.

GDULA, M. R., POTERLOWICZ, K., MARDARYEV, A. N., SHAROV, A. A., PENG, Y., FESSING, M. Y. & BOTCHKAREV, V. A. 2013. Remodeling of Three-Dimensional Organization of the Nucleus during Terminal Keratinocyte Differentiation in the Epidermis. *Journal of Investigative Dermatology*.

GEIGER, B., SPATZ, J. P. & BERSHADSKY, A. D. 2009. Environmental sensing through focal adhesions. *Nat Rev Mol Cell Biol,* 10**,** 21-33.

GOLDMAN, R. D., CLELAND, M. M., MURTHY, S. N. P., MAHAMMAD, S. & KUCZMARSKI, E. R. 2012. Inroads into the structure and function of intermediate filament networks. *Journal of Structural Biology,* 177**,** 14-23.

GOSTYNSKA, K. B., NIJENHUIS, M., LEMMINK, H., PAS, H. H., PASMOOIJ, A. M., LANG, K. K., CASTANON, M. J., WICHE, G. & JONKMAN, M. F. 2015. Mutation in exon 1a of PLEC, leading to disruption of plectin isoform 1a, causes autosomal-recessive skin-only epidermolysis bullosa simplex. *Hum Mol Genet*.

GRANDFIELD, K. & ENGQVIST, H. 2012. Focused Ion Beam in the Study of Biomaterials and Biological Matter. *Advances in Materials Science and Engineering,* 2012**,** 6.

GREEN, K. J. & GAUDRY, C. A. 2000. Are desmosomes more than tethers for intermediate filaments? *Nat Rev Mol Cell Biol,* 1**,** 208-16.

GREEN, K. J., GETSIOS, S., TROYANOVSKY, S. & GODSEL, L. M. 2010. Intercellular junction assembly, dynamics, and homeostasis. *Cold Spring Harb Perspect Biol,* 2**,** a000125.

GREER, E. L. & SHI, Y. 2012. Histone methylation: a dynamic mark in health, disease and inheritance. *Nat Rev Genet,* 13**,** 343-57.

GREGOR, M., OSMANAGIC-MYERS, S., BURGSTALLER, G., WOLFRAM, M., FISCHER, I., WALKO, G., RESCH, G. P., JORGL, A., HERRMANN, H. & WICHE, G. 2014. Mechanosensing through focal adhesion-anchored intermediate filaments. *FASEB J,* 28**,** 715-29.

GRINNELL, F. 2003. Fibroblast biology in three-dimensional collagen matrices. *Trends Cell Biol,* 13**,** 264-9.

GUILLUY, C., OSBORNE, L. D., VAN LANDEGHEM, L., SHAREK, L., SUPERFINE, R., GARCIA-MATA, R. & BURRIDGE, K. 2014. Isolated nuclei adapt to force and reveal a mechanotransduction pathway in the nucleus. *Nature Cell Biology,* 16**,** 376-381.

GUO, M., EHRLICHER, ALLEN J., MAHAMMAD, S., FABICH, H., JENSEN, MIKKEL H., MOORE, JEFFREY R., FREDBERG, JEFFREY J., GOLDMAN, ROBERT D. & WEITZ, DAVID A. 2013. The Role of Vimentin Intermediate Filaments in Cortical and Cytoplasmic Mechanics. *Biophysical Journal,* 105**,** 1562-1568.

HALE, C. M., SHRESTHA, A. L., KHATAU, S. B., STEWART-HUTCHINSON, P. J., HERNANDEZ, L., STEWART, C. L., HODZIC, D. & WIRTZ, D.

2008. Dysfunctional connections between the nucleus and the actin and microtubule networks in laminopathic models. *Biophys J,* 95**,** 5462-75.
HALL, A. & NOBES, C. D. 2000. *Rho GTPases: molecular switches that control the organization and dynamics of the actin cytoskeleton*.
HANG, F. & BARBER, A. H. 2010. Nano-mechanical properties of individual mineralized collagen fibrils from bone tissue. *Journal of The Royal Society Interface,* 8**,** 500-505.
HANG, F., GUPTA, H. S. & BARBER, A. H. 2014. *Nanointerfacial strength between non-collagenous protein and collagen fibrils in antler bone*.
HANG, F., LU, D., BAILEY, R. J., JIMENEZ-PALOMAR, I., STACHEWICZ, U., CORTES-BALLESTEROS, B., DAVIES, M., ZECH, M., BODEFELD, C. & BARBER, A. H. 2011. In situ tensile testing of nanofibers by combining atomic force microscopy and scanning electron microscopy. *Nanotechnology,* 22**,** 365708.
HARRIS, A. R., BELLIS, J., KHALILGHARIBI, N., WYATT, T., BAUM, B., KABLA, A. J. & CHARRAS, G. T. 2013. Generating suspended cell monolayers for mechanobiological studies. *Nat Protoc,* 8**,** 2516-30.
HARRIS, A. R., DAEDEN, A. & CHARRAS, G. T. 2014. Formation of adherens junctions leads to the emergence of a tissue-level tension in epithelial monolayers. *J Cell Sci,* 127**,** 2507-17.
HARRIS, A. R., PETER, L., BELLIS, J., BAUM, B., KABLA, A. J. & CHARRAS, G. T. 2012. Characterizing the mechanics of cultured cell monolayers. *Proceedings of the National Academy of Sciences,* 109**,** 16449-16454.
HE, T., STEPULAK, A., HOLMSTROM, T. H., OMARY, M. B. & ERIKSSON, J. E. 2002. The intermediate filament protein keratin 8 is a novel cytoplasmic substrate for c-Jun N-terminal kinase. *J Biol Chem,* 277**,** 10767-74.
HEER, C. V. 1972. X - Stochastic Processes, Noise, and Fluctuations. *In:* HEER, C. V. (ed.) *Statistical Mechanics, Kinetic Theory, and Stochastic Processes.* Cambridge: Academic Press.
HESSE, M., ZIMEK, A., WEBER, K. & MAGIN, T. M. 2004. Comprehensive analysis of keratin gene clusters in humans and rodents. *Eur J Cell Biol,* 83**,** 19-26.
HEYMANN, J. A. W., SHI, D., KIM, S., BLISS, D., MILNE, J. L. S. & SUBRAMANIAM, S. 2009. 3D Imaging of mammalian cells with ion-abrasion scanning electron microscopy. *Journal of Structural Biology,* 166**,** 1-7.
HIS, W. 1874. *Unsere Körperform und das physiologische Problem ihrer Entstehung Briefe an einen befreundeten Naturforscher / von Wilhelm His,* Leipzig :, F.C.W. Vogel.
HO, C. Y., JAALOUK, D. E., VARTIAINEN, M. K. & LAMMERDING, J. 2013. Lamin A/C and emerin regulate MKL1–SRF activity by modulating actin dynamics. *Nature,* 497**,** 507-511.
HOFFMAN, B. D., GRASHOFF, C. & SCHWARTZ, M. A. 2011. Dynamic molecular processes mediate cellular mechanotransduction. *Nature,* 475**,** 316-323.
HOFMANN, W. A., JOHNSON, T., KLAPCZYNSKI, M., FAN, J. L. & DE LANEROLLE, P. 2006. From transcription to transport: emerging roles for nuclear myosin I. *Biochem Cell Biol,* 84**,** 418-26.

HOUBEN, F., WILLEMS, C. H. M. P., DECLERCQ, I. L. J., HOCHSTENBACH, K., KAMPS, M. A., SNOECKX, L. H. E. H., RAMAEKERS, F. C. S. & BROERS, J. L. V. 2009. Disturbed nuclear orientation and cellular migration in A-type lamin deficient cells. *Biochimica et Biophysica Acta (BBA) - Molecular Cell Research,* 1793**,** 312-324.

HUBER, F., BOIRE, A., LÓPEZ, M. P. & KOENDERINK, G. H. 2015. Cytoskeletal crosstalk: when three different personalities team up. *Current Opinion in Cell Biology,* 32**,** 39-47.

HÜBNER, M. R. & SPECTOR, D. L. 2010. Chromatin Dynamics. *Annual Review of Biophysics,* 39**,** 471-489.

HUELSMANN, S. & BROWN, N. H. 2014. Nuclear positioning by actin cables and perinuclear actin: Special and general? *Nucleus,* 5**,** 219-23.

HUTTER, J. L. & BECHHOEFER, J. 1993. Calibration of atomic-force microscope tips. *Review of Scientific Instruments,* 64**,** 1868-1873.

HYNES, R. O. 2002. Integrins: bidirectional, allosteric signaling machines. *Cell,* 110**,** 673-87.

IKEDA, S., CUNNINGHAM, L. A., BOGGESS, D., HOBSON, C. D., SUNDBERG, J. P., NAGGERT, J. K., SMITH, R. S. & NISHINA, P. M. 2003. Aberrant actin cytoskeleton leads to accelerated proliferation of corneal epithelial cells in mice deficient for destrin (actin depolymerizing factor). *Human Molecular Genetics,* 12**,** 1029-1036.

INGBER, D. E., DIKE, L., HANSEN, L., KARP, S., LILEY, H., MANIOTIS, A., MCNAMEE, H., MOONEY, D. J., PLOPPER, G., SIMS, J. & WANG, N. 1994. Cellular Tensegrity: Exploring How Mechanical Changes in the Cytoskeleton Regulate Cell Growth, Migration, and Tissue PAttern during Morphogenesis. *International Review of Cytology,* 150**,** 52.

INGBER, D. E., MADRI, J. A. & JAMIESON, J. D. 1981. Role of basal lamina in neoplastic disorganization of tissue architecture. *Proc Natl Acad Sci U S A,* 78**,** 3901-5.

INGBER, D. E., WANG, N. & STAMENOVIĆ, D. 2014. Tensegrity, cellular biophysics, and the mechanics of living systems. *Reports on Progress in Physics,* 77**,** 046603.

ISERMANN, P. & LAMMERDING, J. 2013. Nuclear mechanics and mechanotransduction in health and disease. *Curr Biol,* 23**,** R1113-21.

IVANOVSKA, I. L., SHIN, J. W., SWIFT, J. & DISCHER, D. E. 2015. Stem cell mechanobiology: diverse lessons from bone marrow. *Trends Cell Biol*.

IYER, K. V., PULFORD, S., MOGILNER, A. & SHIVASHANKAR, G. V. 2012. Mechanical Activation of Cells Induces Chromatin Remodeling Preceding MKL Nuclear Transport. *Biophysical Journal,* 103**,** 1416-1428.

JACKSON, B., PEYROLLIER, K., PEDERSEN, E., BASSE, A., KARLSSON, R., WANG, Z., LEFEVER, T., OCHSENBEIN, A. M., SCHMIDT, G., AKTORIES, K., STANLEY, A., QUONDAMATTEO, F., LADWEIN, M., ROTTNER, K., VAN HENGEL, J. & BRAKEBUSCH, C. 2011. RhoA is dispensable for skin development, but crucial for contraction and directed migration of keratinocytes. *Mol Biol Cell,* 22**,** 593-605.

JAIN, N., IYER, K. V., KUMAR, A. & SHIVASHANKAR, G. V. 2013. Cell geometric constraints induce modular gene-expression patterns via redistribution of HDAC3 regulated by actomyosin contractility. *Proceedings of the National Academy of Sciences,* 110**,** 11349-11354.

JANMEY, P. A., EUTENEUER, U., TRAUB, P. & SCHLIWA, M. 1991. Viscoelastic properties of vimentin compared with other filamentous biopolymer networks. *J Cell Biol,* 113**,** 155-60.

JANMEY, P. A., SHAH, J. V., JANSSEN, K. P. & SCHLIWA, M. 1998. Viscoelasticity of intermediate filament networks. *Subcell Biochem,* 31**,** 381-97.

JANSSENS, V. & GORIS, J. 2001. Protein phosphatase 2A: a highly regulated family of serine/threonine phosphatases implicated in cell growth and signalling. *Biochem J,* 353**,** 417-39.

JEFFERSON, J. J., LEUNG, C. L. & LIEM, R. K. 2004. Plakins: goliaths that link cell junctions and the cytoskeleton. *Nat Rev Mol Cell Biol,* 5**,** 542-53.

JENSEN, U. B., LOWELL, S. & WATT, F. M. 1999. The spatial relationship between stem cells and their progeny in the basal layer of human epidermis: a new view based on whole-mount labelling and lineage analysis. *Development,* 126**,** 2409-18.

JIMENEZ-PALOMAR, I., SHIPOV, A., SHAHAR, R. & BARBER, A. H. 2012. Influence of SEM vacuum on bone micromechanics using in situ AFM. *Journal of the Mechanical Behavior of Biomedical Materials,* 5**,** 149-155.

JOFFE, B., LEONHARDT, H. & SOLOVEI, I. 2010. Differentiation and large scale spatial organization of the genome. *Curr Opin Genet Dev,* 20**,** 562-9.

JOHNSON, L., CAO, X. & JACOBSEN, S. 2002. Interplay between two epigenetic marks. DNA methylation and histone H3 lysine 9 methylation. *Curr Biol,* 12**,** 1360-7.

JONES, J. C. & GREEN, K. J. 1991. Intermediate filament-plasma membrane interactions. *Curr Opin Cell Biol,* 3**,** 127-32.

JONES, M. C., CASWELL, P. T. & NORMAN, J. C. 2006. Endocytic recycling pathways: emerging regulators of cell migration. *Curr Opin Cell Biol,* 18**,** 549-57.

JUNG, H.-J., TATAR, A., TU, Y., NOBUMORI, C., YANG, S. H., GOULBOURNE, C. N., HERRMANN, H., FONG, L. G. & YOUNG, S. G. 2014. An Absence of Nuclear Lamins in Keratinocytes Leads to Ichthyosis, Defective Epidermal Barrier Function, and Intrusion of Nuclear Membranes and Endoplasmic Reticulum into the Nuclear Chromatin. *Molecular and Cellular Biology,* 34**,** 4534-4544.

KALEV, P. & SABLINA, A. A. 2011. Protein phosphatase 2A as a potential target for anticancer therapy. *Anticancer Agents Med Chem,* 11**,** 38-46.

KAMINO, T., YAGUCHI, T., OHNISHI, T., ISHITANI, T. & OSUMI, M. 2004. Application of a FIB-STEM system for 3D observation of a resin-embedded yeast cell. *J Electron Microsc (Tokyo),* 53**,** 563-6.

KASAHARA, K., KARTASOVA, T., REN, X. Q., IKUTA, T., CHIDA, K. & KUROKI, T. 1993. Hyperphosphorylation of keratins by treatment with okadaic acid of BALB/MK-2 mouse keratinocytes. *J Biol Chem,* 268**,** 23531-7.

KASZA, K. E., BROEDERSZ, C. P., KOENDERINK, G. H., LIN, Y. C., MESSNER, W., MILLMAN, E. A., NAKAMURA, F., STOSSEL, T. P., MACKINTOSH, F. C. & WEITZ, D. A. 2010. Actin filament length tunes elasticity of flexibly cross-linked actin networks. *Biophys J,* 99**,** 1091-100.

KAWSKA, A., CARVALHO, K., MANZI, J., BOUJEMAA-PATERSKI, R., BLANCHOIN, L., MARTIEL, J. L. & SYKES, C. 2012. How actin network

dynamics control the onset of actin-based motility. *Proc Natl Acad Sci U S A,* 109**,** 14440-5.

KETEMA, M. & SONNENBERG, A. 2011. Nesprin-3: a versatile connector between the nucleus and the cytoskeleton. *Biochemical Society Transactions,* 39**,** 1719-1724.

KHATAU, S. B., HALE, C. M., STEWART-HUTCHINSON, P. J., PATEL, M. S., STEWART, C. L., SEARSON, P. C., HODZIC, D. & WIRTZ, D. 2009. A perinuclear actin cap regulates nuclear shape. *Proceedings of the National Academy of Sciences,* 106**,** 19017-19022.

KIELY, M. & KIELY, P. A. 2015. PP2A: The Wolf in Sheep's Clothing? *Cancers (Basel),* 7**,** 648-69.

KIM, S. & COULOMBE, P. A. 2007. Intermediate filament scaffolds fulfill mechanical, organizational, and signaling functions in the cytoplasm. *Genes Dev,* 21**,** 1581-97.

KOCHIN, V., SHIMI, T., TORVALDSON, E., ADAM, S. A., GOLDMAN, A., PACK, C. G., MELO-CARDENAS, J., IMANISHI, S. Y., GOLDMAN, R. D. & ERIKSSON, J. E. 2014. Interphase phosphorylation of lamin A. *J Cell Sci,* 127**,** 2683-96.

KOLSCH, A., WINDOFFER, R., WURFLINGER, T., AACH, T. & LEUBE, R. E. 2010. The keratin-filament cycle of assembly and disassembly. *Journal of Cell Science,* 123**,** 2266-2272.

KONIECZNY, P., FUCHS, P., REIPERT, S., KUNZ, W. S., ZEOLD, A., FISCHER, I., PAULIN, D., SCHRODER, R. & WICHE, G. 2008. Myofiber integrity depends on desmin network targeting to Z-disks and costameres via distinct plectin isoforms. *J Cell Biol,* 181**,** 667-81.

KOSS-HARNES, D., HOYHEIM, B., ANTON-LAMPRECHT, I., GJESTI, A., JORGENSEN, R. S., JAHNSEN, F. L., OLAISEN, B., WICHE, G. & GEDDE-DAHL, T., JR. 2002. A site-specific plectin mutation causes dominant epidermolysis bullosa simplex Ogna: two identical de novo mutations. *J Invest Dermatol,* 118**,** 87-93.

KOSTER, MARIA J. E., SNEL, B. & TIMMERS, H. T. M. 2015. Genesis of Chromatin and Transcription Dynamics in the Origin of Species. *Cell,* 161**,** 724-736.

KOUKLIS, P. D., HUTTON, E. & FUCHS, E. 1994. Making a connection: direct binding between keratin intermediate filaments and desmosomal proteins. *J Cell Biol,* 127**,** 1049-60.

KOURTIDIS, A., NGOK, S. P. & ANASTASIADIS, P. Z. 2013. p120 catenin: an essential regulator of cadherin stability, adhesion-induced signaling, and cancer progression. *Prog Mol Biol Transl Sci,* 116**,** 409-32.

KREPLAK, L., BAR, H., LETERRIER, J. F., HERRMANN, H. & AEBI, U. 2005. Exploring the mechanical behavior of single intermediate filaments. *J Mol Biol,* 354**,** 569-77.

KREPLAK, L., HERRMANN, H. & AEBI, U. 2008. Tensile properties of single desmin intermediate filaments. *Biophys J,* 94**,** 2790-9.

KROGAN, N. J., DOVER, J., KHORRAMI, S., GREENBLATT, J. F., SCHNEIDER, J., JOHNSTON, M. & SHILATIFARD, A. 2002. COMPASS, a histone H3 (Lysine 4) methyltransferase required for telomeric silencing of gene expression. *J Biol Chem,* 277**,** 10753-5.

KU, N. O., AZHAR, S. & OMARY, M. B. 2002. Keratin 8 phosphorylation by p38 kinase regulates cellular keratin filament reorganization: modulation by a keratin 1-like disease causing mutation. *J Biol Chem,* 277**,** 10775-82.

KU, N. O. & OMARY, M. B. 2006. A disease- and phosphorylation-related nonmechanical function for keratin 8. *J Cell Biol,* 174**,** 115-25.

KU, N. O., STRNAD, P., ZHONG, B. H., TAO, G. Z. & OMARY, M. B. 2007. Keratins let liver live: Mutations predispose to liver disease and crosslinking generates Mallory-Denk bodies. *Hepatology,* 46**,** 1639-49.

KU, N. O., TOIVOLA, D. M., STRNAD, P. & OMARY, M. B. 2010. Cytoskeletal keratin glycosylation protects epithelial tissue from injury. *Nat Cell Biol,* 12**,** 876-85.

KUMAR, A., MAITRA, A., SUMIT, M., RAMASWAMY, S. & SHIVASHANKAR, G. V. 2014. Actomyosin contractility rotates the cell nucleus. *Scientific Reports,* 4.

KUROKAWA, I., TAKAHASHI, K., MOLL, I. & MOLL, R. 2011. Expression of keratins in cutaneous epithelial tumors and related disorders--distribution and clinical significance. *Exp Dermatol,* 20**,** 217-28.

LACHNER, M., O'CARROLL, D., REA, S., MECHTLER, K. & JENUWEIN, T. 2001. Methylation of histone H3 lysine 9 creates a binding site for HP1 proteins. *Nature,* 410**,** 116-20.

LAMMERDING, J., FONG, L. G., JI, J. Y., REUE, K., STEWART, C. L., YOUNG, S. G. & LEE, R. T. 2006. Lamins A and C but not lamin B1 regulate nuclear mechanics. *J Biol Chem,* 281**,** 25768-80.

LAMMERDING, J., HSIAO, J., SCHULZE, P. C., KOZLOV, S., STEWART, C. L. & LEE, R. T. 2005. Abnormal nuclear shape and impaired mechanotransduction in emerin-deficient cells. *J Cell Biol,* 170**,** 781-91.

LAMMERDING, J., SCHULZE, P. C., TAKAHASHI, T., KOZLOV, S., SULLIVAN, T., KAMM, R. D., STEWART, C. L. & LEE, R. T. 2004. Lamin A/C deficiency causes defective nuclear mechanics and mechanotransduction. *J Clin Invest,* 113**,** 370-8.

LANCTÔT, C., CHEUTIN, T., CREMER, M., CAVALLI, G. & CREMER, T. 2007. Dynamic genome architecture in the nuclear space: regulation of gene expression in three dimensions. *Nature Reviews Genetics,* 8**,** 104-115.

LE CLAINCHE, C. & CARLIER, M.-F. 2008. *Regulation of Actin Assembly Associated With Protrusion and Adhesion in Cell Migration*.

LEBEYEC, J., XU, R., LEE, S., NELSON, C., RIZKI, A., ALCARAZ, J. & BISSELL, M. 2007. Cell shape regulates global histone acetylation in human mammary epithelial cells. *Experimental Cell Research,* 313**,** 3066-3075.

LEE, C.-H., KIM, M.-S., CHUNG, B. M., LEAHY, D. J. & COULOMBE, P. A. 2012. Structural basis for heteromeric assembly and perinuclear organization of keratin filaments. *Nature Structural & Molecular Biology,* 19**,** 707-715.

LEE, J. S. H., HALE, C. M., PANORCHAN, P., KHATAU, S. B., GEORGE, J. P., TSENG, Y., STEWART, C. L., HODZIC, D. & WIRTZ, D. 2007. Nuclear Lamin A/C Deficiency Induces Defects in Cell Mechanics, Polarization, and Migration. *Biophysical Journal,* 93**,** 2542-2552.

LEE, M. J., RAN BYUN, M., FURUTANI-SEIKI, M., HONG, J. H. & JUNG, H. S. 2014. YAP and TAZ regulate skin wound healing. *J Invest Dermatol,* 134**,** 518-25.

LEHOUX, S. & TEDGUI, A. 2003. Cellular mechanics and gene expression in blood vessels. *J Biomech,* 36**,** 631-43.
LEUBE, R. E., MOCH, M., KÖLSCH, A. & WINDOFFER, R. 2011. "Panta rhei": Perpetual cycling of the keratin cytoskeleton. *BioArchitecture,* 1**,** 39-44.
LI, C. & XU, Q. 2007. Mechanical stress-initiated signal transduction in vascular smooth muscle cells in vitro and in vivo. *Cell Signal,* 19**,** 881-91.
LI, Q., KUMAR, A., MAKHIJA, E. & SHIVASHANKAR, G. V. 2014. The regulation of dynamic mechanical coupling between actin cytoskeleton and nucleus by matrix geometry. *Biomaterials,* 35**,** 961-969.
LI, X., LEHMAN, W. & FISCHER, S. 2010. The Relationship between Curvature, Flexibility and Persistence Length in the Tropomyosin Coiled-Coil. *Journal of Structural Biology,* 170**,** 313-318.
LIEBERMAN-AIDEN, E., VAN BERKUM, N. L., WILLIAMS, L., IMAKAEV, M., RAGOCZY, T., TELLING, A., AMIT, I., LAJOIE, B. R., SABO, P. J., DORSCHNER, M. O., SANDSTROM, R., BERNSTEIN, B., BENDER, M. A., GROUDINE, M., GNIRKE, A., STAMATOYANNOPOULOS, J., MIRNY, L. A., LANDER, E. S. & DEKKER, J. 2009. Comprehensive mapping of long-range interactions reveals folding principles of the human genome. *Science,* 326**,** 289-93.
LIELEG, O., SCHMOLLER, K. M., CLAESSENS, M. M. & BAUSCH, A. R. 2009. Cytoskeletal polymer networks: viscoelastic properties are determined by the microscopic interaction potential of cross-links. *Biophys J,* 96**,** 4725-32.
LIEN, W. H., GUO, X., POLAK, L., LAWTON, L. N., YOUNG, R. A., ZHENG, D. & FUCHS, E. 2011. Genome-wide maps of histone modifications unwind in vivo chromatin states of the hair follicle lineage. *Cell Stem Cell,* 9**,** 219-32.
LIN, D. C., DIMITRIADIS, E. K. & HORKAY, F. 2007. Robust Strategies for Automated AFM Force Curve Analysis—I. Non-adhesive Indentation of Soft, Inhomogeneous Materials. *Journal of Biomechanical Engineering,* 129**,** 430.
LITJENS, S. H. M., DE PEREDA, J. M. & SONNENBERG, A. 2006. Current insights into the formation and breakdown of hemidesmosomes. *Trends in Cell Biology,* 16**,** 376-383.
LIVERPOOL, T. B. 2006. *Active gels: where polymer physics meets cytoskeletal dynamics*.
LLOYD, C., YU, Q. C., CHENG, J., TURKSEN, K., DEGENSTEIN, L., HUTTON, E. & FUCHS, E. 1995. The basal keratin network of stratified squamous epithelia: defining K15 function in the absence of K14. *J Cell Biol,* 129**,** 1329-44.
LODISH H., BERK A., ZIPURSKY S.L. & AL., E. 2000. The Actin Cytoskeleton. *In:* H., F. W. (ed.) *Molecular Cell Biology.* New York.
LOISEL, T. P., BOUJEMAA, R., PANTALONI, D. & CARLIER, M. F. 1999. Reconstitution of actin-based motility of Listeria and Shigella using pure proteins. *Nature,* 401**,** 613-6.
LOMBARDI, M. L., JAALOUK, D. E., SHANAHAN, C. M., BURKE, B., ROUX, K. J. & LAMMERDING, J. 2011. The interaction between nesprins and sun proteins at the nuclear envelope is critical for force transmission between the nucleus and cytoskeleton. *J Biol Chem,* 286**,** 26743-53.

LU, D. & BARBER, A. H. 2012. *Optimized nanoscale composite behaviour in limpet teeth*.

MA, H., HYUN, J., STILLER, P. & CHILKOTI, A. 2004. "Non-Fouling" Oligo(ethylene glycol)- Functionalized Polymer Brushed Synthesized by Surface-Initiated Atom Transfer Radical Polymerization. *Advanced Materials,* 16**,** 4.

MACKINTOSH, F. C. 2006. *Polymer-based models of cytoskeletal networks*

Cytoskeletal Mechanics, Cambridge University Press.

MALHAS, A. N., LEE, C. F. & VAUX, D. J. 2009. Lamin B1 controls oxidative stress responses via Oct-1. *The Journal of Cell Biology,* 184**,** 45-55.

MAMMOTO, A. & INGBER, D. E. 2009. Cytoskeletal control of growth and cell fate switching. *Curr Opin Cell Biol,* 21**,** 864-70.

MAMMOTO, A., MAMMOTO, T. & INGBER, D. E. 2012. Mechanosensitive mechanisms in transcriptional regulation. *Journal of Cell Science,* 125**,** 3061-3073.

MAMMOTO, T. & INGBER, D. E. 2010. Mechanical control of tissue and organ development. *Development,* 137**,** 1407-20.

MANIOTIS, A. J., CHEN, C. S. & INGBER, D. E. 1997. Demonstration of mechanical connections between integrins, cytoskeletal filaments, and nucleoplasm that stabilize nuclear structure. *Proc. Natl. Acad. Sci. USA,* 94**,** 6.

MARDARYEV, A. N., GDULA, M. R., YARKER, J. L., EMELIANOV, V. N., POTERLOWICZ, K., SHAROV, A. A., SHAROVA, T. Y., SCARPA, J. A., CHAMBON, P., BOTCHKAREV, V. A. & FESSING, M. Y. 2014. p63 and Brg1 control developmentally regulated higher-order chromatin remodelling at the epidermal differentiation complex locus in epidermal progenitor cells. *Development,* 141**,** 101-111.

MARGADANT, C., CHARAFEDDINE, R. A. & SONNENBERG, A. 2010. Unique and redundant functions of integrins in the epidermis. *FASEB J,* 24**,** 4133-52.

MARTIN, A. C., GELBART, M., FERNANDEZ-GONZALEZ, R., KASCHUBE, M. & WIESCHAUS, E. F. 2010. Integration of contractile forces during tissue invagination. *J Cell Biol,* 188**,** 735-49.

MARTINS, R. P., FINAN, J. D., FARSHID, G. & LEE, D. A. 2012. Mechanical Regulation of Nuclear Structure and Function. *Annual Review of Biomedical Engineering,* 14**,** 431-455.

MAZUMDER, A., ROOPA, T., BASU, A., MAHADEVAN, L. & SHIVASHANKAR, G. V. 2008. Dynamics of chromatin decondensation reveals the structural integrity of a mechanically prestressed nucleus. *Biophys J,* 95**,** 3028-35.

MAZUMDER, A., ROOPA, T., KUMAR, A., IYER, K. V., RAMDAS, N. M. & SHIVASHANKAR, G. V. 2010. Prestressed nuclear organization in living cells. *Methods Cell Biol,* 98**,** 221-39.

MAZUMDER, A. & SHIVASHANKAR, G. V. 2007. Gold-Nanoparticle-Assisted Laser Perturbation of Chromatin Assembly Reveals Unusual Aspects of Nuclear Architecture within Living Cells. *Biophysical Journal,* 93**,** 2209-2216.

MAZUMDER, A. & SHIVASHANKAR, G. V. 2010. Emergence of a prestressed eukaryotic nucleus during cellular differentiation and development. *J R Soc Interface,* 7 Suppl 3**,** S321-30.

MCBEATH, R., PIRONE, D. M., NELSON, C. M., BHADRIRAJU, K. & CHEN, C. S. 2004. Cell shape, cytoskeletal tension, and RhoA regulate stem cell lineage commitment. *Dev Cell,* 6**,** 483-95.
MENDEZ, M. G., RESTLE, D. & JANMEY, P. A. 2014. Vimentin Enhances Cell Elastic Behavior and Protects against Compressive Stress. *Biophysical Journal,* 107**,** 314-323.
MEYER, R. K. & AEBI, U. 1990. Bundling of actin filaments by alpha-actinin depends on its molecular length. *J Cell Biol,* 110**,** 2013-24.
MIANO, J. M., LONG, X. & FUJIWARA, K. 2007. Serum response factor: master regulator of the actin cytoskeleton and contractile apparatus. *Am J Physiol Cell Physiol,* 292**,** C70-81.
MILANI, M. & DROBNE, D. 2006. Focused Ion Beam Manipulation and Ultramicroscopy of Unprepared Cells. *Scanning,* 28**,** 7.
MIROSLAV, K., TOMÁŠ, M., TOMÁŠ, V. & TOMÁŠ, Š. 2011. Low energy focused ion beam milling of silicon and germanium nanostructures. *Nanotechnology,* 22**,** 105304.
MISTELI, T. 2007. Beyond the sequence: cellular organization of genome function. *Cell,* 128**,** 787-800.
MOCH, M., HERBERICH, G., AACH, T., LEUBE, R. E. & WINDOFFER, R. 2013. Measuring the regulation of keratin filament network dynamics. *Proceedings of the National Academy of Sciences,* 110**,** 10664-10669.
MOEENDARBARY, E., VALON, L., FRITZSCHE, M., HARRIS, A. R., MOULDING, D. A., THRASHER, A. J., STRIDE, E., MAHADEVAN, L. & CHARRAS, G. T. 2013. The cytoplasm of living cells behaves as a poroelastic material. *Nat Mater,* 12**,** 253-61.
MOLECULAR STATION, I. *Chromatin Structure Model* [Online]. Molecular Station Inc. Available: http://www.molecularstation.com/molecular-biology-images/502-dna-pictures/58-chromatin-strucure-model.html?size=big [Accessed 18/05 2012].
MOZZETTA, C., BOYARCHUK, E., PONTIS, J. & AIT-SI-ALI, S. 2015. Sound of silence: the properties and functions of repressive Lys methyltransferases. *Nat Rev Mol Cell Biol,* 16**,** 499-513.
NA, S., CHOWDHURY, F., TAY, B., OUYANG, M., GREGOR, M., WANG, Y., WICHE, G. & WANG, N. 2009. Plectin contributes to mechanical properties of living cells. *Am J Physiol Cell Physiol,* 296**,** C868-77.
NAETAR, N., KORBEI, B., KOZLOV, S., KERENYI, M. A., DORNER, D., KRAL, R., GOTIC, I., FUCHS, P., COHEN, T. V., BITTNER, R., STEWART, C. L. & FOISNER, R. 2008. Loss of nucleoplasmic LAP2[alpha]-lamin A complexes causes erythroid and epidermal progenitor hyperproliferation. *Nat Cell Biol,* 10**,** 1341-1348.
NATSUGA, K. 2015. Plectin-related skin diseases. *J Dermatol Sci,* 77**,** 139-45.
NAUMOVA, N. & DEKKER, J. 2010. Integrating one-dimensional and three-dimensional maps of genomes. *J Cell Sci,* 123**,** 1979-88.
NELSON, W. G. & SUN, T. T. 1983. The 50- and 58-kdalton keratin classes as molecular markers for stratified squamous epithelia: cell culture studies. *J Cell Biol,* 97**,** 244-51.
NEUMANN, S., SCHNEIDER, M., DAUGHERTY, R. L., GOTTARDI, C. J., EMING, S. A., BEIJER, A., NOEGEL, A. A. & KARAKESISOGLOU, I. 2010. Nesprin-2 Interacts with α-Catenin and Regulates Wnt Signaling at

the Nuclear Envelope. *Journal of Biological Chemistry,* 285**,** 34932-34938.
NICOLÁS, F. M. & RICARDO, G. 2006. Measuring phase shifts and energy dissipation with amplitude modulation atomic force microscopy. *Nanotechnology,* 17**,** S167.
NIKOLIC, B., MAC NULTY, E., MIR, B. & WICHE, G. 1996. Basic amino acid residue cluster within nuclear targeting sequence motif is essential for cytoplasmic plectin-vimentin network junctions. *J Cell Biol,* 134**,** 1455-67.
NOIREAUX, V., GOLSTEYN, R. M., FRIEDERICH, E., PROST, J., ANTONY, C., LOUVARD, D. & SYKES, C. 2000. Growing an actin gel on spherical surfaces. *Biophys J,* 78**,** 1643-54.
NORA, E. P., LAJOIE, B. R., SCHULZ, E. G., GIORGETTI, L., OKAMOTO, I., SERVANT, N., PIOLOT, T., VAN BERKUM, N. L., MEISIG, J., SEDAT, J., GRIBNAU, J., BARILLOT, E., BLUTHGEN, N., DEKKER, J. & HEARD, E. 2012. Spatial partitioning of the regulatory landscape of the X-inactivation centre. *Nature,* 485**,** 381-5.
OMARY, M. B., KU, N. O., TAO, G. Z., TOIVOLA, D. M. & LIAO, J. 2006. "Heads and tails" of intermediate filament phosphorylation: multiple sites and functional insights. *Trends Biochem Sci,* 31**,** 383-94.
OSMANAGIC-MYERS, S., GREGOR, M., WALKO, G., BURGSTALLER, G., REIPERT, S. & WICHE, G. 2006. Plectin-controlled keratin cytoarchitecture affects MAP kinases involved in cellular stress response and migration. *The Journal of Cell Biology,* 174**,** 557-568.
OSTLUND, C., FOLKER, E. S., CHOI, J. C., GOMES, E. R., GUNDERSEN, G. G. & WORMAN, H. J. 2009. Dynamics and molecular interactions of linker of nucleoskeleton and cytoskeleton (LINC) complex proteins. *J Cell Sci,* 122**,** 4099-108.
OWARIBE, K., KARTENBECK, J., STUMPP, S., MAGIN, T. M., KRIEG, T., DIAZ, L. A. & FRANKE, W. W. 1990. The hemidesmosomal plaque. I. Characterization of a major constituent protein as a differentiation marker for certain forms of epithelia. *Differentiation,* 45**,** 207-20.
PAIK, W. K., PAIK, D. C. & KIM, S. 2007. Historical review: the field of protein methylation. *Trends Biochem Sci,* 32**,** 146-52.
PAJEROWSKI, J. D., DAHL, K. N., ZHONG, F. L., SAMMAK, P. J. & DISCHER, D. E. 2007. Physical plasticity of the nucleus in stem cell differentiation. *Proceedings of the National Academy of Sciences,* 104**,** 15619-15624.
PALUCH, E. K., NELSON, C. M., BIAIS, N., FABRY, B., MOELLER, J., PRUITT, B. L., WOLLNIK, C., KUDRYASHEVA, G., REHFELDT, F. & FEDERLE, W. 2015. Mechanotransduction: use the force(s). *BMC Biology,* 13.
PAN, X., HOBBS, R. P. & COULOMBE, P. A. 2013. The expanding significance of keratin intermediate filaments in normal and diseased epithelia. *Current Opinion in Cell Biology,* 25**,** 47-56.
PATEL, G. K., WILSON, C. H., HARDING, K. G., FINLAY, A. Y. & BOWDEN, P. E. 2005. Numerous Keratinocyte Subtypes Involved in Wound Re-Epithelialization. *Journal of Investigative Dermatology,* 126**,** 497-502.
PATIL, S., JEDSADAYANMATA, A., WENCEL-DRAKE, J. D., WANG, W., KNEZEVIC, I. & LAM, S. C. 1999. Identification of a talin-binding site in the integrin beta(3) subunit distinct from the NPLY regulatory motif of post-ligand binding functions. The talin n-terminal head domain interacts

with the membrane-proximal region of the beta(3) cytoplasmic tail. *J Biol Chem,* 274**,** 28575-83.
PATWARI, P., CHUTKOW, W. A., CUMMINGS, K., VERSTRAETEN, V. L., LAMMERDING, J., SCHREITER, E. R. & LEE, R. T. 2009. Thioredoxin-independent regulation of metabolism by the alpha-arrestin proteins. *J Biol Chem,* 284**,** 24996-5003.
PEDERSON, T. & AEBI, U. 2005. Nuclear actin extends, with no contraction in sight. *Mol Biol Cell,* 16**,** 5055-60.
PERROTTI, D. & NEVIANI, P. 2013. Protein phosphatase 2A: a target for anticancer therapy. *Lancet Oncol,* 14**,** e229-38.
PETERSON, J. R. & MITCHISON, T. J. 2002. Small molecules, big impact: a history of chemical inhibitors and the cytoskeleton. *Chem Biol,* 9**,** 1275-85.
PFENDNER, E. & UITTO, J. 2005. Plectin gene mutations can cause epidermolysis bullosa with pyloric atresia. *J Invest Dermatol,* 124**,** 111-5.
POH, Y.-C., SHEVTSOV, S. P., CHOWDHURY, F., WU, D. C., NA, S., DUNDR, M. & WANG, N. 2012. Dynamic force-induced direct dissociation of protein complexes in a nuclear body in living cells. *Nature Communications,* 3**,** 866.
POLLARD, T. D. & COOPER, J. A. 1986. Actin and actin-binding proteins. A critical evaluation of mechanisms and functions. *Annu Rev Biochem,* 55**,** 987-1035.
PONTI, A., MACHACEK, M., GUPTON, S. L., WATERMAN-STORER, C. M. & DANUSER, G. 2004. Two Distinct Actin Networks Drive the Protrusion of Migrating Cells. *Science,* 305**,** 1782-1786.
PORTER, R. M., LUNNY, D. P., OGDEN, P. H., MORLEY, S. M., MCLEAN, W. H., EVANS, A., HARRISON, D. L., RUGG, E. L. & LANE, E. B. 2000. K15 expression implies lateral differentiation within stratified epithelial basal cells. *Lab Invest,* 80**,** 1701-10.
PORTET, S., MADZVAMUSE, A., CHUNG, A., LEUBE, R. E. & WINDOFFER, R. 2015. Keratin Dynamics: Modeling the Interplay between Turnover and Transport. *PLoS ONE,* 10**,** e0121090.
PORTET, S., VASSY J FAU - BEIL, M., BEIL M FAU - MILLOT, G., MILLOT G FAU - HEBBACHE, A., HEBBACHE A FAU - RIGAUT, J. P., RIGAUT JP FAU - SCHOEVAERT, D. & SCHOEVAERT, D. 1999. Quantitative analysis of cytokeratin network topology in the MCF7 cell line. *Cytometry,* 35**,** 203-13.
POSTEL, R., KETEMA, M., KUIKMAN, I., DE PEREDA, J. M. & SONNENBERG, A. 2011. Nesprin-3 augments peripheral nuclear localization of intermediate filaments in zebrafish. *Journal of Cell Science,* 124**,** 755-764.
QIN, Z., BUEHLER, M. J. & KREPLAK, L. 2010. A multi-scale approach to understand the mechanobiology of intermediate filaments. *Journal of Biomechanics,* 43**,** 15-22.
RABL, C. 1885. Über Zelltheillung. *Morph. Jb.,* 10**,** 16.
RAINERO, E., HOWE, J. D., CASWELL, P. T., JAMIESON, N. B., ANDERSON, K., CRITCHLEY, D. R., MACHESKY, L. & NORMAN, J. C. 2015. Ligand-Occupied Integrin Internalization Links Nutrient Signaling to Invasive Migration. *Cell Rep*.

RAITH, M., VALENCIA, R. G., FISCHER, I., ORTHOFER, M., PENNINGER, J. M., SPULER, S., REZNICZEK, G. A. & WICHE, G. 2013. Linking cytoarchitecture to metabolism: sarcolemma-associated plectin affects glucose uptake by destabilizing microtubule networks in mdx myofibers. *Skelet Muscle,* 3**,** 14.

RAJAPAKSE, I. & GROUDINE, M. 2011. On emerging nuclear order. *The Journal of Cell Biology,* 192**,** 711-721.

RAMMS, L., FABRIS, G., WINDOFFER, R., SCHWARZ, N., SPRINGER, R., ZHOU, C., LAZAR, J., STIEFEL, S., HERSCH, N., SCHNAKENBERG, U., MAGIN, T. M., LEUBE, R. E., MERKEL, R. & HOFFMANN, B. 2013. Keratins as the main component for the mechanical integrity of keratinocytes. *Proceedings of the National Academy of Sciences,* 110**,** 18513-18518.

RANDO, O. J. & CHANG, H. Y. 2009. Genome-wide views of chromatin structure. *Annu Rev Biochem,* 78**,** 245-71.

RAPPOPORT, J. Z. & SIMON, S. M. 2003. Real-time analysis of clathrin-mediated endocytosis during cell migration. *J Cell Sci,* 116**,** 847-55.

REICHELT, J. 2007. Mechanotransduction of keratinocytes in culture and in the epidermis. *European Journal of Cell Biology,* 86**,** 807-816.

REYES, C. D. & GARCÍA, A. J. 2003. Engineering integrin-specific surfaces with a triple-helical collagen-mimetic peptide. *Journal of Biomedical Materials Research Part A,* 65A**,** 511-523.

REYNAUD, C., SOMMER, F., QUET, C., EL BOUNIA, N. & DUC, T. M. 2000. Quantitative determination of Young's modulus on a biphase polymer system using atomic force microscopy. *Surface and Interface Analysis,* 30**,** 185-189.

REZNICZEK, G. A., ABRAHAMSBERG, C., FUCHS, P., SPAZIERER, D. & WICHE, G. 2003. Plectin 5'-transcript diversity: short alternative sequences determine stability of gene products, initiation of translation and subcellular localization of isoforms. *Hum Mol Genet,* 12**,** 3181-94.

RHEINWALD, J. G. & GREEN, H. 1975. Serial cultivation of strains of human epidermal keratinocytes: the formation of keratinizing colonies from single cells. *Cell,* 6**,** 331-43.

RHEINWALD, J. G. & GREEN, H. 1977. Epidermal growth factor and the multiplication of cultured human epidermal keratinocytes. *Nature,* 265**,** 421-4.

RICE, J. C., BRIGGS, S. D., UEBERHEIDE, B., BARBER, C. M., SHABANOWITZ, J., HUNT, D. F., SHINKAI, Y. & ALLIS, C. D. 2003. Histone methyltransferases direct different degrees of methylation to define distinct chromatin domains. *Mol Cell,* 12**,** 1591-8.

RICE, R. H. & GREEN, H. 1977. The cornified envelope of terminally differentiated human epidermal keratinocytes consists of cross-linked protein. *Cell,* 11**,** 417-22.

ROGERS, M. A., WINTER, H., LANGBEIN, L., BLEILER, R. & SCHWEIZER, J. 2004. The human type I keratin gene family: characterization of new hair follicle specific members and evaluation of the chromosome 17q21.2 gene domain. *Differentiation,* 72**,** 527-40.

ROUX, K. J., CRISP, M. L., LIU, Q., KIM, D., KOZLOV, S., STEWART, C. L. & BURKE, B. 2009. Nesprin 4 is an outer nuclear membrane protein that

can induce kinesin-mediated cell polarization. *Proc Natl Acad Sci U S A,* 106**,** 2194-9.
ROWAT, A. C., FOSTER, L. J., NIELSEN, M. M., WEISS, M. & IPSEN, J. H. 2005. Characterization of the elastic properties of the nuclear envelope. *Journal of The Royal Society Interface,* 2**,** 63-69.
ROWAT, A. C., LAMMERDING, J. & IPSEN, J. H. 2006. Mechanical Properties of the Cell Nucleus and the Effect of Emerin Deficiency. *Biophysical Journal,* 91**,** 4649-4664.
ROWLANDS, A. S., GEORGE, P. A. & COOPER-WHITE, J. J. 2008. Directing osteogenic and myogenic differentiation of MSCs: interplay of stiffness and adhesive ligand presentation. *Am J Physiol Cell Physiol,* 295**,** C1037-44.
RUBANOV, S. & MUNROE, P. R. 2004. FIB-induced damage in silicon. *Journal of Microscopy,* 214**,** 213-221.
RUBIN, J., RUBIN, C. & JACOBS, C. R. 2006. Molecular pathways mediating mechanical signaling in bone. *Gene,* 367**,** 1-16.
RUDINI, N. & DEJANA, E. 2008. Adherens junctions. *Curr Biol,* 18**,** R1080-2.
RUZSNAVSZKY, O., DIENES, B., OLAH, T., VINCZE, J., GALL, T., BALOGH, E., NAGY, G., BATORI, R., LONTAY, B., ERDODI, F. & CSERNOCH, L. 2013. Differential effects of phosphatase inhibitors on the calcium homeostasis and migration of HaCaT keratinocytes. *PLoS ONE,* 8**,** e61507.
SAHIN, O. & ERINA, N. 2008. High-resolution and large dynamic range nanomechanical mapping in tapping-mode atomic force microscopy. *Nanotechnology,* 19**,** 445717.
SAHIN, O., MAGONOV, S., SU, C., QUATE, C. F. & SOLGAARD, O. 2007. An atomic force microscope tip designed to measure time-varying nanomechanical forces. *Nat Nano,* 2**,** 507-514.
SAKAKI, M., KOIKE, H., TAKAHASHI, N., SASAGAWA, N., TOMIOKA, S., ARAHATA, K. & ISHIURA, S. 2001. Interaction between emerin and nuclear lamins. *J Biochem,* 129**,** 321-7.
SANTOS-ROSA, H., SCHNEIDER, R., BANNISTER, A. J., SHERRIFF, J., BERNSTEIN, B. E., EMRE, N. C., SCHREIBER, S. L., MELLOR, J. & KOUZARIDES, T. 2002. Active genes are tri-methylated at K4 of histone H3. *Nature,* 419**,** 407-11.
SCHILLER, H. B., HERMANN, M.-R., POLLEUX, J., VIGNAUD, T., ZANIVAN, S., FRIEDEL, C. C., SUN, Z., RADUCANU, A., GOTTSCHALK, K.-E., THÉRY, M., MANN, M. & FÄSSLER, R. 2013. β1- and αv-class integrins cooperate to regulate myosin II during rigidity sensing of fibronectin-based microenvironments. *Nature Cell Biology,* 15**,** 625-636.
SCHMOLLER, K. M., LIELEG, O. & BAUSCH, A. R. 2008. Cross-linking molecules modify composite actin networks independently. *Phys Rev Lett,* 101**,** 118102.
SCHOENFELDER, S., CLAY, I. & FRASER, P. 2010. The transcriptional interactome: gene expression in 3D. *Curr Opin Genet Dev,* 20**,** 127-33.
SCHÖNHERR, H., FENG, C. L., TOMCZAK, N. & VANCSO, G. J. 2005. Compositional Mapping of Polymer Surfaces by Chemical Force Microscopy Down to the Nanometer Scale: Reactions in Block Copolymer Microdomains. *Macromolecular Symposia,* 230**,** 149-157.

SCHONTHAL, A. H. 2001. Role of serine/threonine protein phosphatase 2A in cancer. *Cancer Lett,* 170**,** 1-13.
SCHOTTA, G., LACHNER, M., PETERS, A. H. & JENUWEIN, T. 2004. The indexing potential of histone lysine methylation. *Novartis Found Symp,* 259**,** 22-37; discussion 37-47, 163-9.
SCHWEIZER, J., BOWDEN, P. E., COULOMBE, P. A., LANGBEIN, L., LANE, E. B., MAGIN, T. M., MALTAIS, L., OMARY, M. B., PARRY, D. A. D., ROGERS, M. A. & WRIGHT, M. W. 2006. New consensus nomenclature for mammalian keratins. *The Journal of Cell Biology,* 174**,** 169-174.
SEGRE, J. A. 2006. Epidermal barrier formation and recovery in skin disorders. *J Clin Invest,* 116**,** 1150-8.
SELTMANN, K., CHENG, F., WICHE, G., ERIKSSON, J. E. & MAGIN, T. M. 2015. Keratins Stabilize Hemidesmosomes through Regulation of beta4-Integrin Turnover. *J Invest Dermatol,* 135**,** 1609-20.
SELTMANN, K., FRITSCH, A. W., KAS, J. A. & MAGIN, T. M. 2013a. Keratins significantly contribute to cell stiffness and impact invasive behavior. *Proceedings of the National Academy of Sciences,* 110**,** 18507-18512.
SELTMANN, K., ROTH, W., KROGER, C., LOSCHKE, F., LEDERER, M., HUTTELMAIER, S. & MAGIN, T. M. 2013b. Keratins mediate localization of hemidesmosomes and repress cell motility. *J Invest Dermatol,* 133**,** 181-90.
SEN, G. L., WEBSTER, D. E., BARRAGAN, D. I., CHANG, H. Y. & KHAVARI, P. A. 2008. Control of differentiation in a self-renewing mammalian tissue by the histone demethylase JMJD3. *Genes & Development,* 22**,** 1865-1870.
SESHACHARYULU, P., PANDEY, P., DATTA, K. & BATRA, S. K. 2013. Phosphatase: PP2A structural importance, regulation and its aberrant expression in cancer. *Cancer Lett,* 335**,** 9-18.
SHEETZ, M. P. & SPUDICH, J. A. 1983. Movement of myosin-coated fluorescent beads on actin cables in vitro. *Nature,* 303**,** 31-5.
SHI, X., MA, Y. Q., TU, Y., CHEN, K., WU, S., FUKUDA, K., QIN, J., PLOW, E. F. & WU, C. 2007. The MIG-2/integrin interaction strengthens cell-matrix adhesion and modulates cell motility. *J Biol Chem,* 282**,** 20455-66.
SHIVASHANKAR, G. V. 2010. *Nuclear mechanics and genome regulation*, Elsevier.
SHIVASHANKAR, G. V. 2011. Mechanosignaling to the Cell Nucleus and Gene Regulation. *Annual Review of Biophysics,* 40**,** 361-378.
SHUMAKER, D. K., DECHAT, T., KOHLMAIER, A., ADAM, S. A., BOZOVSKY, M. R., ERDOS, M. R., ERIKSSON, M., GOLDMAN, A. E., KHUON, S., COLLINS, F. S., JENUWEIN, T. & GOLDMAN, R. D. 2006. Mutant nuclear lamin A leads to progressive alterations of epigenetic control in premature aging. *Proc Natl Acad Sci U S A,* 103**,** 8703-8.
SKAU, C. T., COURSON, D. S., BESTUL, A. J., WINKELMAN, J. D., ROCK, R. S., SIROTKIN, V. & KOVAR, D. R. 2011. Actin filament bundling by fimbrin is important for endocytosis, cytokinesis, and polarization in fission yeast. *J Biol Chem,* 286**,** 26964-77.
SMITH, K. L. & DEAN, S. J. 1998. Tissue repair of the epidermis and dermis. *J Hand Ther,* 11**,** 95-104.

SNIDER, N. T. & OMARY, M. B. 2014. Post-translational modifications of intermediate filament proteins: mechanisms and functions. *Nat Rev Mol Cell Biol,* 15**,** 163-77.

SOLOVEI, I., WANG, A. S., THANISCH, K., SCHMIDT, C. S., KREBS, S., ZWERGER, M., COHEN, T. V., DEVYS, D., FOISNER, R., PEICHL, L., HERRMANN, H., BLUM, H., ENGELKAMP, D., STEWART, C. L., LEONHARDT, H. & JOFFE, B. 2013. LBR and lamin A/C sequentially tether peripheral heterochromatin and inversely regulate differentiation. *Cell,* 152**,** 584-98.

SONG, J. G., KOSTAN, J., DREPPER, F., KNAPP, B., DE ALMEIDA RIBEIRO, E., JR., KONAREV, P. V., GRISHKOVSKAYA, I., WICHE, G., GREGOR, M., SVERGUN, D. I., WARSCHEID, B. & DJINOVIC-CARUGO, K. 2015. Structural insights into Ca2+-calmodulin regulation of Plectin 1a-integrin beta4 interaction in hemidesmosomes. *Structure,* 23**,** 558-70.

SONNENBERG, A. & LIEM, R. K. H. 2007. Plakins in development and disease. *Experimental Cell Research,* 313**,** 2189-2203.

SOSA, B. A., ROTHBALLER, A., KUTAY, U. & SCHWARTZ, T. U. 2012. LINC complexes form by binding of three KASH peptides to domain interfaces of trimeric SUN proteins. *Cell,* 149**,** 1035-47.

SPURNY, R., GREGOR M FAU - CASTANON, M. J., CASTANON MJ FAU - WICHE, G. & WICHE, G. 2008. Plectin deficiency affects precursor formation and dynamics of vimentin networks. *Exp Cell Res,* 314**,** 3570–3580.

STEWART-HUTCHINSON, P. J., HALE, C. M., WIRTZ, D. & HODZIC, D. 2008. Structural requirements for the assembly of LINC complexes and their function in cellular mechanical stiffness. *Experimental Cell Research,* 314**,** 1892-1905.

STRAHL, B. D. & ALLIS, C. D. 2000. The language of covalent histone modifications. *Nature,* 403**,** 41-5.

STRAIGHT, A. F., CHEUNG, A., LIMOUZE, J., CHEN, I., WESTWOOD, N. J., SELLERS, J. R. & MITCHISON, T. J. 2003. Dissecting Temporal and Spatial Control of Cytokinesis with a Myosin II Inhibitor. *Science,* 299**,** 1743-1747.

SULLIVAN, T., ESCALANTE-ALCALDE, D., BHATT, H., ANVER, M., BHAT, N., NAGASHIMA, K., STEWART, C. L. & BURKE, B. 1999. Loss of A-type lamin expression compromises nuclear envelope integrity leading to muscular dystrophy. *J Cell Biol,* 147**,** 913-20.

SVITKINA, T. M., VERKHOVSKY, A. B. & BORISY, G. G. 1996. Plectin sidearms mediate interaction of intermediate filaments with microtubules and other components of the cytoskeleton. *J Cell Biol,* 135**,** 991-1007.

SWIFT, J., IVANOVSKA, I. L., BUXBOIM, A., HARADA, T., DINGAL, P. C., PINTER, J., PAJEROWSKI, J. D., SPINLER, K. R., SHIN, J. W., TEWARI, M., REHFELDT, F., SPEICHER, D. W. & DISCHER, D. E. 2013. Nuclear lamin-A scales with tissue stiffness and enhances matrix-directed differentiation. *Science,* 341**,** 1240104.

SZEVERENYI, I., CASSIDY, A. J., CHUNG, C. W., LEE, B. T., COMMON, J. E., OGG, S. C., CHEN, H., SIM, S. Y., GOH, W. L., NG, K. W., SIMPSON, J. A., CHEE, L. L., ENG, G. H., LI, B., LUNNY, D. P., CHUON, D., VENKATESH, A., KHOO, K. H., MCLEAN, W. H., LIM, Y. P. & LANE, E. B. 2008. The Human Intermediate Filament Database: comprehensive

information on a gene family involved in many human diseases. *Hum Mutat,* 29**,** 351-60.

TERRY, S. J., ELBEDIWY, A., ZIHNI, C., HARRIS, A. R., BAILLY, M., CHARRAS, G. T., BALDA, M. S. & MATTER, K. 2012. Stimulation of cortical myosin phosphorylation by p114RhoGEF drives cell migration and tumor cell invasion. *PLoS ONE,* 7**,** e50188.

THAKAR, R. G., CHENG, Q., PATEL, S., CHU, J., NASIR, M., LIEPMANN, D., KOMVOPOULOS, K. & LI, S. 2009. Cell-Shape Regulation of Smooth Muscle Cell Proliferation. *Biophysical Journal,* 96**,** 3423-3432.

THOMAS, M. C. & CHIANG, C. M. 2006. The general transcription machinery and general cofactors. *Crit Rev Biochem Mol Biol,* 41**,** 105-78.

TIAN, R., GREGOR, M., WICHE, G. & GOLDMAN, J. E. 2006. Plectin Regulates the Organization of Glial Fibrillary Acidic Protein in Alexander Disease. *The American Journal of Pathology,* 168**,** 888-897.

TOIVOLA, D. M., KU, N. O., RESURRECCION, E. Z., NELSON, D. R., WRIGHT, T. L. & OMARY, M. B. 2004. Keratin 8 and 18 hyperphosphorylation is a marker of progression of human liver disease. *Hepatology,* 40**,** 459-66.

TOIVOLA, D. M., ZHOU, Q., ENGLISH, L. S. & OMARY, M. B. 2002. Type II keratins are phosphorylated on a unique motif during stress and mitosis in tissues and cultured cells. *Mol Biol Cell,* 13**,** 1857-70.

TRANCHIDA, D., PICCAROLO, S. & SOLIMAN, M. 2006. Nanoscale Mechanical Characterization of Polymers by AFM Nanoindentations: Critical Approach to the Elastic Characterization. *Macromolecules,* 39**,** 4547-4556.

TRIPATHI, V. & PRASANTH, K. 2011. Cell Nucleus. *iLS. John Willey & Sons, Ltd: Chichester.***,** 13.

UEMATSU, J., NISHIZAWA, Y., SONNENBERG, A. & OWARIBE, K. 1994. Demonstration of type II hemidesmosomes in a mammary gland epithelial cell line, BMGE-H. *J Biochem,* 115**,** 469-76.

VAEZI, A., BAUER, C., VASIOUKHIN, V. & FUCHS, E. 2002. Actin Cable Dynamics and Rho/Rock Orchestrate a Polarized Cytoskeletal Architecture in the Early Steps of Assembling a Stratified Epithelium. *Developmental Cell,* 3**,** 367-381.

VALENCIA, R. G., WALKO, G., JANDA, L., NOVACEK, J., MIHAILOVSKA, E., REIPERT, S., ANDRA-MAROBELA, K. & WICHE, G. 2013. Intermediate filament-associated cytolinker plectin 1c destabilizes microtubules in keratinocytes. *Mol Biol Cell,* 24**,** 768-84.

VAN HOLDE, K. & ZLATANOVA, J. 1995. Chromatin higher order structure: chasing a mirage? *J Biol Chem,* 270**,** 8373-6.

VAN HOLDE, K. & ZLATANOVA, J. 2007. Chromatin fiber structure: Where is the problem now? *Semin Cell Dev Biol,* 18**,** 651-8.

VAN VLIET, K. J., BAO, G. & SURESH, S. 2003. The biomechanics toolbox: experimental approaches for living cells and biomolecules. *Acta Materialia,* 51**,** 5881-5905.

VANNINI, A. 2013. A structural perspective on RNA polymerase I and RNA polymerase III transcription machineries. *Biochim Biophys Acta,* 1829**,** 258-64.

VANNINI, A. & CRAMER, P. 2012. Conservation between the RNA polymerase I, II, and III transcription initiation machineries. *Mol Cell,* 45**,** 439-46.

VASIOUKHIN, V., BAUER, C., YIN, M. & FUCHS, E. 2000. Directed actin polymerization is the driving force for epithelial cell-cell adhesion. *Cell,* 100**,** 209-19.

VASSY, J., BEIL M FAU - IRINOPOULOU, T., IRINOPOULOU T FAU - RIGAUT, J. P. & RIGAUT, J. P. 1996. Quantitative image analysis of cytokeratin filament distribution during fetal rat liver development. *Hepatology,* 23**,** 630-8.

VERSAEVEL, M., GREVESSE, T. & GABRIELE, S. 2012. Spatial coordination between cell and nuclear shape within micropatterned endothelial cells. *Nature Communications,* 3**,** 671.

VIGNJEVIC, D., PELOQUIN, J. & BORISY, G. G. 2006. In vitro assembly of filopodia-like bundles. *Methods Enzymol,* 406**,** 727-39.

VIGNJEVIC, D., YARAR, D., WELCH, M. D., PELOQUIN, J., SVITKINA, T. & BORISY, G. G. 2003. Formation of filopodia-like bundles in vitro from a dendritic network. *J Cell Biol,* 160**,** 951-62.

VINCKIER, A., DUMORTIER, C., ENGELBORGHS, Y. & HELLEMANS, L. 1996. Dynamical and mechanical study of immobilized microtubules with atomic force microscopy. *Journal of Vacuum Science & Technology B,* 14**,** 1427-1431.

VINCKIER, A. & SEMENZA, G. 1998. Measuring elasticity of biological materials by atomic force microscopy. *FEBS Letters,* 430**,** 12-16.

VOGEL, V. & SHEETZ, M. 2006. Local force and geometry sensing regulate cell functions. *Nat Rev Mol Cell Biol,* 7**,** 265-75.

WACHSSTOCK, D. H., SCHWARTZ, W. H. & POLLARD, T. D. 1993. Affinity of alpha-actinin for actin determines the structure and mechanical properties of actin filament gels. *Biophys J,* 65**,** 205-14.

WACHSSTOCK, D. H., SCHWARZ, W. H. & POLLARD, T. D. 1994. Cross-linker dynamics determine the mechanical properties of actin gels. *Biophys J,* 66**,** 801-9.

WAGNER, N. & KROHNE, G. 2007. LEM-Domain Proteins: New Insights into Lamin-Interacting Proteins. *In:* KWANG, W. J. (ed.) *International Review of Cytology.* Academic Press.

WALKO, G., CASTAÑÓN, M. J. & WICHE, G. 2015. Molecular architecture and function of the hemidesmosome. *Cell and Tissue Research,* 360**,** 529-544.

WALKO, G., VUKASINOVIC, N., GROSS, K., FISCHER, I., SIBITZ, S., FUCHS, P., REIPERT, S., JUNGWIRTH, U., BERGER, W., SALZER, U., CARUGO, O., CASTANON, M. J. & WICHE, G. 2011. Targeted proteolysis of plectin isoform 1a accounts for hemidesmosome dysfunction in mice mimicking the dominant skin blistering disease EBS-Ogna. *PLoS Genet,* 7**,** e1002396.

WALLACE, L., ROBERTS-THOMPSON, L. & REICHELT, J. 2012. Deletion of K1/K10 does not impair epidermal stratification but affects desmosomal structure and nuclear integrity. *Journal of Cell Science,* 125**,** 1750-1758.

WANG, K., MCCARTER, R., WRIGHT, J., BEVERLY, J. & RAMIREZ-MITCHELL, R. 1993. Viscoelasticity of the sarcomere matrix of skeletal muscles. The titin-myosin composite filament is a dual-stage molecular spring. *Biophys J,* 64**,** 1161-77.

WANG, N. & INGBER, D. E. 1994. Control of cytoskeletal mechanics by extracellular matrix, cell shape, and mechanical tension. *Biophys J,* 66**,** 2181-9.
WANG, N., TYTELL, J. D. & INGBER, D. E. 2010. Mechanotransduction at a distance: mechanically coupling the extracellular matrix with the nucleus. *Nature Reviews - Molecular Cell Biology,* 10**,** 8.
WANG, Z., SCHONES, D. E. & ZHAO, K. 2009. Characterization of human epigenomes. *Current Opinion in Genetics & Development,* 19**,** 127-134.
WARREN, D. T., TAJSIC, T., MELLAD, J. A., SEARLES, R., ZHANG, Q. & SHANAHAN, C. M. 2010. Novel nuclear nesprin-2 variants tether active extracellular signal-regulated MAPK1 and MAPK2 at promyelocytic leukemia protein nuclear bodies and act to regulate smooth muscle cell proliferation. *J Biol Chem,* 285**,** 1311-20.
WATT, F. M. 1998. Epidermal stem cells: markers, patterning and the control of stem cell fate. *Philos Trans R Soc Lond B Biol Sci,* 353**,** 831-7.
WEI, S. C., FATTET, L., TSAI, J. H., GUO, Y., PAI, V. H., MAJESKI, H. E., CHEN, A. C., SAH, R. L., TAYLOR, S. S., ENGLER, A. J. & YANG, J. 2015. Matrix stiffness drives epithelial-mesenchymal transition and tumour metastasis through a TWIST1-G3BP2 mechanotransduction pathway. *Nat Cell Biol,* 17**,** 678-88.
WESTERMARCK, J. & HAHN, W. C. 2008. Multiple pathways regulated by the tumor suppressor PP2A in transformation. *Trends Mol Med,* 14**,** 152-60.
WICHE, G., OSMANAGIC-MYERS, S. & CASTAÑÓN, M. J. 2015. Networking and anchoring through plectin: a key to IF functionality and mechanotransduction. *Current Opinion in Cell Biology,* 32**,** 21-29.
WILHELMSEN, K. 2005. Nesprin-3, a novel outer nuclear membrane protein, associates with the cytoskeletal linker protein plectin. *The Journal of Cell Biology,* 171**,** 799-810.
WILLERT, K. & JONES, K. A. 2006. Wnt signaling: is the party in the nucleus? *Genes & Development,* 20**,** 1394-1404.
WILSON, K. L. & BERK, J. M. 2010. The nuclear envelope at a glance. *Journal of Cell Science,* 123**,** 1973-1978.
WILSON, K. L. & FOISNER, R. 2010. Lamin-binding Proteins. *Cold Spring Harbor Perspectives in Biology,* 2.
WINDOFFER, R., BEIL, M., MAGIN, T. M. & LEUBE, R. E. 2011. Cytoskeleton in motion: the dynamics of keratin intermediate filaments in epithelia. *The Journal of Cell Biology,* 194**,** 669-678.
WINDOFFER, R., KOLSCH, A., WOLL, S. & LEUBE, R. E. 2006. Focal adhesions are hotspots for keratin filament precursor formation. *J Cell Biol,* 173**,** 341-8.
WINDOFFER, R., WOLL, S., STRNAD, P. & LEUBE, R. E. 2004. Identification of novel principles of keratin filament network turnover in living cells. *Mol Biol Cell,* 15**,** 2436-48.
WINTER, L. & WICHE, G. 2012. The many faces of plectin and plectinopathies: pathology and mechanisms. *Acta Neuropathologica,* 125**,** 77-93.
WOLL, S., WINDOFFER, R. & LEUBE, R. E. 2005. Dissection of keratin dynamics: different contributions of the actin and microtubule systems. *Eur J Cell Biol,* 84**,** 311-28.

WÖLL, S., WINDOFFER, R. & LEUBE, R. E. 2007. p38 MAPK-dependent shaping of the keratin cytoskeleton in cultured cells. *The Journal of Cell Biology,* 177**,** 795-807.

WOODCOCK, C. L. & DIMITROV, S. 2001. Higher-order structure of chromatin and chromosomes. *Curr Opin Genet Dev,* 11**,** 130-5.

WOODCOCK, C. L. & GHOSH, R. P. 2010. Chromatin Higher-order Structure and Dynamics. *Cold Spring Harbor Perspectives in Biology,* 2**,** a000596-a000596.

WYATT, T. P., HARRIS, A. R., LAM, M., CHENG, Q., BELLIS, J., DIMITRACOPOULOS, A., KABLA, A. J., CHARRAS, G. T. & BAUM, B. 2015. Emergence of homeostatic epithelial packing and stress dissipation through divisions oriented along the long cell axis. *Proc Natl Acad Sci U S A,* 112**,** 5726-31.

YOUNG, K. G. & KOTHARY, R. 2005. Spectrin repeat proteins in the nucleus. *BioEssays,* 27**,** 144-52.

ZAIDEL-BAR, R., ZHENHUAN, G. & LUXENBURG, C. 2015. The contractome - a systems view of actomyosin contractility in non-muscle cells. *J Cell Sci*.

ZHANG, H., SUNNARBORG, S. W., MCNAUGHTON, K. K., JOHNS, T. G., LEE, D. C. & FABER, J. E. 2008. Heparin-binding epidermal growth factor-like growth factor signaling in flow-induced arterial remodeling. *Circ Res,* 102**,** 1275-85.

ZHEN, Y. Y., LIBOTTE, T., MUNCK, M., NOEGEL, A. A. & KORENBAUM, E. 2002. NUANCE, a giant protein connecting the nucleus and actin cytoskeleton. *J Cell Sci,* 115**,** 3207-22.

ZHOU, Q., JI, X., CHEN, L., GREENBERG, H. B., LU, S. C. & OMARY, M. B. 2005. Keratin mutation primes mouse liver to oxidative injury. *Hepatology,* 41**,** 517-25.

ZHOU, V. W., GOREN, A. & BERNSTEIN, B. E. 2011. Charting histone modifications and the functional organization of mammalian genomes. *Nat Rev Genet,* 12**,** 7-18.

Appendices

I. Cooperation between actin and keratin networks regulates nuclear mechanotransduction

Filipe V Almeida[1,6], Gernot Walko[2], James R McMillan[3], John A McGrath[4], Gerhard Wiche[5], Asa H Barber[1], John T Connelly[6]*

1. School of Engineering and Materials Science, Queen Mary, University of London, London UK
2. Centre for Stem Cells and Regenerative Medicine, King's College London, London UK
3. The National Diagnostic EB Laboratory, Viapath, St. Thomas' Hospital, London, UK
4. St. John's Institute of Dermatology, King's College London (Guy's Campus), London UK
5. Max F. Perutz Laboratories, Department of Biochemistry and Cell Biology, University of Vienna, Vienna Austria
6. Centre for Cell Biology and Cutaneous Research, Barts and the London School of Medicine and Dentistry, Queen Mary, University of London, London UK

* Corresponding author:
Dr. John Connelly
Centre for Cutaneous Research
4 Newark Street
London E1 2AT
UK

j.connelly@qmul.ac.uk
Tel: +44 207 882 7160
Fax: +44 207 882 7172

Key words: Keratinocyte, Mechanics, Nucleus, Keratin, Cyoskeleton, Plectin

Abstract:

The transmission of mechanical forces to the nucleus is important for intracellular positioning, mitosis, and cell motility, yet the contribution of specific components of the cytoskeleton to nuclear mechanotransduction remains unclear. In this study, we examine how cross-talk between F-actin and keratin networks controls the 3D nuclear morphology of keratinocytes. Using micro-patterned surfaces to precisely manipulate cell shape, we find that cell adhesion and spreading regulate the size and shape of the nucleus. Disruption of the keratin cytoskeleton through loss of plectin promoted greater nuclear deformation, which depended on acto-myosin contractility. Nuclear morphology did not depend on direct linkage of the keratin cytoskeleton with the nuclear membrane, rather loss of plectin reduced keratin filament density around the nucleus. We further demonstrate that keratinocytes have abnormal nuclear morphologies in the epidermis of plectin-deficient, epidermolysis bullosa patients. Together, our data demonstrate that plectin is an essential regulator of nuclear morphology *in vitro* and *in vivo* and protects the nucleus from mechanical deformation.

Introduction:

Mechanical and biophysical interactions between cells and their surrounding environment regulate essential processes, such as growth (Chen et al., 1997), survival (Chen et al., 1997), migration (Pelham and Wang, 1997), and differentiation (Connelly et al., 2010; Engler et al., 2006; McBeath et al., 2004), and in some instances contribute to disease progression (Paszek et al., 2005). Integrin-based adhesions and the actin cytoskeleton are classic physical linkages between cells and the extracellular matrix and regulate various aspects of cellular mechano-sensing (Dupont et al., 2011; Engler et al., 2006; McBeath et al., 2004). Nevertheless, how these intracellular structures transform mechanical forces into biochemical signals and influence cell behaviour remains unclear.

Recent evidence suggests that the nucleus itself may be a central mechano-sensing element within the cell. Expression levels of Lamin A/C, a main structural component of the nucleus, correlate with bulk tissue mechanics and at a molecular level, mediate gene expression and stem cell differentiation (Swift et al., 2013). The nucleus also independently adapts to external forces via phosphorylation of the nuclear membrane protein Emerin (Guilluy et al., 2014). Furthermore, chromatin has been proposed to undergo rapid conformational changes when an external mechanical stimulus is applied (Iyer et al., 2012). Thus, the transmission of forces to the nucleus may be a critical component of cellular mechanotransduction.

The nucleus physically connects to the cytoskeleton via the LINC (Linker of Nucleoskeleton and Cytoskeleton) complex, which comprises nesprins, SUN1/2, and the nuclear lamina. The integrity of this linkage is essential for maintaining nuclear shape, integrity, and positioning within the cell (Gundersen and Worman, 2013; Isermann and Lammerding, 2013). Indeed, the disruption of the LINC complex or the nuclear lamina leads to dramatic morphological changes in the nucleus (Lammerding et al., 2004), as well as defects in mitotic spindle orientation (Hale et al., 2008) and cell migration (Khatau et al., 2012; Lee et al., 2007; Zhang et al., 2009). Moreover, mutations in the genes encoding these structural proteins have been implicated in a

variety of diseases, including progeria (Goldman et al., 2004), muscular dystrophy (Bonne et al., 1999), and deafness (Horn et al., 2013).

The nesprin family of proteins localise to the outer nuclear membrane and contain extra-nuclear domains that provide the first point of contact between the cytoskeleton and the nucleus (Zhang et al., 2001). While the different nesprin chains interact with distinct components of the cytoskeleton, each has a conserved KASH domain that binds SUN1/2 within the inter-membrane space. SUN1/2 in turn bind to nuclear lamina proteins, thereby forming a continuous physical link between the cytoskeleton and the nucleoskeleton (Starr and Fridolfsson, 2010, 1). Nesprin-1 and nesprin-2 giant bind to F-actin microfilaments (Zhang et al., 2001; Zhen et al., 2002), whereas nesprin-4 couples the nuclear membrane to microtubules via the kinesin-1 motor protein (Roux et al., 2009). Additionally, nesprin-3 connects to intermediate filaments via plectin (Wilhelmsen et al., 2005), a large (500 kDa) cytolinker that not only cross-links intermediate filaments to each other, but also links them to the nuclear membrane, the actin cytoskeleton, and integrin receptors (Castañón et al., 2013).

While the actin cytoskeleton and LINC complex control nuclear mechanotransduction for some cell types (Li et al., 2014; Versaevel et al., 2012), the role of intermediate filaments in force transmission to the nucleus is less clear. In epidermal keratinocytes, the keratin cytoskeleton contributes significantly to overall cell rigidity and could potentially influence nuclear mechanotransduction (Kröger et al., 2013; Ramms et al., 2013; Seltmann et al., 2013). In this study we investigate the mechanisms of force transmission to the nucleus in keratinocytes using micro-patterned polymer substrates, which allow for precise control over single cell adhesion and spreading. We demonstrate that cooperation between the keratin cross-linking protein, plectin, and the actin cytoskeleton regulates nuclear deformation in response to defined biophysical cues. Furthermore, the nuclear morphology of keratinocytes in the epidermis of epidermolysis bullosa simplex (EBS) patients with plectin deficiency is perturbed. Together, our findings provide new insights into the complex process of nuclear mechanotransduction and demonstrate a novel function for plectin in epidermal keratinocytes.

Results:

Keratinocyte shape specifies nuclear morphology independently of acto-myosin contractility

To assess how cell shape affects the nuclear morphology of primary human keratinocytes, single cells were seeded onto micro-patterned collagen substrates of different sizes and shapes: circular islands of 20, 30 and 50 μm diameter and elliptical islands of shape factor 8 (SF = major/minor axis) with an equivalent area to 30 μm diameter islands. The resultant 3D nuclear morphology was analysed by confocal microscopy 3 hours after seeding when the cells on the larger islands were fully spread (Fig 1A). The cross-sectional areas of the nuclei increased significantly as cells spread progressively on the 30 μm and 50 μm islands (Fig 1B), while the height of the nucleus decreased slightly (Fig 1C). Because the increase in area was proportionally greater than the decrease in height, cell spreading on the 50 μm islands resulted in approximately 40% increase in nuclear volume compared to cells on the 20 μm substrates (Fig 1D). In addition to nuclear size, cell shape also correlated with nuclear shape. The nuclei of cells on the elliptical SF8 islands were more elongated, switching from oblate (disk-like) to prolate (zeppelin-like) ellipsoids, compared to cells on SF1 substrates (Fig 1E). These results indicate that primary keratinocyte shape defines nuclear morphology, consistent with the response of other cell types (Li et al., 2014; Versaevel et al., 2012).

As the actin cytoskeleton is a key regulator of cell mechanics and directly links to the nucleus (Li et al., 2014; Zhen et al., 2002), we next investigated the role of cytoskeletal tension in cell shape-induced nuclear deformation. Although inhibition of acto-myosin contractility with blebbistatin completely blocked actin stress fibre formation, the cross-sectional areas of nuclei on 20 μm and 50 μm islands were unaffected (Fig 1F,G). A similar response was observed in cells treated with the Rho-kinase inhibitor Y27632, and even complete disruption of actin polymerisation with latrunculin only partially blocked cell-shape induced nuclear expansion on the 50 μm islands (Fig S1A,B). We conclude that the actin cytoskeleton is not solely responsible for maintaining nuclear morphology in keratinocytes.

1. Plectin mediates cell shape-induced nuclear deformation

The keratin network of intermediate filaments is a major structural and mechanical component of keratinocytes (Ramms et al., 2013; Seltmann et al., 2013). We therefore sought to determine how this cytoskeletal structure contributed to the regulation of nuclear morphology. We examined mouse keratinocytes lacking the gene for plectin (*Plec*), which controls keratin cytoskeletal organisation via filament cross-linking (Castañón et al., 2013; Rezniczek et al., 1998; Steinböck et al., 2000). As previously described (Osmanagic-Myers et al., 2006), *Plec*-null keratinocytes (KO) had a more elongated, spindle-like morphology (Fig 2A), and the keratin filaments were thicker and less dense compared to wild-type (WT) cells (Fig 2B). Correlating with overall cell morphology on non-patterned surfaces, the nuclei of KO keratinocytes were significantly larger and more elongated than WT cells. We then analysed the nuclear morphology of WT and KO cells cultured on micro-patterned substrates to control for changes in cell shape and determine the direct effect of plectin on the nucleus. Like human keratinocytes, WT mouse cells displayed larger nuclei when allowed to spread on 50 μm islands and more elongated nuclei on SF8 islands (Fig 2E-H). The response to the micro-patterned surfaces was significantly more pronounced in *Plec* KO cells, with nuclear area increasing from approximately 150 μm^2 to 220 μm^2 on the 50 μm substrates and the aspect ratio increasing from 2 to 3 on the SF8 substrates (Fig 2E-H). It is interesting to note that the level of nuclear deformation in KO cells was similar to that of HeLa cells, which express a distinct pattern of cytokeratins from epidermal keratinocytes (Moll et al., 1982) (Fig S1). These findings indicate that in the absence of plectin, the nuclei of keratinocytes are more sensitive to extracellular physical cues and that plectin is a key regulator of nuclear morphology.

2. Cross-talk between plectin and acto-myosin contractility regulates keratin filament organisation and nuclear morphology

To understand the mechanism by which plectin regulates nuclear morphology, we next examined the organisation of various adhesive and cytoskeletal structures in WT and *Plec* KO keratinocytes. KO cells displayed reduced staining for the hemidesmosomal integrin α6 (Fig 3A), and more elongated focal adhesions, which appeared to associate with keratin filaments (Fig 3B). Both WT and KO cells were competent to form actin stress fibres (Fig 3C); however, the KO cells were more sensitive to inhibition of acto-

myosin contractility with blebbistatin. In WT cells, blebbistatin reduced keratin filament thickness, but the dense network structure was maintained (Fig 3C). By contrast, treatment of KO cells with blebbistatin resulted in a dramatic collapse of the keratin network (Fig 3C). These results suggest that cooperation between the actin and keratin cytoskeletons modulates keratinocyte structure and that the keratin network prevents a complete collapse of cell morphology even in the absence of acto-myosin tension.

To test whether cross-talk between actin and keratin also influences nuclear mechanics, we next examined the effects of blebbistatin on the nuclear morphology of WT and *Plec* KO cells on micro-patterned substrates. Blebbistatin treatment abolished the differences in nuclear cross-sectional area and elongation on the 50 μm and SF8 micro-patterns, respectively (Fig 4A-D). Thus, acto-myosin contractility is required for plectin-dependent changes in nuclear deformation. The reduced nuclear elongation caused by blebbistatin treatment (Fig 4B,D) in particular suggests that tensile forces from the actin cytoskeleton promote nuclear deformation, and the more pronounced elongation in KO cells (Fig 4B,D) suggests that the keratin cytoskeleton opposes these forces and protects the nucleus from deformation.

3. The keratin cytoskeleton modulates nuclear morphology independently of direct linkage to the nuclear membrane

Plectin is a well-established cytolinker within the epidermis, and as demonstrated here and by others, it controls keratin filament organisation (Osmanagic-Myers et al., 2006). Plectin also connects intermediate filaments such as vimentin to the nuclear membrane via nesprin-3 (Wilhelmsen et al., 2005). Therefore, loss of plectin may potentially affect nuclear morphology either by disrupting the direct physical linkage and force transmission between the cytoskeleton and the nucleus or indirectly through changes in keratin structure and cellular mechanics. We examined the expression and localisation of plectin and nesprin-3 in mouse keratinocytes. In WT cells, plectin co-localised with keratin filaments in the cytoplasm but not the nucleus, as would be expected based on its function as a keratin cross-linker (Osmanagic-Myers et al., 2006) (Fig 5A). Similarly, diffuse nesprin-3 staining was only observed in the cytoplasm of WT keratinocytes, whereas in 3T3 fibroblasts it specifically localised to the nuclear

membrane (Fig 5B). Previous studies have demonstrated low nesprin-3 expression within the epidermis, and mice lacking nesprin-3 have a normal skin phenotype (Ketema et al., 2013). These findings suggest that in keratinocytes, plectin and nesprin-3 do not directly link keratins to the nuclear membrane.

To determine how disruption of nuclear-cytoskeletal linkages influences nuclear morphology in keratinocytes, we overexpressed a dominant negative nesprin (DN-KASH), which comprises a KASH domain for localisation to the nuclear membrane but lacks any extra-nuclear cytoskeletal binding domains (Zhang et al., 2001). Compared to GFP overexpression, DN-KASH had no effect on WT nuclei (Fig 5C-D), which in conjunction with the immunofluorescence data, further supports an indirect role of plectin in nuclear mechanotransduction. Interestingly, DN-KASH expression in *Plec* KO cells reduced nuclear area to WT levels (Fig 5D). This effect may be due to disruption of the linkage between other nesprins (e.g. nesprin-1 and nesprin-2 giant) and the actin cytoskeleton, which is required for nuclear expansion in the absence of plectin.

4. Plectin dynamically mediates the effect of cell crowding on nuclear morphology

In addition to single cell adhesion and spreading, we also sought to determine the role of plectin in regulating cell-cell interactions and nuclear morphology within multi-cell structures. WT and *Plec* KO cells were seeded onto large micro-patterns of 200 μm in diameter at either low (37,500 per cm^2) or high (225,000 per cm^2) densities, and the 3D nuclear morphology was assessed by confocal microscopy. At low density (minimum to completely cover the micro-pattern), similar numbers of WT and KO cells adhered to the patterns, and the nuclei of the KO cells were significantly larger than WT (Fig 6A-C), consistent with the single cell experiments. When seeded at high density, however, there were significantly more KO cells per micro-patterned island than WT cells. The nuclear volume of KO cells at high density was also significantly smaller than at low density, while seeding density had no effect on the nuclear volume of WT cells. Intriguingly, the KO cells' nuclei were more elongated in the apical direction (Z axis) compared to the WT cells at both densities (Fig 6D-E). These results indicate that plectin is indeed important for cell density sensing. In the absence of plectin, keratinocytes are more sensitive to cell crowding, which in turn affects cell packing and

nuclear deformation, and may reflect defects in the keratin cytoskeleton and cellular mechanics.

To investigate the plasticity and dynamics of nuclear deformation, we next took advantage of dynamically adhesive micro-patterns developed in our laboratory (Costa et al., 2014) and investigated nuclear morphology when keratinocytes were released from the micro-patterns and induced to migrate. Cells were seeded onto 200 μm islands at high density for 12 hours, then activated to migrate by functionalisation of the surrounding polymer brushes with a collagen mimetic peptide (Reyes and García, 2003) (Fig 6F). Nuclear cross-sectional area remained relatively constant in WT cells migrating onto the functionalised surfaces, while nuclear area increased significantly in *Plec* KO cells within 6 hours of activation (Fig 6G). These results demonstrate that reduced nuclear area caused by cell crowding in KO cells is reversible, and the nuclei expand again when cells are allowed to migrate and spread.

5. Nuclear morphology is perturbed in the epidermis of EBS-MD patients

In human skin, mutations in the *PLEC* gene cause the blistering disease epidermolysis bullosa simplex with muscular dystrophy (EBS-MD) (McLean et al., 1996; Smith et al., 1996; Winter and Wiche, 2013). To investigate whether plectin also influences nuclear mechanics *in vivo*, we analysed the morphology of nuclei in the epidermis of four EBS-MD patients with confirmed plectin deficiency (Table S1). Compared to normal epidermis, the nuclei of basal keratinocytes in the EBS-MD samples were significantly smaller, less circular, and elongated in the apical direction (Fig 7A-D). These findings demonstrate that plectin also regulates the nuclear morphology of human keratinocytes *in vivo*. Moreover, the more apically elongated nuclei observed in the EBS-MD samples are consistent with the *in vitro* effects of cell crowding and suggest that *PLEC* mutations may directly influence nuclear morphology within the epidermis via changes in keratin structure and cellular mechanics.

Discussion:

In this study we examined the mechanisms of force transmission from external adhesive cues to the nucleus of epidermal keratinocytes. We took advantage of micro-patterned

collagen substrates to precisely control the adhesion and spreading of single cells, as well as crowding in multi-cell clusters. Our results demonstrate that in keratinocytes, the size and shape of the nucleus changes in response to defined biophysical cues, and the extent of this deformation is controlled by cross-talk between plectin and acto-myosin contractility. Plectin is required for maintaining a dense keratin network and dampens nuclear deformation induced by either cell spreading or crowding. Interestingly, this effect does not appear to involve direct linkage of plectin to the nuclear membrane. Based on these findings we propose a model in which the keratin cytoskeleton provides a rigid network that resists both tensile and compressive forces imposed on the cell and protects the nucleus from excessive deformation.

Plectin is a well-established regulator of cytoskeletal architecture across different cell types. Consistent with our findings, the absence of plectin in keratinocytes induces the formation of thicker keratin filament bundles, with noticeably larger voids within the meshwork (Osmanagic-Myers et al., 2006). Loss of plectin in keratinocytes results in increased MAP kinase activity and enhanced cell migration (Osmanagic-Myers et al., 2006). However, this response appears to be cell-type specific. In fibroblasts, plectin is necessary for localisation of vimentin intermediate filaments to focal adhesions at the cell periphery (Burgstaller et al., 2010; Spurny et al., 2008) and inhibits cell motility (Gregor et al., 2014). MCF-7 breast cancer cells similarly acquire a slower, less protrusive phenotype in the absence of plectin (Boczonadi et al., 2007). Plectin also impacts the organisation of the intermediate filament protein glial fibrillary acidic protein (GFAP) in astrocytes, and contributes to the fibrotic phenotype of R239C GFAP mutant cells (Tian et al., 2006). Finally, loss of plectin reduces fibroblast stiffness and impairs force transmission (Na et al., 2009). Thus, plectin is a key regulator of cellular mechanics, and our data add a new dimension to this function, specifically in the control of nuclear morphology. Given the cell type-specific function of plectin in cytoskeletal organisation and migration, its role in force transmission to the nucleus for other cell types will be an important area of investigation in future studies.

Here, we provide evidence that plectin indirectly protects the nucleus from deformation via keratin filament cross-linking rather than direct linkage to the nuclear membrane. Consistent with this result, crystallographic characterisation of keratin filament bundles

recently revealed that the disulphide bond responsible for the X-shaped coiled-coil heterodimers is enriched in the perinuclear region of basal keratinocytes of the epidermis, where it is thought to stabilise a cage of keratin around the nucleus and provide mechanical support in early stages of differentiation (Lee et al., 2012). In other studies, epidermal specific overexpression of mutant Lamin A/C (progerin) led to abnormal nuclear morphology in keratinocytes (Wang et al., 2008), and in some instances progerin overexpression promoted hyperproliferation and hair loss (Sagelius et al., 2008). These findings demonstrate that, in addition to the keratins, the nuclear lamina is important for maintaining keratinocyte nuclear morphology, and further suggest that disruption of nuclear mechanics does indeed influence epidermal cell function.

While plectin clearly regulates keratinocyte nuclear morphology, the direct impact on cell behaviour and disease progression remains unclear. Changes in the size and shape of the nucleus could potentially affect chromatin structure and gene expression. During terminal differentiation in the mouse epidermis, increased clusters of heterochromatin accompany decreased nuclear volume (Gdula et al., 2013), and our own studies have shown that histone acetylation correlates with cell adhesion and spreading on micro-patterned substrates (Connelly et al., 2011). Similarly, chromatin de-condensation follows nuclear softening in embryonic stem cells (Chalut et al., 2012), and direct mechanical stimulation of HeLa cells causes rapid de-compaction of chromatin (Iyer et al., 2012). While there is a strong association between nuclear deformation, chromatin remodelling, and cell behaviour, a definitive causative relationship has yet to be established.

Clinically, mutations in plectin (plectinopathies) manifest into different symptoms according to the missing isoforms (Winter and Wiche, 2013), while keratin 14 mutations themselves disrupt keratin filament mechanics (Russell et al., 2004) and lead to distinct forms of EBS (Coulombe et al., 1991). In future studies, investigation of how other types of plectin mutations, such as in EBS Ogna (Walko et al., 2011), and EBS caused by keratin mutations may affect nuclear morphology will be of great importance. Moreover, identifying a potential role for nuclear mechanics in the

pathophysiology of blistering skin diseases could shed new light on our understanding and treatment of these complex and painful conditions.

7. Materials and Methods:

6. *Fabrication of micro-patterned substrates*

In order to control adhesive area, patterned polymerised (oligo ethylene glycol methacrylate) (POEGMA) brushes were utilised. Briefly, master silicon moulds were created by photolithography and used to cast poly-dimethylsiloxane stamps. The micro-patterned stamps were inked with the thiol initiator, ω-mercaptoundecyl bromoisobutyrate, and brought into conformal contact with gold-coated coverslips for 15 seconds to deposit the initiator as a self-assembled monolayer. Atom transfer radical polymerisation (ATRP) of the monomeric solution oligo(ethylene glycol) methacrylate (OEGMA; M_n 360 for –OH brushes) and oligo(ethylene glycol) methyl ether methacrylate (M_n 300 for -CH3 terminated brushes), was carried out in a water/ethanol (4:1) solution of OEGMA (1.6 M), Cu(II)Br (3.3 mM), 2,2-bipyridine (82 mM) and Cu(I)Cl (33 mM). The reaction was performed at room temperature from 0.25-1h. For dynamically adhesive micro-patterns, substrates were further modified with alkyne moieties as previously described (Costa et al., 2014). Following sterilisation with 70% ethanol, patterned substrates were coated with 20 μg/ml of rat type I collagen (BD Biosciences) in PBS for 1 h at 37 °C. Substrates were rinsed three times with 1 mM HCl and twice with PBS. All chemicals were from Sigma Aldrich unless otherwise indicated.

7. *Cell culture*

Primary human keratinocytes were isolated from neonatal foreskin and maintained on a feeder layer of J2 3T3 fibroblasts, as previously described (Rheinwald and Green, 1977). Cells were cultured in FAD medium containing 1 part Ham's F12 (Life Technologies), 3 parts DMEM (Life Technologies), 10^{-4} M adenine, 10% FBS (Biosera), 1% penicillin/streptomycin (Life Technologies), 0.5 μg/ml hydrocortisone, 5 μg/ml insulin, 10^{-10} M cholera toxin and 10 ng/ml EGF (Peprotech). Immortalised *Plec* (-/-) and (+/+) mouse keratinocyte cell cultures were established from Plec (-/-)/p53 (-/-) and Plec (+/+)/p53 (-/-) mice as previously described (Andrä et al., 2003) and

maintained in EpiLife medium with Human Keratinocyte Growth Supplement (Life Technologies). NIH 3T3 cells were maintained in DMEM supplemented with 10% FBS and 1% penicillin/streptomycin. For seeding onto micro-patterned substrates, regardless the type of substrate, both primary human and mouse keratinocytes were trypsinised (passages ranging 2–8 for pHK and 8-18 for the MK) and re-seeded onto the micro-patterned substrates at varying densities ranging 10,000-25,000 cells/cm^2. Cells were allowed to adhere for 0.5-1 h and then rinsed three times with fresh medium. Where indicated, cells were treated for 3 hours with 50 μM Blebbistatin (Merck Millipore), 1 μM Latrunculin (Merck Millipore), 10 μM Y27632 (Merck Millipore), or carrier control (0.1% DMSO). To activate cell migration out of the micro-patterns, substrates were functionalised with a collagen mimetic peptide containing the GFOGER motif (Reyes and García, 2003) (Activotec). Cells were exposed to 1 mg/mL GFOGER in phenol-free DMEM containing 0.5% Irgacure 2959. The coupling reaction was initiated by exposure to 365 nm light from an LED array (Cetoni, Germany) for 1 min. After exposure, substrates were immediately washed three times with DMEM.

8. EB skin samples

Plectin deficient EBS-MD and control skin biopsies were provided by the EB Laboratory at St. Thomas' Hospital (Viapath, London). Ethical approval was obtained from Guy's and St. Thomas' NHS Trust Research Ethics committee, code 07/H0802/104 (PI: JA McGrath). Following informed consent, a shave biopsy of normal-appearing, rubbed skin was biopsied from the arm or thigh following local anaesthetic with 2% lignocaine. Skin biopsies were transported to the EB Laboratory where they were washed on a rotator in PBS at 4°C. Samples were then embedded and mounted in Tissue-Tek® OCT compound (Agar Scientific) and snap frozen in liquid nitrogen-cooled n-heptane for storage at -80°C until 5-7 μm cryostat skin sections were cut using a Bright OTF500 cryostat (Bright Instruments). Plectin deficient samples were previously identified by the EB Laboratory by negative staining with at least two out of six anti-plectin diagnostic antibodies.

9. Plasmids and transfection

Mouse keratinocytes were cultured in Epi-life medium for 24 h prior to transfection. Cells were transfected for 3 h using 1 μl Lipofectamine 2000 (Life Technologies) and 1 μg of DNA per 10^5 cells. The dominant negative nesprin (DN-KASH) construct was kindly provided by Dr. Derek Warren (King's College London) and has been described previously (Zhang et al., 2001).

10. *Immunofluorescence imaging and quantification*

For immunofluorescence microscopy, cells were fixed with 4% paraformaldehyde (PFA) and permeabilised with 0.2% Triton X-100 in PBS for 10 min at room temperature and washed three times in PBS. Samples were blocked for 1 h in 10% bovine serum plus 0.25% fish gelatin, incubated with primary antibodies for 1 h at room temperature or at 4 °C overnight, and incubated with secondary antibodies (Life Technologies, 1:1000) for 1 h at room temperature. Samples were mounted on glass slides with Mowiol reagent. The following primary antibodies were used for immunofluorescence staining: Lamin A/C (Santa Cruz Biotechnology, Ms 636, 1:200), K14 (Cancer Research UK, Ms LL002, 1:500), K14 (Covance, Rb polyclonal, 1:5000), α6 integrin (BD Biosciences, Rat GoH3, 1:100), paxillin (BD Biosciences, Ms 177, 1:200), plectin (Ms 10F6, 1:2) (Walko et al., 2011), and nesprin-3 (gift from Arnoud Sonnenberg, Rb polyclonal, 1:100). F-actin was labelled with phalloidin-AlexaFluor 488 (Life Technologies, 1:500).

High-resolution images were acquired with either a Zeiss 510 or 710 confocal microscope. For low magnification epi-fluorescence microscopy, either Leica DMI4000 or Leica DMI5000 were used. ImageJ was used for two dimensional data analysis of epi-fluorescent images. For the processing and analysis of z-stacks of single cells, a MatLab (MathWorks) script was developed. Briefly, each frame was threshold using Otsu's method. As the pixel area through the z-stacks followed a normal distribution, the height was determined by counting the frames resembling a pixel area superior within $\mu \pm 0.64\sigma^2$ of the fitted Gaussian curve. For the quantification of 3D geometry, Imaris (Bitplane) was used to fit an ellipsoid to the DAPI signal and calculate volume, ellipticity (both prolate and oblate) and XYZ axes (both absolute and normalised lengths). To determine whether the nucleus was oriented in the apical or lateral direction, the sine of the angle between the major axis of the fitted ellipsoid (*c* axis) and

the X-Y plane was calculated. Nuclei oriented in the apical direction were defined as having angles above 45^{o} ($\sin(\emptyset) \approx 0.71$ of normalised vector).

11. *Statistical analysis*

All data were analysed by one- or two-factor ANOVA and Tukey's test for posthoc analysis. Significance was determined by $P < 0.05$.

Acknowledgements:

We would like to the thank Dr. Derek Warren (King's College London) for helpful discussions about nuclear-cytoskeletal linkages and providing the DN-KASH constructs. We would also like to thank Prof. Arnoud Sonnenberg for providing the Nesprin-3 antibody; Dr. Patricia Costa for assistance with the dynamically adhesive micro-patterns: and Dr. Guillaume Charras for helpful discussions and advice on cellular mechanics. This work was funded by the BBSRC (BB/J000914/1) and Barts and the London Charity (Grant 442/1032).

Author contributions:

FVA designed and carried out experiments and co-wrote the manuscript. GWa and GWi generated the *Plec* KO mice and cell lines and advised on experimental design. JRM and JAM provided EBS-MD skin samples and assisted with the analysis. AHB advised on experimental design and data analysis. JTC supervised the project, carried out experiments, and co-wrote the manuscript.

References:

Andrä, K., Kornacker, I., Jörgl, A., Zörer, M., Spazierer, D., Fuchs, P., Fischer, I. and Wiche, G. (2003). Plectin-isoform-specific rescue of hemidesmosomal defects in plectin (-/-) keratinocytes. *J. Invest. Dermatol.* **120**, 189–197.

Boczonadi, V., McInroy, L. and Määttä, A. (2007). Cytolinker cross-talk: periplakin N-terminus interacts with plectin to regulate keratin organisation and epithelial migration. *Exp. Cell Res.* **313**, 3579–3591.

Bonne, G., Di Barletta, M. R., Varnous, S., Becane, H. M., Hammouda, E. H., Merlini, L., Muntoni, F., Greenberg, C. R., Gary, F., Urtizberea, J. A., et al. (1999). Mutations in the gene encoding lamin A/C cause autosomal dominant Emery-Dreifuss muscular dystrophy. *Nat Genet* **21**, 285–8.

Burgstaller, G., Gregor, M., Winter, L. and Wiche, G. (2010). Keeping the vimentin network under control: cell-matrix adhesion-associated plectin 1f affects cell shape and polarity of fibroblasts. *Mol. Biol. Cell* **21**, 3362–3375.

Castañón, M. J., Walko, G., Winter, L. and Wiche, G. (2013). Plectin-intermediate filament partnership in skin, skeletal muscle, and peripheral nerve. *Histochem. Cell Biol.* **140**, 33–53.

Chalut, K. J., Höpfler, M., Lautenschläger, F., Boyde, L., Chan, C. J., Ekpenyong, A., Martinez-Arias, A. and Guck, J. (2012). Chromatin decondensation and nuclear softening accompany Nanog downregulation in embryonic stem cells. *Biophys. J.* **103**, 2060–2070.

Chen, C. S., Mrksich, M., Huang, S., Whitesides, G. M. and Ingber, D. E. (1997). Geometric control of cell life and death. *Science* **276**, 1425–8.

Connelly, J. T., Gautrot, J. E., Trappmann, B., Tan, D. W., Donati, G., Huck, W. T. and Watt, F. M. (2010). Actin and serum response factor transduce physical cues from the microenvironment to regulate epidermal stem cell fate decisions. *Nat Cell Biol* **12**, 711–8.

Connelly, J. T., Mishra, A., Gautrot, J. E. and Watt, F. M. (2011). Shape-induced terminal differentiation of human epidermal stem cells requires p38 and is regulated by histone acetylation. *PLoS One* **6**, e27259.

Costa, P., Gautrot, J. E. and Connelly, J. T. (2014). Directing cell migration using micropatterned and dynamically adhesive polymer brushes. *Acta Biomater*.

Coulombe, P. A., Hutton, M. E., Letai, A., Hebert, A., Paller, A. S. and Fuchs, E. (1991). Point mutations in human keratin 14 genes of epidermolysis bullosa simplex patients: genetic and functional analyses. *Cell* **66**, 1301–1311.

Dupont, S., Morsut, L., Aragona, M., Enzo, E., Giulitti, S., Cordenonsi, M., Zanconato, F., Le Digabel, J., Forcato, M., Bicciato, S., et al. (2011). Role of YAP/TAZ in mechanotransduction. *Nature* **474**, 179–83.

Engler, A. J., Sen, S., Sweeney, H. L. and Discher, D. E. (2006). Matrix elasticity directs stem cell lineage specification. *Cell* **126**, 677–89.

Gdula, M. R., Poterlowicz, K., Mardaryev, A. N., Sharov, A. A., Peng, Y., Fessing, M. Y. and Botchkarev, V. A. (2013). Remodeling of three-dimensional organization of the nucleus during terminal keratinocyte differentiation in the epidermis. *J. Invest. Dermatol.* **133**, 2191–2201.

Goldman, R. D., Shumaker, D. K., Erdos, M. R., Eriksson, M., Goldman, A. E., Gordon, L. B., Gruenbaum, Y., Khuon, S., Mendez, M., Varga, R., et al. (2004). Accumulation of mutant lamin A causes progressive changes in nuclear architecture in Hutchinson-Gilford progeria syndrome. *Proc Natl Acad Sci U S A* **101**, 8963–8.

Gregor, M., Osmanagic-Myers, S., Burgstaller, G., Wolfram, M., Fischer, I., Walko, G., Resch, G. P., Jörgl, A., Herrmann, H. and Wiche, G. (2014). Mechanosensing through focal adhesion-anchored intermediate filaments. *FASEB J.* **28**, 715–729.

Guilluy, C., Osborne, L. D., Van Landeghem, L., Sharek, L., Superfine, R., Garcia-Mata, R. and Burridge, K. (2014). Isolated nuclei adapt to force and reveal a mechanotransduction pathway in the nucleus. *Nat. Cell Biol.* **16**, 376–381.

Gundersen, G. G. and Worman, H. J. (2013). Nuclear positioning. *Cell* **152**, 1376–1389.

Hale, C. M., Shrestha, A. L., Khatau, S. B., Stewart-Hutchinson, P. J., Hernandez, L., Stewart, C. L., Hodzic, D. and Wirtz, D. (2008). Dysfunctional connections between the nucleus and the actin and microtubule networks in laminopathic models. *Biophys. J.* **95**, 5462–5475.

Horn, H. F., Brownstein, Z., Lenz, D. R., Shivatzki, S., Dror, A. A., Dagan-Rosenfeld, O., Friedman, L. M., Roux, K. J., Kozlov, S., Jeang, K.-T., et al. (2013). The LINC complex is essential for hearing. *J. Clin. Invest.* **123**, 740–750.

Isermann, P. and Lammerding, J. (2013). Nuclear mechanics and mechanotransduction in health and disease. *Curr. Biol.* **23**, R1113–1121.

Iyer, K. V., Pulford, S., Mogilner, A. and Shivashankar, G. V. (2012). Mechanical activation of cells induces chromatin remodeling preceding MKL nuclear transport. *Biophys. J.* **103**, 1416–1428.

Ketema, M., Kreft, M., Secades, P., Janssen, H. and Sonnenberg, A. (2013). Nesprin-3 connects plectin and vimentin to the nuclear envelope of Sertoli cells but is not required for Sertoli cell function in spermatogenesis. *Mol. Biol. Cell* **24**, 2454–2466.

Khatau, S. B., Bloom, R. J., Bajpai, S., Razafsky, D., Zang, S., Giri, A., Wu, P.-H., Marchand, J., Celedon, A., Hale, C. M., et al. (2012). The distinct roles of the

nucleus and nucleus-cytoskeleton connections in three-dimensional cell migration. *Sci Rep* **2**, 488.

Kröger, C., Loschke, F., Schwarz, N., Windoffer, R., Leube, R. E. and Magin, T. M. (2013). Keratins control intercellular adhesion involving PKC-α-mediated desmoplakin phosphorylation. *J. Cell Biol.* **201**, 681–692.

Lammerding, J., Schulze, P. C., Takahashi, T., Kozlov, S., Sullivan, T., Kamm, R. D., Stewart, C. L. and Lee, R. T. (2004). Lamin A/C deficiency causes defective nuclear mechanics and mechanotransduction. *J. Clin. Invest.* **113**, 370–378.

Lee, J. S. H., Hale, C. M., Panorchan, P., Khatau, S. B., George, J. P., Tseng, Y., Stewart, C. L., Hodzic, D. and Wirtz, D. (2007). Nuclear lamin A/C deficiency induces defects in cell mechanics, polarization, and migration. *Biophys. J.* **93**, 2542–2552.

Lee, C.-H., Kim, M.-S., Chung, B. M., Leahy, D. J. and Coulombe, P. A. (2012). Structural basis for heteromeric assembly and perinuclear organization of keratin filaments. *Nat. Struct. Mol. Biol.* **19**, 707–715.

Li, Q., Kumar, A., Makhija, E. and Shivashankar, G. V. (2014). The regulation of dynamic mechanical coupling between actin cytoskeleton and nucleus by matrix geometry. *Biomaterials* **35**, 961–969.

McBeath, R., Pirone, D. M., Nelson, C. M., Bhadriraju, K. and Chen, C. S. (2004). Cell shape, cytoskeletal tension, and RhoA regulate stem cell lineage commitment. *Dev Cell* **6**, 483–95.

McLean, W. H., Pulkkinen, L., Smith, F. J., Rugg, E. L., Lane, E. B., Bullrich, F., Burgeson, R. E., Amano, S., Hudson, D. L., Owaribe, K., et al. (1996). Loss of plectin causes epidermolysis bullosa with muscular dystrophy: cDNA cloning and genomic organization. *Genes Dev.* **10**, 1724–1735.

Moll, R., Franke, W. W., Schiller, D. L., Geiger, B. and Krepler, R. (1982). The catalog of human cytokeratins: patterns of expression in normal epithelia, tumors and cultured cells. *Cell* **31**, 11–24.

Na, S., Chowdhury, F., Tay, B., Ouyang, M., Gregor, M., Wang, Y., Wiche, G. and Wang, N. (2009). Plectin contributes to mechanical properties of living cells. *Am. J. Physiol., Cell Physiol.* **296**, C868–877.

Osmanagic-Myers, S., Gregor, M., Walko, G., Burgstaller, G., Reipert, S. and Wiche, G. (2006). Plectin-controlled keratin cytoarchitecture affects MAP kinases involved in cellular stress response and migration. *J. Cell Biol.* **174**, 557–568.

Paszek, M. J., Zahir, N., Johnson, K. R., Lakins, J. N., Rozenberg, G. I., Gefen, A., Reinhart-King, C. A., Margulies, S. S., Dembo, M., Boettiger, D., et al. (2005). Tensional homeostasis and the malignant phenotype. *Cancer Cell* **8**, 241–54.

Pelham, R. J. and Wang, Y. (1997). Cell locomotion and focal adhesions are regulated by substrate flexibility. *Proc Natl Acad Sci U S A* **94**, 13661–5.

Ramms, L., Fabris, G., Windoffer, R., Schwarz, N., Springer, R., Zhou, C., Lazar, J., Stiefel, S., Hersch, N., Schnakenberg, U., et al. (2013). Keratins as the main component for the mechanical integrity of keratinocytes. *Proc. Natl. Acad. Sci. U.S.A.* **110**, 18513–18518.

Reyes, C. D. and García, A. J. (2003). Engineering integrin-specific surfaces with a triple-helical collagen-mimetic peptide. *J Biomed Mater Res A* **65**, 511–523.

Rezniczek, G. A., De Pereda, J. M., Reipert, S. and Wiche, G. (1998). Linking integrin alpha6beta4-based cell adhesion to the intermediate filament cytoskeleton: direct interaction between the beta4 subunit and plectin at multiple molecular sites. *J. Cell Biol.* **141**, 209–225.

Rheinwald, J. G. and Green, H. (1977). Epidermal growth factor and the multiplication of cultured human epidermal keratinocytes. *Nature* **265**, 421–4.

Roux, K. J., Crisp, M. L., Liu, Q., Kim, D., Kozlov, S., Stewart, C. L. and Burke, B. (2009). Nesprin 4 is an outer nuclear membrane protein that can induce kinesin-mediated cell polarization. *Proc. Natl. Acad. Sci. U.S.A.* **106**, 2194–2199.

Russell, D., Andrews, P. D., James, J. and Lane, E. B. (2004). Mechanical stress induces profound remodelling of keratin filaments and cell junctions in epidermolysis bullosa simplex keratinocytes. *J. Cell. Sci.* **117**, 5233–5243.

Sagelius, H., Rosengardten, Y., Hanif, M., Erdos, M. R., Rozell, B., Collins, F. S. and Eriksson, M. (2008). Targeted transgenic expression of the mutation causing Hutchinson-Gilford progeria syndrome leads to proliferative and degenerative epidermal disease. *J Cell Sci* **121**, 969–78.

Seltmann, K., Fritsch, A. W., Käs, J. A. and Magin, T. M. (2013). Keratins significantly contribute to cell stiffness and impact invasive behavior. *Proc. Natl. Acad. Sci. U.S.A.* **110**, 18507–18512.

Smith, F. J., Eady, R. A., Leigh, I. M., McMillan, J. R., Rugg, E. L., Kelsell, D. P., Bryant, S. P., Spurr, N. K., Geddes, J. F., Kirtschig, G., et al. (1996). Plectin deficiency results in muscular dystrophy with epidermolysis bullosa. *Nat. Genet.* **13**, 450–457.

Spurny, R., Gregor, M., Castañón, M. J. and Wiche, G. (2008). Plectin deficiency affects precursor formation and dynamics of vimentin networks. *Exp. Cell Res.* **314**, 3570–3580.

Starr, D. A. and Fridolfsson, H. N. (2010). Interactions between nuclei and the cytoskeleton are mediated by SUN-KASH nuclear-envelope bridges. *Annu Rev Cell Dev Biol* **26**, 421–44.

Steinböck, F. A., Nikolic, B., Coulombe, P. A., Fuchs, E., Traub, P. and Wiche, G. (2000). Dose-dependent linkage, assembly inhibition and disassembly of

vimentin and cytokeratin 5/14 filaments through plectin's intermediate filament-binding domain. *J. Cell. Sci.* **113 (Pt 3)**, 483–491.

Swift, J., Ivanovska, I. L., Buxboim, A., Harada, T., Dingal, P. C. D. P., Pinter, J., Pajerowski, J. D., Spinler, K. R., Shin, J.-W., Tewari, M., et al. (2013). Nuclear lamin-A scales with tissue stiffness and enhances matrix-directed differentiation. *Science* **341**, 1240104.

Tian, R., Gregor, M., Wiche, G. and Goldman, J. E. (2006). Plectin regulates the organization of glial fibrillary acidic protein in Alexander disease. *Am. J. Pathol.* **168**, 888–897.

Versaevel, M., Grevesse, T. and Gabriele, S. (2012). Spatial coordination between cell and nuclear shape within micropatterned endothelial cells. *Nat Commun* **3**, 671.

Walko, G., Vukasinovic, N., Gross, K., Fischer, I., Sibitz, S., Fuchs, P., Reipert, S., Jungwirth, U., Berger, W., Salzer, U., et al. (2011). Targeted proteolysis of plectin isoform 1a accounts for hemidesmosome dysfunction in mice mimicking the dominant skin blistering disease EBS-Ogna. *PLoS Genet.* **7**, e1002396.

Wang, Y., Panteleyev, A. A., Owens, D. M., Djabali, K., Stewart, C. L. and Worman, H. J. (2008). Epidermal expression of the truncated prelamin A causing Hutchinson-Gilford progeria syndrome: effects on keratinocytes, hair and skin. *Hum Mol Genet* **17**, 2357–69.

Wilhelmsen, K., Litjens, S. H., Kuikman, I., Tshimbalanga, N., Janssen, H., Van den Bout, I., Raymond, K. and Sonnenberg, A. (2005). Nesprin-3, a novel outer nuclear membrane protein, associates with the cytoskeletal linker protein plectin. *J Cell Biol* **171**, 799–810.

Winter, L. and Wiche, G. (2013). The many faces of plectin and plectinopathies: pathology and mechanisms. *Acta Neuropathol.* **125**, 77–93.

Zhang, Q., Skepper, J. N., Yang, F., Davies, J. D., Hegyi, L., Roberts, R. G., Weissberg, P. L., Ellis, J. A. and Shanahan, C. M. (2001). Nesprins: a novel family of spectrin-repeat-containing proteins that localize to the nuclear membrane in multiple tissues. *J. Cell. Sci.* **114**, 4485–4498.

Zhang, X., Lei, K., Yuan, X., Wu, X., Zhuang, Y., Xu, T., Xu, R. and Han, M. (2009). SUN1/2 and Syne/Nesprin-1/2 complexes connect centrosome to the nucleus during neurogenesis and neuronal migration in mice. *Neuron* **64**, 173–87.

Zhen, Y.-Y., Libotte, T., Munck, M., Noegel, A. A. and Korenbaum, E. (2002). NUANCE, a giant protein connecting the nucleus and actin cytoskeleton. *J. Cell. Sci.* **115**, 3207–3222.

Figures legend

Figure 1: Keratinocyte shape specifies 3D nuclear morphology.

Primary human keratinocytes were cultured on either circular collagen islands with diameters of 20, 30, and 50 μm, or ellipses (SF8 with equivalent area of 30 μm). (A) Representative immunofluorescence images of F-actin (green), Lamin A/C (red), and DAPI (blue) through the central plane of the cell were obtained by confocal microscopy. (B) Quantification of the maximum cross-sectional area, (C) height, (D) volume, and (E) geometrical shape coefficients was performed for cells on each of the micro-patterns using z-stack confocal images. (F) Representative confocal images of primary human keratinocytes cultured on 50 μm islands and treated with carrier (0.1% DMSO) or 50 μM blebbistatin. (G) Quantification of cross-sectional area. Scale bars equal 10 μm. Data represent mean ± SEM (N=3 experiments). *$P < 0.05$ compared to 20 μm; §$P < 0.05$ compared to 30 μm.

Figure 2: Plectin mediates cell shape-induced nuclear deformation.

(A) Representative bright field images of cell morphology for *Plec* +/+ (WT) and -/- (KO) keratinocytes. (B) Representative images of keratin 14 (K14) organisation and nuclear morphology (DAPI) of WT and KO cells. Scale bars equal 10 μm. (C) Quantification of nuclear cross-sectional area and (D) aspect ratio of WT and KO cells cultured on non-patterned surfaces. (E) Representative bright field images and (F) DAPI fluorescence of WT and KO cells on 50 μm and SF8 micro-patterns. Scale bars equal 50 μm. (G) Quantification of nuclear cross-sectional area and (H) aspect ratio of WT and KO cells on circular 20, 30, or 50 μm islands or SF8 islands. All data represent mean ± SEM (N=3 experiments). *P < 0.05 compared to WT.

Figure 3: Plectin regulates organisation of adhesive and cytoskeletal structures.

Representative confocal immunofluorescence images of (A) keratin 14 (K14) and integrin α6 and (B) K14 and paxillin localisation in WT and KO keratinocytes. (C) K14 and F-actin images of WT and KO cells treated with carrier (0.1% DMSO) or 50 μM blebbistatin. Scale bars equal 10 μm.

Figure 4: Cross-talk between actin and keratin regulates nuclear morphology.

Representative DAPI fluorescence images of WT and KO keratinocytes on (A) 50 μm and (B) SF8 micro-patterns. Cells were treated with carrier (0.1% DMSO) or 50 μM blebbistatin. Scale bars equal 50 μm (C) Quantification of nuclear cross-sectional area on 50 μm islands and (D) aspect ratio on SF8 patterns. All data represent mean ± SEM (N=3 experiments). *P < 0.05 compared to WT.

Figure 5: Plectin regulates nuclear morphology independently of direct linkage to the nuclear membrane.

(A) Immunofluorescence images of plectin, keratin 14 (K14), and DAPI localisation in WT and KO keratinocytes. (B) Immunofluorescence images of nesprin-3 and DAPI localisation in WT mouse keratinocytes and NIH 3T3 fibroblasts. (C) Fluorescent images of dominant negative nesprin-GFP (DN-KASH) expression in WT and KO keratinocytes. All scale bars equal 10 μm. (D) Quantification of nuclear area in WT and KO cells transiently transfected with DN-KASH or GFP alone. All data represent mean ± SEM (N=3 experiments). *P < 0.05 compared to WT.

Figure 6: Plectin influences cell crowding and nuclear morphology in multi-cell structures.

(A) Representative confocal images of DAPI stained WT and *Plec* KO cells seeded on 200 μm islands at low (37,500 per cm^2) and high (225,000 per cm^2) densities. (B) Quantification of the number of nuclei per pattern and (C) nuclear volume. (D) Representative 3D reconstruction of DAPI stained nuclei. Yellow nuclei show those preferentially aligned with Z-axis. (E) Quantification of the percentage of nuclei preferentially elongated in the Z-axis (angle of major axis 45° above XY plane). Data represent mean ± SEM (N=3 experiments). *P < 0.05 comparing WT versus KO; ψP < 0.05 comparing low versus high density seeding. (F) Representative fluorescence images of F-actin and DNA of WT and KO cells before (0 hours) and 3 and 6 hours after photo-activated coupling of the collagen-mimetic peptide (GFOGER) to the surrounding polymer surface. (G) Quantification of nuclear morphology at times 0, 3, and 6 hours after activation with the GFOGER peptide. Data represent the mean ± SD (n>72 cells) of a representative experiment. *P < 0.05 comparing WT and KO at 6 hours.

Figure 7: Nuclear morphology is perturbed in plectin deficient epidermis.

(A) Representative images of DAPI stained frozen sections from biopsies of normal neonatal and adult and EBS-MD skin. Scale bars equal 10 μm. (B) Quantification of nuclear cross-sectional area, (C) aspect ratio, and (D) circularity of basal keratinocytes. At least 100 cells were measured per specimen. Data represent the mean ± SEM (N=4 patients). *P<0.05 compared to normal skin.

Figures

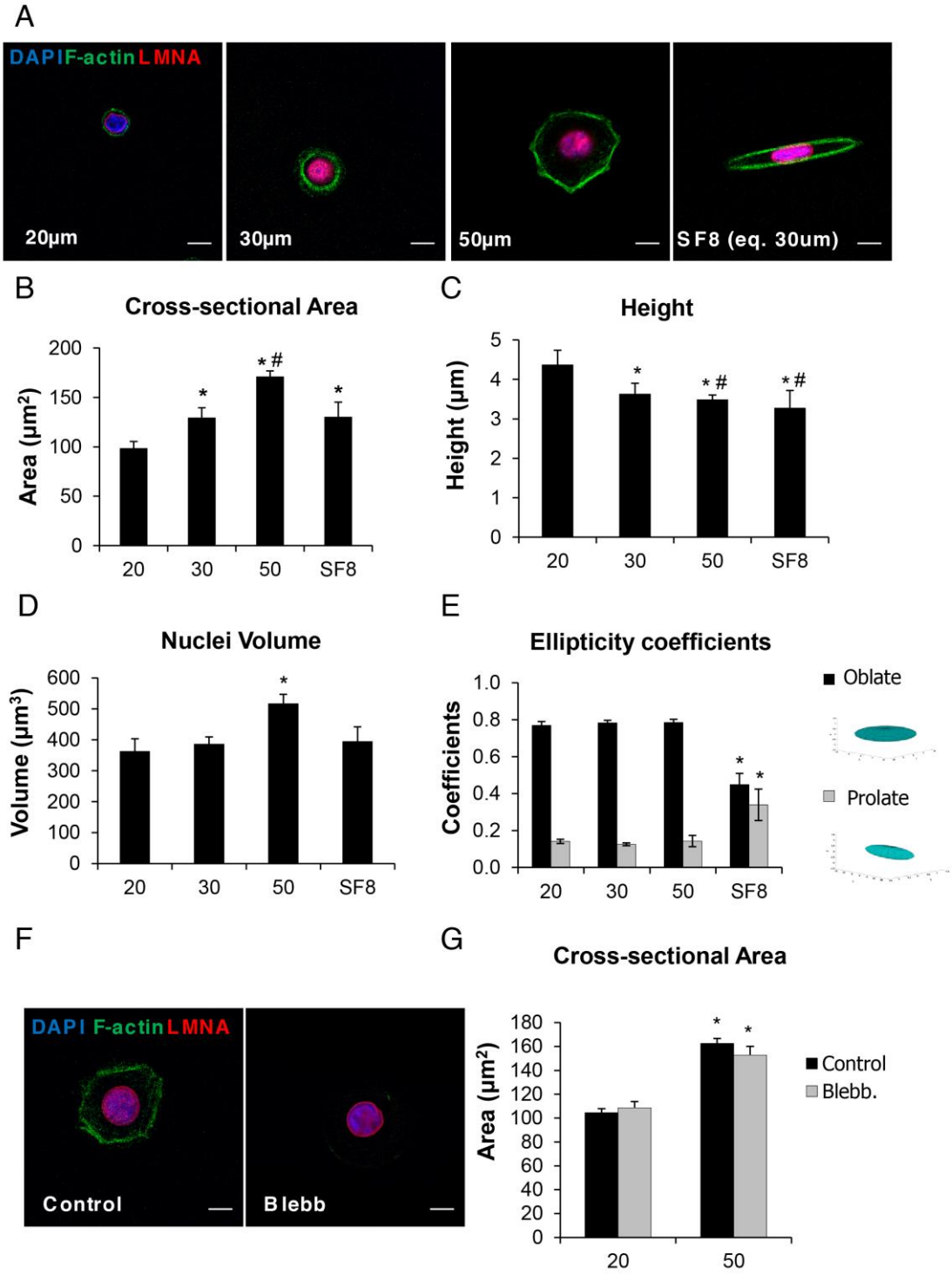
A
DAPI F-actin LMNA
20µm
30µm
50µm
SF8 (eq. 30um)
B
Cross-sectional Area
Area (µm²)
200
150
100
50
0
20
30
50
SF8
C
Height
Height (µm)
5
4
3
2
1
0
D
Nuclei Volume
Volume (µm³)
600
500
400
300
200
100
0
E
Ellipticity coefficients
Coefficients
1.0
0.8
0.6
0.4
0.2
0.0
Oblate
Prolate
F
DAPI F-actin LMNA
Control
Blebb
G
Cross-sectional Area
Area (µm²)
180
160
140
120
100
80
60
40
20
0
Control
Blebb.

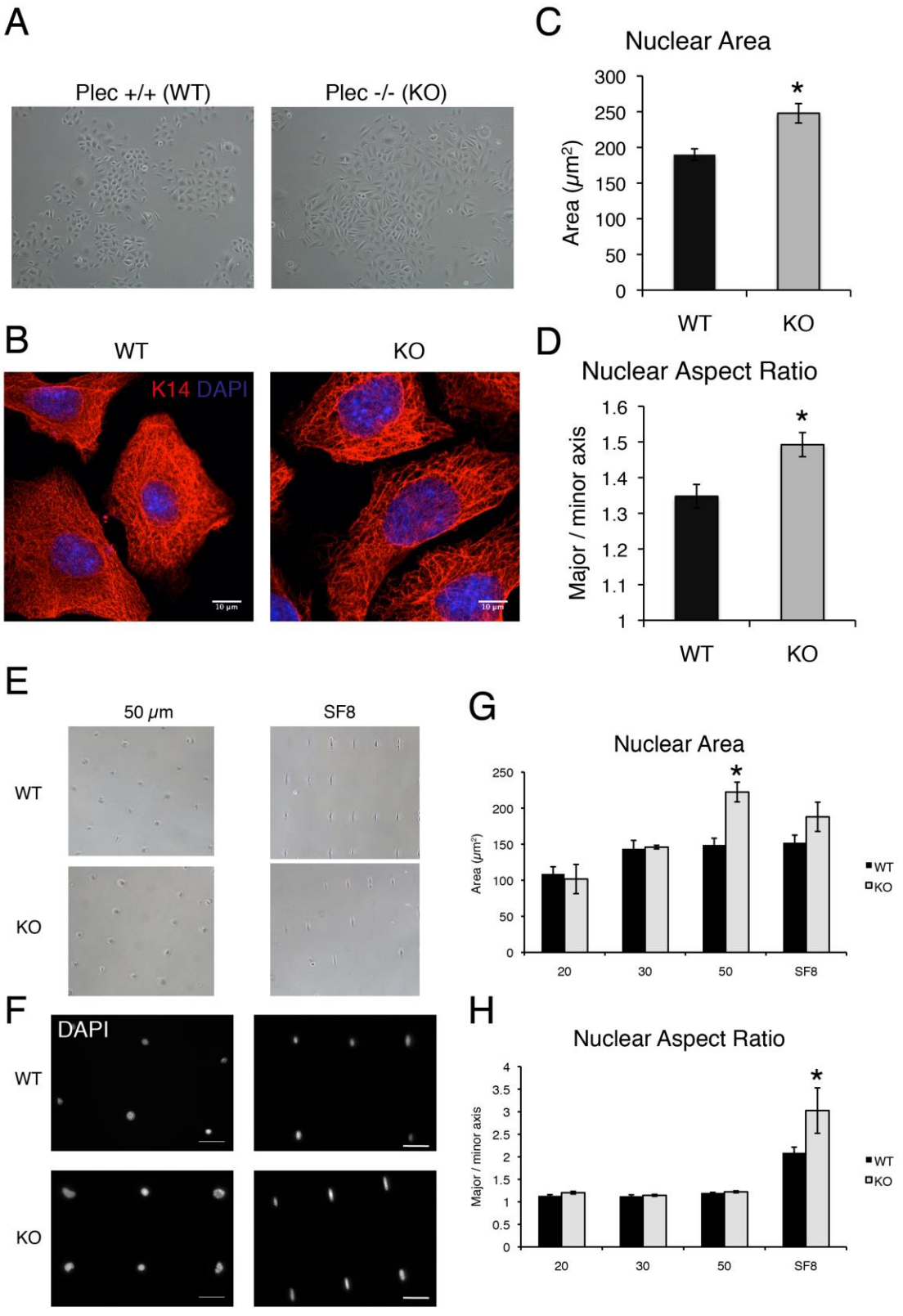
A
Plec +/+ (WT)
Plec -/- (KO)
B
WT
KO
K14 DAPI
C
Nuclear Area
Area (μm²)
300
250
200
150
100
50
0
*
WT
KO
D
Nuclear Aspect Ratio
Major / minor axis
1.6
1.5
1.4
1.3
1.2
1.1
1
*
WT
KO
E
50 μm
SF8
WT
KO
F
DAPI
WT
KO
G
Nuclear Area
Area (μm²)
250
200
150
100
50
0
*
20
30
50
SF8
WT
KO
H
Nuclear Aspect Ratio
Major / minor axis
4
3.5
3
2.5
2
1.5
1
0.5
0
*
20
30
50
SF8
WT
KO

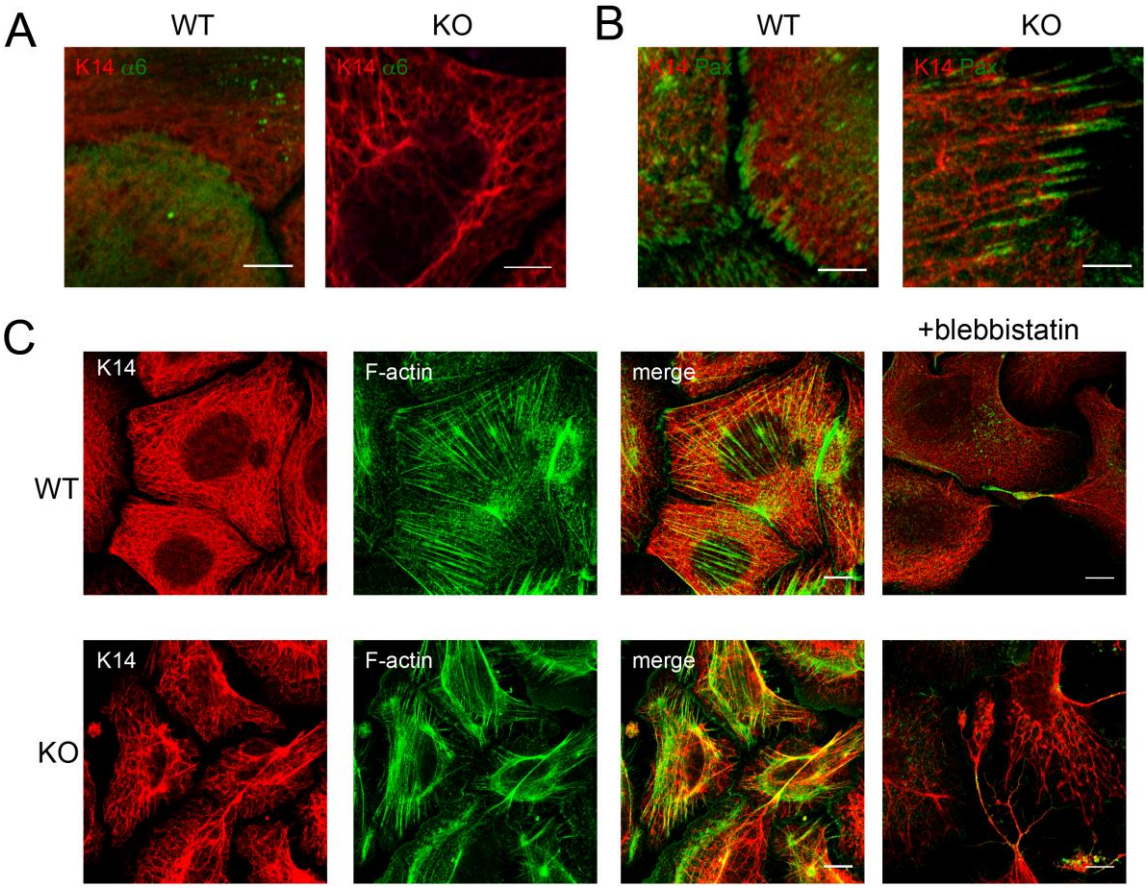
A
WT
KO
K14 α6
K14 α6
B
WT
KO
K14 Pax
K14 Pax
C
+blebbistatin
WT
KO
K14
F-actin
merge
K14
F-actin
merge

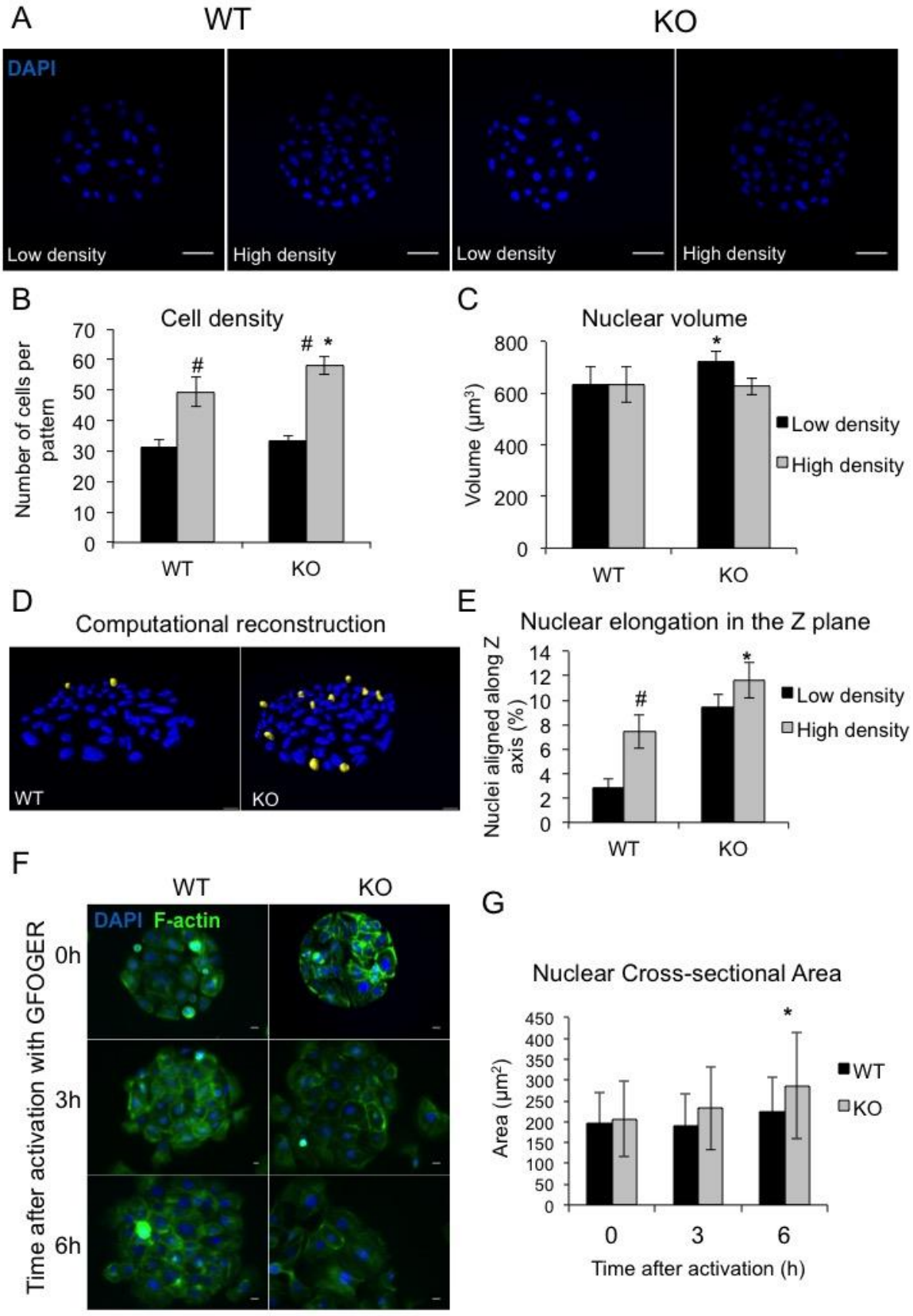
A
WT
KO
DAPI
Low density
High density
Low density
High density
B
Cell density
Number of cells per pattern
70
60
50
40
30
20
10
0
#
*
WT
KO
C
Nuclear volume
Volume (μm³)
800
600
400
200
0
*
Low density
High density
WT
KO
D
Computational reconstruction
WT
KO
E
Nuclear elongation in the Z plane
Nuclei aligned along Z axis (%)
14
12
10
8
6
4
2
0
#
*
Low density
High density
WT
KO
F
WT
KO
DAPI F-actin
Time after activation with GFOGER
0h
3h
6h
G
Nuclear Cross-sectional Area
Area (μm²)
450
400
350
300
250
200
150
100
50
0
*
WT
KO
0
3
6
Time after activation (h)

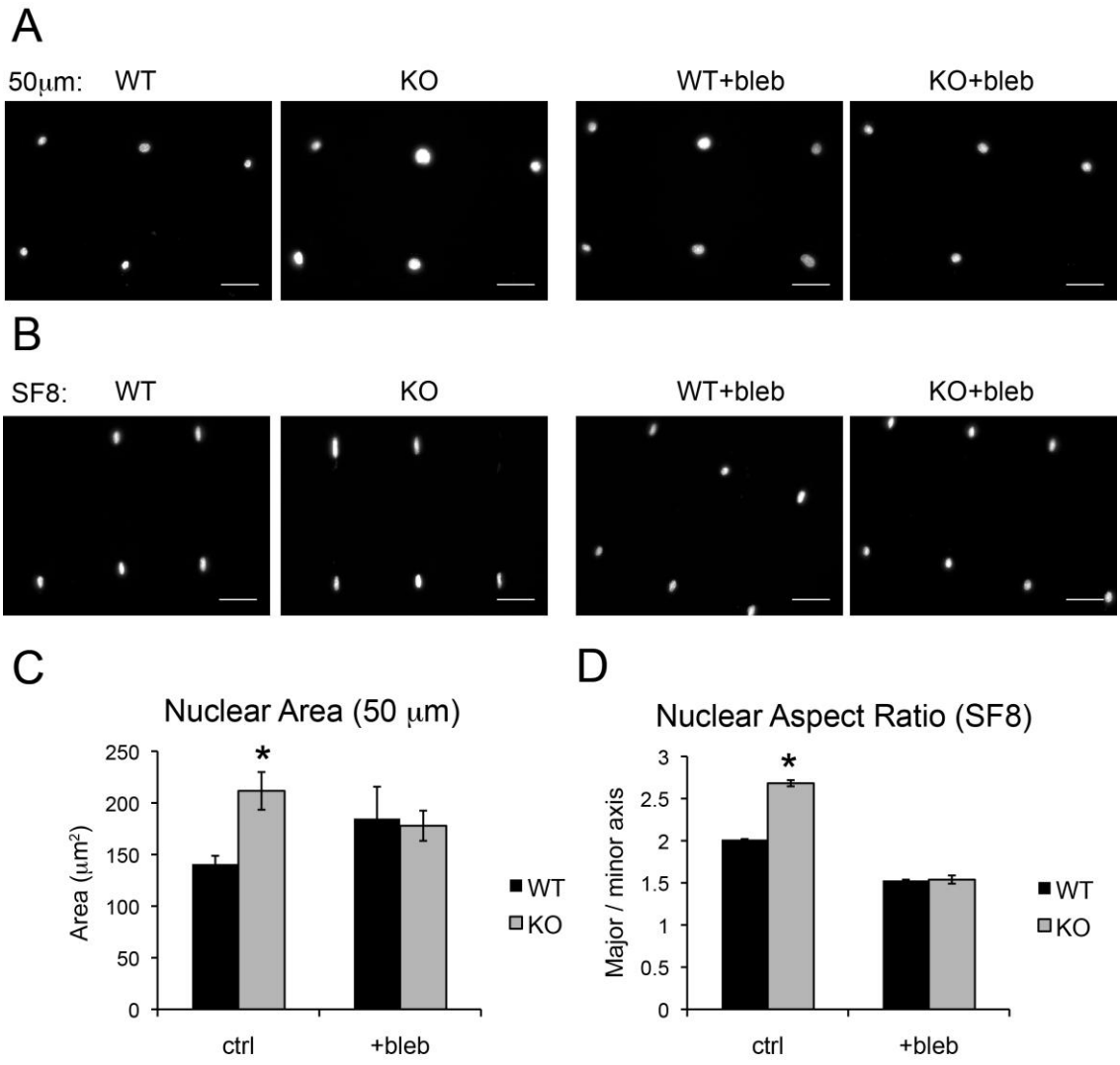
A
50μm:
WT
KO
WT+bleb
KO+bleb
B
SF8:
WT
KO
WT+bleb
KO+bleb
C
Nuclear Area (50 μm)
Area (μm²)
250
200
150
100
50
0
*
ctrl
+bleb
WT
KO
D
Nuclear Aspect Ratio (SF8)
Major / minor axis
3
2.5
2
1.5
1
0.5
0
*
ctrl
+bleb
WT
KO

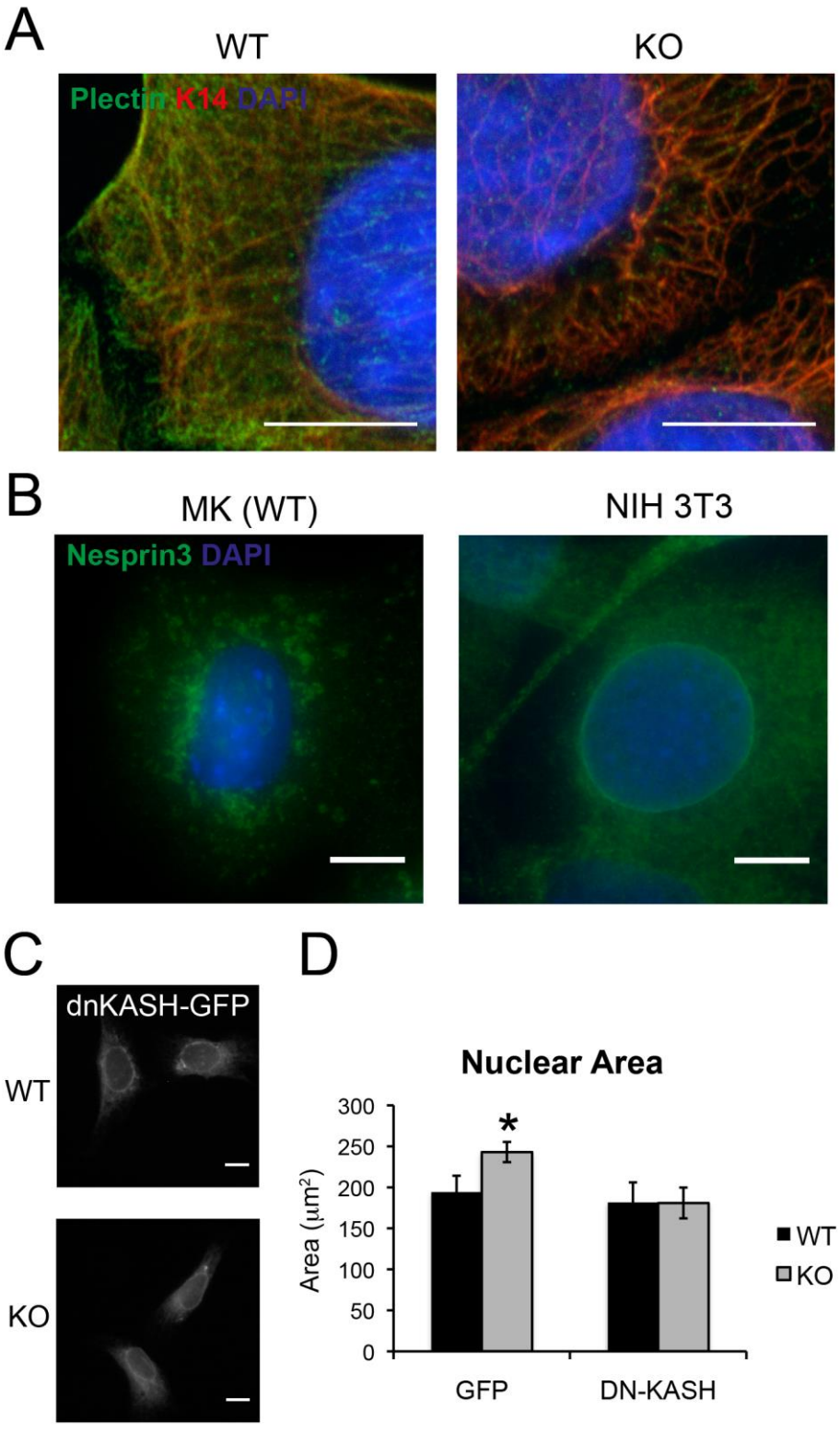
A
WT
KO
Plectin K14 DAPI
B
MK (WT)
NIH 3T3
Nesprin3 DAPI
C
dnKASH-GFP
WT
KO
D
Nuclear Area
Area (μm²)
300
250
200
150
100
50
0
*
GFP
DN-KASH
WT
KO

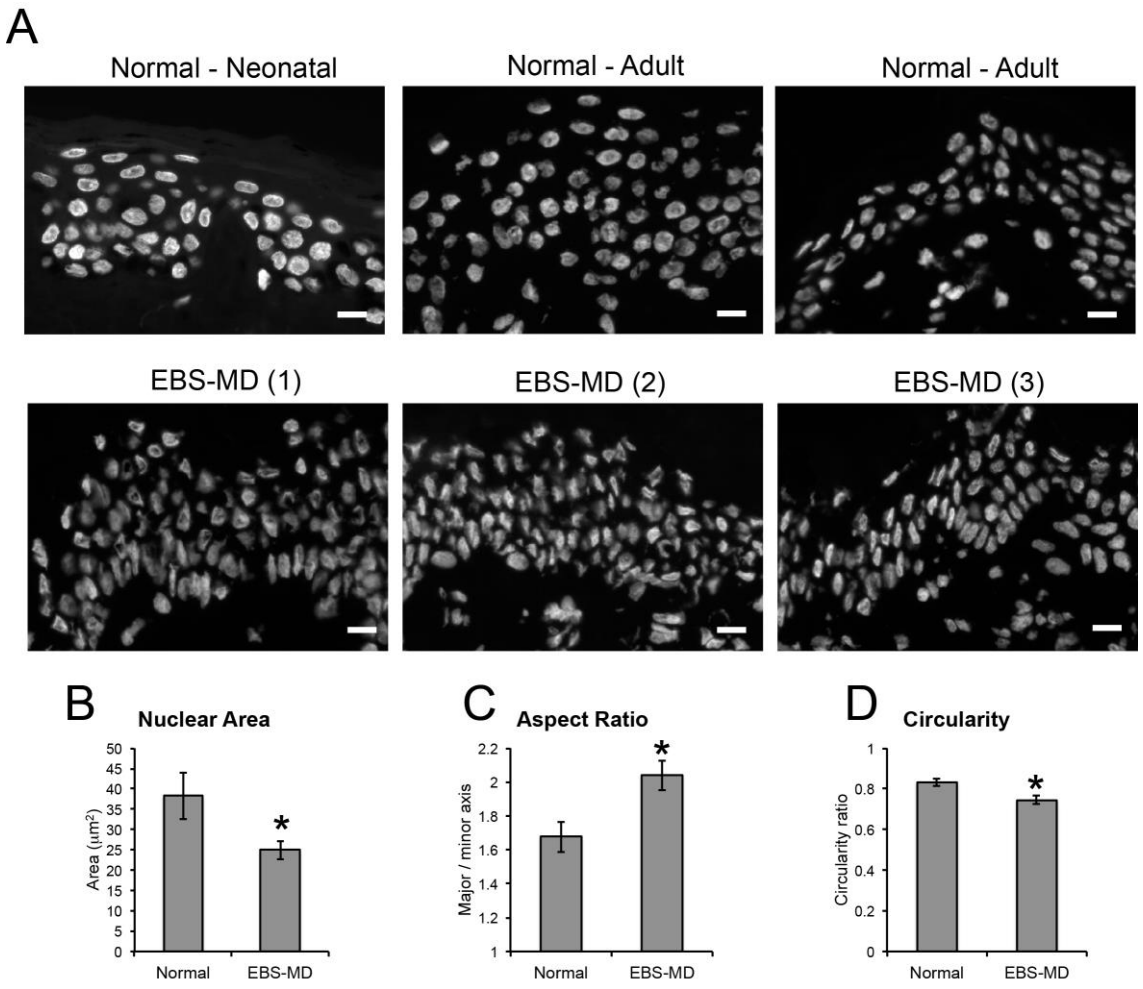
A
Normal - Neonatal
Normal - Adult
Normal - Adult
EBS-MD (1)
EBS-MD (2)
EBS-MD (3)
B
Nuclear Area
Area (μm²)
50
45
40
35
30
25
20
15
10
5
0
*
Normal
EBS-MD
C
Aspect Ratio
Major / minor axis
2.2
2
1.8
1.6
1.4
1.2
1
*
Normal
EBS-MD
D
Circularity
Circularity ratio
1
0.8
0.6
0.4
0.2
0
*
Normal
EBS-MD

II. 3D confocal data analysis: calculating nuclear height and cross-sectional area of Z-stacks

```
function heightCS(L,Ch,N,PS,Z)
%v1.2.1,11/04/2015
%thresholding
%Blue channel is used
%L - letter/character that identifies each condition for consequent
tif
%files - e.g. 'a;b;c' - has to be a string ;
%Ch - channel desirable for analysis:  1(468, blue),2(488, green), 3
(555, red)
%N - nr of collected images/stacks (not frames)
%optional labels to be displayd. By default, 20um, 30um, 50um and SF8-
30um
%are assumed to correspond to the first, second, till the last
%respectively. Note that the order must match with the first inserted
%letter/characters that identify the sample in the respective tif
files

%%  Lets read several images in one unique folder and organise it in a
matrix with syntax starting in 'v' for each collected sample;
sep=strfind(L,',');
names=regexprep(L,',','');
cellCondID = cell(length(names),N);
if ~exist('PS','var') && ~exist('Z','var')
    PS = 0.18;% microns
    Z = 0.31;
elseif ~exist('Z','var')
     Z = 0.31;
end
conf1 = 0.98;
conf2 = 0.64;
for cond=1:size(L,2)-size(sep,2) % to analyse EACH condition -
assuming that the user inserts one character per condition separated
by ';' !!
%% Locating and loading DAPI channel (C1-)
cellN = 1; % counting the real number of different cells to be
analysed queue
    for sample = 1:N %identifies each cell
        [non,A]= fileattrib(strcat('C',int2str(Ch),'-
',names(cond),sprintf('%02d',sample),'*'));
        if isstruct(A)
            cellCondID {cond,cellN} =
strcat(names(cond),sprintf('%02d',cellN));
            for frame=1:length(A)
                tempp(:,:,frame) =
imread(A(frame).Name(max(strfind(A(frame).Name,'\'))+1:end));
            end
            eval(horzcat(cellCondID {cond,cellN},' = tempp;'))
            cellN = cellN + 1;
        elseif ~isstruct(A) && exist('A','var')
            warning(strcat(cellCondID {cond,cellN},'_DOES NOT
EXIST'));
        end
        clear tempp
    end
```

```
     %searches for the files beggining with file_name as initials - b
containes the number of different images found with the desirable
syntax
end
clear tempp cellN A sample cond frame

%% cellCondID now contains the names of the black%white images which
are ready to be used for morphometric measurements
%first of all, it is necessary to determine the useful/desirable
frames
%that correspond to the nucleus volume - imperative second threshold
(area)
%         confidence1 = 1.4;
%         confidence2 = 0.64;
fid0 = fopen(horzcat('RAW_DATA.txt'),'w');
fprintf(fid0,'%s %s %s %s \n','SAMPLE', 'Height(um)',
'CS_area(um2)','Average_Intensity');
for cond2=1:size(cellCondID,1) %goes through the conditions
    for sample2=1:size(cellCondID,2) %goes through the sample
(individual z-stack)
        if exist(cellCondID{cond2,sample2},'var')~=0
            temp=eval(cellCondID{cond2,sample2});
            %% Thresholding DAPI and filtering
            % v containes the names which allocates each the stack of
DAPI.
            %lets now filter (2D median filter) and convert the images
for binary by applying Otsu's method
            %(calculates the proper threshold, here adopted to be the
highest of each
            %sample) - goal is to do morphometric analysis
            for fr0=1:size(temp,3) %assuming that all the images are
512*512, lets calculate the ideal threshold for each frame (fr)
                frame=medfilt2(temp(:,:,fr0));
                thresh(fr0)=graythresh(frame);
            end
            thresh2 = smooth(thresh,0.3,'loess');
            %% Thresholding based on Gaussian fit of Oslo's
thresholding levels (graythresh function above)
            try
                [gaussianCheck gof]=
fit((1:length(thresh2))',thresh2,'gauss1');
            catch
                warning(horzcat('Fitting of the Gaussian function to
threshold distribution impossible. Sample ignored: ',
cellCondID{cond2,sample2}))
                h(cond2, sample2) = 0;
                cs_area(cond2, sample2) = 0;
                stack_int(cond2, sample2) = 0;
            end
            if exist('gaussianCheck','var')
                if gaussianCheck.b1 < 0 || gaussianCheck.b1 > length
(thresh2) || gof.rsquare < 0.8
                    warning(horzcat('Threshold levels do not obay to a
Gaussian-like distribution. Sample ignored: ',
cellCondID{cond2,sample2}))
                    h(cond2, sample2) = 0;
                    cs_area(cond2, sample2) = 0;
                    stack_int(cond2, sample2) = 0;
                elseif round(gaussianCheck.b1) > 0 &&
round(gaussianCheck.b1) < length (thresh2)
```

```
                    indexH1 = round(gaussianCheck.b1-
(gaussianCheck.c1*conf1));
                    indexH2 =
round(gaussianCheck.b1+(gaussianCheck.c1*conf1));
                    indexCS1 = round(gaussianCheck.b1-
(gaussianCheck.c1*0.85));
                    indexCS2 =
round(gaussianCheck.b1+(gaussianCheck.c1*0.85));
                    if indexH1 > 0  && indexH2 < length(thresh2) %&&
gof.rsquare > 0.8
                        nucFramH = indexH1:indexH2;
                        nucFramCS = indexCS1:indexCS2;
                        threshold (1) = mean ([thresh(nucFramH(1))
thresh(nucFramH(end))]);
                        threshold (2) = mean([thresh(nucFramCS(1))
thresh(nucFramCS(end))]);
                    elseif indexH1 <= 0  && indexH2 <
length(thresh2)%&& gof.rsquare > 0.8
                        nucFramH = 1:indexH2;
                        threshold (1) = mean([thresh(nucFramH(1))
thresh(nucFramH(end))]);
                        if indexCS1 <= 0
                            nucFramCS = 1:indexCS2;
                            threshold (2) = mean([thresh(nucFramCS(1))
thresh(nucFramCS(end))]);
                        else
                            nucFramCS = indexCS1:indexCS2;
                            threshold (2) = mean([thresh(nucFramCS(1))
thresh(nucFramCS(end))]);
                        end
                    elseif indexH1 > 0  && indexH2 > length(thresh)
%&& gof.rsquare > 0.8
                        nucFramH = indexH1:length(thresh2);
                        threshold (1) = mean ([thresh(nucFramH(1))
thresh(nucFramH(end))]);
                        if indexCS2 > length(thresh2)
                            nucFramCS = indexCS1:length(thresh);
                            threshold (2) = mean([thresh(nucFramCS(1))
thresh(nucFramCS(end))]);
                        else
                            nucFramCS = indexCS1:length(thresh);
                            threshold (2) = mean([thresh(nucFramCS(1))
thresh(nucFramCS(end))]);
                        end
                    else
                        warning(horzcat('Limits of Gaussian curve out
of data boundaries. Threshold used is the one from first or last
frames: ', cellCondID{cond2,sample2}))
                        nucFramH = 1:length(thresh);
                        threshold (1) = mean ([thresh(nucFramH(1))
thresh(nucFramH(end))]);
                        if indexCS1 > 0 && indexCS2 < length(thresh2)
                            nucFramCS = indexCS1:indexCS2;
                            threshold (2) = mean([thresh(nucFramCS(1))
thresh(nucFramCS(end))]);
                        elseif indexCS1 < 0 && indexCS2 <
length(thresh2)
                            nucFramCS = 1:indexCS2;
                            threshold (2) = mean([thresh(nucFramCS(1))
thresh(nucFramCS(end))]);
```

```
                        elseif indexCS1 > 0 && indexCS2 >
length(thresh2)
                            nucFramCS = indexCS1:length(thresh);
                            threshold (2) = mean([thresh(nucFramCS(1))
thresh(nucFramCS(end))]);
                        else
                            warning(horzcat('Impossible to set the
threshold. Sample ignored: ', cellCondID{cond2,sample2}))
                            h(cond2, sample2) = 0;
                            cs_area(cond2, sample2) = 0;
                            stack_int(cond2, sample2) = 0;
                        end
                    end
                    if exist('threshold','var') &&
length(threshold)==2 && length(nucFramH) <= length(thresh2) &&
length(nucFramH)>3
                        [gaussianCheck3 quality3] =
fit(nucFramH',thresh2(nucFramH),'gauss1');
%%Thresholding and applying binary morphometric operations
                        if quality3.rsquare > 0.80
                            for fr=1:size(temp,3)
                                % applying binary filters to sharp the
nuclei:
                                im (:,:,fr) =
im2bw(temp(:,:,fr),threshold(1)); %threshold is the mean of the whole
intensity's coeff. curves
                                im2 (:,:,fr) =
im2bw(temp(:,:,fr),threshold(2)); % stronger threshold for area
calculation
                                im (:,:,fr) =
bwmorph(im(:,:,fr),'open');
                                im2 (:,:,fr) =
bwmorph(im2(:,:,fr),'open');
                                im (:,:,fr) =
bwmorph(im(:,:,fr),'majority');
                                im2 (:,:,fr) =
bwmorph(im2(:,:,fr),'majority');
                                im (:,:,fr) =
imfill(im(:,:,fr),'holes');
                                im2 (:,:,fr) =
imfill(im2(:,:,fr),'holes');
                                area(fr) = bwarea(im(:,:,fr));
%temporary variable for the area - needed to decide the beginning and
ending of the nuclei
                                maskNuc(:,:,fr) =
immultiply(temp(:,:,fr),im2(:,:,fr));
                                intDist(fr) =
sum(sum(maskNuc(:,:,fr)))/(length(maskNuc(:,:,fr)>0));
                            end
                            %% Locating the frames correspondent to
the actual nucleus
                            [gaussianCheck2 gof]=
fit((1:length(area))',smooth(area,0.3,'loess'),'gauss1');
                            if  gaussianCheck2.b1 > 1 &&
gaussianCheck2.b1 < length(area) &&
gaussianCheck2.b1+gaussianCheck2.c1 < (length(area)+8) &&
gaussianCheck2.b1-gaussianCheck2.c1 >-8 && gof.rsquare >0.8
                                cs_area (cond2,sample2) =
length(find(maskNuc(:,:,round(gaussianCheck2.b1)) > 0))*(PS^2); % area
= nr of positive pixels of the cross-sectional frame (mean of last &
initial nuclear frames) * pixel size
```

```
                                h(cond2,sample2) =
abs(gaussianCheck2.b1+(gaussianCheck2.c1*conf2)-(gaussianCheck2.b1-
(gaussianCheck2.c1*conf2)))*Z; %counts the frames of dapi signal and
multiplies it for Z to conver it to microns
                                stack_int (cond2,sample2) =
intDist(round(gaussianCheck2.b1));
                            else
                                warning(horzcat('Area Thresholding
failed. Sample ignored: ', cellCondID{cond2,sample2}))
                                h(cond2, sample2) = 0;
                                cs_area(cond2, sample2) = 0;
                                stack_int(cond2, sample2) = 0;
                            end
                        else
                            warning(horzcat('Quality of Gaussian-like
distribution not satisfatory. Sample ignored: ',
cellCondID{cond2,sample2}))
                            h(cond2, sample2) = 0;
                            cs_area(cond2, sample2) = 0;
                            stack_int(cond2, sample2) = 0;
                        end
                    elseif exist('threshold','var') &&
length(threshold)==1 && length(nucFramH) <= length(thresh2)
                        warning('Single threshold
applied.:',cellCondID{cond2,sample2})
                        [gaussianCheck3 quality3] =
fit(nucFramH',thresh2(nucFramH),'gauss1');
%%Thresholding and applying binary morphometric operations
                        if quality3.rsquare > 0.80
                            for fr=1:size(temp,3)
                                % applying binary filters to sharp the
nuclei:
                                im (:,:,fr) =
im2bw(temp(:,:,fr),threshold); %threshold is the mean of the whole
intensity's coeff. curves
                                im2 (:,:,fr) =
im2bw(temp(:,:,fr),threshold); % stronger threshold for area
calculation
                                im (:,:,fr) =
bwmorph(im(:,:,fr),'open');
                                im2 (:,:,fr) =
bwmorph(im2(:,:,fr),'open');
                                im (:,:,fr) =
bwmorph(im(:,:,fr),'majority');
                                im2 (:,:,fr) =
bwmorph(im2(:,:,fr),'majority');
                                im (:,:,fr) =
imfill(im(:,:,fr),'holes');
                                im2 (:,:,fr) =
imfill(im2(:,:,fr),'holes');
                                area(fr) = bwarea(im(:,:,fr));
%temporary variable for the area - needed to decide the beginning and
ending of the nuclei
                                maskNuc(:,:,fr) =
immultiply(temp(:,:,fr),im2(:,:,fr));
                                intDist(fr) =
sum(sum(maskNuc(:,:,fr)))/(length(maskNuc(:,:,fr)>0));
                            end
                        else
```

```
                            warning(horzcat('Quality of Gaussian-like
distribution not satisfatory. Sample ignored: ',
cellCondID{cond2,sample2}))
                            h(cond2, sample2) = 0;
                            cs_area(cond2, sample2) = 0;
                            stack_int(cond2, sample2) = 0;
%                                 break
                        end
                        %% Locating the frames correspondent to the
actual nucleus
                        [gaussianCheck2 gof]=
fit((1:length(area))',smooth(area,0.3,'loess'),'gauss1');
                        if  gaussianCheck2.b1 > 1 && gaussianCheck2.b1
< length(area) && gaussianCheck2.b1+gaussianCheck2.c1 <
(length(area)+8) && gaussianCheck2.b1-gaussianCheck2.c1 >-8 &&
gof.rsquare >0.8
                            cs_area (cond2,sample2) =
length(find(maskNuc(:,:,round(gaussianCheck2.b1)) > 0))*(PS^2); % area
= nr of positive pixels of the cross-sectional frame (mean of last &
initial nuclear frames) * pixel size
                            h(cond2,sample2) =
abs(gaussianCheck2.b1+(gaussianCheck2.c1*conf2)-(gaussianCheck2.b1-
(gaussianCheck2.c1*conf2)))*Z; %Height is defined by guassian limits
(-c*(-conf2)+c*conf2)
                            stack_int (cond2,sample2) =
intDist(round(gaussianCheck2.b1));
                        else
                            warning(horzcat('Area Thresholding failed.
Sample ignored: ', cellCondID{cond2,sample2}))
                            h(cond2, sample2) = 0;
                            cs_area(cond2, sample2) = 0;
                            stack_int(cond2, sample2) = 0;
%                                 break
                        end
                    else
                        warning(horzcat('Area Thresholding failed.
Sample ignored: ', cellCondID{cond2,sample2}))
                        h(cond2, sample2) = 0;
                        cs_area(cond2, sample2) = 0;
                        stack_int(cond2, sample2) = 0;
%                           break
                    end
                else
                    warning(strcat('Parameter values considered zero,
because following condition does not
exist.',char(cellCondID{cond2,sample2})));
                    cs_area(cond2,sample2) = 0;
                    h(cond2,sample2) = 0;
                    stack_int(cond2,sample2) = 0;
                end
            end
            clear thresh* area nucFram1 frame intDist index* gaussian*
            %% Reporting raw data - column basis; writes sample_ID,
height, cross-sectional area, followed by averaged intensity of the
whole stack
            fprintf(fid0,'%s %4.4f %4.4f %4.4f
\n',horzcat(names(cond2),'_',int2str(sample2)), h(cond2,sample2),
cs_area(cond2,sample2), stack_int(cond2,sample2));
        end
        try
            % Averaging out the data
```

```
            pos = h(cond2,:) > 0; % Knock-down of zero values by
firstly locating them,
            pos1 = cs_area(cond2,:) > 0;
            pos2 = stack_int(cond2,:) > 0;
            avH(cond2) = mean(h(cond2,pos));% and operating only
those!
            sdH(cond2) = std(h(cond2,pos));
            avA(cond2) = mean(cs_area(cond2,pos1));
            sdA(cond2) = std(cs_area(cond2,pos1));
            asstack_int(cond2) = mean(stack_int(cond2,pos2));
            sdstack_int(cond2) = std(stack_int(cond2,pos2));
            nn(cond2) = sum(pos);
            nnn(cond2) = sum(pos1);
            nnnn(cond2) = sum(pos2);
        catch
            warning (strcat('_NO DATA IS recognised - NUCLEUS NOT
DETECTED in the condition _',char(cellCondID{cond2,sample2})));
        end
    end
end
fclose(fid0);
space='______';
ii=1:size(names,2);
p=1;
pp=1;
while p<=size(names,2)
    namess(pp:pp+size(strcat(names(ii(p)),space),2)-
1)=strcat(names(ii(p)),space);
    p=p+1;
    pp=size(namess,2)+1;
end
fprintf('\n\n The Height (um) is: \n\n');
disp(strcat('_____________',namess));
fprintf('\n\n AVE.');
disp(avH);
fprintf('\n\n StD.');
disp(sdH);
fprintf('\n\n The Area (um^2) is: \n\n');
fprintf('\n\n AVE.');
disp(avA);
fprintf('\n\n StD.');
disp(sdA);
fidH=fopen('height.txt','w');
fidHR=fopen('height_raw.txt','w');
fidA=fopen('area.txt','w');
fidAR=fopen('area_raw.txt','w');
conds=sprintf('%s',names)';
fprintf(fidH,'%s \n', '       N    X (um)    St. Dev.');
fprintf(fidA,'%s \n', '       N    X (um^2)   St. Dev.');
fprintf(fidHR,'%s \n', ' The Height');
fprintf(fidAR,'%s \n', ' The Area');

print='\n ';
cab = sprintf('\b\b\b\b');
for zz=1:size(conds,1)

    fprintf(fidH,'%c % 6.0f % 4.3f % 4.4f\n',conds(zz), nn(zz),
avH(zz), sdH(zz));
    tf(fidA,'%c % 6.0f % 4.3f % 4.4f\n',conds(zz), nnn(zz), avA(zz),
sdA(zz));
```

```
    print = strcat(print,' %4.3f ');
    cab = strcat(cab,conds(zz));
end
fprintf(fidHR,'\n %s \n', cab);
fprintf(fidAR,'\n %s \n', cab);
for ref=1:size(h,2)
    fprintf(fidHR,strcat(print,'\n'), h(:,ref)');
    fprintf(fidAR,strcat(print,'\n'), cs_area(:,ref)');
end

fclose(fidH);
fclose(fidA);
fclose(fidHR);

end
```

III. Radial profile analysis of multichannel fluorescent images

```
function MCRA(L,centroidCh,analysisCh,maskCh,PS) %Multi-Channel Radial
Analysis of A particular immuno-channel
%%% Version 1.3.2 - 13/04/2015
%L - letter/character that identifies each condition for consequent
tif
%files - e.g. 'a,b,c' - has to be a string ;
%Ch - channel desirable for analysis:  1(468, blue),2(488, green), 3
(555, red)
%N - nr of collected images/stacks (not frames)
%optional labels to be displayd. By default, 20um, 30um, 50um and SF8-
30um
%are assumed to correspond to the first, second, till the last
%respectively. Note that the order must match with the first inserted
%letter/characters that identify the sample in the respective tif
files
%mask1 - used for centroid determination

%%  Lets read several images in one unique folder and organise it in a
matrix with syntax starting in 'v' for each collected sample;
sep=strfind(L,',');
Analys={};
if exist('PS','var') == 0
    PS=0.18;
end
names=regexprep(L,',','');
staining = {''}; %setting treatments - extra conditions such as the
marker analysed (e.g. lamin A/C)
prefix = ''; %calling prefix of file name - contemplated in the file
name
heading1 = {}; % for saving in last
heading2 = {}; % for saving in last
for treatment = 1:length(staining)
    for pattern=1:size(L,2)-size(sep,2) % to analyse EACH condition -
assuming that the user inserts one character per condition separated
by ',' !!
            %% Locating and loading DAPI channel (C1-)
```

```
            file_name=strcat(prefix,names(pattern)); % syntax is as
prefix_treatment-condition.tif, being condition=patternNumber
            [non1,B1]= fileattrib(strcat(file_name,'*')); %searches
for the files beggining with file_name as initials - b containes the
number of different images found with the desirable syntax
            if maskCh ~= centroidCh
                misMatch = 1;
            end

            if isstruct(B1)==1 %&& isstruct(B2)==1 && length(B1) ==
length(B2)
                for K=1:size(B1,2) %seek for the particular tif file -
identified by the 2 last digits; K is each individual frame per
condition
                    temp =
imread(B1(K).Name(max(strfind(B1(K).Name,'\'))+1:end));
                    images(:,:,K) = temp (:,:,analysisCh);% stacks it
in 'images' matrix
                    centroid_im(:,:,K) = temp (:,:,centroidCh);
                    if exist ('misMatch','var')
                        mask_im(:,:,K) = temp (:,:,maskCh);
                    end
                    if [size(images,1) size(images,2)] ==
[size(centroid_im,1) size(centroid_im,2)] %checks for equal
resolutions
                        resolution = size(images,1); %used to check
image bounderies at the polar analysis
                    end

                end
                %creating variables and saving respective image stacks
                Analys{treatment,pattern} =
strcat(staining(treatment),'_',char(names(pattern))); %generates
variable names automatically saving it in a string matrix where rows
are the conditions (a, b, c...),
                                                                %cond;
columns are the particular variable names (if exists - 'corr' is
created to avoid empty v cells.
                evalc([char(Analys{treatment,pattern}) '= images']); %
attributes to each variable in 'v' the respective image.
                CENTROID_IM{treatment,pattern} =
strcat('centroid_im',staining(treatment),'_',char(names(pattern)));
%generates variable names automatically saving it in a string matrix
where rows are the conditions (a, b, c...),
                                                                %cond;
columns are the particular variable names (if exists - 'corr' is
created to avoid empty v cells.
                evalc([char(CENTROID_IM{treatment,pattern}) '=
centroid_im']); % attributes to each variable in 'v' the respective
image.

                if exist('misMatch','var')
                    MASK_IM{treatment,pattern} =
strcat('mask_im',staining(treatment),'_',char(names(pattern)));
%generates variable names automatically saving it in a string matrix
where rows are the conditions (a, b, c...),

%cond; columns are the particular variable names (if exists - 'corr'
is created to avoid empty v cells.
```

```
                    evalc([char(MASK_IM{treatment,pattern}) '=
mask_im']); % attributes to each variable in 'v' the respective image.
                end
                clear images mask_im
            elseif isstruct(B1)==1 && isstruct(B2)==1 && length(B1) ~=
length(B2)
                warning(strcat(file_name,'_ Number of Centroid &
Analysing channel not consistent'));
            elseif isstruct(B1)==1 && isstruct(B2)~=1
                warning(strcat(file_name,'_ Centroid channel not
detected'))
            else
                warning(strcat(file_name,'_ Images not found. Check
syntax'));
            end
    end
end
    %% Thresholding and filtering
    row3 = ones(size(Analys));
for row=1:size(Analys,1) %going through treatments
        row1 = 1;
        row2 = 1;
    for col=1:size(Analys,2) %going trough conditions
        row_int = 1;
        col_int = 1;
        pointer2 = 1;
        if ~isempty(Analys{row,col})  &&
~isempty(CENTROID_IM{row,col})
            %opening stacks for centroid, analysis and maskng
            centroid_im =
eval(strcat(char(CENTROID_IM{row,col}),';'));% centroid stack
            analysis_im = eval(strcat(char(Analys{row,col}),';'));%
analysis stack
            if exist('MASK_IM','var')
                mask_imm = eval(strcat(char(MASK_IM{row,col}),';')); %
maskings stack
            end
            %going through each frame
            for fr=1:size(analysis_im,3)
                im = analysis_im(:,:,fr);
                centroid_imm = centroid_im(:,:,fr);
                im2 =
zeros(size(centroid_imm,1),size(centroid_imm,2));
                centroid_thresh =
mean(centroid_imm(edge(centroid_imm)>0))*0.6; % threshold level
coincides with edge image
                im2 (centroid_imm (:,:) > centroid_thresh) = 1;
                im2 = bwmorph(im2,'dilate',5);
                im2 = imfill(im2,'holes');
                im3 = bwareaopen(im2,50); % despeckling analysis
channel
                if exist('MASK_IM','var') %in case masking channel
exists
                    temp2 = mask_imm(:,:,fr);
                    imm = zeros(size(temp2,1),size(temp2,2));
                    mask_thresh = mean(temp2(edge(temp2)>0))*0.6;
                    imm (temp2 (:,:) > mask_thresh) = 1;
                    im4 = bwmorph(imm,'dilate',5);
                    im4 = imfill(im4,'holes');
                    im4 = bwareaopen(im4,50);
```

```
                else % if masking channel does not exist, limits of
analysis channel ought to be its own thresholded image
                    im4 = im3;
                end
                try %Trying to use regionprops to get
automatically/acccurately the centroid
                    ref = regionprops(im3,'centroid');
                    x0 = round(ref.Centroid(1));
                    y0 = round(ref.Centroid(2));
                catch %alternatively, using peak of sum intensity
function throughout X and Y
                    for ii = 1:size(im3,2)
                        xpos (round(ii)) =
sum(double(im3(round(ii),:)));
                        ypos(round(ii)) =
sum(double(im3(:,round(ii))));
                    end
                    y0 = find ( smooth(xpos,20) == max
(smooth(xpos,20)),1,'first');
                    x0 = find ( smooth(ypos,20) == max
(smooth(ypos,20)),1,'first');
                end
                clear xpos ypos
                cs_area (col,fr)= length(find(im4 > 0)); %defines the
area of thresholded image as the number of positive pixels
                %% Measuring radial intensity
                int_flag = 1; % flag to see how many interations were
tried in the polar readings
                interations = 3;
                for P=1:round(((cs_area(col,fr)/pi())^0.5)*1.3)
%defining distance vector P in pixels
                    B2 = atan(inv(P));
                    M = (2*(pi()-B2))/(B2*(2*pi()-B2)); %interval
coefficient
                    O = 0:B2:2*pi()+B2;
                    for AN=1:size(O,2) %defining revolution angle
                        try
                            if
im4(round(P*sin(O(AN)))+y0,round(P*cos(O(AN)))+x0) > 0 %considers only
the positive thresholded points
                                int (fr,P,AN) =
im(round(P*sin(O(AN)))+y0,round(P*cos(O(AN)))+x0); %reading im -
channel to be analyses
                            end
                        catch
                            if round(P*sin(O(AN)))+y0 < 0 ||
round(P*sin(O(AN)))+y0 > resolution || round(P*cos(O(AN)))+x0 < 0 ||
round(P*cos(O(AN)))+x0 >resolution
                                warning('Image edges encountered')
                                break
                            elseif round(P*sin(O(AN)))+y0 < 0 ||
round(P*sin(O(AN)))+y0 > resolution || round(P*cos(O(AN)))+x0 < 0 ||
round(P*cos(O(AN)))+x0 >resolution && int_flag >= size(O,2)
                                warning('Intensity profile failed')
                                break
                            end
                        end
                    end
                    try
```

```
                        [fr2 row_int0 col_int0] = size(int); %reads
the actual dimensions of intensity matrix, filtering any unsuccessful
polar reading
                    catch
                        if ~exist('int','var') && P==1
                            warning ('Image is unreadable for polar
analysis. Centroid')
                        elseif ~exist('int','var') && P > 1 &&
int_flag < interations
                            int (fr,P,AN) =0;
                            int_flag = int_flag + 1;
                            continue
                        elseif ~exist('int','var')&& P > 1 && int_flag
> interations
                            break
                        end
                    end
                    if col_int0 > col_int
                        col_int = col_int0;
                    end
                        if  row_int0 >= P && sum(int(fr2,P,:))==0
                            av_rad_int (fr2,P) = 0;
                            std_rad_int (fr2,P) = 0;
                            radial_n(fr2,P) = 0;
                        elseif row_int0 >= P
                            av_rad_int (fr2,P) = mean
(double(int(fr2,P,1:col_int0))); %mean of the read intensities for a
particular 'p'
                            std_rad_int (fr2,P) = std
(double(int(fr2,P,1:col_int0)));
                            radial_n (fr2,P) = col_int0; %variable
indicating the maximum O considered in each frame - used in further
interpolation
                        end

                end
                distance (fr2) = row_int0; %variable indicating the
maximum P considered in each frame - used in further interpolation
                pointer = size(av_rad_int,2);
                if pointer > pointer2
                    pointer2 = pointer;
                end
                original = double(im).*double(im2); %creates the
masked nuclei frame
                av_int (fr2,:) = sum (original(original > 0)) / sum
(im2(im2 > 0)); % calculates the averaged intensity: sum of masked
intnsity values / sum of positive pixels correspondent to the nucleus
                clear imm im2 im im3 int
            end
        %% Avering out the radial intensity profile both in absolute
and interpolated form
            flag0 = 0;
            %Performing interpolation and averaging, respectively
            for neg=1:size(av_rad_int,1)
                if sum(av_rad_int(neg,:))>0 %interpolate only if the
av_rad_int curve is positive numbers and the begins with first 3
numbers of  are positive
                    flag0 = flag0 +1;
                    interp_fr_int (neg,:)=
interp1(0:1/(((size(av_rad_int(neg,1:distance(neg)),2)-
```

```
1))):1,av_rad_int(neg,1:distance(neg)),0:1/(100-1):1); %interpolation
of averaged curve (just the previously averaged bit - distance(fr)
                    pos_av_rad_int (flag0,:) = av_rad_int(neg,:);
%creates a positive variable of av_rad_int
                    pos_std_rad_int (flag0,:) = std_rad_int(neg,:);
%creates a positive variable of std_rad_int
                    pos_radial_n(flag0,:) = radial_n(neg,:);
                else
                    interp_fr_int (neg,:) = zeros(1,100);
                    continue
                end
            end
            flag2 = 1;
            %Ignoring negative interpolated curves - creating pos
            %(from positive) variable. Thus, both peripherical and
core
            %intensity area are calculated.
            periphery = 70:91;
            core = 1:20;
            for negg = 1:size(interp_fr_int,1)
                if sum(interp_fr_int(negg,:))>0
                    pos_interp_fr_int (flag2,:)=
interp_fr_int(negg,:);
                    periph_int(flag2,:) =
trapz(periphery,interp_fr_int(flag2,periphery));
                    core_int(flag2,:) =
trapz(core,interp_fr_int(flag2,core));
                    cs_area2(flag2,:) = cs_area(col,negg); % creating
new cs_area for the curves that are indeed interpolated
                    frameID(flag2,:) = negg;
                    pos_av_int(flag2,:) = av_int(negg);
                    flag2 = flag2 + 1;
                end
            end

            %% Averaging both positive averaged curves
            for PPP = 1:size(pos_av_rad_int,2)
                flag4 = 1; %enables the location of COLUMNS to be
analysed - it's undesirable the reading of zeros outside the read P
(above)
                if size(pos_interp_fr_int,1)>1 &&
size(pos_av_rad_int,1)>1
                    av_fr_int (PPP) = mean
(pos_av_rad_int(pos_av_rad_int(:,PPP)>0,PPP));
                   %Calculating the standard deviation out of previous
SD
                    N_SD (:,PPP)= (pos_radial_n(:,PPP)-
1).*(pos_std_rad_int(:,PPP).^2);
                    N_AV_RAD (:,PPP) =
pos_radial_n(:,PPP).*(pos_av_rad_int(:,PPP).^2);
                    AV (PPP) = mean(pos_av_rad_int(:,PPP))^2;
                    std_fr_int (PPP)= 1/(sum(pos_radial_n(:,PPP))-1) *
(((sum(N_SD(:,PPP)) + sum(N_AV_RAD(:,PPP)) - sum(pos_radial_n(:,PPP))
* AV(PPP)))^0.5);
                    if PPP==distance(flag4) %deciding when the maximum
P (above) was reached
                        flag4 = flag4+1;
                    end
                    n_number (col) = size(pos_av_rad_int,1);
%determining the number of measured curves
```

```
                elseif size(pos_interp_fr_int,1)==1 &&
size(pos_av_rad_int,1)==1
                    av_fr_int = pos_av_rad_int';
                    n_number (col) = size(pos_av_rad_int,1);
                    std_fr_int = zeros(size(pos_av_rad_int,1),1);
                end
            end

            %Avering positive interpolated curves - naturally, does
not take into
            %account all the measured points, once the interpolation
curve is
            %determined out of the averaged one.
            if size(pos_interp_fr_int,1)>1 && size(pos_av_rad_int,1)>1
                av_fr_int_interp = mean(pos_interp_fr_int)';
                std_fr_int_interp = std(pos_interp_fr_int)';
                n_number (col) = size(pos_interp_fr_int,1);
%determining the number of measured curves
            elseif size(pos_interp_fr_int,1)==1 &&
size(pos_av_rad_int,1)==1
                av_fr_int_interp = pos_interp_fr_int';
                std_fr_int_interp =
zeros(size(pos_interp_fr_int,1),1);
                n_number (col) = size(pos_interp_fr_int,1);
            end
        else
            av_fr_int_interp = zeros(100,1);
            std_fr_int_interp = zeros(100,1);
            av_fr_int = zeros(1,10);
            std_fr_int = zeros(1,10);
            frameID = 0;
            cs_area2 =0;
            periph_int=0;
            core_int=0;
            pos_av_int=0;
        end
            record1(:,:,row) = [av_fr_int_interp std_fr_int_interp];
            record2(:,:,row) = [av_fr_int' std_fr_int'];
            heading1 = horzcat (heading1,repmat([{names(col)} '
'],1,size(record1,2))); %size profiles recordings
            heading2 = horzcat (heading2,repmat([staining(row) '
'],1,size(record1,2)));
            record3(:,:,row) = [frameID cs_area2 periph_int core_int
pos_av_int];
            RAD_INT{row,col} =
genvarname(strcat('radint_',staining(row),'_',names(col))); %RAD_INT
containes generated variable's names of the interpolated profile of
all conditions
            evalc([char(RAD_INT{row,col}) '=record1(:,:,row)']); %
average of interpolated curves and respective standard deviation
            [row0 col1 w] = size(record1);
                if row0>row1
                    row1 = row0;
                end
            RAD{row,col} =
genvarname(strcat('rad_',staining(row),'_',names(col))); %RAD
containes generated variable's names of the ONLY averaged profile of
all samples
            evalc([char(RAD{row,col}) '=record2(:,:,row)']); % average
and standard deviation
```

```
            [row00 col2 ww] = size(record2);
                if row00>row2
                    row2 = row00;
                end
            DESC{row,col} =
genvarname(strcat('desc_',staining(row),'_',names(col))); %DESC
containes the areas od peripherical and core intensity, plus the
overall intensity (average) and cs_area(2)
            evalc([char(DESC{row,col}) '=record3(:,:,row)']); %
average and standard deviation
            [row000 col3 www] = size(record3);
                if row000>row3(row)
                    row3(row) = row000;
                end
            clear av_fr_int av_rad_int int pos_interp_fr_int
interp_fr_int int av_rad_int pos_av_rad_int av_fr_int_interp
std_fr_int_interp av_fr_int std_fr_int record1 record2 record3
pos_std_rad_int pos_radial_n N_SD N_AV_RAD AV std_fr_int
            clear frameID cs_area2 periph_int core_int pos_av_int
    end
end


    %% saving the interpolated radial results
    fid1 = fopen('radial_results_interpol.txt','w');
    fprintf(fid1,'%s \n', char(heading1));
    fprintf(fid1,'%s \n', char(heading2)');
    fprintf(fid1,'%s \n', repmat(horzcat('X(a.u.) ','SD
'),1,numel(RAD_INT)));
    matrix=zeros(row1,col1*numel(RAD_INT));
    initial = 1;
    monomer = '%5.2f ';
    for Z1 = 1:size(RAD_INT,1) %goes through all the conditions saved
in RAD_INT. Z1 - treatment; Z2 - pattern
        for Z2 = 1:size(RAD_INT,2)
            if ~isempty(RAD_INT{Z1,Z2})
                temp_matrix=eval(char(RAD_INT{Z1,Z2})); %reads
temporarily RAD_INT(Z)
                last = initial+size(temp_matrix,2)-1;
                matrix (1:length(temp_matrix),initial:last)=
temp_matrix; %creates a master matrix with all the interpolated curves
saved in different condition variables
                initial = last +1;
                clear temp_matrix
            end
        end
    end
    writting = repmat(monomer,1,size(matrix,2));
    for ZZ=1:length(matrix)
        fprintf(fid1,strcat(writting,'\n '), matrix(ZZ,:)');
    end
    fclose(fid1);
    save('RADIAL_interp_result','matrix');

    %% saving the radial results - averages only as the RAW data
    fid2 = fopen('radial_results.txt','w');
    fprintf(fid2,'%s \n', char(heading1));
    fprintf(fid2,'%s \n', char(heading2)');
    fprintf(fid2,'%s \n', repmat(horzcat('X(a.u.) ','SD
'),1,numel(RAD)));
```

```
    matrix2=zeros(row2,col2*numel(RAD));
    initial = 1;
    monomer = '%5.2f ';
    for Z1 = 1:size(RAD,1) %goes through all the conditions saved in
RAD_INT. Z1 - treatment; Z2 - pattern
        for Z2 = 1:size(RAD,2)
            if ~isempty(RAD{Z1,Z2})
                temp_matrix=eval(char(RAD{Z1,Z2})); %reads temporarily
RAD_INT(Z)
                last = initial+size(temp_matrix,2)-1;
                matrix2 (1:length(temp_matrix),initial:last)=
temp_matrix; %creates a master matrix with all the interpolated curves
saved in different condition variables
                initial = last +1;
                clear temp_matrix
            end
        end
    end
    writting = repmat(monomer,1,size(matrix2,2));
    for ZZ=1:length(matrix2)
        fprintf(fid2,strcat(writting,'\n '), matrix2(ZZ,:)');
    end
    fclose(fid2);
    save('RADIAL_result','matrix2');

    %% Saving cross-sectional area, n number, core and peripherical
intensities
    fid3 = fopen ('CONF_DESCRIPTIVE_DATA.txt','w');
    matrix3=zeros(sum(row3),col3);
    initial = 1;
    for Z1 = 1:size(DESC,1) %treatment
        for Z2 = 1:size(DESC,2) %pattern
            if ~isempty(DESC{Z1,Z2})
                temp_matrix=eval(char(DESC{Z1,Z2}));
                last = initial+size(temp_matrix,1)-1;
                matrix3 (initial:(initial+size(temp_matrix,1)-
1),1:size(temp_matrix,2))= temp_matrix;
                ID_matrix(initial:(initial+size(temp_matrix,1)-1)) =
repmat({[staining{Z1} '_' names(Z2)]},1,size(temp_matrix,1));
                initial = last +1;
                clear temp_matrix
            end
        end
    end
    fprintf(fid3,horzcat(' ID ','Cross_sectional_Area(X, um2)
','core_intensity(X,a.u.) ','peripherical_intensity(X,a.u.)
','average_intensity(X,a.u.) \n'));
    for ZZ=1:size(matrix3,1)
        if sum(matrix3(ZZ,:)) > 0 && ~isempty(ID_matrix(ZZ))
            fprintf(fid3,'%s %1.0f %4.2f %6.3f %6.3f
%6.3f\n',strcat(ID_matrix{ZZ}),matrix3(ZZ,:));
        else
            continue
        end
     end
    fclose(fid3);
    save('CONF_DESCRIPTIVE_DATA','matrix3');
end
```

IV. JPK data analysis: reading and saving individual curves in a readable format

```
function JPK_curves(reference,output)
%%% Version 2.1 - 06/04/2013
%% reading and organising JPK curves results - it saves each curve
with apropriate cell ID
% reference - input file containing the name of each file (first
column)
% and respective cell ID number (second column) - must be a .csv file;
% structure must be third column; model the 4th and lastly the cell
type as
% the 5th. SYNTAX MUST BE CONSISTENT!
% Output is the syntax for the output files - optional
%  Auto-generated by MATLAB - opening cellID matrix created on Excel
%% Import the data
[~, ~, newData1] = xlsread(reference);
newData1(cellfun(@(x) ~isempty(x) && isnumeric(x) &&
isnan(x),newData1)) = {''};
% result:
    % data = cell ID number - double matrix;
    % textdata = file name of raw curve - ATTENTION, is not a text
file

%% Identifying curve characteristics - based on reference file
for k=1:length(newData1)
    file_name = newData1{k,1};
    cellID = newData1{k,2};
    structure = newData1{k,3};
    model =  newData1{k,4};
    cellType = newData1{k,5};
    if isempty(file_name)
        warning('occasional error reading reference file - row may be
empty. Check file!')
        break
    end

    %% reading the txt file
    if sum(strfind(file_name,'.txt')) ~= 0
        [non,C]= fileattrib(file_name); % ignores the format of file,
naturally
    elseif sum(strfind(file_name,'.jpk-force')) ~= 0
        [non,C]= fileattrib(strcat(file_name(1:end-10),'.txt'));
    else
        warning ('File name contained in the reference matrix not
found: ',file_name);
    end

    if isstruct(C)
       fid = fopen(C.Name);
        l=1; %line related flag - incremented when text line
corresponds to actual data
        s = 0; %line related flag - identifies the curve segment
contained in headings
        %% line by line reading
        tline = fgetl(fid); %reads next line in text file fid.
            while ischar(tline)
```

```
                if ~isempty(tline) && ~strncmp('#',tline,1)  &&
~feof(fid)
                    eval([segmentID{s}, '(l,:) = str2num(tline);']);
                    l=l+1;
                    tline = fgetl(fid);
                elseif ~isempty(tline) && strncmp('#',tline,1) &&
~feof(fid)
                    if strncmp('# fancyNames:',tline,13)
                        delim = strfind(tline,'"');
                        ini = 1:2:length(delim);
                        fin = 2:2:length(delim);
                        for i=1:length(ini)
                            eval(['variables',segmentID{s},
'{i}=tline(delim(ini(i))+1:delim(fin(i))-1);'])
                        end
                    elseif strncmp('# units:',tline,8)
                        delim = strfind(tline,' ');
                        loc = 2:length(delim);
                        eval(['units',segmentID{s},
'=tline(delim(loc)+1);']);
                    elseif strncmp('# segment: ',tline,11)
                        s = s+1;
                        segmentID {s}= tline(strfind(tline,':
')+2:end);
                    end
                    tline = fgetl(fid);
                elseif isempty(tline) && exist('segmentID','var') &&
~feof(fid)
%                     endFlag = endFlag+1;
                    l=1;
                    tline = fgetl(fid);
                elseif feof(fid) && exist('segmentID','var') %being the
end of text file and with at least 1 segment read
                    break
                end
            end
            fclose(fid);
    else
        error('File could not be read.')
    end

    %% generating individual ID for the file
    if exist('output','var')
        [non,CC]=
fileattrib(horzcat('Curve_',output,'_',structure(1:4),'_',model(1:4),'
_',cellType,'_',int2str(cellID),'*'));
        if strcmp(CC,'No such file or directory.') % checking if
previous curve with same ref was created.
            sec = 1;
        else
            sec=length(CC)+1;
        end
        appendicite = '';
        for j=1:length(segmentID)
            try

save(horzcat('Curve_',output,'_',structure(1:4),'_',model(1:4),'_',cel
lType,'_',int2str(cellID),'.',int2str(sec),'_','.mat'),
['variables',segmentID{j}], ['units',segmentID{j}],
segmentID{j},appendicite)
```

```
            catch
                warning(['More than one possible segment per curve.
Curve ignored:  ', file_name])
            end
            appendicite = '-append';
            eval(['clear ',segmentID{j}]);
        end

        clear units* variables* segmentID{:}
    else
        appendicite = '';
        for j=1:length(segmentID)

save(horzcat('Curve_',structure(1:4),'_',model(1:4),'_',cellType,'_',i
nt2str(cellID),'.',int2str(sec),'_','.mat'),
['variables',segmentID{j}], ['units',segmentID{j}],
segmentID{j},appendicite)
            appendicite = '-append';
            eval(['clear ',segmentID{j}]);
        end
        clear units* variables* segmentID{:}
    end
end
clear sec
```

```
function hertz(input,K)
%% V.1.7. - 29/04/2013, ignoring linear correction shit
%% Measuring the Elastic moduli of data presenting the "input" syntax
% The system will read only curves with syntax "Curves*"
% Reading the file
[A,newData1] = fileattrib (horzcat('Curve_',input,'*'));
combE = double.empty(2,5,0);
hertzCurve = 0;
for curve=1:length(newData1)
    CP = [];
    dir = newData1(curve).Name;
    loc = strfind(dir,'\');
    fileName {curve} = dir(loc(end)+1:end);
    hertzCheck = sum(strfind(fileName{curve},'Hert'));
    relaxationCheck = sum(strfind(fileName{curve},'Forc'));
    load(fileName{curve});
    % the variables contained in loaded file are
    % 'extend','retract', 'variables*' and 'units*' of both extend and
retract curves.
    % The first two correspond to the raw data - to each column of
    % the curve e.g extend(:,1), the correspondent variable
designation and units
    % are contained in variablesextend(1) and unitextend,
respectively. The
    % respective units are defined by latest (string) being each
character the unit according with SI
    %% Reading units and converting everything to nanoscale
    variables = whos('variables*');
    for i=1:length(variables)
        variablesName = variables(i).name; %reads the name of the
variable
        variable = eval(variablesName); %evaluates it
        if length(variablesName) > length('variables') %checks for the
variables* in order to exclude 'variables' array itself
            segmentID =
variablesName(regexp(variablesName,'variables','end')+1:end); %creates
an segment identifier
            for j=1:length(variable)
                if strcmp(variable{j},'Height') %spots the z-
displacements column
                    eval(['zDispUnit = units' segmentID '(j);']);
                    switch zDispUnit
                        case 'm'
                            scalar = 1E9;
                        case 'mm'
                            scalar = 1E6;
                        case 'um'
                            scalar = 1E3;
                        case 'nm'
                            scalar = 1;
                    end
                    eval(['zDisp' segmentID ' = flipud(' segmentID
'(:,j)).*scalar;']); %flips the curve upside down to nm
                elseif strcmp(variable{j},'Vertical Deflection')
                    eval(['vDeflUnit = units' segmentID '(j);']);
                    switch vDeflUnit
                        case 'N'
                            scalar = 1E9;
```

```
                        case 'mN'
                            scalar = 1E6;
                        case 'uN'
                            scalar = 1E3;
                        case 'nN'
                            scalar = 1;
                    end
                    eval(['vDefl' segmentID ' =' segmentID
'(:,j).*scalar;']);
                end
            end
        end
    end
        clear variable*
        %% Identifying the sample and curve
        uScore = strfind(fileName{curve},'_');
        dot = strfind(fileName{curve},'.');
        fileNameStr = fileName{curve};
        sampleID {curve} = fileNameStr(uScore(end-2)+1:uScore(end-1)-
1);
        cellID {curve} = fileNameStr(uScore(end-1)+1:dot(1)-1);
        curveID {curve} = fileNameStr(dot(1)+1:uScore(end)-1);
        structureID {curve} = fileNameStr(uScore(2)+1:uScore(3)-1);
    if hertzCheck ~= 0 && ~isempty(who('zDispextend')) &&
~isempty(who('vDeflextend')) %Elasticity test
        zDisp = zDispextend;
        vDefl = vDeflextend;
        indLim = 100; %indentation limit vector [nm]
        intIndVector = 0:indLim/(10-1):indLim; % creates the
interpolated indentation vector for representation
        if length(zDisp)>100 && length(vDefl)>100
            hertzCurve = hertzCurve +1; % Hertzian only read curve
            disp(horzcat('Processing:  ',sampleID {hertzCurve},cellID
{hertzCurve},curveID{curve},structureID {hertzCurve},'...'))
            %% Implementing pre-processing
            % Linear search for best aggregate fit of line and Hertz-
type power law
            limit1 = 5; % number minimum of point for fitting
interations
            % using extend curve for processing
            for k=1:length(zDisp)-(limit1*2)
                xi = sprintf('%6.16f',zDisp(end-(limit1+k))); %fitting
is very sensitive to the precision of this value!
                yi = sprintf('%4.16f',vDefl(end-(limit1+k)));
                s = fittype( strcat(yi,'+(a*(x-(',xi,')).^(3/2))'),
'independent', 'x', 'dependent', 'y' );
                f = fitoptions (s);%             [pFit1 pError1] =
fit(zDisp(end-(limit1+k):end),vDefl(end-
(limit1+k):end),f,'problem',{vDefl(end-(limit1+k)),zDisp(end-
(limit1+k)),3/2});
                f.Lower = 0;
                f.StartPoint = 0;
                f.Upper =1;
                try
                    [pFit1 pError1] = fit(zDisp(end-
(limit1+k):end),vDefl(end-(limit1+k):end),s,f);
                    [lFit1 lError1] = fit(zDisp(1:end-(limit1+k-
1)),vDefl(1:end-(limit1+k-1)),'poly1');
                    aError (k) = pError1.rmse + lError1.rmse; %
aggregate error
```

```
                    powerE (k) = pError1.rsquare; %rsquare error for
alternative CP determination - in accordance with visual inspection
                catch %if fitting cannot be carried on, error is kept
the same
                    aError (k) = max(aError);
                    powerE (k) = max(powerE);
                end
            end
            %% Finding CP
            mseCP = length(zDisp) - find(aError ==
min(aError),1,'first') - limit1; %Contact point
            fitTol = max(powerE)-0.08; % defines the fit quality for
contact point (secondary) calculation
            rsquareCP = find(fliplr(powerE) > fitTol,1,'first') +
limit1; %Contact point
            if  ~isempty(mseCP) && ~isempty(rsquareCP) && rsquareCP <=
length(zDisp) && mseCP <= length(zDisp)
                CP = [mseCP; rsquareCP];
            elseif isempty(mseCP) && ~isempty(rsquareCP)
                CP = vDefl(rsquareCP);
                reportComm = 'Contact point based on RSQUARE is used';
            elseif ~isempty(mseCP) && isempty(rsquareCP)
                CP = vDefl(mseCP);
                reportComm = 'Contact point based on MSE is used';
            else
                warning(horzcat('Contact point could not be determine
-  ',sampleID {hertzCurve},cellID
{hertzCurve},curveID{curve},structureID {hertzCurve}))
                combE (:,:,hertzCurve) = 0;
            end
            clear aError powerE
            if ~isempty(CP)
                % Set up fittype and options.
                ft = fittype( 'smoothingspline' );
                opts = fitoptions( ft );
                opts.SmoothingParam = 5E-007; %obtained by visual
inspection - cftool
                %% Data smoothing
                [smoothfit, gof] = fit( zDisp, vDefl, ft, opts );
                svDefl = feval(smoothfit,zDisp);
                lzDisp = zDisp;
                lsvDefl = svDefl;
                lvDefl = vDefl;
%                 end
                clear initial final %d2zDisp d3zDisp vDefl zDisp
svDefl
                for cp = 1:length(CP) % Processing using two distict
CP detection procedures
                    %% Calculating Strain Limit
                    if CP(cp) > 0 && length(lvDefl) > CP(cp) &&
length(lsvDefl) > CP(cp)
                        tipSampleSepa = (lzDisp-lzDisp(CP(cp)))-
((lsvDefl-lsvDefl(CP(cp)))./K); %tip-sample separation vector
                        for p=1:length(indLim)
                            indLimInde = find(tipSampleSepa >
indLim(p),1,'first');
                            if ~isempty(indLimInde) && length(lzDisp)
== length(lvDefl)
                                %% Setting distance tolerance between
fitted function and the original curve @ the CP
                                RMSE = dsp.RMS;
```

```
                                dTole = step (RMSE,lsvDefl);
                                strLsvDefl =
sprintf('%4.16f',lvDefl(CP(cp)));
                                strLzDisp =
sprintf('%6.16f',lzDisp(CP(cp)));
                                ff =
fittype(horzcat(strLsvDefl,'+(a*(x-(',strLzDisp ,')).^(3/2))'),
'independent', 'x', 'dependent', 'y' );
                                optss = fitoptions(ff);
                                optss.Lower = 0;
                                optss.StartPoint = 0;
                                optss.Upper =1;
                                pFit2 =
fit(lzDisp(CP(cp):end),lsvDefl(CP(cp):end),ff,optss);
                                powerFit2 = feval(pFit2,lzDisp);
%creates the hertzian fitted curve from CP(cp):end
                                if dTole < abs(powerFit2 (CP(cp)) -
lsvDefl(CP(cp))) %further preprocessing is required - distance
tolerance is overcame
                                    dToleF = find(abs(powerFit2 -
lsvDefl) < dTole); % seeks for points where distance tolerance is obay
                                    dToleF_CP = dToleF - CP(cp);
%subtracts CP(cp) in order to check for the closests indexes
                                    ppCP(cp) =
dToleF_CP(find(abs(dToleF_CP) > 0,1,'first'))+CP(cp); %% REDUNDUNT TRY
WAS TAKEN FROM HERE
                                    %% Pre-processing
                                        if exist('ppCP(cp)','var') &&
ppCP(cp)-indLimInde >= 5 % further preprocessing not necessary
                                            contTipSampleSepa =
tipSampleSepa(ppCP(cp):indLimInde);
                                            contF =
lsvDefl(ppCP(cp):indLimInde);
                                            ss =
fittype('b*x^(3/2)','independent', 'x', 'dependent', 'y');
                                            optss = fitoptions(ss);
                                            optss.Lower = 0;
                                            optss.Upper = 6000; %
determined so the Elastic moduli does not overcome kilopascal range
                                            optss.StartPoint = 0;
                                            [pFit3 pError3] =
fit(contTipSampleSepa-contTipSampleSepa(1),contF-contF(1),ss,optss);
%fitting TipSampleSeparation[nm] Vs F[nN] to determine E
                                            if pError3.rsquare >
fitTol*0.70
                                                combE(cp,p,hertzCurve)
= pFit3.b*(2.25/(4*sqrt(10E3)))*1E9; %pFit3.b*(1E-9/(1E-
9^(3/2)))*(2.25/(4*(1E-5)^0.5));%Elastic modulus for the CP assumed -
F = 4*(R^0.5)/(3*(1-v^2))*E*(ind^3/2)
                                            else
                                                comment = 'Quality of
fitting not satisfactory. Sample ignored: ';

warning(horzcat(comment,sampleID {hertzCurve},cellID
{hertzCurve},curveID{curve},structureID {hertzCurve}));
                                                combE(cp,p,hertzCurve)
= 0;
                                            end
                                    elseif exist('ppCP(cp)','var')
&& ~isempty(ppCP(cp)) && ppCP(cp)-indLimInde <5;
```

```
                                                comment = 'Not enough
points for contact-region curve. Curve ignored. Sample: ';
                                                warning
(horzcat(comment,sampleID {hertzCurve},cellID
{hertzCurve},curveID{curve},structureID {hertzCurve}))
                                                combE(cp,p,hertzCurve) =
0;
                                            elseif exist('ppCP(cp)','var')
&& isempty(ppCP(cp))
                                                comment = 'Contact point
is not within the distance tolerance and correction is not possible.
Curve ignored. Sample: ';
                                                warning
(horzcat(comment,sampleID {hertzCurve},cellID
{hertzCurve},curveID{curve},structureID {hertzCurve}))
                                                combE(cp,p,hertzCurve) =
0;
                                            end
                                        elseif indLimInde-CP(cp) >= 5%
preprocessing not necessary - dTole not overcame and there's enough
points for the fitting
                                            contTipSampleSepa=
tipSampleSepa(CP(cp):indLimInde);
                                            contF =
lsvDefl(CP(cp):indLimInde);
                                            ss =
fittype('b*x^(3/2)','independent', 'x', 'dependent', 'y');
                                            optss = fitoptions(ss);
                                            optss.Lower = 0;
                                            optss.Upper = 6000;
                                            optss.StartPoint = 0;
                                            [pFit3 pError3] =
fit(contTipSampleSepa-contTipSampleSepa(1),contF-contF(1),ss,optss);
%fitting TipSampleSeparation[nm] Vs F[nN] to determine E
                                            if pError3.rsquare > fitTol*0.70
                                                combE(cp,p,hertzCurve) =
pFit3.b*(2.25/(4*sqrt(10E3)))*1E9;%Elastic modulus for the CP assumed
- F = 4*(R^0.5)/(3*(1-v^2))*E*(ind^3/2)
                                            else
                                                comment = 'Quality of fitting
not satisfactory. Sample ignored: ';

warning(horzcat(comment,sampleID {hertzCurve},cellID
{hertzCurve},curveID{curve},structureID {hertzCurve}));
                                                combE(cp,p,hertzCurve) = 0;
                                            end
                                        elseif indLimInde-CP(cp) < 5
                                            comment = 'Distance tolerance not
overcame but not enough points for the fitting. Sample ignored: ';
                                            warning(horzcat(comment,sampleID
{hertzCurve},cellID {hertzCurve},curveID{curve},structureID
{hertzCurve}))
                                            combE(cp,p,hertzCurve) = 0;
                                        end
                                    elseif isempty(indLimInde) &&
length(lzDisp)-CP(cp) > 5
                                        comment = 'Indentation limit not
found, probably outside curve bounderies. Fitting is still
performed:';
```

```
                                    warning(horzcat(comment,sampleID
{hertzCurve},cellID {hertzCurve},curveID{curve},structureID
{hertzCurve}))
                                    contTipSampleSepa=
tipSampleSepa(CP(cp):end);
                                    contF = lsvDefl(CP(cp):end);
                                    ss =
fittype('b*x^(3/2)','independent', 'x', 'dependent', 'y');
                                    optss = fitoptions(ss);
                                    optss.Lower = 0;
                                    optss.Upper = 6000;
                                    optss.StartPoint = 0;
                                    [pFit3 pError3] =
fit(contTipSampleSepa-contTipSampleSepa(1),contF-contF(1),ss,optss);
%fitting TipSampleSeparation[nm] Vs F[nN] to determine E
                                    if pError3.rsquare > fitTol*0.70
                                        combE(cp,p,hertzCurve) =
pFit3.b*(2.25/(4*sqrt(10E3)))*1E9;%Elastic modulus for the CP assumed
- F = 4*(R^0.5)/(3*(1-v^2))*E*(ind^3/2)
                                    % convertion nano- to meter- scale -
a2=a1*(n/(n^1.5))
                                    else
                                        comment = 'Quality of fitting not
satisfactory. Sample ignored: ';
                                        warning(horzcat(comment,sampleID
{hertzCurve},cellID {hertzCurve},curveID{curve},structureID
{hertzCurve}));
                                        combE(cp,p,hertzCurve) = 0;
                                    end
                                else
                                    comment = 'Fitting not possible -
line241. Sample ignored: ';
                                    warning(horzcat(comment,sampleID
{hertzCurve},cellID {hertzCurve},curveID{curve},structureID
{hertzCurve}))
                                    combE(cp,p,hertzCurve) = 0;
                                end
                                clear limit2
                            end
                        else
                            comment = 'Contact point is either not
positive or out of curve boundaries. Sample ignored: ';
                            warning (horzcat(comment,sampleID
{hertzCurve},cellID {hertzCurve},curveID{curve},structureID
{hertzCurve}))
                            combE (cp,:,hertzCurve) = 0;
                        end
                    end %for - different contact points
                else
                    comment = 'Contact point not found. Sample ignored: ';
                    warning (horzcat(comment,sampleID {hertzCurve},cellID
{hertzCurve},curveID{curve},structureID {hertzCurve}))
                    combE (:,:,hertzCurve) = 0;
                end %@ the CP checkpoint - if not existent, combE is
assumed 0
                clear CP

                %% Constructing cell array containing IDs and respective E
                hertzM {hertzCurve,1} = sampleID{hertzCurve};
                hertzM {hertzCurve,2} = cellID{hertzCurve};
```

```
            hertzM {hertzCurve,3} = curveID{hertzCurve};
            hertzM {hertzCurve,4} = structureID{hertzCurve};
            %% Interpolation
            intContF (:,hertzCurve) = interp1(contTipSampleSepa -
contTipSampleSepa(1),contF-contF(1),intIndVector);
            clear contF contTipSampleSepa
            if exist('reportComm','var')
                hertzM {hertzCurve,5} = reportComm;
            end
        elseif relaxationCheck ~=0
            comment = 'relaxation model not implemented yet - Betch!';
            warning (horzcat(comment,sampleID {curve},cellID
{curve},curveID{curve},structureID {curve}))
        else
            comment = 'Check reference file as input! Model check
failed.';
            warning (horzcat(comment,sampleID {curve},cellID
{curve},curveID{curve},structureID {curve}))
        end
    end % 1st if @ the hertzCheck
end % 1st for - curve is defined as nr of curves within the folder
    %%Reading different sampleID's in the previously read curves
    save(strcat('raw_data',input,'.mat'),'hertzM','combE','int*');
end
```